Sulfur cycle through the ages, from rivers to sedimentary carbonates

Guillaume Paris

C R P G | Centre de Recherches Pétrographiques et Géochimiques

Sulfur cycle through the ages, from rivers to sedimentary carbonates

Le cycle du soufre à travers les âges, des rivières aux carbonates sédimentaires.

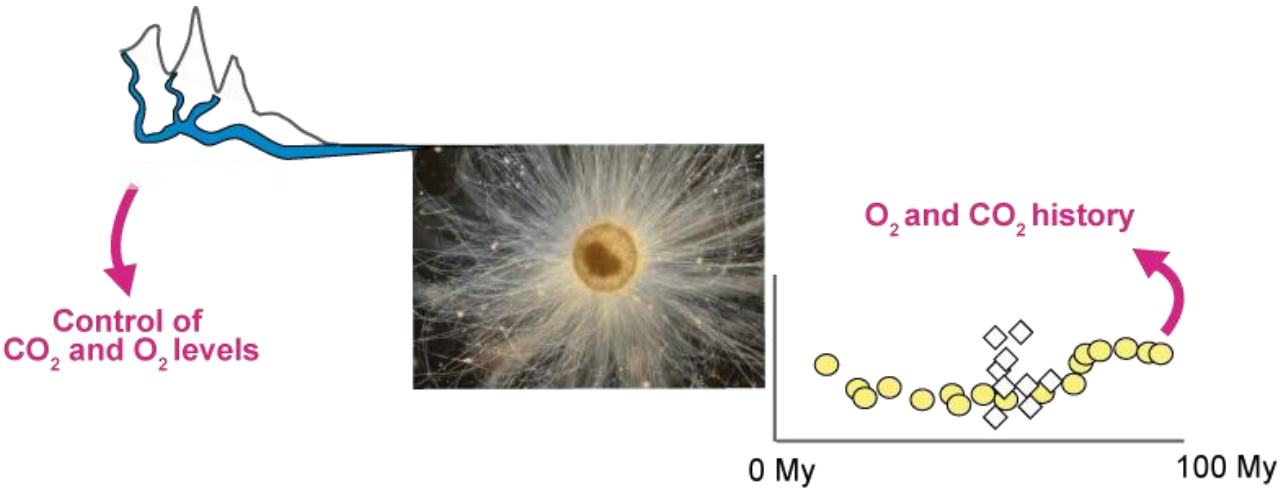

Guillaume Paris

Habilitation à Diriger les Recherches

Soutenue le 11 décembre 2023

Géosciences

Ecole doctorale Sirena

Sulfur cycle through the ages, from rivers to sedimentary carbonates

Cycle du soufre à travers les âges, des rivières aux carbonates sédimentaires.

Habilitation à Diriger les Recherches

Guillaume Paris

Soutenue le 11 décembre 2023 devant le jury composé de

Rapporteurs/rapportrices

Magali Ader, Professor	IPGP
Vincent Balter, DR CNRS	LGL-TPE
Adina Paytan, Professor	UCSC

Examinateurs/examinatrices

Vincent Busigny, Professor	IPGP
Christian France-Lanord, DR CNRS	CRPG
Emmanuelle Pucéat, Professor	Biogéosciences
Edward Tipper, Professor	University of Cambridge

Remerciements

Abstract

I would like to thank my family, my friends, my collaborators and all the people I had the chance to meet over the years, in the lab and elsewhere. Merci à Anne, Chiara, Claire, Guillaume, Ted pour les relectures, les excitants projets qui nous réunissent et, ainsi qu'à mes parents, Gérald et Rustine, pour le soutien sans faille au cours de la rédaction de ce mémoire.

Full text

First, I want to thank all the students, grad students and postdocs I've been given the chance to work with over the years, especially Vicky, Ted, Caroline, Sanjeev, Mark, Yigal and Arbia. Working with you was stimulating and I've learned a lot.

Je veux vous remercier tous et toutes au CRPG, qui m'avez offert des collaborations stimulantes et excitantes depuis mon arrivée, des échanges humaines, des bières, des sorties cinés, qui avez gardé Rustine, ainsi que toutes les personnes qui m'ont aidé au fil des années de ma candidature CNRS et de la découverte de la vie académique. Merci à vous Guillaume, Précie, Celia, Evelyn, Charlotte, Julien, PH, Laurette, Thomas, Yves, Raphael, Mary, Christian et merci à Bernard et David de m'avoir inclus dans le module de géochimie. Je veux aussi remercier les PAR et leur soutien sans faille, technique, scientifique, administratif, humain – la vie du CRPG vous doit énormément. Merci à vous l'équipe d'IRISS, Catherine, Damien, Aimeryc, Christiane et Camille, et merci également Bruno, Isabelle, Aurélie et tous les membres de l'équipe administrative. Merci à vous tous et toutes qui m'avez donné un coup de main, échangé autour d'un café, au CRPG, au sein d'OTELo, à la DR06 ou encore au sein de l'UL.

Je veux remercier particulièrement mes collaborateurices amis ou amies de nombreuses années, Annachiara, Julien, Jérôme, Claire, Pascale, Anne, Ted. Je veux remercier aussi les membres du monde Paléos pour tous les échanges, l'organisation des GDR et écoles, la vie de la communauté : merci Guillaume, Guillaume, Guillaume, Guillaume, et quelques non-Guillaumes: Emmanuelle, Yannick, Alicia, Pierre, Nathalie et toutes les personnes avec qui j'ai pu échanger au fil des années. Merci aux membres du groupe de lecture biomin !! J'en apprends toujours autant à chaque lecture.

Et une pensée spéciale pour les membres de la Section 18 – c'est une mission exigeante, difficile, et émotionnellement coûteuse, et vous la rendez excitante, enrichissante, motivante et avant tout humaine et inoubliable.

France is wonderful, the world is too! There are so many people I met at Caltech that I need to thank as well. Jess and Alex, and all of you who made Caltech an unforgettable human and scientific adventure: Adam, Sophie, Ted, Nithya, Anna, Anne, Uri, Jena, Katie, Marion, Caltech-Morgan, Emmanuel, Virginie, Seth, Masha, and also Paul, Hollywood-Morgan, Rob, Ashton, Parc-de-triomphe-John, Cyrus, Christopher.

I also want to thank all the sulfur people throughout the world who makes this community an exciting and thriving area, whether we had the opportunity to collaborate or not. I'm always incredibly happy to meet you during international conferences or other opportunities, in particular Sasha, Itay, David and Sam. I also deeply enjoyed all the opportunities I had to meet people of the biomineralization world, in particular the Catalina people.

Merci à tous ceux et toutes celles qui ont traversé l'Atlantique lorsque j'étais à Caltech, but also thanks to all of you who crossed the Atlantic since I moved to France.

Bea, Benjamin, Emelyne, Emmanuel, Gérald, JP, Juliane, Laurie, Marie, Marie-Laure, Matthieu, Matthieu, Maxime, Séverine, Stéphanie et Virginie le monde académique et les années de doutes, de quête d'un poste, de déménagements, de coups durs auraient été bien plus dures sans vous. Merci pour tout. Je vous dois tant. Merci pour les heures d'échanges, les verres, les partages, la culture, le soutien moral inconditionnel. Merci à toute la nouvelle génération, en particulier les filleul.e.s: Eli, Victor, Ninon et Margot.

Je sais que j'oublie plein de gens et je m'en excuse.

Enfin, Rustine et Cagibi, Minouit aussi, et bien sûr Duchesse et Vany, je sais que vous n'avez jamais trop eu votre mot à dire et je vous en remercie d'autant plus.

Je vais néanmoins devoir clôre cette liste, sur ma famille car il va sans dire que je ne serai pas ici sans vous. Merci tatas, tontons, cousins, cousines de toutes générations. Merci Michèle, notamment pour toutes ces fois où tu m'héberges rue des Francs-Bourgeois. Merci à mes grands-parents même s'ils ne sont plus là, et à Marie-Noëlle et Joseph qui nous ont quittés trop tôt. Et enfin, merci Papa, merci Maman, merci JD, merci Bertrand, merci Anna, merci Olga, merci Eleni, merci Yanis et bienvenu à Sasha

Table des matières

Remerciements i
Table des matières iii
Introduction 1
Chapter I. The sulfur cycle and the composition of the ocean-atmosphere system 3
I. Long-term evolution of the Earth's surface: the example of the last 100 million years. 3
II. The canonical view of the long-term CO_2 and O_2 control. 5
III. The meaning of the sulfur isotopic composition of seawater sulfate and its links to the carbon and oxygen cycles. 9
IV. Microbial sulfate reduction and sulfur isotopes. 13
V. Sulfur contribution to weathering. 25
VI. Conclusion. 29
Chapter II. The use of the MC-ICP-MS method to measure sulfur isotopes. 31
I. Sulfur isotope abundance ratio measurements: an overview. 31
II. Measurement procedure. 33
III. Experimental results. 37
IV. Discussion. 40
V. The V-CDT scale: use with caution. 44
VI. Conclusion. 45
Chapter III. The geological records of the sulfur cycle. 47
I. The main archives for $\delta^{34}S_{sw}$. 47
II. Comparison between the records. 52
III. Past evolution of the sulfur cycle. 56
IV. Conclusion: the importance of a proper archive and stratigraphy. 59
Chapter IV. Carbonate Associated Sulfate (CAS): a work in progress. 60
I. Where and what is sulfur in biogenic carbonates? 61
II. Transport of ions and control of the composition of the biomineralizing fluid. 65
III. Carbonate associate sulfate: nature and control. 75
IV. Sulfur isotope composition of carbonates. 86
V. Conclusion. 92
Chapter V. Why are CAS so often different from other records? A history of diagenesis, and of new information to be extracted from the sedimentary record. 94
I. Post-depositional processes. 94
II. Diagenetic processes affecting sulfur isotopes. 99
III. Revisiting $\delta^{34}S_{CAS}$ variations under the prism of diagenesis. 109
IV. Conclusion. 115
Chapter VI. Reconstructing past $\delta^{34}S_{sw}$ and diagenetic processes across the K-Pg boundary. 117
I. Oceanic carbon and sulfur cycle of the K-Pg boundary. 117
II. A new combined sulfur record from benthic and planktic foraminifera. 122
III. Reconstruction of the sulfur cycle. 126
IV. Conclusion. 132
Annex I: Calcium isotopes: new calibrations, and additional paleoenvironmental information. 134
I. Introduction. 134
II. Calcium isotopes: different experiments, different protocols, contradictory results. 134
III. Aim of the new experiments, method, and results. 134
IV. Discussion. 134
V. Conclusion. 134
Annex II. Research project: the sulfur cycle reconstructed, from rivers to the depths of the ocean. 136
I. Interactions between biogeochemical cycles control the composition of the ocean-atmosphere system. 136
II. Methodology, approach, and tasks 136
Annex III: Resume, research management, teaching, outreach, supervision 147
I. Resume 147
II. Supervised students and postdoctoral collaborators. 153
III. Societal and environmental impact. 154
IV. Fundings. 156
V. Teaching and outreach. 157
VI. Research management. 158
General conclusion. 161
List of bibliographical references 163
Abstract/résumé 186
Abstract 186
Résumé 186

Introduction

The carbon and oxygen biogeochemical cycles have controlled the composition of the ocean-atmosphere system throughout Earth's history. These two fundamental cycles are linked by widely studied processes: (1) photosynthesis and its associated opposed flux, the oxidation of organic matter, and (2) carbonate precipitation coupled with weathering and its counter-flux, reversed weathering. The third flux/counter flux, less well characterized, is the formation and burial of pyrite, which releases oxygen and CO_2 on geological timescales and its counter-flux, the oxidation of pyrite at the surface of continents, which disrupts weathering and lead to atmospheric oxygen consumption. Sulfur isotopes are a prime tool for studying the current and ancient sulfur cycle, and shed light on the interactions between sulfur, carbon, and oxygen cycling. My work has focused on improving our understanding of the carbonate archive as a recorder of the sulfur cycle, and on the parameters that control the S isotopic composition of rivers and of the ocean.

In order to describe and more thoroughly quantify the modern and ancient sulfur cycle, I have structured my research, as well as the projects of the different grad students and postdocs I've been supervising and collaborating with, through different questions over the years. Thanks to a new method I developed for measuring sulfur isotope abundance ratios from small samples by MC-ICP-MS, I centered my research on the modern and past evolution of the sulfur cycle. The first axis of my research focuses on the modern sulfur cycle. How well do we understand the interactions between the carbon, oxygen and sulfur cycles and the mechanisms that control the modern sulfur isotope ratios of the ocean? Many additional constraints on the modern sulfur cycle are still needed. For example, it is important to constrain sulfur's role in continental weathering, which we worked on, for instance, during Mark Torres's and Chenyang Jin's PhD and in collaboration with Erica Erlanger, Andrea Burke and Dimitri Laurent during their postdoctoral years. Additionally, it is important to better understand sulfur fractionation during microbial processes, on which I worked through Min-Sub Sim's postdoc and my own work.

The second main axis of my research concerns reconstructing ocean sulfur isotope ratios back in time, using carbonate associated sulfate as an archive. Do biogenic carbonates record the sulfur isotopic composition of seawater? Answering this question requires considering isotope fractionation during S incorporation in carbonates from an inorganic point of view, and the problem of vital effects. These projects formed the basis of part of Yigal Barkan's PhD and Caroline Thaler's postdoc. There is indeed a lot to be understood about how sulfate is managed during biomineralization, since it plays many roles, both as an inhibitor and facilitator.

Is this sulfur isotope ratio preserved throughout the rock's history? Possibly, but we need to understand the processes of diagenesis and metamorphism at work, as demonstrated by Ted Present's PhD. Finally, can we use carbonate associated sulfate to extract useful information about biogeochemical cycles and paleoenvironmental conditions? Most likely, if the conditions above are well understood and constrained, which we demonstrated during the PhD work of Vicky Rennie and Arbia Jouini.

It is within this general framework that much of my research, for the past and upcoming decades, falls. In addition to these questions, which concern the study of the Earth throughout its history, sulfur is an element whose cycle is strongly perturbed by human activities, and I am increasingly interested in the modern sulfur cycle, weathering, and pollution, though I will not detail this part of my work, through - for instance - the postdoctoral research of Sanjeev Dasari.

This memoire is structured as follows. After a general introduction of the biogeochemical cycles investigated here and why the sulfur isotope ratios that we can measure in seawater and rivers can bring critical information about the composition of the ocean-atmosphere system, I will introduce the analytical developments I led on the MC-ICP-MS. Following this presentation, I will present and compare the different archives of the geological sulfur cycle and why carbonate associated sulfate is of particular interest. I will then focus on this archive and present where we now stand on our knowledge of sulfur, and more particularly sulfate incorporation in carbonates. I will also describe how we showed that diagenesis impacts carbonate associated sulfate and how this signal alteration is actually a source of paleoenvironmental information in itself. I will finally focus on the results we obtained on the K-Pg boundary.

The chapters that follow will contain work I contributed to, directly or through collaborations with postdoctoral fellows and supervision of grad students, and how this work has contributed to move the field forward. Not all of my work will be detailed here, so that I am able to focus specifically on the geological sulfur cycle. Each chapter starts with a global introduction on the topic before going into detail in my contributions, and those of my collaborators.

I will then conclude with where I want to take my research in the next ten years. A first annex will discuss all of my non-scientific contributions to the scientific communities I belong to and a second annex will discuss a recently developing aspect of my research on calcium isotope ratio in carbonates.

Chapter I. The sulfur cycle and the composition of the ocean-atmosphere system.

In order to introduce my work on the sulfur cycle, I will start with an overview of the carbon and oxygen cycles. A brief introduction to the sulfur cycle itself, and its interaction with the carbon and oxygen cycles, will be completed by the description of different contributions I contributed to through collaborations with postdoctoral fellows and grad students: Mark Torres, Andrea Burke, Mins-Sub Sim, Dimitri Laurent and Erica Erlanger, as well as my own work in collaboration with Sean Crowe.

I. Long-term evolution of the Earth's surface: the example of the last 100 million years.

Interactions between the biogeochemical cycles of carbon, oxygen and sulfur regulate the chemical composition of the ocean-atmosphere system, and hence atmospheric concentrations of CO_2, a greenhouse gas of particular importance in the context of global warming. CO_2 plays an essential role in controlling Earth's climate, which has been marked by a slow first order cooling over the past 100 Myr as atmospheric CO_2 levels have slowly declined (e.g. Li and Elderfield, 2013; Rae et al., 2021). To fully anticipate the consequences of rising anthropogenic CO_2, we need to continually improve our understanding of the controls of atmospheric CO_2 levels on all time scales.

Today, atmospheric CO_2 represents around 2% of the inorganic carbon present in the ocean-atmosphere system, which can be considered as a single entity on timescales longer than 50,000 years. Limestone and sedimentary organic matter are the main carbon reservoirs at the Earth's surface, and any imbalance in the flow of carbon into or out of these sediments can generate major fluctuations in atmospheric CO_2 levels (Berner, 1991).

The last 100 Myr of Earth History provide a fundamental example of how geologic imbalances in carbon fluxes have driven changes in atmospheric CO_2 and global temperatures, as those imbalances led to the cold climate under which Humans evolved and that they are now disrupting (Fig. 1).

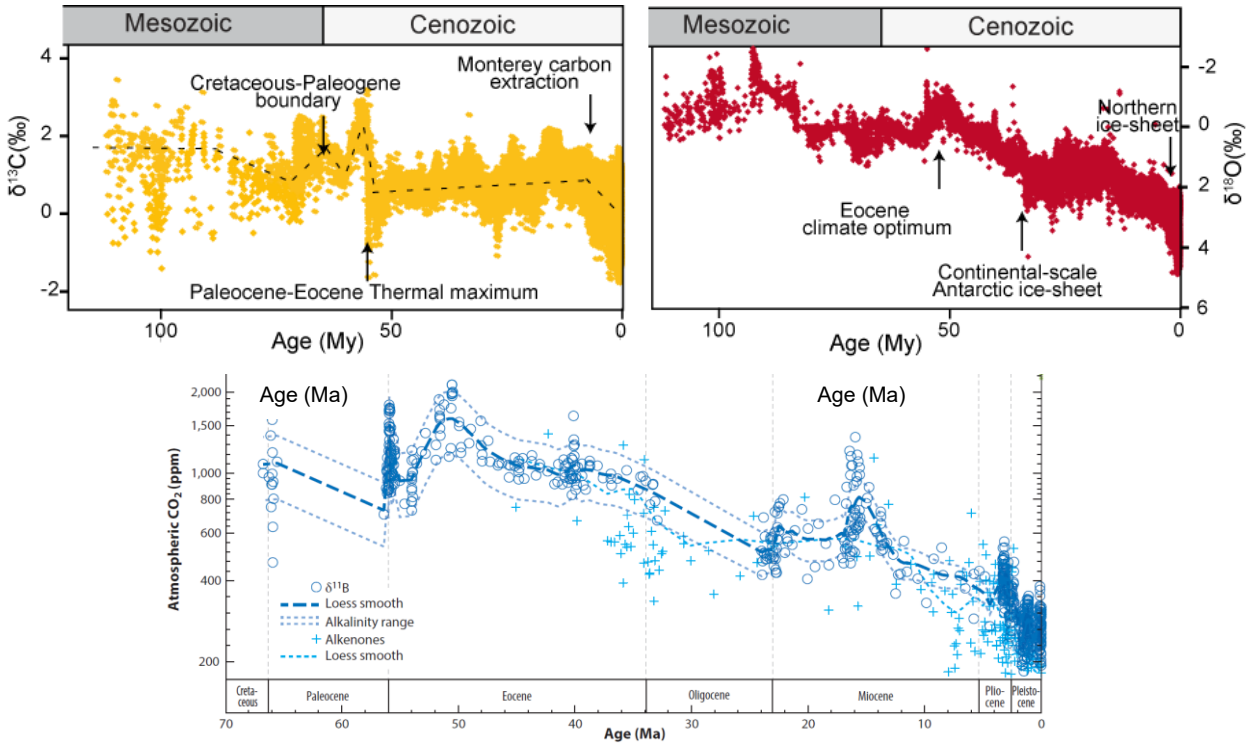

Figure 1. Upper panels : stacked $\delta^{13}C$ and $\delta^{18}O$ records from benthic foraminifera for the past 120 Myr, against some paleoenvironmental milestones (Cramer et al., 2009; Friedrich et al., 2012; Zachos et al., 2001). $\delta^{13}C = (({}^{13}C/{}^{12}C)_{sample}/({}^{13}C/{}^{12}C)_{V\text{-}PDB} - 1)$ and $\delta^{18}O = (({}^{18}O/{}^{16}O)_{sample}/({}^{18}O/{}^{16}O)_{V\text{-}PDB} - 1)$ with V-PDB the Vienna Pee Dee Belemnite reference material (Stichler, 1995). Lower panel: compilation of proxy-based CO_2 reconstruction for the Cenozoic (Rae et al., 2021)

Over this period, the stable carbon isotope composition measured in foraminifera tests (their shells) is one of the main archives used to reconstruct imbalances in carbon fluxes (e.g. (e.g. Berner et al., 1983; Craig, 1953; Cramer et al., 2009; Friedrich et al., 2012; Landergren, 1954; Zachos et al., 2001; Westerhold et al., 2020) that led to the first order continuous CO_2 decrease of the Cenozoic (e.g. Anagnostou et al., 2016; Berner, 1991; Rae et al., 2021). Records of Earth's surface temperature help contextualize carbon cycle changes. They can be reconstructed using the oxygen isotope composition of the calcareous tests, which depend on temperature along with other physico-chemical parameters of the seawater in which the individual lived (e.g. Cramer et al., 2009; Emiliani and Edwards, 1953; Friedrich et al., 2012; Urey, 1951; Zachos et al., 2001; Westerhold et al., 2020). The $\delta^{18}O$ data reveal that the carbon cycle evolution drove a global decrease in atmospheric CO_2 levels that led the Earth towards its current cold period, marked by the glacial-interglacial alternations in place since the Pleistocene. The last 100 Myr thus represent a pivotal period in the history of our planet's environment. While the carbon and oxygen cycles are being intensively explored over this period, the sulfur cycle needs to be more greatly characterized and better constrained. We will nonetheless first start with the description of the carbon cycle.

Much like carbon and oxygen isotopes, sulfur isotopes represent an essential tool for deciphering the processes controlling the sulfur cycle. Sulfur has four stable isotopes, ^{32}S (~95%), ^{34}S (~5%), and the minor isotopes ^{33}S and ^{36}S. Isotope abundance ratios are reported in ‰ deviation from the Vienna Canyon Diablo Troilite standard (V-CDT), under the δ notation ($\delta^{34}S = (^{34}S/^{32}S)_{sample}/(^{34}S/^{32}S)_{V\text{-}CDT} - 1$; (Stichler, 1995). They constitute the tool of choice at the heart of my research that I use to tackle various questions on the controls and evolution of the sulfur cycle, mainly through the investigation of modern rivers and the reconstruction of past seawater $\delta^{34}S$ values. This first chapter will connect the use of sulfur isotopes to our understanding and exploration of the carbon and oxygen cycles and present the main contributions of my work to these questions.

II. The canonical view of the long-term CO_2 and O_2 control.

1. Dissolved Inorganic Carbon.

Though atmospheric CO_2 represents the main cause of concern when it comes to the ongoing climate crisis, it is far from being the most abundant form of carbon at Earth's surface. The carbon, present in the atmosphere in the form of gaseous CO_2, represents ~800 GtC. It is present in the ocean either as dissolved inorganic carbon (DIC, 38000 GtC) or organic matter. DIC is simply the sum of all the dissolved inorganic carbon species in seawater, dominated at seawater pH by the bicarbonate ion.

$$DIC = [CO_{2\text{-}aq}] + [H_2CO_3] + [HCO_3^-] + [CO_3^{2-}].$$

At the pH values of seawater (roughly between 7.5 to 8.3), the dominant species is the bicarbonate ion.

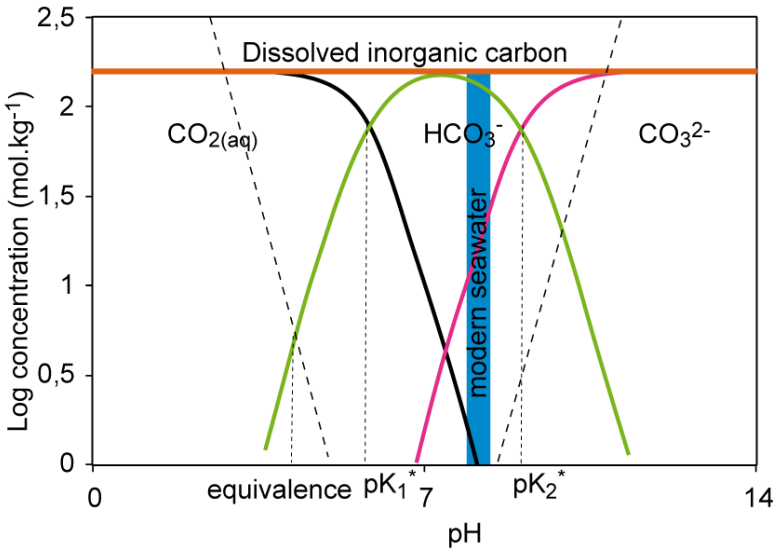

Figure 2. Carbon speciation in the modern ocean as a function of pH. $CO_{2(aq)}$ is the sum of dissolved CO_2 and H_2CO_3. K_1^* and K_2^* are the apparent dissociation constants.

DIC has been described at length multiple times, as well as the various constants of the system. Henry's constant describes the temperature-dependent relationship between the partial pressure of atmospheric CO_2 and the concentration of dissolved CO_2 ($CO_{2(aq)}$).

$$pCO_2 \xleftrightarrow{K_H} CO_{2(aq)}$$

Other carbon species follow successive equilibrium described by the dissociation constants K_1 and K_2:

$$CO_2 + H_2O \xleftrightarrow{K_1} HCO_3^- + H^+ \xleftrightarrow{K_2} CO_3^{2-} + 2H^+$$

As concentration is easier to determine than activity, apparent dissociation constants can be used instead, defined by:

$$K_1^* = \frac{[HCO_3^-][H^+]}{[CO_{2(aq)}]} \text{ and } K_2^* = \frac{[CO_3^{2-}][H^+]}{[HCO_3^-]}$$

K_1^* and K_2^* depend on temperature, pressure, and salinity.

2. The biological pump.

CO_2 can be used in the ocean or on the surface of continents by autotrophic organisms, in particular within the framework of oxygenic photosynthesis, which uses the energy of light to produce organic matter from CO_2. By doing so, it leads to the release of O_2, according to the simplified balance:

$$H_2O + CO_2 \rightarrow CH_2O + O_2.$$

If the organic matter escapes aerobic respiration, a respiration which uses O_2 as an electron acceptor, then carbon is trapped in marine (or continental) sediments. In sediments, less than a few percent of organic matter produced in the photosynthetic zone is preserved (Klaas and Archer, 2002; Le Quéré et al., 2005; Middelburg et al., 1993; Sundquist, 1985),

$$CH_2O + O_2 \rightarrow H_2O + CO_2.$$

Thus, the photosynthesis and respiration tandem constitutes the biological pump, which contributes to control the O_2 and CO_2 levels of the ocean and the atmosphere (e.g. Berner, 1994, 1991). Over the long timescales, the evolution of CO_2 and O_2 is linked to either organic matter export in the water column and its preservation of organic matter in marine sediments, the burial of newly produced continental organic matter, or oxidation of sedimentary organic matter during riverine transport (e.g. Bouchez et al., 2010; Galy et al., 2007; Märki et al., 2021).

Overall, organic matter in sediments represents an estimated amount of 15 $\times 10^6$ GtC (Dupré et al., 2003).

3. Alkalinity and carbonate production.

Organic matter is not the only reservoir of sedimentary carbon. Sediments also contain inorganic carbon, in the form of limestone, dolostone, chalk or any rock containing calcium carbonate minerals. Overall, such sediments trap represents ~60$\times 10^6$ GtC (e.g. Dupré et al., 2003) and the carbonate factory is thus a major sink of carbon.

In the ocean, calcium and hydrogen carbonate ions are used by calcifying organisms for the synthesis of calcium carbonates (e.g. coral skeletons, foraminifera tests, bivalve shell, coccoliths).

The chemical composition of seawater regarding inorganic carbon chemistry can be fully described combining DIC, alkalinity and pH. Alkalinity has been defined in many different ways (Dickson, 1992; Turchyn et al., 2021; Zeebe and Wolf-Gladrow, 2001). It can be described as the number of protons to add to 1 kg of seawater at 25°C to decrease its pH down to 4.5, a pH close to the equivalence point of HCO_3^- , the main proton donor in a seawater where the carbonate system dominates alkalinity (Fig. 2). The value of 4.5 has been partially arbitrarily defined in order to provide a reference frame for all seawater samples (Dickson, 1981). Practically, alkalinity is thus the number of moles of hydrogen ion equivalent to the excess of proton acceptors over proton donors in 1 kg of seawater. Proton acceptors are bases formed from weak acids with a dissociation constant $K \leq 10^{-4.5}$ (Dickson, 1981). For instance, for each mole of CO_3^{2-}, two moles of proton must be added as the dominant inorganic carbon species at a pH value of 4.5 is H_2CO_3, and one mole of proton must be added for each mole of HCO_3^- . Thus, considering the carbonate system only, alkalinity would be:

$$A = [HCO_3^-] + 2[CO_3^{2-}]$$

This quantity is sometimes referred to as the “Carbonate Alkalinity” or CA. When considering all the species contributing to alkalinity in the ocean, the total alkalinity TA is described as:

$$TA = [HCO_3^-] + 2[CO_3^{2-}] + [H_3BO_4^-] + [HO^-] + [HPO_4^{2-}] + 2[PO_4^{3-}]...$$
$$+ [NH_3] + [HS^-] + 2[S^-] - [H^+] - [H_3PO_4] - [HSO_4^-].$$

Carbonate precipitation is usually described using the dominant DIC species at ambient seawater pH, HCO_3^-:

$$Ca^{2+} + 2HCO_3^- \rightarrow CaCO_3 + CO_2 + H_2O$$

Thus, carbon precipitation uses up to units of alkalinity and one unit of DIC, while releasing one unit of CO_2 and acidifying seawater and it is often referred to as the “counter-pump”,

compared to the organic pump. To understand its role in the long-term capture of atmospheric CO2, carbonate precipitation must be considered in regard to the continuous supply of alkalinity and DIC to the ocean through weathering.

4. Weathering and carbonate precipitation.

Silicate weathering, coupled with the precipitation of carbonate rocks in the ocean, is generally presented as one of the main outflows of CO_2 from the atmosphere on geological time scales (Berner, 1993; Dupré et al., 2003; Ebelmen, 1855; Gaillardet et al., 1999; Kump et al., 2000; Louvat and Allègre, 1997; West et al., 2005). Carbonate weathering, on long time-scales, is carbon-neutral even though it acts as a short term carbon sink (Gaillardet et al., 2019). CO_2 drawdown occurs through the breakdown of calcium silicates, which promotes the formation of bicarbonate ions and the release of calcium ions, increasing DIC and alkalinity delivery to the ocean:

$$H_2O + 2CO_2 + CaSiO_3 \rightarrow Ca^{2+} + 2HCO_3^- + SiO_2$$

In the ocean, calcium and bicarbonate ions are used by calcifying organisms to synthesize calcium carbonates (e.g. coral skeletons, foraminifera tests, bivalve shells, coccoliths). This reaction consumes one unit of DIC and two units of alkalinity.

$$Ca^{2+} + 2HCO_3^- \rightarrow CaCO_3 + CO_2 + H_2O$$

The coupling of the two reactions above shows that for every atom of carbon that participates in weathering, one atom of carbon is fixed and eventually incorporated in the sediments, making this process a long-term carbon sink.

$$CO_2 + CaSiO_3 \rightarrow CaCO_3 + SiO_2$$

In this view, silicate weathering act as a thermostat because it regulates CO_2 concentrations in the atmosphere, only to be disrupted by tectonic events such as mountain building (Raymo et al., 1988; Walker et al., 1981). This canonical description of the carbon and oxygen cycles has been constantly evolving for various reasons. First, the relationship between climate and weathering is extremely complicated, depends on lithology and mineralogy, and is extremely hard to extrapolate to a global scale (Beaulieu et al., 2012; Deng et al., 2022; Gislason et al., 1996; Goddéris et al., 2008; Millot et al., 2002; Tipper et al., 2021; von Blanckenburg, 2006; West et al., 2005). The global silicate weathering flux might be over-estimated (Tipper et al., 2021) and organic matter sedimentation, especially in tectonically active areas like the Himalayas and the Bengal fan, might be a bigger carbon sink (e.g. Galy et al., 2007). Finally, metamorphic carbon fluxes might be underestimated, up to the point that the traditional view of orogenesis as an efficient inorganic carbon sink might be less systematic than previously

thought (Erlanger et al., in review; Gaillardet and Galy, 2008). Furthermore, the sulfur cycle comes into play when it comes to weathering, which we will develop in the next paragraph.

When establishing how much CO_2 is consumed by weathering, it is necessary to tease apart the nature of weathered lithologies and understand if dissolved cations come from silicates, carbonates or shales (e.g. Gaillardet et al., 1999; Kemeny and Torres, 2021; Torres et al., 2016). To do so, chemical and isotopic analyses of river waters are a tool of choice, together with an inversion model in order to establish the budget of cations coming from each lithology (e.g. Gaillardet et al., 1999; Kemeny et al., 2021; Kemeny and Torres, 2021; Märki et al., 2021; Tipper et al., 2006; Torres et al., 2016; Turchyn et al., 2013). Doing so is required to determine the source of the Total Dissolved Solid (TDS) load of the river and thus the nature of the weathered lithologies. One can calculate first how much of the dissolved inorganic carbon in rivers comes from dissolved carbonate rocks, oxidized organic matter or from dissolved atmospheric CO_2 and second how much calcium comes from carbonate or silicate weathering. As only silicate weathering ultimately allows new calcium carbonate precipitation, such calculations are thus necessary to estimate atmospheric CO_2 drawdown from weathering.

III. The meaning of the sulfur isotopic composition of seawater sulfate and its links to the carbon and oxygen cycles.

1. A brief overview of the sulfur cycle.

The contributions of sulfur to the carbon and oxygen cycles are manifold. Sulfur, with its multiple redox states from (-II) – $S^{2-}/HS^{-}/H_2S$ to (+VI) – sulfate SO_4^{2-}, plays multiple roles in electron transfers in biochemical metabolisms or in geochemical processes. It is involved in organic matter respiration in anaerobic environments and influences weathering. In addition, the redox state changes of sulfur are often associated to sulfur isotope fractionations, which makes sulfur isotopes a useful tool in describing the sulfur cycle, and thus into bringing new constraints to the carbon and oxygen cycles that will be described through this chapter.

Sulfur is delivered to Earth's surface by volcanism and hydrothermalism as H_2S or SO_2 and is readily oxidized to sulfate in the modern oxidizing atmosphere. Sulfate cumulates into the ocean, where it is currently concentrated at 28 mmol/L, with a residence time of 10 to 20 Myr (Bottrell and Newton, 2006; Canfield, 2004; Fike et al., 2015; Paytan et al., 2004). Sulfate can be utilized by Microbial Sulfate Reduction (MSR) and reduced to sulfide, which can precipitate to pyrite. Thus, sulfur can leave the ocean either as oxidized (sulfate in evaporites) or reduced (sulfide in pyrite) sulfur. Evaporite and pyrite are the two main fluxes of sulfur out of the ocean (noted respectively as F_{evap} and F_{pyr} in Fig. 3). These sediments may be carried to the mantle or outcrop on the surface of continents, where they are subjected to weathering. Rivers then carry sulfur back to the ocean, resulting from a mixture of sulfate produced by the dissolution

of evaporites and sulfate produced by the oxidation of pyrite, as well as sulfur emitted by human activities (which, along with hydrothermalism and mantle inputs through volcanoes and mid oceanic ridges, make up the final input flux F_{in}).

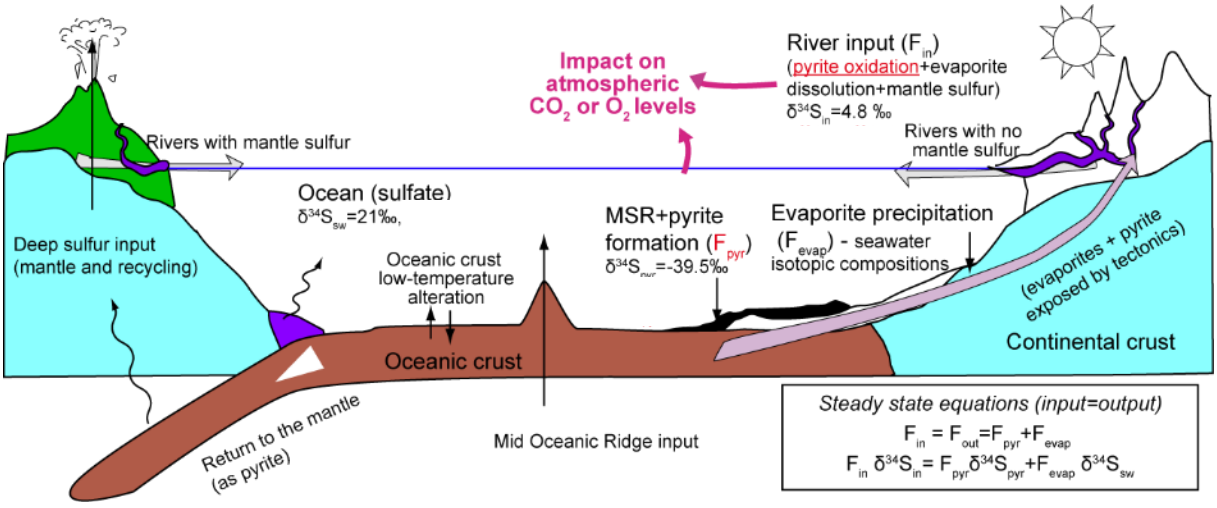

Figure 3. Simplified sulfur cycle with the main input (Fin) and output (F_{pyr} and F_{evap}) fluxes. Human influence (e.g. acid rain, fertilizers) is not shown. Isotopic values from Tostevin et al. (2014); Burke et al. (2018).

2. The parameters that control $\delta^{34}S_{sw}$.

Atmospheric O_2 and CO_2 levels are connected to the sulfur cycle, which can be reconstructed using $\delta^{34}S_{sw}$ as a central parameter, as well as exploring the modern sulfur cycle that sets the modern $\delta^{34}S_{sw}$ value through the contribution of pyrite oxidation to continental weathering and pyrite formation in sediments. Sulfate in seawater is a major sulfur reservoir with $\delta^{34}S$ value close to + 21‰ with respect to meteorite sulfur, and its isotopic composition is sustained by microbial sulfate reduction (Ault and Kulp, 1959; Kaplan et al., 1963; Kaplan and Rittenberg, 1964; Thode et al., 1953). Conceptually, the sulfur cycle is much like the carbon cycle (Fig. 4; e.g. Fike et al., 2015). Oxidized in the ocean, sulfur can be taken out by precipitation of its oxidized form (as evaporite for sulfur - F_{evap}, carbonate for carbon - F_{carb}) or biological reduction (MSR and pyrite precipitation for sulfur - F_{pyr}, photosynthesis for carbon - F_{org}), the biological processes inducing a major isotopic fractionation favoring the lighter isotope (Rees, 1973; Thode et al., 1953).

It is often using such a simplified cycle that the evolution of sulfur isotopes is explored (Fig. 4 and 5). As a result, models rely on the following parameters: fractionation during MSR, sulfate concentration in the ocean, pyrite or evaporite burial flux, pyrite or evaporite weathering flux.

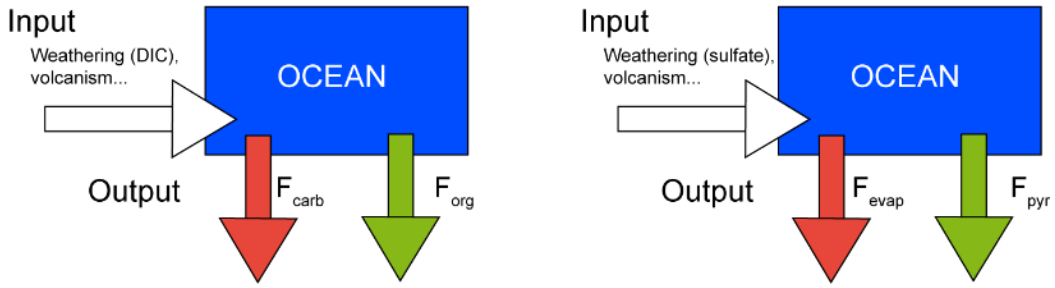

Figure 4. Conceptual carbon and sulfur cycle models

Evaporites precipitate out of the ocean with very little fractionation (Raab and Spiro, 1991) and the isotopic composition of seawater is controlled by the fractionation between pyrite and seawater ($^{34}\alpha_{pyr\text{-}sw}$).

$$^{34}\alpha_{pyr\text{-}sw} = (^{34}S/^{32}S)_{pyrite}/(^{34}S/^{32}S)_{seawater}$$

Most of the fractionation is due to MSR (e.g. Rees, 1973), which preferentially uptakes the light ^{32}S isotope in which pyrite is enriched, and the $\delta^{34}S$ value of pyrite ($\delta^{34}S_{pyr}$) is thus lower than that of seawater $\delta^{34}S_{sw}$. The fractionation associated with MSR will be detailed below. The burial flux of pyrite F_{pyr} is therefore one of the controlling elements of $\delta^{34}S_{sw}$, since evaporites have the same isotopic composition as seawater (Fike et al., 2015; Fig. 3 and 4). The $\delta^{34}S$ value of the ocean is also influenced by rivers, and the average isotope ratio of the river input to the ocean ($\delta^{34}S_{in}$) depends mainly on the relative contribution of evaporite dissolution and pyrite oxidation (Burke et al., 2018; Calmels et al., 2007; Wortmann and Paytan, 2012). In return, the isotope ratio of sulfate dissolved in rivers can help reconstruct the various contributions of pyrite oxidation and evaporite dissolution to the riverine budget of sulfate, as detailed previously (Erlanger et al., in review; Kemeny et al., 2021; Torres et al., 2016; Turchyn et al., 2013).

3. What constraints does $\delta^{34}S_{sw}$ bring to our understanding of the sulfur cycle?

To the first order, assuming steady state, the variability of the isotopic composition of oceanic sulfur is set by the combination of these elements.

First, the budget of sulfur can be described with M the total amount of sulfur in the ocean:

$$\frac{dM}{dt} = F_{in} - (F_{evap} + F_{pyr})$$

The same equation holds true for ^{34}S and can be simplified using the δ notation:

$$\frac{d(M \times \delta^{34}S_{sw})}{dt} = F_{in}\ \delta^{34}S_{in} - (F_{evap} \times \delta^{34}S_{evap} + F_{pyr} \times \delta^{34}S_{pyr})$$

If we assume steady state and that the isotopic composition of evaporite is identical to that of seawater, and using f_{pyr} as the relative burial flux or pyrite, the equation can be simplified as

$$\delta^{34}S_{sw} = \delta^{34}S_{in} + \varepsilon_{pyr} \times f_{pyr}$$

Where ε_{pyr} represents the total fractionation between sulfate and pyrite (e.g. Fike et al., 2015; Kurtz et al., 2003).

$$\varepsilon_{pyr} = ({}^{34}\alpha_{pyr\text{-}sw} - 1) \times 1000\ ‰$$

Sulfur isotope abundance ratios can eventually help us by providing estimations of sulfur fluxes in the modern and past ocean.

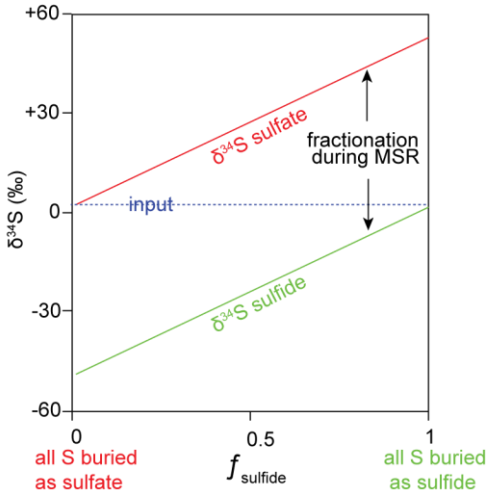

Figure 5. Steady state description of the control of $\delta^{34}S_{sw}$

For instance, because the $\delta^{34}S$ value of modern seawater is close to + 21 ‰, if one assumes an average 40 ‰ fractionation between sulfate and pyrite and use the canonical value of 3 ‰ for $\delta^{34}S_{in}$, one will find that $f_{pyr} \sim 0.4$. Estimates of sulfur fluxes have varied with estimates of F_{pyr} around 4 to 6.10^{13} gS/yr and estimates of F_{evap} ranging from 3 to 6.10^{13} gS/yr (e.g. Kah et al., 2004; Newton and Bottrell, 2007). A stronger constrain can be put on f_{pyr} using ^{33}S as well, which puts a range on f_{pyr} between 0.1 and 0.45, with the likeliest values between, 0.2 and 0.35 (Tostevin et al., 2014). In addition, $\delta^{34}S$ can be reconstructed throughout geological times and thus help us constrain the evolution of those parameters.

To do so, we need to be able to fully understand the modern sulfur cycle, its ties to the carbon and oxygen cycles, and the size, nature and isotope ratios of modern sulfur fluxes. It is clear however that many unknowns are present in our description of the sulfur cycle in the model presented above. First, the weathering flux isotopic composition has been mostly inferred rather than constrained until Burke et al. (2018). Second, assumptions are required on the average value of ε_{pyr}, while this value can drastically change in space and time (e.g. Canfield, 2004; Fike and Grotzinger, 2008; Pasquier et al., 2021). Third, new fluxes can probably complete our canonical of the sulfur cycle, such as the burial of sulfur associated to organic

matter, which becomes possibly important during times of global oceanic anoxia and might even contribute to increase the burial of organic matter (Raven et al., 2021, 2018).

The next section of this chapter will address what we know about the modern sulfur cycle and how my work contributed to improve this knowledge, mostly regarding weathering processes, but also fractionation associated to MSR.

IV. Microbial sulfate reduction and sulfur isotopes.

This next part will focus on the sulfur cycle interactions with the carbon and oxygen cycles, through microbial sulfate reduction, the process that ultimately sets the $\delta^{34}S$ values of rivers and of the ocean.

1. Carbon, oxygen, and sulfur cycle connections during microbial sulfate reduction in sediments.

Microbial sulfate reduction is a key metabolism in anaerobic environments, which leads to the reoxidation of 50% of the organic matter present in sediments (Canfield and Raiswell, 1999) and only one of the numerous reactions involving sulfur, through reactions of reduction, oxidation, and disproportionation (e.g. Fike et al., 2016; Fig. 6).

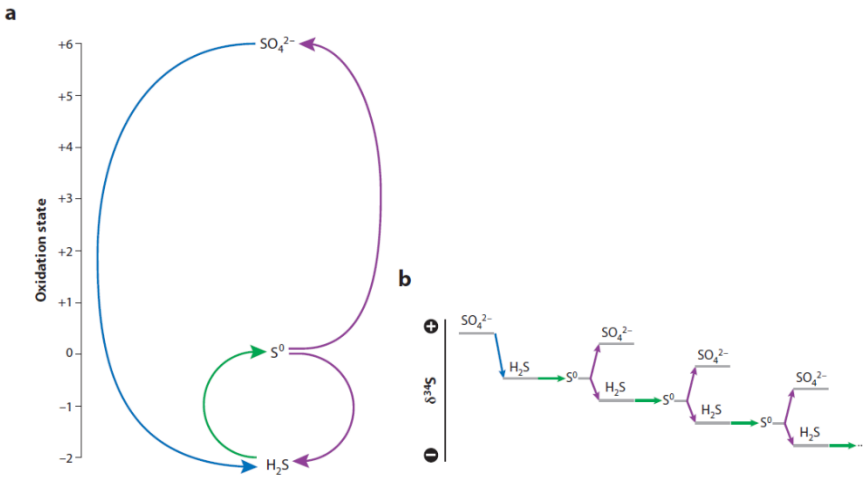

Figure 6. (a) Major microbial sulfur redox reaction involved in sulfur metabolisms: Sulfate reduction (blue); sulfide oxidation (green) to a more oxidized state between elemental sulfur S^0 and sulfate; and disproportionation of elemental sulfur or other intermediate-valence sulfur species (purple). (b) Combined isotopic effect of sulfur metabolisms: MSR produces ^{34}S-depleted sulfide. Subsequent cycles of oxidation (minimal isotopic fractionation) and disproportionation (yielding ^{34}S-enriched sulfide and ^{34}S-depleted sulfide) produce increasingly ^{34}S-depleted H_2S (figure from Fike et al., 2016).

Even though modern sulfate reducers can also produce energy through aerobic respiration (Dilling and Cypionka, 1990), most sulfur metabolisms are ancient and appeared probably as early as ~3.5 Ga, if not earlier (Philippot et al., 2007; Shen et al., 2001). MSR is an anaerobic

respiration process in which sulfate acts as an electron acceptor when oxygen is not available, which thus couples the carbon and sulfur cycles. The reaction can be simplified as follows:

$$SO_4^{2-} + 2\ CH_2O \rightarrow H_2S + 2\ HCO_3^-$$

MSR modifies alkalinity, increases DIC and leads to the formation of pyrite as well as the formation of authigenic carbonates. Pyrite is a mainly biogenic iron sulfide produced in ocean sediments. During marked marine anoxic events, MSR can even occur in the water column, above the sediment-water interface (Owens et al., 2013). There is a positive global correlation between pyrite formation and organic matter burial, as the latter only forms in environment rich in the former, and modern marine sediments are characterized by an overall C/S ratio of 3.(Berner, 1984; Raiswell and Berner, 1986). In addition, incorporation of sulfur to organic matter, during diagenesis or in the suboxic parts of the water column, makes it more resistant to oxidation (e.g. Burdige, 2007; Hebting et al., 2006; Raven et al., 2021, 2018), contributing to a correlation between C and S burial.

Given these relationships the main mechanism leading to decoupled C and S burial is the deposition of organic matter on land, where sulfate occurs at lower concentrations and where pyrite formation is limited (Berner and Raiswell, 1983). This general observation has lead the scientific community to question whether or not the carbon and sulfur cycles are always coupled, or if there are periods of Earth history when they become uncoupled (e.g. Kurtz et al., 2003; Rennie et al., 2018).

The role of pyrite formation in delivering carbon back to the ocean-atmosphere system links the sulfur cycle to the level of oxygenation of our planet's surface (Berner, 2006; Canfield, 2004; Planavsky et al., 2012, 2011). Pyrite oxidation is an O_2 sink, thus leading to the idea that pyrite formation is an O_2 source (Broecker, 1970). These canonical links between the carbon, sulfur and oxygen cycles underscore the importance of constraining the sulfur cycle.

2. Other occurrences of MSR.

i. In the water column.

It is worth noting that sulfate reduction does not occur only in sediments. It has also been documented within the OMZ (oxygen minimum zone) of the ocean, though the sulfur cycle is often described as cryptic because reduced sulfur is quickly reoxidized (Callbeck et al., 2018; Canfield et al., 2010; Johnston et al., 2014). Particulate sulfides can be exported away from the OMZ (de Souza et al., 2022); sulfurization can make organic matter more resistant to respiration and contribute to increased export of both organic carbon and reduced sulfur (Raven et al., 2021). Such processes might because preeminent during periods of extension of the OMZ, such as Oceanic Anoxic Events, the Paleocene-Eocene Thermal Maximum and

possibly under the ongoing climate crises triggered by human activities (Raven et al., 2018; Yao et al., 2018).

MSR also occurs in stratified water columns, either in the ocean, in basins such as Cariaco or the Black Sea, or in stratified lakes, such as Lake Matano (e.g. Crowe, Paris et al., 2014; Gomes and Hurtgen, 2015).

ii. In wetlands.

In wetlands, high rates of MSR can be sustained despite the low sulfate concentrations characteristic of most continental waters, which has led to describe a cryptic sulfur cycle on land as well (Guo et al., 2020; Howarth and Teal, 1979; Ng et al., 2020), that receives increasing attention. This is because wetlands are the main natural source of atmospheric methane, a gas with a greenhouse effect much more potent than CO_2 (Wuebbles and Hayhoe, 2002). Because MSR is slightly more energetically efficient than methanogenesis, it might actually help to reduce the occurrence of methanogenesis, and thus methane emissions, in wetlands, though this is disputed (Gauci et al., 2004; Pester et al., 2012; Wieder et al., 1990).

3. The Rees pathway.

i. The original Rees model.

The first results produced by controlled growth of sulfate reducers revealed that the intensity of fractionation was directly controlled by the reduction rate, suggesting that the reaction sequence involved two consecutive steps that could both be rate-controlling (Fig. 7; Harrison and Thode, 1958). This study first postulated the complexity of the reduction process, with the question of whether sulfate activation or S-O breaking is the rate controlling step (Harrison and Thode, 1958). At low rates, the fractionation (25 ‰) is similar to abiotic reduction fractionation (22 ‰), suggesting that step II controls the isotopic effect. This is because, once sulfate is reduced to sulfite, all subsequent steps fully consume the sulfite once produced. By contrast, at higher rates, step I becomes the dominant one.

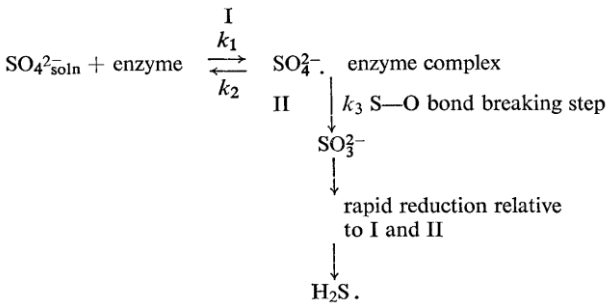

Figure 7. The precursor of the Rees pathway (Harrison and Thode, 1958)

It was quickly discovered that activation of sulfate occurred through reaction with Adenosine TriPhosphate to form Adenosine PhosphoSulphate through the action of the ATP-sulfurylase (Peck Jr, 1962). In order to accelerate the formation of APS, the other end product, PPi, must be removed. Rees et al. (1973) calculated a 50 ‰ fractionation associated to MSR of culture experiments as well as natural population in the Black Sea. To do so, they supposed a 25 ‰ isotopic effect associated both to APS reduction to sulfite and, unlike Harrison and Thode, to sulfite reduction to H_2S.

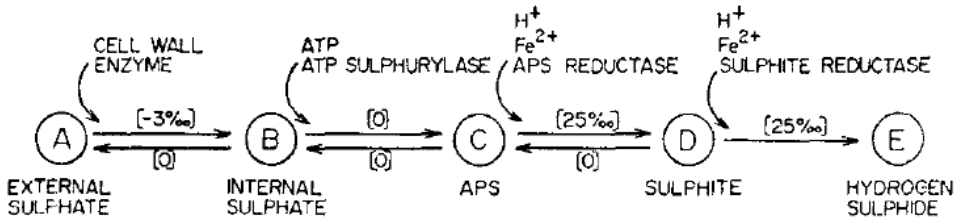

Figure 8. The original Rees pathway (Rees, 1973) with the fractionations associated to the forward and backward fluxes.

The Rees model (Fig. 8) follows four assumptions: no effect of concentration on fractionation, full reversibility from external sulfate to internal sulfite, the fractionation must be evaluated at steady state, H_2S must be evacuated as it is produced (Rees, 1973). The results of Rees et al. concluded with the following points. At low sulfate concentration, all reactions proceed onwards and the only fractionation that is expressed is that associated to the uptake of sulfate from the medium, -3 ‰. The other extreme case is when all reactions process such as equilibrium between onwards and backwards reactions is reached, and a maximum fractionation of 47 ‰ is calculated, which reproduces the maximum fractionation that was then observed. In addition, in culture experiments of *D. desulfuricans* in an environment containing $H_2{}^{35}S$, anaerobic oxidation of H_2S back to sulfate was observed (Trudinger and Chambers, 1973). Overall, the variability of sulfur isotope fractionation is linked to the reversibility of the process.

ii. Evolution of the Rees pathway.

It was first suggested that the onset of sulfate-sulfide fractionation occurred 800 Myr ago (Thode et al., 1953), before more detailed work suggests that the fractionation occurred stepwise very early on, with MSR being an ancient metabolism, already effective in the Archean . However, these early experiments contributed to set the idea that the maximum fractionation possibly attained by sulfate reduction was of 50 ‰, and that higher fractionation observed in marine pyrites or certain environments had to be linked to additional processes such as sulfate disproportionation (Canfield and Teske, 1996). However, many recent investigations have revisited the maximum fractionation associated to MSR, reaching values

up to 70 ‰, thus capturing most environments (Leavitt et al., 2013; Sim et al., 2011b). Various investigations have also used the $^{18}O/^{16}O$ oxygen isotope ratio of sulfate ($\delta^{18}O_{SO4}$). They also display an inverse relationship with csSRR and bring additional constraints on the fluxes of reduced sulfur in and out of the cell since they are particularly sensitive to reduced sulfur reoxidation (e.g. Antler et al., 2017; Brunner et al., 2005).

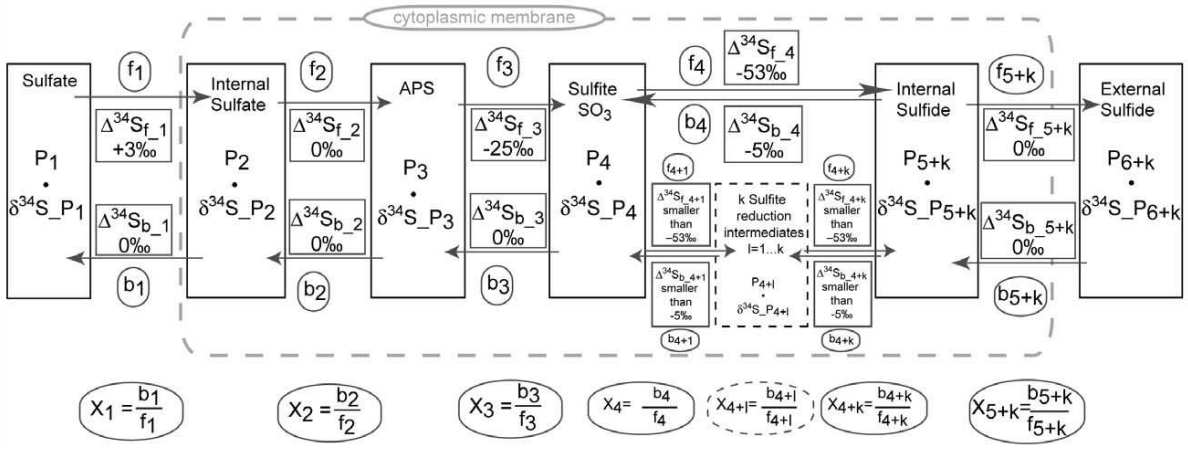

Figure 9. The revisited Rees pathway with either direct oxidation of sulfite to sulfide or multiple step reduction (Brunner and Bernasconi, 2005)

As more experimental results became available, as well as more data from natural communities, it became necessary to revisit the Rees model. Two modifications were brought. The observation of trithionate and thiosulfate intermediates indicate that intermediate reduction steps are necessary where Rees assumed a one-step reaction from sulfide to sulfite (Fitz and Cypionka, 1990). Brunner and Bernasconi (2005) revisited Rees 's model by adding additional intermediate and modifying the isotopic effect associated to the reduction of sulfite, proposed to be overall -53 ‰ (Fig. 9).

Additional elements can complexify the model, such as leakage of intermediate sulfur compounds that can accumulate in the growth media, exchange between the different internal sulfur pools or exchange with the outside of the cell (Bradley et al., 2011; Brunner et al., 2005; Canfield et al., 2006). Mostly, those models rely on similar assumptions where fractionation factors are set for each given step and the total fractionation expressed will depend on the fluxes/back fluxes within the cell. In this framework, the maximum fractionation is the equilibrium fractionation, itself being the sum of the kinetic fractionation that occur at each step (Brunner and Bernasconi, 2005).

Overall, it might be possible that no step is actually rate-limiting (Wing and Halevy, 2014). In their model, the authors used a different approach and decided to link sulfur isotope fractionation with reaction reversibility and intracellular metabolite concentrations. In this model, sulfate and sulfide concentrations outside the cell are set. For each step, the

relationship between backward and forward reactions is thermodynamically calculated based on the concentration of each metabolite, including APS and PPi. The overall description of the model is very similar to the Rees model, with only one reduction step from sulfite to H_2S, which is assigned a kinetic isotope effect of 22 ‰. The results show an overall interplay of rates and external concentration in controlling the fractionation, with the highest fractionation for the higher concentration and lowest rates, in agreement with experimental data.

iii. Multiple sulfur isotopes: the Pacman plots.

A new constraint was provided by conceptual developments using the minor sulfur isotopes, ^{33}S and ^{36}S (Farquhar et al., 2003; Ono et al., 2006a). Here, we will focus on ^{33}S. Sulfur isotope ratios can also be described using the notation $\delta'^{3x}S$ defined as

$$\delta'^{3x}S = \ln[(^{3x}S/^{32}S)_{sample}/(^{3x}S/^{32}S)_{V\text{-}CDT}]$$

reported in ‰, like the δ values. The relationship between ^{32}S, ^{3x}S, and ^{34}S is reported as

$$\Delta^{3x}S = \delta'^{3x}S - \lambda_{ref}^{3x} \times \delta'^{34}S$$

Where λ_{ref}^{3x} is the room temperature equilibrium mass fractionation law factor, which is 0.515 for $\Delta^{33}S$ (Farquhar et al., 2003).

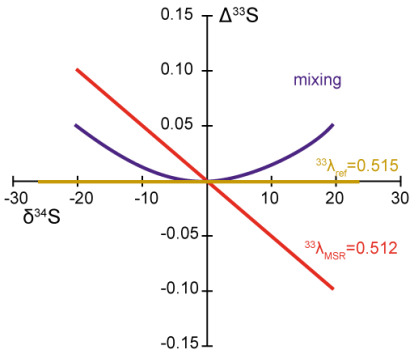

Figure 10. Examples of mass fractionation laws in a triple isotope space

Mass dependent fractionations (MDF) are characterized by $\Delta^{33}S = 0$ ‰ and mass independent fractionations (MIF) by $\Delta^{33}S \neq 0$‰. Processes like MSR are mass-dependent but follow a fractionation law with a λ^{3x} value different from the reference. Sulfur isotopes of sulfide produced by MSR are thus characterized by $\Delta^{33}S \neq 0$‰, despite MSR being a MDF process. Similarly, mixing can generate small non-zero $\Delta^{33}S$ values (Fig. 10).

The minor isotopes of sulfur have provided additional insights into the different metabolic pathways (Fig. 11). First, the initial Rees model fails to capture existing data in the δ-Δ space, unless the fractionation factors used for each step are the thermodynamically calculated fractionation factor (Farquhar et al., 2003; Johnston et al., 2007, 2005).

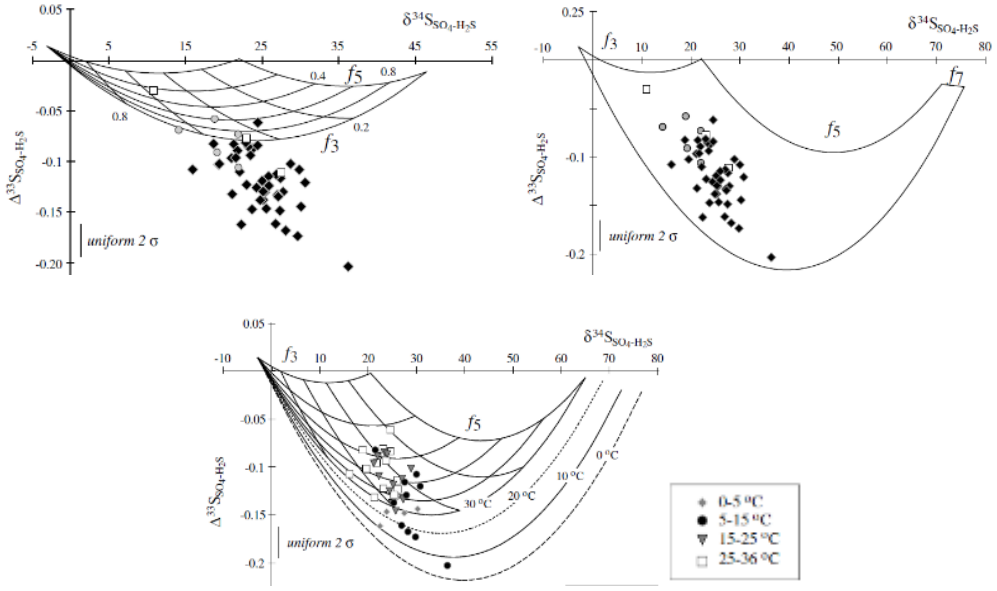

Figure 11. Multiple sulfur isotope plots exploring the domain of values that can be achieved through different fractionations and pathways describing MSR. In the upper left panel, f_3 is the mass balance on the entire cell and f_5 the backflow from sulfide to sulfate and fractionations follow the Rees pathway. In the upper right panel, f_7 is the back reaction from the intermediate between sulfite and sulfide back to sulfite, and fractionations follow equilibrium at low temperatures. In the bottom panel, the effect of higher temperatures indicated (f_7 = 0, figures and data from Johnston et al., 2007 - diamonds - with data from Farquhar et al., 2003 – squares and Johnston et al., 2005 – circles).

Furthermore, the addition of an additional step between sulfite and H_2S, the trithionate pathway, allows to capture the most fractionation data points. The Wing and Halevy (2014) model further explores the relationship between ^{32}S, ^{33}S and ^{34}S and brings further constraints in terms of the relationship between the kinetic and equilibrium fractionations occurring between the different sulfur pools in the cell. Overall, the use of multiple sulfur isotope ratios provides strong constraints that the Rees model is too simplistic, and that the fractionations that were proposed must be revisited, with fractionations up to 70 ‰ that can be explained by MSR alone (Wing and Halevy, 2014).

iv. Intracellular sulfur isotope ratio measurements.

Independently of expectations of the Rees pathway for sulfur isotope fractionations, an alternative path to constrain the isotopic effects associated to the different steps of MSR is to determine the fractionation associated to the different enzymes involved. A first focus was put on the detailed understanding of Dsr, the dissimilatory sulfide reductase, probably the most important enzyme in MSR. The sulfite reduction steps require a combination of Dsr proteins: the enzyme DsrAB in association with DsrC, and, for the final reduction step, the membrane-bound complex DsrMK(JOP) (Fig. 12; Bradley et al., 2011; Santos et al., 2015; Venceslau et al., 2014).

Within this pathway, Leavitt et al. (2015) led experiments to understand the fractionation associated to the DsrAB reduction step. They found a fractionation of -15.3 ± 2 ‰, associated to this step. The authors of this study underline the fact that this value aligns nicely with the lowest fractionation observed in marine environments and high-rate cultures, suggesting that it might be, in such conditions, the rate-controlling step of the MSR process. *In vitro* culture allowed Sim et al. (2021) to determine the fractionation associated to the Apr (APS reductase) enzyme, which catalyzed the reduction of APS to sulfite. The fractionation was determined to be 20.3 ± 0.5‰ and 20.1 ± 0.8 ‰ at 32 and 20 °C, respectively (Sim et al., 2019). In contrast to Leavitt et al. (2015), they concluded that it was APS reduction, rather than sulfite reduction, which appeared to limit in vivo dissimilatory sulfate reduction at high respiration rates. Overall, the sum of these fractionations seems to exceed the overall reduction fractionation used in the Wing and Halevy model, implying the need to revisit their assumptions.

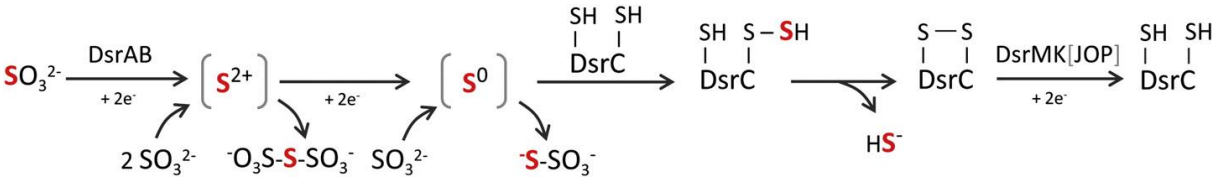

Figure 12. MSR pathway enlightening the role of the Dissimilatory Sulfate Reductase enzyme (Venceslau et al., 2014)

In Sim et al. (2017), we measured the sulfur isotope composition of different in vivo sulfur metabolites, growing *Desulfovibrio alaskensis*, an incomplete reducer, in a ^{33}S spiked medium. This approach was only allowed by the measurement method described in Chapter II (Paris et al., 2013). Instead of focusing on a given step, this approach has the benefit of considering MSR as a whole. During the exponential phase, the most oxidized sulfur pool inside the cell (SO_4^{2-}+APS) is enriched by up to +49 ‰ compared to the external reservoir, while the overall sulfate-sulfide fractionation is small, on the order of ~5 ‰ or less.

This observation suggests that the sulfate reduction rate is as fast as the sulfate uptake rate during the exponential growth phase, while sulfate reduction rates drastically diminish as cells enter the early stationary phase. Then, the intracellular quantity of sulfate remains high, making the sulfate transport reversible. All these results suggest (1) the existence of a significant intracellular sulfate reservoir and (2) that the rate of sulfate exchange across the membrane substantially exceeds sulfate reduction rates, allowing the expression of sulfur isotope fractionation in the stationary phase. Such a strong reservoir effect might contribute to the inverse correlation between sulfur isotope fractionation and cell-specific sulfate reduction rate of sulfate reduction.

4. Parameters influencing sulfur isotope fractionation during MSR.

Because of the importance of MSR in the main biogeochemical cycles on Earth, the community has worked to gain extensive knowledge on the parameters that control sulfur isotope fractionation between sulfate and the produced sulfide. It should be noted that in most studies about MSR, the fractionation is given as the fractionation between sulfate and sulfide (and not the produced sulfide and the initial sulfate) and is reported as $\delta^{34}S_{SO42-}$-$\delta^{34}S_{H2S}$. It is thus a positive value.

i. Sulfate concentration.

Culture experiments of single-strain and natural populations led to the observation that sulfur isotope fractionation seemed to be suppressed at low sulfate concentration, i.e. lower than 200 µmol/L (Habicht et al., 2002). This observation has since been both confirmed and nuanced. Additional culture experiments showed that the concentration at which the expressed fractionation is muted depends on the investigated species (e.g. Bradley et al., 2016; Sim, 2019; Fig. 13a).

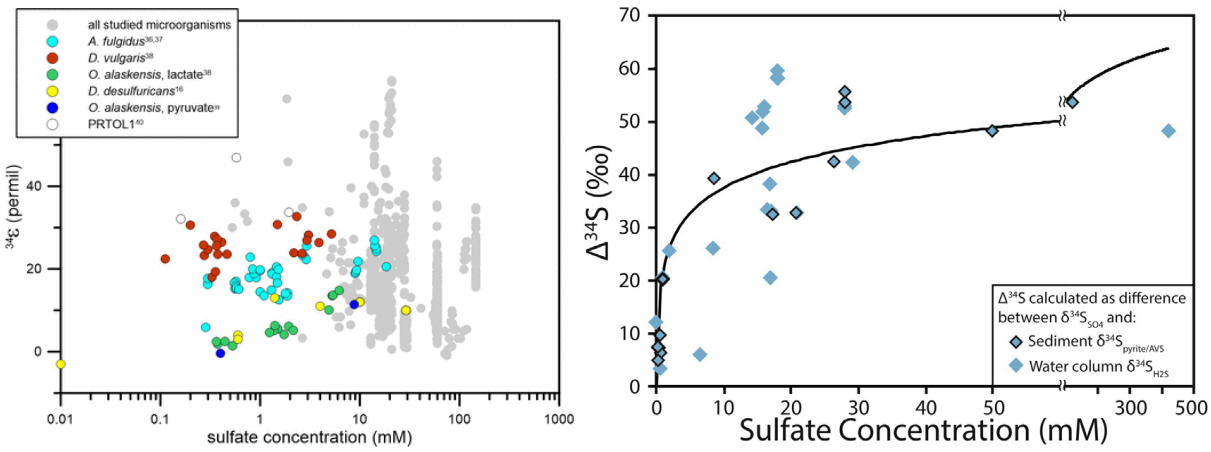

Figure 13. Influence of sulfate concentration on sulfate-sulfide fractionation, in culture experiments (left panel from Sim et al., 2022) and in euxinic environments (right panel from Gomes et and Hurtgen., 2015).

By contrast, natural low-sulfate environments such as Lake Matano in Indonesia reveal that, even at the micromolar level, significant fractionation occurs (Crowe, Paris et al., 2014, Fig. 14). In this lake where MSR occurs in the water column, we produced a sulfur isotope profile showing that a fractionation of 20 ‰ can be expressed between sulfate and sulfide at concentrations lower than 25 µmol/L. Nonetheless, a global compilation of fractionation factors measured in euxinic environments suggests that full fractionation (> 30 ‰) is only expressed at concentrations above 10 mmol/L (Gomes and Hurtgen, 2015).

At the cellular level, the underlying mechanism is that, at low sulfate concentration, the reversibility of sulfate uptake diminishes, thus making it the controlling step of the overall

expressed fractionation, as sulfate pumped into the cell is quantitatively reduced to sulfite. As a result, no additional fractionation can be expressed (e.g. Wing and Halevy, 2014; Sim et al., 2023; Fig. 13a). At the sediment or water-column level, other processes are involved, such as diffusion, advection, pore fluid (or water column) reoxidation, and Rayleigh distillation that all contribute to the final expressed fractionation (e.g. Crowe, Paris et al., 2014; Gomes and Hurtgen, 2015; Jørgensen, 1979)

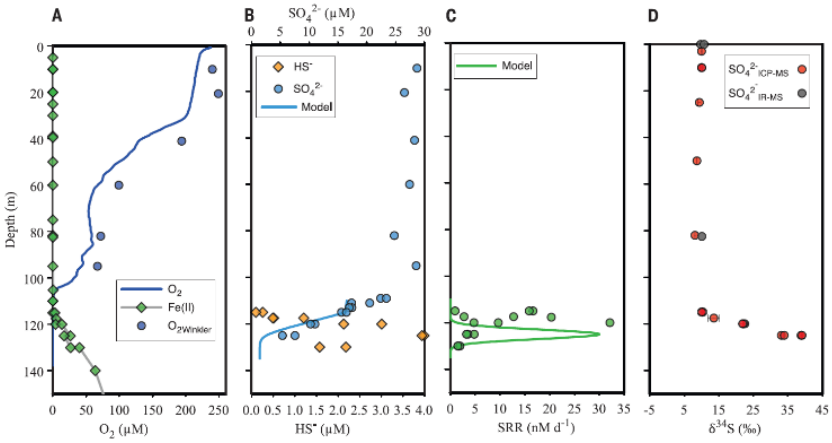

Figure 14. Chemical stratification, sulfate reduction rate and sulfur isotope ratios (as $\delta^{34}S$) of sulfate at Lake Matano (Indonesia) showing significant fractionation despite low sulfate concentrations (figure from Crowe, Paris et al., 2014).

ii. Sulfate reduction rate.

The first experiments showed that the fractionation was proportional to sulfate concentration and inversely proportional to cell specific sulfate reduction rates, usually noted csSRR, hereafter simplified as sulfate reduction rate (Chambers et al., 1975; Harrison and Thode, 1958; Kaplan and Rittenberg, 1964). In this relationship, the lower the rate, the higher the fractionation, until a certain limit set by the thermodynamic equilibrium between sulfate and sulfide (e.g. Brunner and Bernasconi, 2005). At low rates, the maximum magnitude of fractionation observed is that of thermodynamic equilibrium (Canfield et al., 2010; Farquhar et al., 2003; Leavitt et al., 2013; Wing and Halevy, 2014).

Most experiments and dataset cover reduction rates ranging from 0.002 to 860 fmol of SO_4^{2-}.cell^{-1}.day^{-1} (Sim et al., 2023, Fig. 15). The one exception to this trend comes from culture experiments at extremely low rates (0.002-0.2 10^{-16} to 10^{-18} $fmol_{SO42-}$.cell^{-1}.day^{-1}; Davidson et al., 2009) and the exact trends can depend on the strain that is investigated (Sim et al., 2023). In natural environments, the rate-fractionation trend is likely conditioned by the nature and availability of the organic matter, as well as, to a lesser extent, temperature.

Overall, the concentration effect previously described could be a threshold effect but is also linked to sulfate reduction rates. A Michaelis-Menchen like relationship where fractionation is

proportional to the rate at which sulfate is imported into the cell and inversely proportional to the cell-specific SRR, at which electrons are provided (Bradley et al., 2016). In addition, at low sulfate concentration, models suggest that lower fractionation does not occur if sulfate reduction rates are low, thus showing the interplay between both parameters (Wing and Halevy, 2014).

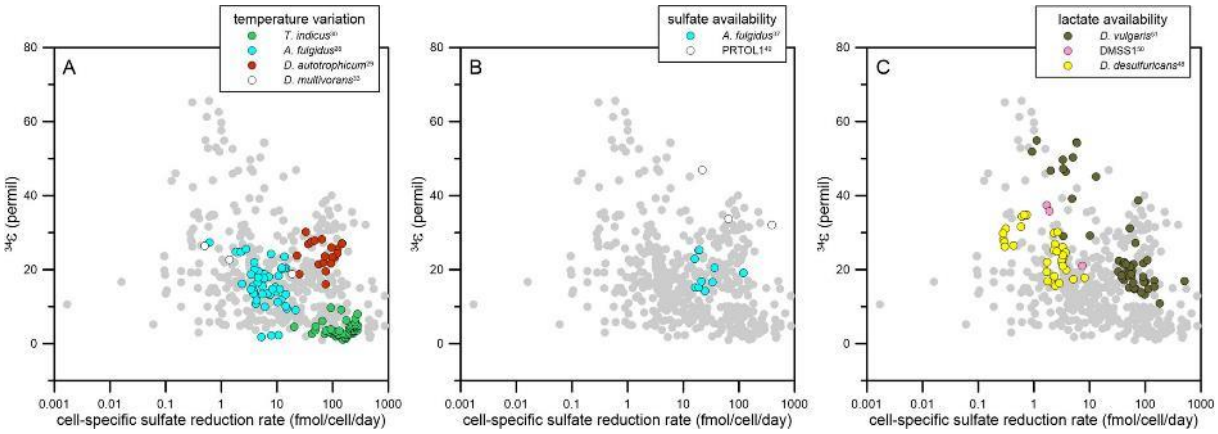

Figure 15. Influence of csSRR on the fractionation of sulfur isotopes between sulfate and sulfide

iii. Temperature.

Temperature also influences the fractionation between sulfate and sulfide (e.g. Canfield et al., 2006; Johnston et al., 2007), though in a non-linear way. Temperature might play in two cases. First, temperature modifies the equilibrium fractionation between sulfate and sulfide, which is the maximum fractionation that can be reached during MSR. Second, temperature might modify the reversibility of the different reactions, rather than enzymatic kinetics (Sim et al., 2023). If APS reduction is indeed the controlling step (Sim et al., 2021), then faster APS reduction at higher temperatures would limit the backward reaction from APS to sulfate and reduce the sulfur isotope fractionation. A similar line of reasoning could be followed if DsrC was the limiting step (Leavitt et al., 2015). Overall, variations associated to temperature change remain limited, below 10 ‰. Thus, temperature is not the main factor controlling sulfur isotope fractionation in natural environments.

iv. Electron donors.

With early culture experiments (Harrison and Thode, 1958) came the notion that the final fractionation could depend on the electron donor provided to the cell, which is to say the organic substrate given to the cell to reduce sulfate. Cells grown on H_2 or lactate tend to produce a relatively small isotope effect, though it can depend on the species that is investigated (e.g. Sim et al., 2011b). By contrast, larger sulfur isotope effect can be obtained using carbohydrates or aromatic substrates, as summarized in Fig. 16 (Sim et al., 2023). Thus,

the same cells, grown on different substrates, can generate sulfur isotope fractionations from 6 to 66 ‰, which virtually covers up the entire range of fractionation observed in nature (Sim et al., 2011a).

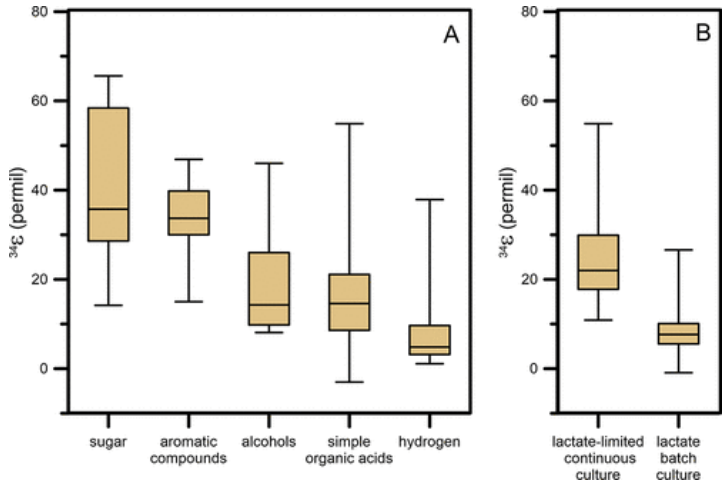

Figure 16. Influence of the nature of the electron donor (organic substrate) used during MSR (Sim et al., 2023)

However, the nature of the organic substrate is not the only aspect that matters. Its abundance must also be taken into account, as microbes grown on lactate, but in depleted conditions, were also able to express high fractionation between sulfate and sulfide (Leavitt et al., 2013).

Unlike sulfate concentration, the mechanism at play here might be linked to the reversibility of APS and sulfite reduction (Sim et al., 2023). Though this has not been directly determined, experimental conditions reducing the flow of electrons going through MSR (mutation, iron limitation, enhancing other pathways such as nitrogen fixation) all lead to higher fractionation. As a result, the higher fractionations observed with more oxidized organic matter, or less abundant electron donor, could potentially increase the intracellular oxidation state and increase the reversibility of the reduction steps, thus increasing the overall fractionation (Sim et al., 2023).

In conclusion, the fractionation associated to sulfate reduction can vary between ~0 ‰ and + 70 ‰ depending on sulfate reduction rates, the nature and availability of the electron donor, and to a lesser extent sulfate concentration and temperature. To better understand the fractionation and its causes, it is important to understand the exact pathway involved.

5. Summary.

MSR is thus a critical metabolic pathway in anaerobic environments. It reduces sulfate to sulfide, which can be incorporated in pyrite. Because organic matter is reduced, MSR is a player in the carbon cycle. During reduction, sulfur isotopes are fractionated, and the reduced

sulfur carries a $\delta^{34}S$ value lower than sulfate. As a result, pyrite is usually isotopically lower than seawater sulfate and evaporites.

The fractionation between sulfate and sulfide depends on the nature of the electron donor, on sulfate reduction rates and to some extent to sulfate concentrations. I contributed to these questions through measurements of $\delta^{34}S$ values in water samples from lake Matano to investigate fractionation at low sulfate concentrations and showed that despite concentrations lower than 30 µmol/L, a 20 ‰ fractionation occurred (Crowe, Paris et al., 2014). I also collaborated with Min-Sub Sim during his postdoctoral stay, and we contributed to understanding intracellular processes during MSR. In particular, the next chapter will show how my methodological developments enabled the first measurements of sulfate (Sim et al., 2017).

V. Sulfur contribution to weathering.

1. Sulfuric vs. carbonic acid.

Sulfur occurs in sediment mostly as evaporite and pyrite. Evaporites such as gypsum mostly precipitate in restrained basin oceans. Sulfate evaporites constitutes a major component of evaporitic sequences from sulfate-rich oceans such as today's (e.g. Hardie et al., 1996). As explained previously, pyrite is a reduced sulfur mineral (FeS_2). When exposed on land to oxidized waters or atmosphere, pyrite oxidizes. The oxidation can occur through direct oxygen consumption of oxygen or through Fe^{3+} reduction (e.g. Calmels et al., 2007):

$$FeS_2 + 3.5O_2 + H_2O \rightarrow Fe^{2+} + 2SO4^{2-} + 2H^+$$

$$FeS_2 + 14Fe^{3+} + 8H_2O \rightarrow 15Fe^{2+} + 2SO4^{2-} + 16H^+$$

Pyrite oxidation leads to the production of sulfuric acid (H_2SO_4), which competes with carbonic acid to dissolve surface rocks and lowers the CO_2 consumption linked to weathering (Beaulieu et al., 2011; Calmels et al., 2007; Galy and France-Lanord, 1999; Li et al., 2008; Torres et al., 2017; Turchyn et al., 2013).

$$CaSiO_3 + H_2SO_4 \rightarrow Ca^{2+} + SO_4^{2-} + H_2O + SiO_2$$

In addition, if sulfuric acid ever comes into contact with carbonate rocks, it will lead to their dissolution according to the following reaction:

$$CaCO_3 + H_2SO_4 \rightarrow Ca^{2+} + SO_4^{2-} + H_2O + CO_2$$

In the first case, no CO_2 is consumed and the effectiveness of weathering as a CO_2 sink is reduced. In the second case, weathering can even become a source of CO_2 towards the atmosphere, in contrast to the picture of continental weathering as a long-term CO_2 sink described above (e.g. Torres et al., 2016).

2. The example of the Madre de Dios.

A way to assess the contribution of pyrite oxidation is the one we followed in Torres et al. (2016) during his PhD work at USC under Josh West's supervision for samples of the Madre de Dios River, a major tributary of the Madeira River. To establish a full weathering budget, it is necessary to evaluate, in addition to the origin of the cations, the nature of the acid involved. In Fig. 17, z represents the relative contribution of sulfuric vs. carbonic acid, while R represents the fraction of cations sourced from carbonate weathering as opposed to silicate weathering.

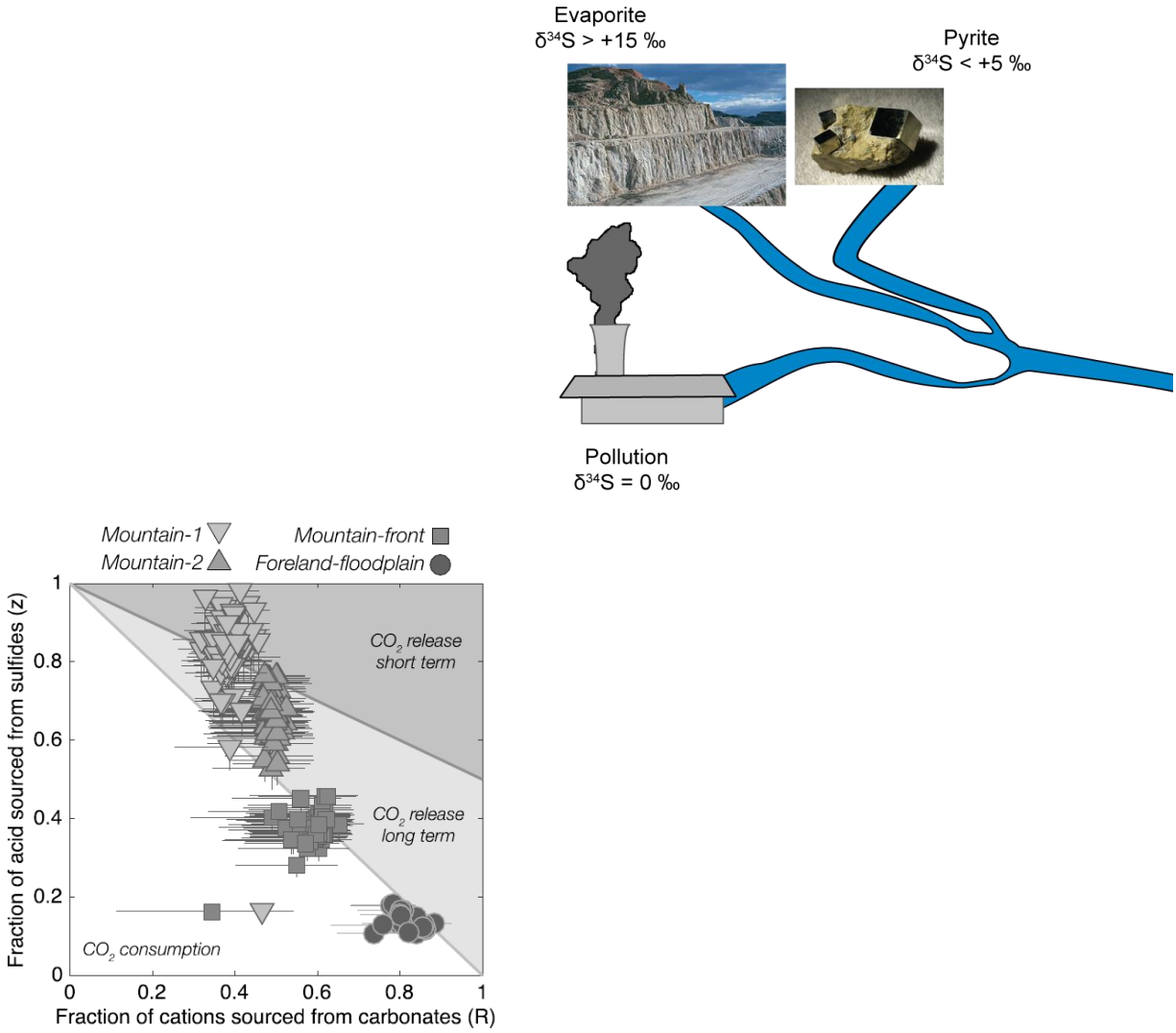

Figure 17. Results of inversion models for the Andean Madre de Dios River mainstem in a space where the fraction of acid sourced from sulfide oxidation is plotted against the fraction of cations sourced from carbonates (figure from Torres et al., 2016). Right panel: schematic vision of how evaporite and pyrite isotopic composition combine to generate the river signal.

The fraction of dissolved sulfate produced by pyrite oxidation is determined by the sulfur isotope ratio of the dissolved sulfate in the river, as pyrites tend to have a lower sulfur isotope abundance ratio value than evaporites. The fraction of cations from carbonates is calculated

from an inversion model combining major elements and $^{87}Sr/^{86}Sr$ ratios (Torres et al., 2016). In this process, though sulfur is not necessarily conservative, whether in concentration or isotopic composition (Turchyn et al., 2013), sulfur isotopes are a critical tool to evaluate the respective contributions of reduced and oxidized sulfur to the riverine budget. Sulfate concentrations and $\delta^{18}O_{SO4}$ values are also necessary to get a full comprehension of the processes occurring, as well as $\Delta^{17}O_{SO4}$ values (Calmels et al., 2007; Erlanger et al., in review; Galy and France-Lanord, 1999; Killingsworth et al., 2022, 2018; Li et al., 2008)Results for the Madre de Dios fall in different fields of the plot defined by the consequences on CO_2 emission or consumption (Fig. 17). As explained previously, $CaCO_3$ precipitation requires two moles of alkalinity and one mole of DIC. As a result, a long-term sequestration of carbon in sediments requires a riverine input defined by z=1-R. If all cations come from carbonates (R = 1), then no acid can be sulfuric, and if all acid is sulfuric, no carbonates should be present. The short-term sequestration is based on a riverine input of one unit of alkalinity for one unit of DIC. If there is less alkalinity than DIC, pH increases and CO_2 can be released, if there is more alkalinity than DIC, CO_2 can be stored as DIC during riverine transportation. This line is defined by z = 1 - R/2. Thus, depending on local parameters that control weathering, such as the local slope, uplift and fresh material supply, when physical erosion delivers particle faster than chemical weathering can process them up to the point that, sulfide oxidation might actually prevail over carbonic as a weathering agent, turning weathering into a source of CO_2 rather than a sink (Torres et al., 2016).

3. Weathering, tectonics, karstogenesis and world budget.

On a bigger scale, sulfuric acid can also contribute to karstogenesis, as we evidenced in the North Pyrenees during Dimitri Laurent's postdoctoral work and was also explored in other places such as the Carlsbad (USA) and Frasassi (Italy) caves (Hill, 1990; Macalady et al., 2007). This work demonstrated interglacial hypogenic karstogenesis was due to the action of sulfuric acid, and that it came from the oxidation of Thermal Sulfate Reduction (TSR), which is an additional connection between tectonics, weathering, climate and the carbon cycle (Laurent et al., 2023, 2021).

I also contributed to a world survey of sulfur isotope ratios from world rivers through Andrea Burke's postdoctoral work. Our study revealed a global budget of 1.3 ± 0.2 Tmol/yr from pyrite oxidation (vs. 1.5 ± 0.2 Tmol/yr from evaporite dissolution, Burke et al., 2018; Fig. 18). We confirmed that pyrite oxidation has long been underestimated (~0.5 Tmol/yr; François and Walker, 1992), and our results are thus in agreement with local studies suggesting higher fluxes (Calmels et al., 2007; Li et al., 2008).

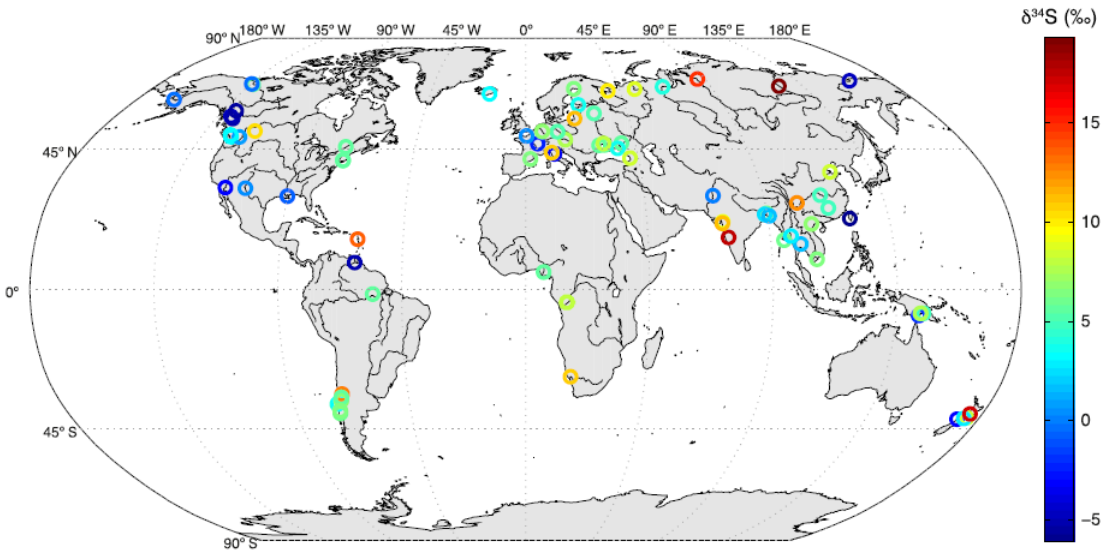

Figure 18. Global map indicating the main stem rivers measured and the $\delta^{34}S$ values (figure from Burke et al., 2018).

As a result, and because pyrite oxidation produces much more sulfuric acid than previously thought, it has been suggested to act as a CO_2 source that has limited the Cenozoic cooling (Torres et al., 2014). However, more O_2 is consumed than CO_2 is released during sulfide weathering, which leads to lower global organic matter respiration levels and additional CO_2 sequestration. Once past the initial release of CO_2 from carbonate dissolution on a 10 Myr timescale, an increase of pyrite oxidation would lead to an increase of organic matter burial and thus to an decrease in atmospheric CO_2 levels (Maffre et al., 2021). Nonetheless, sulfur cycle at the surface of continents is complex, and pyrite oxidation has many consequences on the surface cycles of oxygen and carbon. In addition, investigating the sulfur cycle is also necessary because it is one of the most disturbed by human activities, with around 1/3 of the sulfate transported by rivers today estimated to come from anthropogenic activities (Meybeck, 1987).

In conclusion, additional work on weathering and the intricated relationship between sulfur, inorganic and organic carbon is necessary, as well as the imbrication between deep and critical zone carbon emissions and the role of tectonics, in order to fully understand the connection between weathering and the carbon cycle. In this regard, sulfur isotope ratios are a critical tool and I am working on additional sites, such as the Himalayas (PhD work of Chenyang Jin, supervised by Julien Bouchez at IPGP and ongoing work with Christian France-Lanord and Maarten Lüpker) and the Apennines (postdoctoral work of Erica Erlanger at the Max Planck Institute and at CRPG; (Erlanger et al., in review). In addition to better understanding of weathering processes, the $\delta^{34}S$ value of rivers is of interest to explore and constraint the evolution of the $\delta^{34}S$ of the ocean, one of the most exploited geochemical signals to reconstruct the past evolution of the ocean-atmosphere system.

4. Sulfur is a critical player in weathering processes.

Oxidation of pyrite generates sulfuric acid and consumes atmospheric oxygen. The consumption of oxygen can be direct, or it can occur through re-oxidation of iron reduced during pyrite oxidation. In any case, the end product is sulfuric acid, which can modulate CO_2 consumption during weathering, or even lead to CO_2 emissions. Isotope ratios measured in sulfate, in particular $^{34}S/^{32}S$, provides necessary information on the amount of sulfuric acid produced by pyrite oxidation and contributes to improving estimates of weathering budgets.

Weathering connects the carbon, sulfur and oxygen cycles and delivers the main input of sulfur to the ocean, with a value determined during Andrea's Burke postdoctoral visit (Burke et al., 2018). I contributed to the PhD work of Mark Torres and Chenyang Jin as well as to the postdoctoral work of Erica Erlanger and other ongoing works on the riverine budgets of rivers over the world to improve our understanding of the role played by sulfur during weathering (Erlanger et al., in review; Torres et al., 2016), even in the specific situation of karstogenesis, through a collaboration with Dimitri Laurent during his postdoc years at Georessources (Laurent et al., 2023, 2021).

VI. Conclusion.

The sulfur cycle has many interactions with the carbon and oxygen cycles. Sulfate delivered to the ocean can precipitate as evaporites or be microbially reduced to sulfide and precipitated as pyrite. MSR fractionates sulfur isotopes and sustain a heavy isotopic signature of sulfate in the ocean. On land, pyrite oxidation generates sulfuric acid that can dissolve sedimentary carbonates and release CO_2 to the atmosphere. In all these processes, sulfur isotope ratios allow us to better describe and quantify the fluxes, even though many unknowns remain.

I contributed to investigations of the role of pyrite oxidation in counteracting silicate weathering as a carbon sink and to better understand the signature of sulfate delivered to the ocean (Torres et al., 2016; Burke et al., 2019; Erlanger et al., in review) as well as the role of sulfuric acid in karstogenesis (Laurent et al., 2023, 2021). I also contributed with investigations fractionation during MSR in culture and natural environments (Crowe, Paris et al., 2014; Sim et al., 2016). Recently, and in particular during Sanjeev Dasari's postdoctoral work, I've been also focusing on sulfur isotopes from atmospheric aerosols, either trapper in ice cores to understand atmospheric chemistry perturbations by volcanic eruptions or collected in New Delhi and on the Tibetan Plateau to assess the influence of urban pollution (Dasari et al., 2023, 2022a, 2022b; McConnell et al., 2017).This work is not described here.

All these studies were enabled thanks to analytical developments I led to allow measurement of small samples (Paris et al., 2013) and that I will describe in the following chapter, before

developing reconstruction of past $\delta^{34}S_{sw}$ and how my work contributed to improve the use of CAS as an archive.

Chapter II. The use of the MC-ICP-MS method to measure sulfur isotopes.

I. Sulfur isotope abundance ratio measurements: an overview.

1. 70 Years of analytical progress.

Many analytical advances have been made over the last 70 years since the first sulfur isotope measurement on a Gas Source Mass Spectrometer (GS-MS) as SO_2 (Thode et al., 1961; Wanless and Thode, 1953). Following the SO_2 technique, the onset of SF_6-based analyses offered three new advantages (Hulston and Thode, 1965). First, unlike oxygen, fluorine is monoisotopic, limiting the number of isotopologues. Second, there are no spectral interferences around the SF_6 masses, thus allowing measurement of the entire isotopic system of S. Finally, no memory effect is observed as SF_6 is not a "sticky" gas.

This method is widely used and allows great precision but requires extensive sample preparation. Sulfur needs first to be reduced to H_2S and then trapped as Ag_2S before being fluorinated. The SF_6 produced is then analyzed using Isotope ratio Mass Spectrometry (IRMS). Significant progress has been made, allowing smaller and smaller samples to be analyzed, down to 150 nmol S (Ono et al., 2006b; Ueno et al., 2015) yet this decreased sample size can be accompanied by a loss of precision on $\delta^{34}S$ measurement results. The SF_6 method allowed exploration of the processes generating non-zero $\Delta^{33}S$ and $\Delta^{36}S$ values (customarily referred to as Mass-Independent Fractionation, MIF) of sulfur isotopes in extraterrestrial (meteorites) and terrestrial (Archean sediments, sulfur aerosols trapped in ice cores) samples, contributing to improving the understanding of the evolution of the Earth's (and even Mars's) atmosphere (Farquhar et al., 2000a, 2000b; Hulston and Thode, 1965; Savarino et al., 2003; Thiemens, 1999; Thode and Rees, 1971).

Progress also came from the measurement of oxygen isotopes in sulfate by IRMS, either as $\delta^{18}O$ or $\Delta^{17}O$ (Bao et al., 2000; Claypool et al., 1980). An ever-increasing variety of techniques are used to measure S isotopes in various types of samples at different scales, such as Thermal Ionization MS (Paulsen and Kelly, 1984), Inductively Coupled Plasma MS (ICP-MS) (Mason et al., 1999; Menegario et al., 1998; Prohaska et al., 1999), Secondary Ion Mass Spectrometry (SIMS) (Deloule et al., 1986; Pimminger et al., 1984), and more recently laser spectroscopy (Christensen et al., 2007), ICP-MS/MS (Leyden et al., 2021) or Orbitrap Mass Spectrometry (Neubauer et al., 2020), the latter allowing also 'clumped' sulfate isotopologue measurement.

2. The onset of MC-ICP-MS measurements.

The measurements of sulfur isotopes by ICP-MS started only in the late 1990s because of major interferences on each isotope. To prevent such interferences, a first attempt to measure $^{34}S/^{32}S$ ratios came from measuring the ratio between m/z 48 (^{32}S-$^{16}O^+$) and 50 (^{34}S-$^{16}O^+$) (Menegario et al., 1998). For 1 mL of sample solutions with a sulfur concentration of 17 mg L^{-1}, the authors measured using transient peaks and achieved a precision better than 10 ‰ (1sd). Direct measurements at m/z 32 and 34 were first achieved using a mass spectrometer equipped with a radiofrequency-only hexapole as a reaction/collision cell in which a mixture of Xe and H_2 was introduced (Mason et al., 1999). Charge transfers occurring in the cell increased the S^+/O_2^+ ratio. This approach produced $\delta^{34}S$ values with a 1sd reproducibility between 2 and 3 ‰ for solutions with sulfur concentrations between 10 and 50 mg l^{-1} (or 300 to 1500 µmol L^{-1}). Simultaneously, using a double focusing sector field mass spectrometer, Prohaska et al. (1999) obtained an intermediate precision of 0.4 ‰ 1sd using 10 ng S or less for one individual measurement. Samples were measured for 2 min and replicated ten times. To decrease the $^{16}O_2^+$ interference at m/z 32, they used a microconcentric nebulizer and a desolvating membrane. Craddock et al. (2008) first developed the measurement of $\delta^{34}S$ on the Multi-Collector ICP-MS Neptune for both bulk and in-situ analysis. They demonstrated that, since multicollection allows the simultaneous collection of ^{34}S and ^{32}S isotopes, it decreases the risk of being sensitive to fluctuations in plasma conditions. They obtained a typical external reproducibility (2σ) between 0.2 and 0.45 ‰.Together with appropriate wet chemistry, the MC-ICP-MS approach has allowed increasingly smaller sample sizes to be measured (Das et al., 2012). In addition, the MC-ICP-MS can be used with liquid samples or be coupled to laser ablation or Gas Chromatograph systems (Amrani et al., 2009; Craddock et al., 2008; Raven et al., 2015). Paris et al. (2013) further improved the liquid sample MC-ICP-MS method and first demonstrated the capacity of this instrument to measure unbiased $\Delta^{33}S$, though with external reproducibility typically one order of magnitude higher than the SF_6 method (0.20 ‰ instead of 0.02 ‰).

However, in many studies that I contributed to, MC-ICP-MS analyses were not used to try to determine $\Delta^{33}S$ variations smaller than 0.15 ‰ , and (e.g. Laurent et al., 2021; Torres et al., 2017). Yet, small deviations from the reference mass fractionation law (i.e. $\Delta^{33}S < 0.20$ ‰) provide useful information on the sulfur cycle (e.g. Farquhar et al., 2003; Johnston et al., 2005; Ono et al., 2006a). In order to overcome this issue, I undertook analytical tests to document the ability of the Neptune to measure unbiased and precise $\Delta^{33}S$ in small samples. By doing so, I demonstrated that the MC-ICP-MS method is able to produce unbiased values, with an external precision close to that of the SF_6 method, for samples containing 25-50 nmol S. The

current chapter documents the current method used to measure sulfur isotopes at CRPG as well as the most recent developments, submitted and under revision at GGR.

II. Measurement procedure.

1. Sample preparation.

Three kinds of samples were used: seawater, silver sulfide samples (IAEA-S-1, 2, 3 isotope standards), elemental sulfur (IAEA-S-4) and Na_2SO_4 salts. Acids were purified at CRPG by sub-boiling distillation using a DST-1000 system (Savillex) and high purity water (HPW with 18.2 MΩ·cm conductivity) was produced by an Elga system (Veolia). Unless stated otherwise, all acids used in the following protocols are purified. PFA vials (Savillex) used in this study were rinsed 5 times in HPW, heated overnight at 80°C in ~8 mol/L reagent grade HNO_3, rinsed 5 times with HPW, heated overnight at 80°C in ~6 mol/L reagent grade HCl, rinsed again 5 times with HPW. The interior of the vials was refluxed for 24h at 160 °C using a drop of HNO_3 and rinsed 5 more times with HPW. Vials must be handled carefully because gloves commonly used in the lab have been found to be a source of sulfur contamination. The resin is not recycled, and columns are stored in ~1.1 mol/L reagent grade HCl.

i. IAEA isotope standards.

Roughly 0.5 mg of IAEA-S-1, 2, 3 (silver sulfide) and 4 (elemental sulfur) were weighed and poured into PFA vials. Aqua regia, made by mixing 2 mL of HNO_3 and 2 mL of distilled HCl, was added and the vials were placed on a hot plate for 24h at 160°C. After this oxidizing step, the aqua regia was evaporated and the dry residue was diluted in 1 mL of HPW.

ii. Synthetic solutions.

Prior to sample analysis, 1 L of bracketing isotope standard (BIS) solution at 10 mmol/L of Na_2SO_4 in 0.5 mol/L HNO_3 was prepared, the same HNO_3 solution used as the introduction medium for MC-ICP-MS measurements (Paris et al., 2013). I then mixed three different solutions in different proportions: the BIS solution, another solution made of Na_2SO_4 previously analyzed for $\delta^{34}S$ and $\Delta^{33}S$ (S-MIF-1; Geng et al., 2019), provided by Joel Savarino, and Atlantic seawater (SW) also used as an long-term full repeatability isotope standard. All solutions intended for processing through column chemistry were prepared so that their sulfate concentration was as close to 1 mmol/L as possible to facilitate the standard addition experiments. Solutions were mixed in various proportions, allowing a total sulfate amount of 300 nmol S to be loaded on each column. By doing so, I ensure an equal sample to chemistry blank ratio for all samples. One mL of bracketing isotope standard was evaporated and afterwards diluted again in 10 mL of HPW before mixing with other solutions. For S-MIF-1,

14.2 mg of salt were dissolved in 10 mL of HPW. S-MIF-1' was prepared by mixing 100 µL of BIS at 1 mmol/L and 900 µL of S-MIF-1 at 1 mmol/L. Finally, for Seawater, 100 µL of natural seawater solution were diluted in 2.7 mL of HPW. Then, three samples were prepared by standard addition of the bracketing isotope standard (BIS) and seawater solutions while five samples were prepared by standard addition of the BIS and S-MIF-1' solutions. All samples were then purified by column chemistry.

2. Column chemistry.

After mixing, each sample was purified using the anion-exchange resin AG1X8 (Bio-Rad, 100-200 mesh). In this procedure, the resin is batch cleaned by rinsing it first in HPW three times to remove smaller particles. It is then rinsed in 8 mol/L reagent grade HNO_3 and left overnight. After this step, the resin is rinsed again three times in HPW and is then ready for use. The protocol is very similar to the one used previously (e.g. Burke et al., 2018; Paris et al., 2014a). As the capacity of the resin is 1.7 meq/mL, varying cation/SO_4^{2-} ratios in the samples require variable amounts of resin. Except if stated otherwise, 600 µL of resin are introduced on disposable 10 mL Bio-Rad columns. Once loaded, the resin is rinsed twice with 2×10 column volumes (CV) of ~1.5 mol/L HNO_3. This first step is designed to remove all traces of sulfate, following previous publications (e.g. Das et al., 2012; Paris et al. 2013, 2014). A strong concentration is used because NO_3^- has a lower affinity for the resin than sulfate and it is thus necessary to saturate the active sites of the resin with nitrate ions. The second step consists of running 2×10 CV of ~3.5 mol/L HCl through the resin because Cl^- has a lower affinity for the resin than NO_3^-. The resin is then conditioned with 1×10 CV of ~0.03 % mol/L HCl to remove excess Cl^- from the interstitial volume. The sample is introduced in a total volume of 1 mL and the resin is rinsed with 3×7.5 CV of HPW to remove major cations from the resin before elution with 3×2 CV of 0.45 mmol/L HNO_3 to ensure complete elution of sulfate (Paris et al., 2014). The final elution volume is dried down. Doing so allows the sample to be later diluted with the proper introduction medium before analysis on the Neptune.

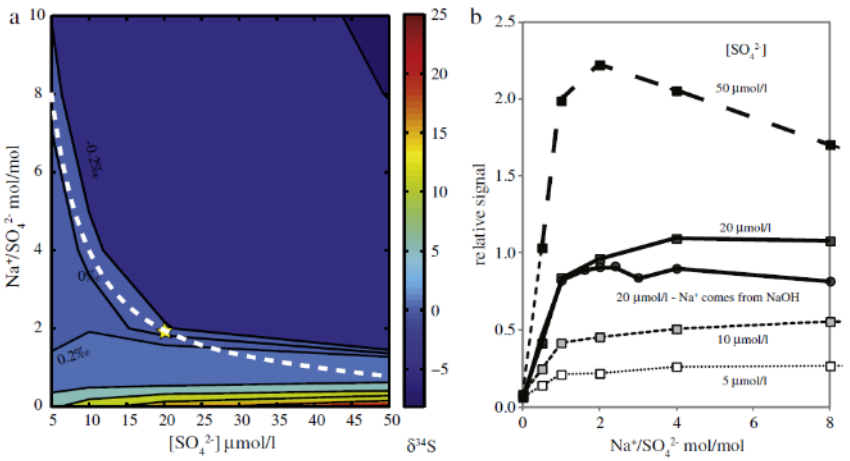

Figure 19. Influence of Na addition on the relative signal obtained on the Neptune using the Aridus.

Before introduction into the MC-ICP-MS, the solutions that were run on the columns are dried down and then diluted in 0.6 mol/L HNO_3, usually in 1 mL, depending on the amount of sulfur in the purified sample. Care is taken to run solutions with a known sulfate concentration, equal to or lower than that of the bracketing isotope standard and a sodium concentration equal to that of the bracketing isotope standard solution, which is necessary to ensure S transmission through the Aridus (Fig. 19, Paris et al., 2013). Here, depending on the run and the amount of sulfur available, the Na_2SO_4 molarity of the bracketing isotope standard solution is 20 or 40 µmol/L. The proper amount of sample is taken and transferred to a 4 ml PTFE vial for isotopic analysis. In the vial, Na^+ is added as NaOH from a 2.3 mmol/L stock solution.

The amount added is calculated so that the final solution matches the sodium molarity of the sample with that of the bracketing isotope standard (40 or 80 µmol/L Na, depending on the bracketing isotope standard used for the run). Finally, I add 0.6 mol/L HNO_3 to reach the required final volume as well as the appropriate Na^+ and SO_4^{2-} concentrations. By doing so, I ensure that the solvent composition (HNO_3 and Na^+ concentration) of the bracketing isotope standard and that of the "samples" are the same.

The minimum amount required for one run on the Neptune is 0.35 mL. Depending on the samples, the final volume varies from 0.5 to 4 mL. Instrumental background is measured in the same 0.6 mol/L HNO_3 solution as used for the dilutions, with the same Na^+ concentration as the bracketing isotope standard and the samples.

3. Isotope abundance ratio measurements.

Sulfur isotope abundance ratios are measured on the Thermo Fischer Scientific MC-ICP-MS Neptune Plus installed at CRPG in 2011. Samples are introduced in ~0.5 mol/L HNO_3 using an ESI PFA-50 nebulizer (with a measured uptake rate of about 60 µl/min) and a Cetac Aridus II. The Aridus II contains a PTFE spray chamber at 110°C and a desolvating PTFE membrane heated at 160 °C to remove solvent vapor. The addition of a cation other than H^+ is necessary to ensure proper transmission through the Aridus. Here, I use Na^+ following Paris et al., 2013, but NH_4^+ can also be used (Albalat et al., 2016). At the start of each run, the ion source is tuned using the BIS solution diluted to a final concentration of 20 or 40 µmol/L depending on the session. The tuning aims to optimize sensitivity, decrease isobaric interferences, increase the signal stability, and improve the mass resolution as much as possible. After optimization of the torch position, I search for the best combination of the various gas flows through iterative tuning (sample gas and auxiliary gas on the Neptune, sweep gas and additional gas on the Aridus).

All three peaks at m/z of 32, 33 and 34, are affected by isobaric interferences mostly due to isotopologues of O_2 and SH with similar m/z ratios in addition to the $^{32}S^+$, $^{33}S^+$ and $^{34}S^+$ ions of interest (Craddock et al., 2008; Paris et al., 2013). The m/z peak 36 used to measure $^{36}S^+$ intensity is affected by a major $^{36}Ar^+$ interference and I do not attempt to measure this minor isotope. The m/z ratio of the interferences are heavier than that of the S^+ ions of interest, leaving an interference-free shoulder on the low-mass side of the peak. The signal for measuring ^{32}S abundance is measured in the central faraday cup and heavy isotopes ^{33}S and ^{34}S in faraday cups H1 and H3, respectively. The reference peak is m/z 34 because it is the least affected by interferences. The m/z position used to collect ^{32}S is slightly offset on the left of the sulfur plateau and ^{33}S even more (Paris et al., 2013). The relative position of the central cup is chosen such that the signal for each isotope is measured in the middle of the interference free plateau, which seats on the left side on the peak. Special attention is given to the ^{33}S plateau, which is 4 mDa wide (Fig. 20).

Once the respective positions of the peaks are chosen, raw signal intensity $^{34}S/^{32}S$ and $^{33}S/^{32}S$ ratios are collected to ensure that the raw $\Delta^{33}S$ value is 0.007 ‰ within ± 0.100 ‰ and that no significant interferences affect the signals measured on the collected masses. The 0.007 ‰ value is the value determined for the BIS. Intensity ratios are measured in high resolution mode to allow optimal mass resolution. We typically aim at reaching a M/ΔM value between 8000 and 10000 using the 5 % - 95 % valley definition (Weyer and Schwieters, 2003) though most of the data here were acquired with an effective resolving power of 6000, due to a slightly worn entrance slit. The latter does not seem to affect the results.

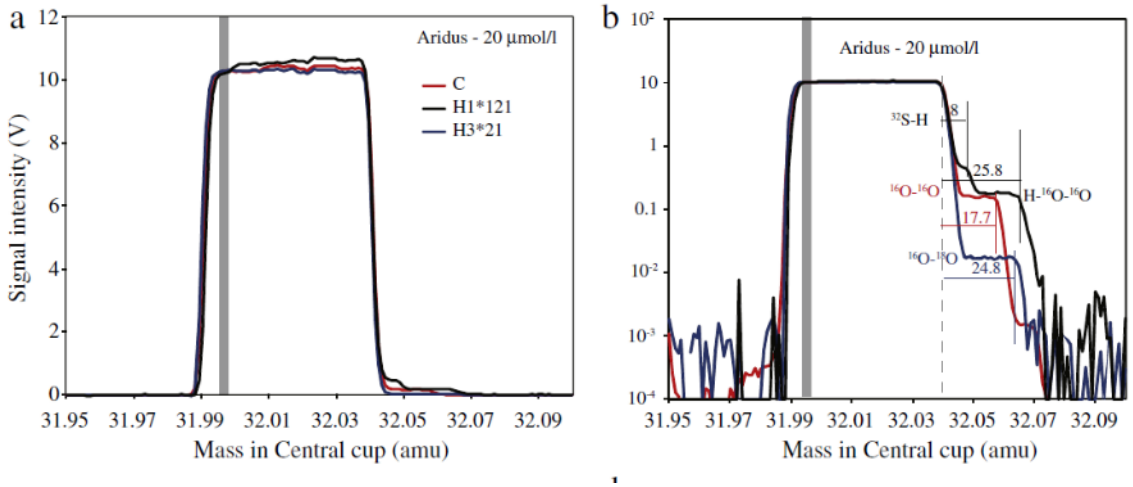

Figure 20. Peak shapes for ^{32}S, ^{33}S and ^{34}S using the Aridus in linear (a) and log (b). Interferences are indicated.

Intensity ratios are collected in 50 cycles of 4.194 s integration time each, following our previous work on the topic, providing a mean ratio value (e.g. Paris et al., 2013). The standard error of the mean of the 50 cycles at the 95 % confidence interval level (2se) provides the "internal error". Collection of a mean ratio thus lasts about four minutes, where the first minute corresponds to the solution uptake time. A sequence consists of running the bracketing isotope standard between each sample, each intercalated with a wash and an instrumental measurement. Taking into account the time required to also measure the $^{34}S/^{32}S$ and $^{33}S/^{32}S$ ratios of the bracketing isotope standard and the instrumental blanks before and after the sample of interest, the complete cycle of data collection to provide a $\delta^{34}S$ value lasts ~25 min. For each sample, 3 to 5 individual measurement results are obtained. These are usually run at 20 µmol/L following Paris et al. (2013). However, as the goal of the current study is to establish the precision that can be obtained for $\Delta^{33}S$ measurements by MC-ICP-MS, I used a sulfate concentration of 40 µmol/L for the $\Delta^{33}S$ bias tests, which yields a signal intensity of ~30V for $^{32}S^{+}$.

4. Data processing.

The data processing is done offline. Each sample or bracketing isotope standard is processed using a MATLAB script that removes outliers within the 50 cycles. The script also allows to manually chop the beginning or the end of the 50 cycles, should a problem occur such as a sample running out of solution or a longer uptake time. The script is available on demand and is based on the script initially developed at Caltech for uranium isotope ratio measurements. Using an offline spreadsheet, both $^{34}S/^{32}S$ and $^{33}S/^{32}S$ ratios are first independently corrected for the instrument background using the average of the background measured before and after the isotope ratio considered (bracketing isotope standard or sample). Finally, the mass drift is corrected using the isotope ratios determined for our bracketing isotope standard and assuming a linear variation between two consecutive bracketing isotope standards, following Paris et al., 2013. Once each individual $\delta^{34}S$ and $\Delta^{33}S$ mean values are calculated, a mean value (and standard deviation) of the instrument replicate population is calculated for each sample. The 2σ value is used to estimate the instrumental intermediate repeatability. When the same sample has been purified independently a repeated number of times indicated in the different tables, and the result of the purification measured as an individual sample, the uncertainty provided is a "full" intermediate repeatability where the uncertainty accounts for purification and instrumental repeatability and will represent the precision at which the values are obtained. All processed values are provided relative to the V-CDT scale (Paris, 2023).

III. Experimental results.

1. Bias.

Our stock solution of bracketing isotope standard is a 10 mmol/L solution of Na_2SO_4 diluted in 0.6 mol/L HNO_3 solution. To establish the value of the Na_2SO_4 bracketing isotope standard I ran the solution against the IAEA-S-1 isotope standard, which defines the V-CDT scale. The $\delta^{34}S$ value of the S-1 isotope standard is defined as being -0.300 ‰ exactly (Coplen and Krouse, 1998) and its $\Delta^{33}S$ value is 0.094 ± 0.004 ‰, following Geng et al., 2019. Numerically, this translates into $^{34}S/^{32}S$ and $^{33}S/^{32}S$ ratios of 0.0441493 and 0.0078768 respectively for IAEA-S-1, using a numerical value for the $^{34}S/^{32}S$ and $^{33}S/^{32}S$ ratio values of the virtual V-CDT isotope standard of exactly 0.0441626 ($^{32}S/^{34}S$=22.6436 ± 0.0020, k=1) and 0.0078772 ($^{32}S/^{34}S$=126.948 ± 0.047, k=1), respectively (Ding et al., 2001). Here, in order to compare only the uncertainty produced by the protocol described (purification and measurement), I follow Farquhar and Wing (2015) and Geng et al. (2019) and do not propagate the uncertainty associated to the determination of the sulfur isotope abundance ratios of the IAEA-S-1 standard. As a result, full expanded uncertainties cannot be discussed here, only the uncertainty of the measurement result. I use these values to establish the isotope ratios of our bracketing isotope standard. To do so, I processed three aliquots of the IAEA-S-1 isotope standard as described above and ran each independently purified aliquot as a bracketing isotope standard and use our in-house bracketing isotope standard (BIS) as a sample, 6 successive times on the Neptune for each purified IAEA-S-1 solution. Results are presented in Table S1, where I also show what would be the value of our $^{33}S/^{32}S$ ratio using the reference value of -0.055 ‰ for the $\delta^{33}S$ value of the IAEA-S-1 isotope standard (Ono et al., 2012). Once the bracketing isotope standard calibrated, I run the purified international isotope standards IAEA-S-2, 3 and 4 and compare our results against published values. Results are presented in Table S2 and compared to published values for the different isotope standards, showing that the MC-ICP-MS allows measurement of sulfur isotope ratios in full agreement with other methods. Results for the synthetic solutions and comparison standards are presented in Fig. 21.

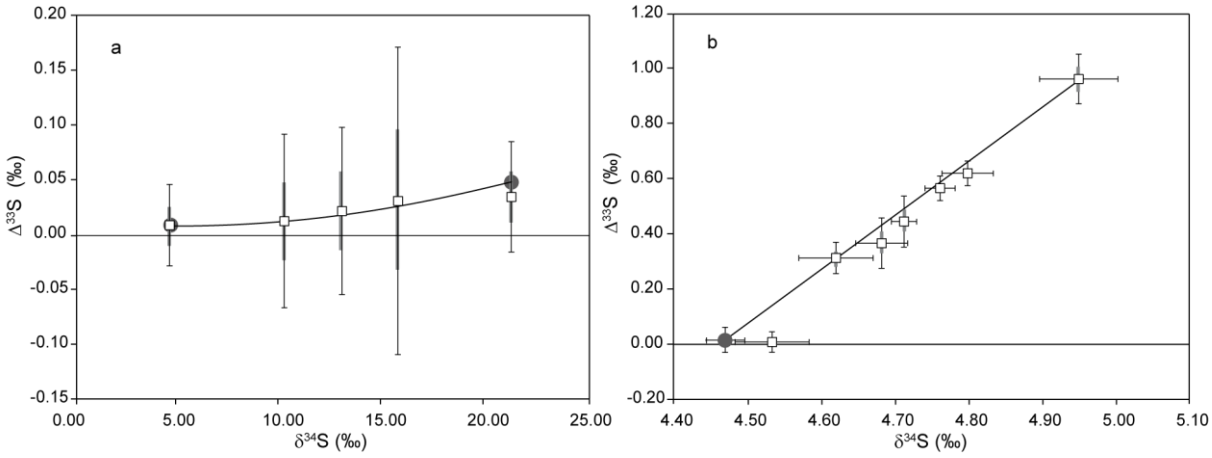

Figure 21. Measurement results for the standard additions between the bracketing isotope standard and S-MIF-1 (panel a) and seawater (panel b). Intermediate instrument repeatability is plotted as the standard deviation at the 95% confidence interval (2σ) of the instrumental mean value determination replicates. The thicker grey lines indicate the standard error of the mean at the 95 % confidence interval level (2se) for $\Delta^{33}S$ values. The endmembers of the mixing lines (grey circles) are the mean of values obtained from replicates (the same original sample purified independently more than once and ran during different sessions) as shown in table 2 and S1. The white squares represent the mean value of 5 measurement results for a single purification. Black lines are theoretical mixing curves between the endmembers.

2. Concentration tests.

To evaluate the analytical precision for smaller samples, the first step was to run the bracketing isotope standard diluted with the blank solution (0.6 mol/L HNO_3 with 80 µmol/L NaOH) against the BIS itself at 40 µmol/L. I also run a purified sample seawater and isotope standard IAEA-S-3 at different sulfate concentrations on the Neptune as they provide high and low ends of the $\delta^{34}S$ scale, using a bracketing isotope standard concentration of 20 µmol/L. In each case, I use NaOH concentration matching that of the bracketing isotope standard (in this case, 80 µmol/L of Na^+ as the bracketing isotope standard concentration is 40 µmol/L). The last test consists of ensuring that purification of smaller samples would not generate any concentration bias. To do so, I run 100 µL of diluted seawater (each containing initially 28 nmol S) on smaller, handmade, PFA columns, containing 50 µL of resin each. In Fig. 22, values are reported as a function of relative intensity, which is the intensity obtained for ^{32}S of the sample over that of the bracketing isotope standard. In each case, there is no significant variation of the $\delta^{34}S$ or $\Delta^{33}S$ values and the instrumental intermediate mean value remains identical within uncertainty (2σ - full intermediate repeatability). The uncertainty however remains roughly constant for relative intensities down to 0.5 (2σ lower than 0.3 ‰) and increase only for the lowest relative concentrations (2σ up to 0.9 ‰).

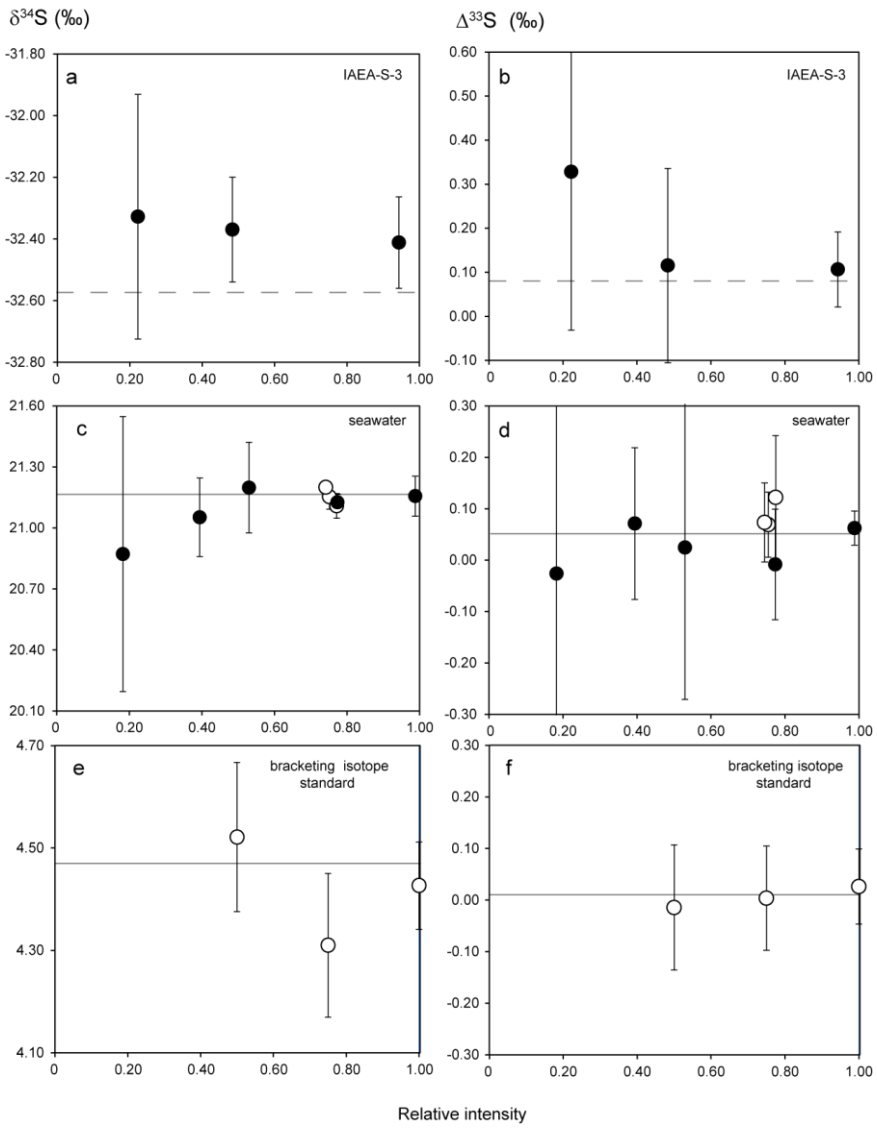

Figure 22. Influence of the amount of sulfur analyzed on measurement bias for the isotope standard IAEA-S-3 (a, b, bracketing isotope standard at 20 µmol/L), seawater (c, d bracketing isotope standard at 20 µmol/L – closed circles ; only 28 nmol S of purified seawater against a bracketing isotope standard at 40 µmol/L – open circles) and the unpurified diluted bracketing isotope standard as a sample (e, f bracketing isotope standard at 40 µmol/L). Intermediate repeatability precisions are given at the 95 % confidence interval (2σ).

IV. Discussion.

1. Potential bias of $\delta^{34}S$ measurements.

The means $\delta^{34}S$ values obtained here for IAEA-S-2 and IAEA-S-3 are 22.21 ± 0.10 ‰ and -32.41 ± 0.15 ‰ (2σ), respectively. Uncertainties are provided as a full intermediate repeatability of 3 independent purification of each standard analyzed independently 5 times each on the MC-ICP-MS. “Full” and instrument intermediate repeatability are identical, suggesting no additional contribution of the purification step to the uncertainty. Thus, instrument and “full” intermediate repeatability can be used to assess the level of precision.

The ability to obtain unbiased isotope ratios by MC-ICP-MS is shown through the comparison of our data with previously published values and the values assigned by the International Atomic Energy Agency, hereafter reference values (IAEA, 2020). The assigned reference values are 22.62 ± 0.16 ‰ and - 32.49 ± 0.16 ‰ (2σ, IAEA, 2020). Uncertainties are provided as the 95 % confidence interval expanded uncertainty of the mean $\delta^{34}S$ value calculated from independent measurements performed in different laboratories using either Gas source IRMS or a double-spike TIMS techniques (IAEA, 2020; Mann et al., 2009). However, as no uncertainty is attached to the value of IAEA-S-1, the expanded uncertainty here is only determined by the standard deviation of the population of individual values from the chosen techniques. Standard IAEA-S-1 is used as the ground value against which our bracketing isotope standard is anchored. IAEA-S-1 has an assigned $\delta^{34}S$ value of -0.30 ‰ and its uncertainty is zero by definition (IAEA, 2020). For intercomparison purposes however, an uncertainty of 0.06 ‰ (2σ) is attributed to the $\delta^{34}S$ value of the isotope standard (IAEA, 2020). However, regardless of the nature of the uncertainty provided in the literature, the uncertainty of the IAEA-S-1 standard is not considered, and neither is that of the in-house reference isotope standard of the laboratories, as this uncertainty is considered to not affect instrumental repeatability. Only instrumental (and here with the contribution of the chemical purification) uncertainty is provided. This must be kept in mind in the comparison discussed below.

For IAEA-S-2, roughly two sets of values exist in the literature. Values between 22.50 ‰ and 22.70 ‰ all come from IRMS, either through SF_6 or SO_2 measurements, while values between 22.20 and 22.45 ‰ are based on IRMS or MC-ICP-MS methods. The spread is similar for IAEA-S-3, though, for the latter, part of the spread might be related to the isotopic heterogeneity of the standard (Mann et al., 2009). IAEA-S-4 (Qi and Coplen, 2003) is less extensively used and fewer published values are available.

The results obtained here mostly agree with existing data, both in terms of $\delta^{34}S$ and $\Delta^{33}S$ (see Table 1), though the MC-ICP-MS $\delta^{34}S$ value for IAEA-S-2 (22.21 ± 0.10 ‰) obtained here is slightly lower than the reference value (22.62 ± 0.16 ‰, IAEA, 2020). There is a minor, statistically significant spread observed between the values obtained by different studies, and our method does not particularly differ from any other approach. The $\delta^{34}S$ value obtained here is in full agreement with other MC-ICP-MS published results and with IRMS values reported from MIT (e.g. 22.24 ± 0.27 ‰ (2σ); Ono et al., 2012 – uncertainty is given as the 95 % confidence interval from 8 replicate measurements).

This minor discrepancy is not related to laboratory contamination or instrument background correction. Indeed, the Total Procedural Blank of our process is lower than 0.5 nmol S. The TPB thus represents about ~0.1 ‰ of the total sulfur introduced on the columns. Because the $\delta^{34}S$ of the blank is comprised between 0 and 5 ‰ it would affect the value of IAEA-S-3 more

than the value of IAEA-S-2, and our IAEA-S-3 value is in full agreement with published values. The offset is also not due to the instrumental background signal on our instrument. Indeed, the concentration tests show that as soon as enough sulfur is introduced into the MC-ICP-MS, the mean value remains unbiased. IAEA-S-2 was run in the same conditions as the other standards, which suggests that the instrumental background correction does not come into play. Because these two isotope standards bracket most of the values found on Earth, it is confirmed here that MC-ICP-MS allows us to measure unbiased $\delta^{34}S$ values, at least for $\delta^{34}S$ values between -32 and +22 ‰.

The results for seawater (21.14 ± 0.08 ‰) fall within the range of values published since the V-CDT scale exist (Table 2). The $\delta^{34}S$ value for seawater in this study slightly differs from that obtained in previous work on the MC-ICP-MS by about 0.15 ‰ (Paris et al., 2013), though the values agree within uncertainty (2σ – full intermediate repeatability). It should be also noted that for both studies, the calibrations were made independently and that each is anchored in the V-CDT scale independently and that each bracketing isotope standard has a roughly 0.10 ‰ uncertainty (2σ - full intermediate repeatability) associated (0.15 ‰ and 0.08 ‰ for the 2013 and this this study, respectively). Taking into account the 0.06 ‰ (k=2) uncertainty on IAEA-S-1, the expanded uncertainties are 0.16 and 0.05 ‰ (k=2). In addition, our previous value was the mean of 35 measurement results of individual natural samples while the current value is the mean of different measurements from the same standard seawater bottle. For all the reasons above, it can be considered that this offset is extremely small and indicates that the two independent calibrations (at Caltech and at CRPG) are robust.

2. Limits of quantification of $\Delta^{33}S$ values in small samples.

Most processes on Earth's surface generate sulfur isotope fractionations according to mass-dependent processes where $\delta'^{33}S = \lambda^{33} \times \delta'^{34}S$. In this equation $\lambda^{33}_{ref} = 0.515$, the equilibrium reference fractionation coefficient at room temperature (Johnston, 2011). There are however different types of situations where $\Delta^{33}S$, the deviation from this fractionation line, can be non-zero: true mass-independent fractionation (MIF) processes, or mass-dependent processes where the fractionation law factor λ^{33} slightly deviates from the reference value λ^{33}_{ref}, for instance because of biological processes, or during mixing or distillation processes (e.g. Farquhar et al., 2003; Johnston et al., 2005; Ono et al., 2006a). Though the latter processes are mass-dependent, they generate non-zero $\Delta^{33}S$ values and are thus usually grouped with the MIF generating processes.

As the end goal is to compare the ability of the MC-ICP-MS to provide $\Delta^{33}S$ values with an uncertainty comparable to the SF_6 method, the uncertainty provided here as full intermediate repeatability is compared to the precision provided for δ33S calculated from SF_6

measurements results as the 2σ value of repeated measurements of the same samples. The MC-ICP-MS used here is sufficiently sensitive to distinguish the subtle $\Delta^{33}S$ variations created by such processes. First, MC-ICP-MS data fully agree with published values of $\Delta^{33}S$ values for seawater and S-MIF-1. The lack of bias in the standard addition experiments shown in Fig. 21 is the first assessment of $\Delta^{33}S$ bias on any instrument. All the values fall on the theoretical mixing trend. As a result, despite 2σ values that can vary by a factor of 3, the mean value is not biased. Importantly, comparison of the Na_2SO_4 solution, the seawater and standard addition experiment 2 shows that the MC-ICP-MS is able to resolve $\Delta^{33}S$ differences down to 0.05 ‰, since the smallest uncertainty achieved is 0.03 ‰ (2σ, full intermediate repeatability). As a result, uncertainty associated to $\Delta^{33}S$ calculations could probably be estimated as the 95 % confidence interval of the standard error of the mean from the population of mean values (2se) and overlap with precision achieved from SF_6 measurement results, using 300 nmol S.

In order to assess how precise the calculation of $\Delta^{33}S$ can be, we will explore the samples with the lowest concentrations (Fig. 22). Doing so is of importance for at least two reasons. (1) The internal error (the standard error of the mean of the 50 cycles at the 95 % confidence interval level, 2se), directly depends on the amount of sulfur analyzed, up to a certain point where plasma flicker dominates. The nature of the relationship depends on the magnitude of the Johnson noise of the detectors (e.g. John and Adkins, 2010; Paris et al., 2013). When evaluating intermediate reproducibility (i.e. taking into account the effect of bracketing and instrument background correction), the direct correlation with concentration is less strong for sulfur isotope ratio measurement results. Thus, the relationship between intermediate precision and sample concentration must be assessed. (2) Correlations between individual measurements $^{34}S/^{32}S$ and $^{33}S/^{32}S$ during SF_6 measurements reveals a correlation that induces a more precise $\Delta^{33}S$ compared to $\delta^{33}S$ and $\delta^{34}S$ while this is not the case on the MC-ICP-MS (Paris et al., 2013). Developing a way to calculate more precise $\Delta^{33}S$ values is therefore required.

Decreasing the sample size from 300 nmol S to 30 nmol S does not alter the precision of the $\Delta^{33}S$ calculations. A triplicate measurement of seawater samples representing 28 nmol S each yields a $\Delta^{33}S$ value of 0.05 ± 0.06 ‰ (2σ – full intermediate repeatability, Table S3). Both the mean and the precision are thus identical to the measurement results using samples of 300 nmol S. However, decreasing the amount of sulfur introduced to a relative intensity of 0.18, which corresponds to 4 nmol of sulfur introduced in the instrument, has a clear effect on the uncertainty (2σ – full intermediate repeatability). The mean values nonetheless agree within uncertainty. Overall, the ability to resolve small $\Delta^{33}S$ variations is lost, as the instrument intermediate repeatability becomes larger than 0.2 ‰. In order to resolve $\Delta^{33}S$ variations smaller than 0.2 ‰, at least 16 nmol must be introduced in the instrument. Routinely,

measurement results of 30 nmol S samples result in unbiased $\Delta^{33}S$ values with an uncertainty around 0.05 ‰ (2σ). Altogether, these results show that the values determined by MC-ICP-MS can allow us not only to determine true mass-independent processes (schematically, $\Delta^{33}S$ > 0.2 ‰) but also to distinguish minor isotope effects ($\Delta^{33}S$ < 0.2 ‰) arising from mixing, distillation, or minor changes in the mass fractionation law.

V. The V-CDT scale: use with caution.

Sulfur isotopes were previously reported against the Canyon Diablo Troilite isotope standard (CDT). Because the CDT isotope standard turned out to be inhomogeneous and became unavailable, a new reference was defined at the 1993 Vienna Conference, the Vienna-CDT scale (Beaudoin et al., 1994; Gonfiantini et al., 1995; Robinson, 1995). This new scale is based on the International Atomic Energy Agency (IAEA) S-1 isotope standard. In this scale, the $^{34}S/^{32}S$ is assigned a $\delta^{34}S$ value of -0.30 ‰ in the V-CDT scale (Coplen and Krouse, 1998; Krouse and Coplen, 1997) while the $\delta^{33}S$ of the IAEA-S-1 isotopic standard has not been set. It has been measured at -0.047 ± 0.37 ‰ (Ding et al., 2001) -0.055 ‰ ± 0.16 ‰ 1sd (Ono et al., 2007) ; or -0.061 ‰ ± 0.03 ‰ (Wing and Farquhar, 2015) against V-CDT. The V-CDT scale is virtual as there is no isotope standard with $\delta^{33}S = \delta^{34}S = 0$‰ and slightly different $\delta^{33}S$ values are reported for the IAEA-S-1 reference standard.

When it comes to such a level of analytical precision, two aspects become critical. First, the way of calculating $\Delta^{33}S$ must be considered. $\Delta^{33}S$ is calculated here using equation 3. As evoked in the introduction, different definitions exist. For instance, Ono et al., 2012 use the same equation as equation 3, while Geng et al. calculate $\Delta^{33}S$ following equation 4.

$$\Delta^{33}S = \delta^{33}S - [(\delta^{34}S/1000+1)^{0.515} - 1] \times 1000 \text{ (equation 4).}$$

In most cases, the different expressions yield extremely close values. However, when it comes to strong deviations from $\Delta^{33}S=0$, the difference can be perceptible. For instance, in the case of the proposed isotope standard S-MIF-1, using equation 3 produces a value of 9.44 ± 0.09 ‰, while using equation 4 results in a $\Delta^{33}S$ value of 9.54 ± 0.09 ‰, as published in Geng et al. (2019). This source of uncertainty is not taken into account in the articles cited here. In order to ensure proper comparison, and to be influenced only by analytical precision, I use equation 3 and recalculate previously published $\Delta^{33}S$ values when necessary (see all the tables).

The second sensitive aspect is the choice of the $\Delta^{33}S$ value assigned to IAEA-S-1 as difference choices of this value exist. In all the references listed here, the $\delta^{34}S$ of IAEA-S-1 is set at -0.30 ‰, in agreement with the definition of the V-CDT scale. However, $\Delta^{33}S$ values ranging from 0.094 ‰ to 0.107 ‰ can be found for IAEA-S-1, which corresponds to $\delta^{33}S$ ranging from -0.061 ‰ to -0.047 ‰, respectively (Ding et al., 2001; Ono et al., 2012; Wing and Farquhar,

2015). It is necessary to agree on what this value is as the IRMS SF_6 routinely yields values with precisions better than 0.02 ‰ (2σ). Defining an unbiased $\Delta^{33}S$ value of seawater is a goal of different publications and is a good example of why the values chosen for IAEA-S-1 matter (Ono et al., 2012; Paris et al., 2013; Tostevin et al., 2014). All the published values for modern seawater agree and indicate that seawater has a non-zero $\Delta^{33}S$ value, that is slightly positive (~0.05 ‰). Yet, the IAEA-S-1 normalization is different in each of these publications (Table 1). Tostevin et al. (2014) assumed that the $\Delta^{33}S$ value of the international standard was 0.107 ‰, Ono et al. (2012) used 0.100 ‰ and Paris et al. (2013) used 0.094 ‰. When renormalizing using 0.094 ‰ for the $\Delta^{33}S$ value of IAEA-S-1 as assumed here, the $\Delta^{33}S$ values measured for seawater become 0.036 ± 0.014 ‰, 0.044 ± 0.007 ‰ to 0.050 ± 0.030 ‰ (2σ) instead of having identical mean values. Similarly, if a value of 0.100 ‰ is assumed for IAEA-S-1, the respective mean values would become 0.042 ‰, 0.050 ‰ and 0.056 ‰. As $\delta^{34}S$ and $\delta^{33}S$ are independently anchored in the V-CDT scale, it is necessary to converge towards a common definition of $\delta^{33}S$ to allow comparisons of data from different labs and establish a proper budget of ^{32}S, ^{33}S and ^{34}S in the external reservoirs of the Earth.

VI. Conclusion.

I document here the first standard addition experiments demonstrating that MC-ICP-MS allow us to calculate unbiased $\delta^{34}S$ and $\Delta^{33}S$ values. The results show that $\Delta^{33}S$ values obtained from MC-ICP-MS measurement results are and with a satisfactory precision for samples as small as 20 nmol S introduced in the instrument. When considering the full intermediate repeatability into account, thus including the purification step, a precision of 0.05 ‰ (2σ) can be obtained from 30 nmol of sulfur. This makes the MC-ICP-MS a useful instrument to estimate small $\Delta^{33}S$ deviations. Though the results are not as precise as those obtained from SF_6 measurements, the approach described here is ideal for the analysis of trace sulfate in natural waters or carbonate samples, making both techniques complementary to each other.

The analytical development I led using Multi-collector Inductively Coupled Mass Spectrometry has allowed the community to work on much smaller samples. Over the last decade, the decrease in sample size required to measure $^{34}S/^{32}S$ ratios permitted by MC-ICP-MS helped improve our knowledge of the sulfur cycle on land, in the ocean, in sediments, and back in time. Applications ranged from exploration of Archean or recent atmospheric processes (Dasari et al., 2023, 2022b, 2022a; McConnell et al., 2017), incorporation of sulfate in carbonates (Barkan et al., 2020; Paris et al., 2014b) and past biogeochemical cycles (Crowe et al., 2014; Paris et al., 2020, 2014a; Present et al., 2019, 2015; Rennie et al., 2018), aspects that will be described in Chapter III to V, as well as weathering and other critical aspects of the

modern sulfur cycles, as described in Chapter I (Burke et al., 2018b; Crowe et al., 2014; Erlanger et al., in review; Laurent et al., 2023, 2021; Sim et al., 2017; Torres et al., 2016).

In addition, the differences between the calibrations chosen for $\delta^{33}S$ calculations, though consistent within a laboratory, can generate differences that must be addressed. For instance, in the case of modern seawater, the different results yield consistently positive values. However, when calculated in a consistent way, differences occur that are sufficient to impact interpretations of the sulfur cycle interpretations. As a result, a global agreement should be found in order to allow interlaboratory data comparison and not relative evolution of a signal.

Chapter III. The geological records of the sulfur cycle.

The isotopic composition of sulfur in seawater can be reconstructed using different sedimentary archives: evaporites, barite and carbonates. This chapter aims to introduce those archives and the progress made over the last 60 years of exploration of reconstruction of the Phanerozoic sulfur cycle. Because one my main contribution to the Phanerozoic sulfur cycle occurred through Victoria Rennie's PhD work on the Cenozoic, a focus will be provided on the last 60 million years of Earth's history through a major breakthrough allowed thanks to the MC-ICP-MS approach: the establishment of the first monospecific foraminifer $\delta^{34}S$ record.

It is important to note that though we won't discuss $\delta^{18}O_{SO4}$ in detail, the oxygen isotopic composition of sulfate can be also used to measure to help document the variations of the sulfur cycle in the past (e.g. Claypool et al., 1980; Turchyn et al., 2004, 2009), with a record now covering the last 130 Myr (Waldeck et al., 2022).

I. The main archives for $\delta^{34}S_{sw}$.

Early in the 1960s, sulfur isotope ratios have been recognized to be almost identical in seawater and precipitating gypsum (Thode et al., 1961), with a fractionation by +1 to 2 ‰ in gypsum relative to dissolved sulfate (Thode and Monster, 1964), thus leading to the idea that changes in ancient evaporites (Macnamara and Thode, 1950) were due to secular changes of the sulfur isotope ratio of seawater. As a result, it has been documented very early in the investigations of ancient evaporites (Ault and Kulp, 1959; Buschendorf et al., 1963; Nielsen and Ricke, 1964; Thode and Monster, 1964, 1965) that their sulfur isotopic is not constant with time, and the notion of large imbalance within the sulfur cycle at the Earth's surface was developed. This idea led to the production of the first datasets documenting the geological history of seawater sulfate $\delta^{34}S$ values (Holser and Kaplan, 1966; Nielsen, 1973 cited in Schidlowski et al., 1977), that fueled different models of the sulfur cycle (see Chapter I). Many investigations rely on sulfur in pyrite to reconstruct past aspects of biogeochemical cycles. An example of a thorough review on the topic can be found elsewhere (Fike et al., 2015).

1. Evaporites.

Gypsum ($CaSO_4.2H_2O$) is the first archive that has been used to reconstruct the sulfur isotopic composition of seawater sulfate. In 1980, Claypool and collaborators produced a synthetic $\delta^{34}S$ curve of seawater sulfate based on worldwide marine evaporites with a temporal coverage of the entire Phanerozoic (Fig. 23), as well as a $\delta^{18}O$ record of seawater sulfate.

For the first time, long-term changes in $\delta^{34}S_{sw}$, but also in $\delta^{18}O_{sw}$ of seawater sulfate, were documented and interpreted. However, for most of the Phanerozoic, large changes observed in $\delta^{34}S$ are not accompanied by equivalent changes in $\delta^{18}O$, with the exception of the Permian (Claypool et al., 1980). As $\delta^{18}O$ and $\delta^{34}S$ of sulfate react both to evaporite precipitation and dissolution as well as to pyrite formation, difference could be explained by the lower sensitivity of $\delta^{18}O$ to sulfide oxidation. However, the new model developed to take advantage of this new dataset produces calcium and oxygen depletions deemed unreasonable by the authors and fails to reproduce the sharp rises in $\delta^{34}S$ such as those observed in the Devonian or the Triassic (Claypool et al., 1980).

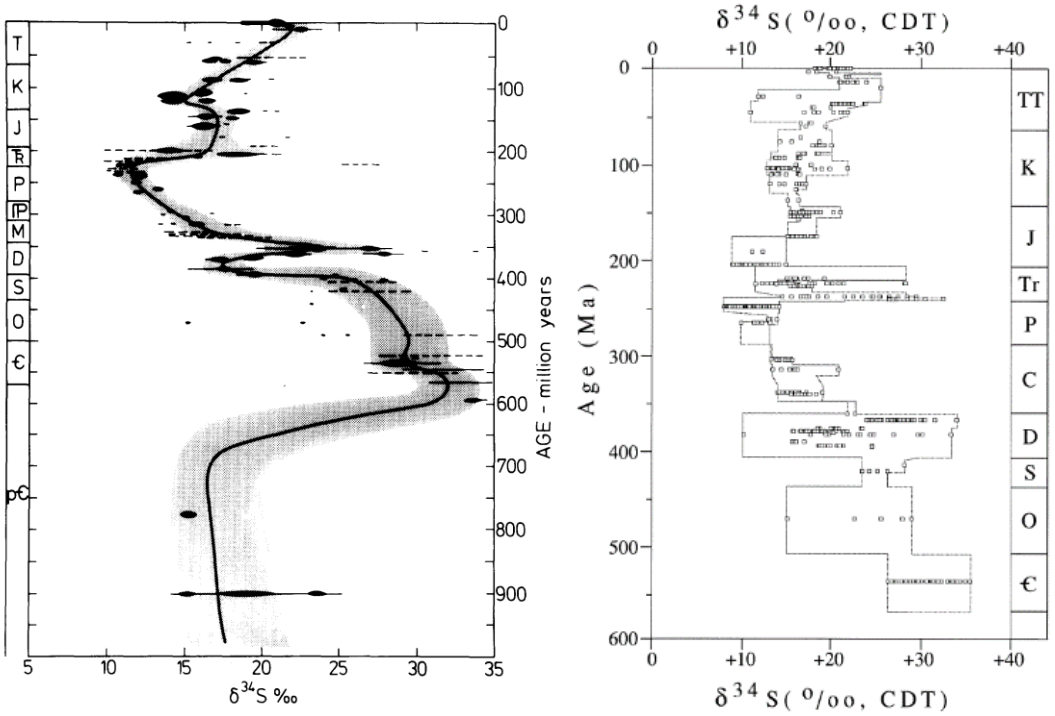

Figure 23. The first compilation of $\delta^{34}S$ values measured using the evaporitic record (figures from Claypool et al., 1980 – left; Strauss, 1997 – right).

Following Claypool's first global compilation, more evaporite-based records have been produced, until the following compilation produced almost 20 years later, and another compilation over the Phanerozoic 40 years after Claypool et al.'s work (Present et al., 2020; Strauss, 1997). The seawater sulfate-gypsum fractionation is now estimated at +1.6 ‰ (Raab and Spiro, 1991).

However, despite the invaluable contribution of the evaporite record to our knowledge of the past sulfur cycle, significant short-term variations can be observed, without clear knowledge of their meaning, whether they represent quick oscillations in the sulfur cycle or evolution of the brine from which the evaporite precipitated (e.g. Holser, 1977), or even an ocean

heterogeneous at times (e.g. Claypool et al., 1980) thus leading the way to the use of other archives of past seawater sulfate $\delta^{34}S$.

2. Carbonate associated sulfate.

Gypsum is not the only sedimentary archive that record the $\delta^{34}S$ value of seawater. Very early on, limestones have been used as well to understand the secular variations of the latter (Kaplan et al., 1963).

The first carbonate-based high resolution record was produced in 1989, over the Neogene, using sulfate present in foraminifera shells (Burdett et al., 1989), which confirmed the values measured from evaporites, though with a higher time resolution and a more continuous temporal coverage (Fig. 24).

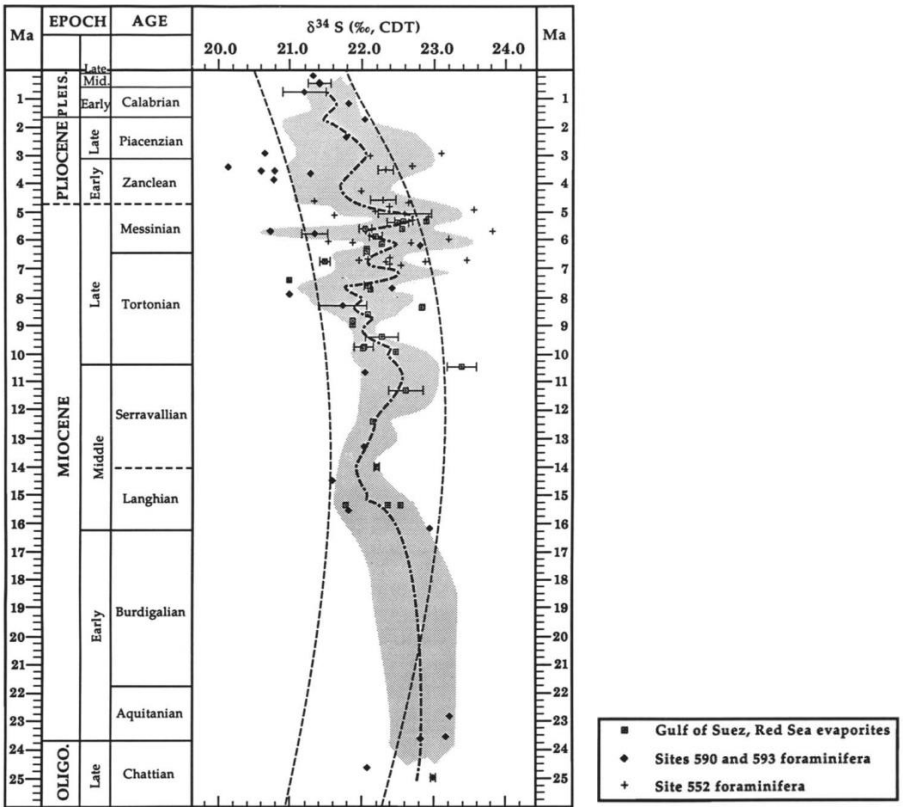

Figure 24. The first $\delta^{34}S$ record based on CAS extracted from mixed foraminifera (figure from Burdett et al., 1989).

Sulfate present in trace elements in carbonates, usually named CAS (Carbonate Associate Sulfate) and sometimes SSS (Structurally Substituted Sulfate) became a tool of choice to reconstruct the sulfur cycle at different timescales and through various events, due to the ubiquity of calcium carbonates in the sedimentary record.

Following studies focusing on specific time events (Kaiho et al., 1999; Kampschulte et al., 2001; Ohkouchi et al., 1999) a first global Phanerozoic record was produced using a

combination of bulk rocks and brachiopod shells (Kampschulte and Strauss, 2004; Fig. 25), revealing a global trend similar to that of evaporites, though sometimes with even more pronounced short-term scatter, such as around the Cambrian-Ordovician boundary.

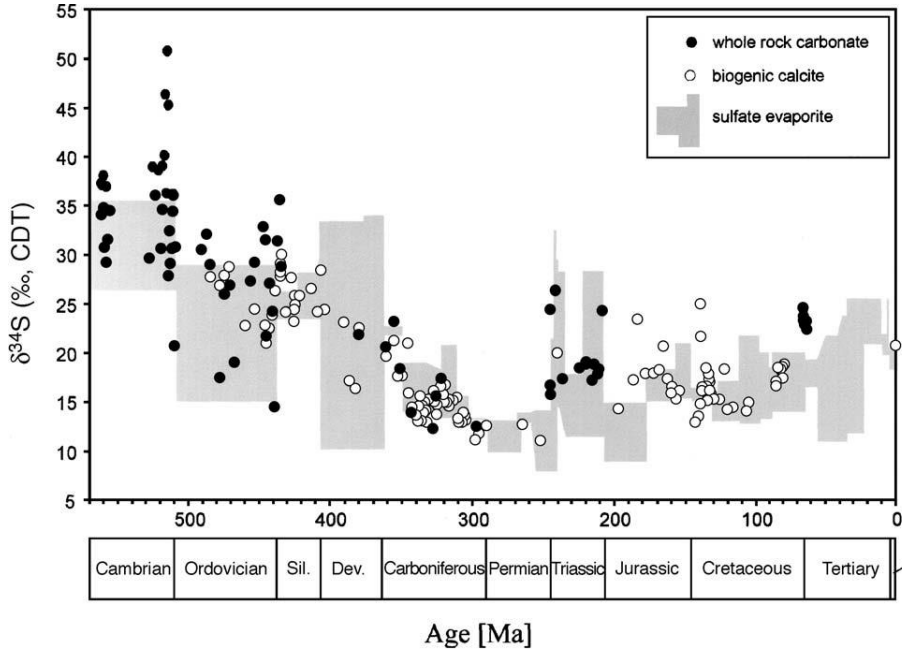

Figure 25. The Phanerozoic CAS record of Kampschulte and Strauss (2004), comparing biogenic and bulk record data with the evaporitic record. Black circles are bulk carbonates and white circles are biogenic samples.

Over the last twenty years, CAS have been intensively used to create seawater $\delta^{34}S$ records throughout all of Earth's history, from the Archean to the Cenozoic. A global compilation for the Phanerozoic has been recently established (Present et al., 2020) and is reproduced hereafter. This compilation includes the foraminifera record that I will present in detail in section II.2. A longer-term compilation has also been proposed all the way to the Archean-Proterozoic boundary, though it is less complete for the Phanerozoic than Present et al.'s (Crockford et al., 2019).

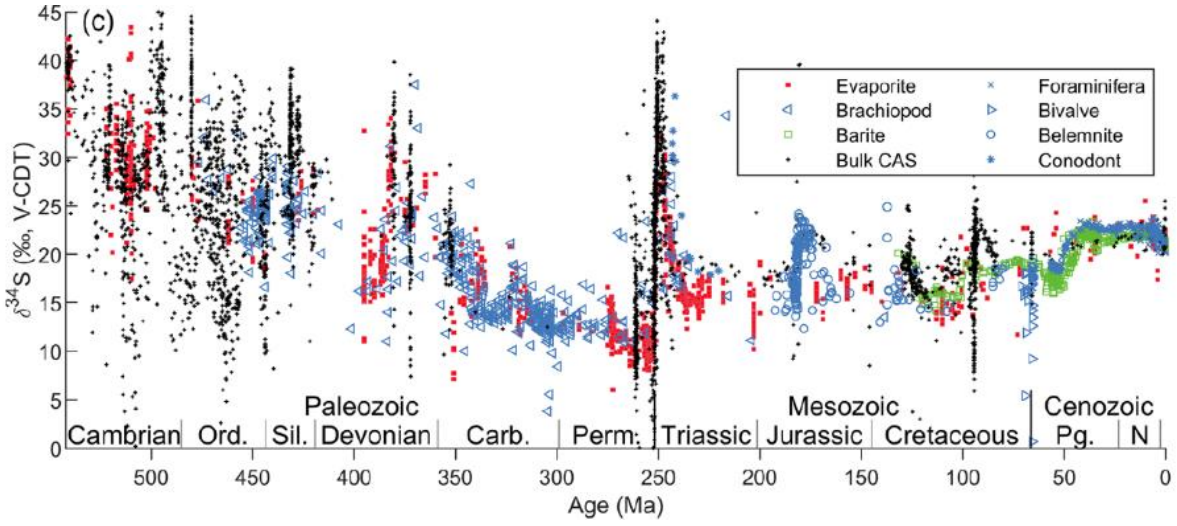

Figure 26. The Phanerozoic CAS record compilation of Present et al. (2020)

3. Barites.

In parallel to the increasing use of CAS as an archive for seawater $\delta^{34}S$, barites have also been used for similar purposes. Barite can be either produced in the water column or in sediments, but pelagic barite is easily recognized as it forms microcrystals occurring within fecal debris throughout the water column. The degradation of organic matter within such micro-environment may provide conditions necessary for the precipitation of $BaSO_4$. (Dehairs et al., 1980). In addition, the chemical composition and Sr isotope ratios of barites can help ensure their marine origin (Goldberg et al., 1969; Paytan et al., 2002, 1993).

Modern barites record seawater value within a 1 ‰ range and enough material has been uncovered from various IODP sites to establish a record covering first the Cenozoic, then the last 130 Myr (Paytan et al., 2004, 1998; Fig. 27).

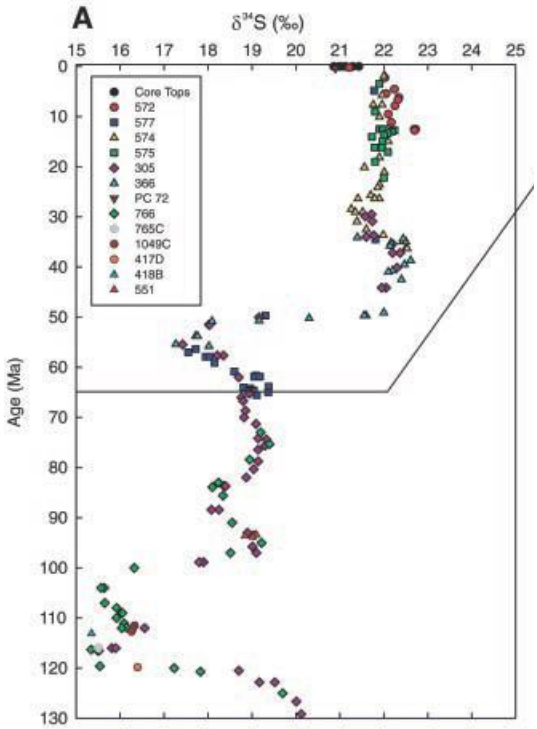

Figure 27. The $\delta^{34}S$ barite record over the last 130 Myr (Paytan et al., 2004)

More records have completed the initial dataset, either through long-term studies combining $\delta^{34}S$ and $\delta^{18}O$ of barite (Turchyn et al., 2009) or through high resolution records of specific events (e.g. Yao et al., 2018). An up-to-date compilation of all data is also provided in Present et al. (2020).

Now that each archive and record has been described, we will compare them in order to understand their strengths and weaknesses and use the comparison between each record to improve them.

II. Comparison between the records.

1. The variability is not the same for all archives: barite, the gold standard?

Various conclusions can be drawn from comparing the records. First of all, those archives reveal a major trend. The further we go back in time, the higher the variability, which has been more than once interpreted as the reflection of lower sulfate concentrations in the ocean (Algeo et al., 2015; Kah et al., 2004; Planavsky et al., 2012). However, for such an interpretation to be true, the meaning of each archive must be assessed, as all archives display a different variability and evaporites and CAS, only archives available prior to 130 My, tend to display more variability than barite (Present et al., 2020; Fig. 28).

Barite is often considered the gold standard because it is an archive that is very resistant to diagenesis. It offered the first unarguable insight into the Meso-Cenozoic sulfur cycle, revealing major shifts whose interpretation remains debated (e.g. Rennie et al., 2018; Wortmann and Chernyavsky, 2007, 2007; Yao and Paytan, 2020). However, barite precipitation in, and sedimentation through, the water column itself is complex.

Seawater is undersaturated with respect to barite and its formation occurs in microenvironments enriched in barium and thus enriched in respired organic matter (Griffith and Paytan, 2012). In the Southern Ocean, $BaSO_4$ precipitation occurs as an amorphous phase prior to barite crystallization, below the first few hundred meters (Stroobants et al., 1991). There, at depths greater than 200 m, organic aggregates are dispersed, possibly as a reflection of where microorganism activity occurs, and individual barite crystals are released in the water column. Yet, laboratory experiments suggest that barite is soluble in the water column and that, as a result, pelagic barite that reached ocean sediments has been shielded from seawater by organic aggregates (Light et al., 2023). As a result, barite slowly precipitates over hundreds of meters through the water column, in an environment where organic matter is concentrated. In addition, especially in the Oxygen minimum zone, local sulfur cycle modification could occur through the sulfur cryptic cycle (Callbeck et al., 2018; Canfield et al., 2010; Johnston et al., 2014; Raven et al., 2021). Though this local cycling don't lead to a local change in $\delta^{34}S_{sw}$ values, its effect on seawater sulfur isotopes is not documented in the past.

Overall, barite provides nonetheless a unique archive against which CAS and evaporites can be compared. Moving further back in time, prior to 130 Myr ago, pelagic barite crystals are unavailable, forcing us to rely on carbonates and evaporites.

2. Evaporites, a discontinuous record.

There are limitations that are inherent to the evaporitic record. First, evaporite deposition is discontinuous, and evaporites are easily dissolved. As a result, the record is discontinuous by

nature, with potential stratigraphic gaps on the order of ten million years. In addition, the precision at which biostratigraphic and magnetostratigraphic dating of evaporites can be established is limited due to the nature of the biologic communities and the low magnetic mineral content of evaporites, though careful work can contribute to a solid chronostratigraphic frame (Bernasconi et al., 2017). Furthermore, microbial sulfate reduction can occur during evaporite deposition and contribute to the evolution of the sulfur isotope ratio of the brine and of the deposited evaporites (Ault and Kulp, 1959; Guibourdenche et al., 2022; Kah et al., 2004). In addition, secondary modification due to thermal sulfate reduction may also occur and obscure the initial composition of the evaporite (Laurent et al., 2021; Vinogradov, 2007). Finally, some evaporite sequences may be of continental origin (Hardie, 1984), or at least strongly influenced by riverine inputs (Aloisi et al., 2022; Utrilla et al., 1992). For all these reasons, though they constitute a necessary archive and the only one known to form directly through massive deposition from seawater, they must be carefully studied to access seawater composition.

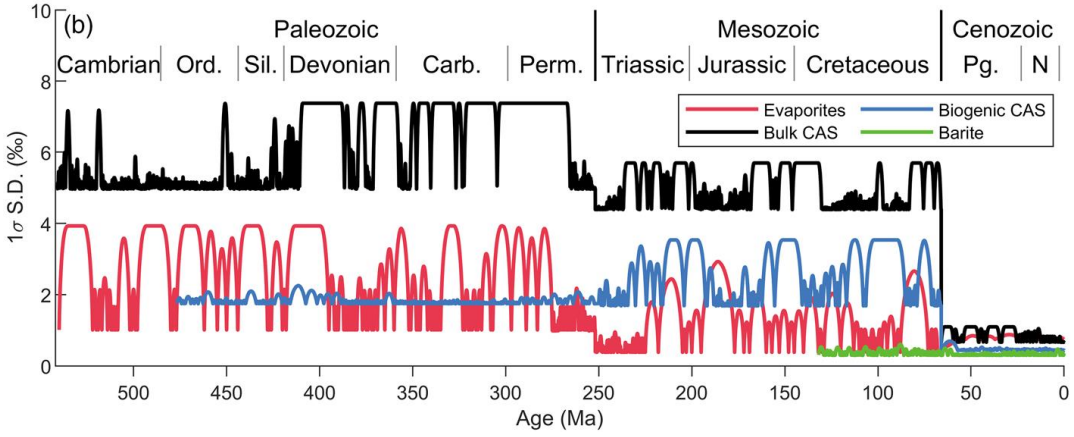

Figure 28. Estimates of $\delta^{34}S_{sw}$ archives' variability, showing an increase of variability back in time for evaporites and CAS, and the additional variability of bulk CAS compared to biogenic CAS, of CAS in general compared to evaporite, and the greater variability in all archives compared to barite, except for biogenic CAS in the Cenozoic (figure from Present et al., 2020).

3. CAS, an archive requiring improvements.

Carbonates also display a variability significantly beyond that of barite, and sometimes of evaporites (Present et al., 2020). A comparison over the Meso-Cenozoic reveals that barite has the lowest variability of all archives (Fig. 28 and 29). This variability could be linked to the fact that barite has a lower possible resolution than carbonates do. As a result, changes could be captured by carbonates and not by barite. However, this hypothesis is not supported by the statistical analysis of Present et al. (2020). In addition, over the Cenozoic, residence time of sulfate in the ocean tends to be incompatible with local changes, making this hypothesis even more unlikely. Many other parameters can come into play, that often complicate the use of

carbonates as a geochemical archive: vital effects or diagenesis. I will detail in Chapters IV and V ten years of progress on these questions. This careful appraisal of CAS as an archive, one of the main focuses of my research since 2010, has allowed us to produce the one carbonate record that displays a variability identical to that of barite: the record based on monospecific foraminifer samples, established by Rennie et al. (2018). This 60 Myr record demonstrates that barite and CAS can be equally reliable archives.

4. CAS and barite records over the last 130 Myr.

Overall, carbonate records display a variability that barite records do not, which questions the meaning of the CAS-based records. The source of variability must be understood. In Rennie et al. (2018), we reexplored the Cenozoic variations of $\delta^{34}S_{sw}$ using CAS from hand-picked monospecific foraminifer samples from a combination of oceanic coring IODP sites (Fig. 29). With the exception of the partial record from Toyama et al. (2020), published afterwards, it is the only CAS record that reproduces the variations displayed by the barite records (Paytan et al., 1998; Toyama et al., 2020; Yao et al., 2020a). The most intriguing Cenozoic $\delta^{34}S_{sw}$ feature is an approximatively 5 ‰ positive shift occurring around at ~52 Ma. This major shift, hard to explain in an ocean with high sulfate concentrations, has been fueling many interrogations regarding its origin and its coupling, or decoupling, to the carbon cycle (Kurtz et al., 2003; Paytan et al., 1998; Rennie et al., 2018; Wortmann and Paytan, 2012; Yao et al., 2020a; Yao and Paytan, 2020). The implications of its origin are very important in terms of alkalinity, carbon, oxygen, and calcium cycles, and yet, it remains debated. The improved resolution of the foraminifera record helped bring a refined understanding of the relationship between $\delta^{34}S_{sw}$ and $\delta^{13}C$ (Rennie et al., 2018).

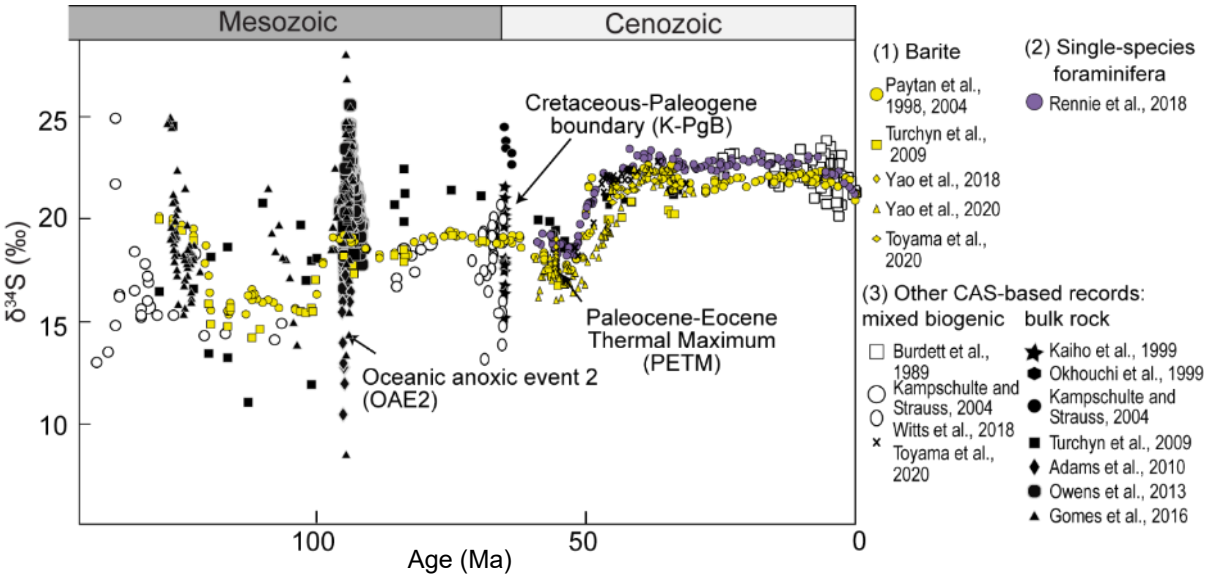

Figure 29. Synthesis of the CAS and barite data covering the last 140 Myr revealing that CAS records tend to display a greater variability than barite, with the notable exception of the foraminifera record by Rennie et al. (2018)

There are however some discrepancies between the Cenozoic barites and foraminifera records. Yao et al. (2020) re-evaluated the age model of the foraminifera record and improved the resolution of the barite record, which allowed them to produce an even more detailed comparison between the two records. They translated the data of Rennie et al. (2018) onto the GTS 2012 timescale. As the Rennie record is also a composite record, it generates noticeable differences depending on the choice of timescales. In particular, major age differences occur for IODP site 1265 (Fig. 30).

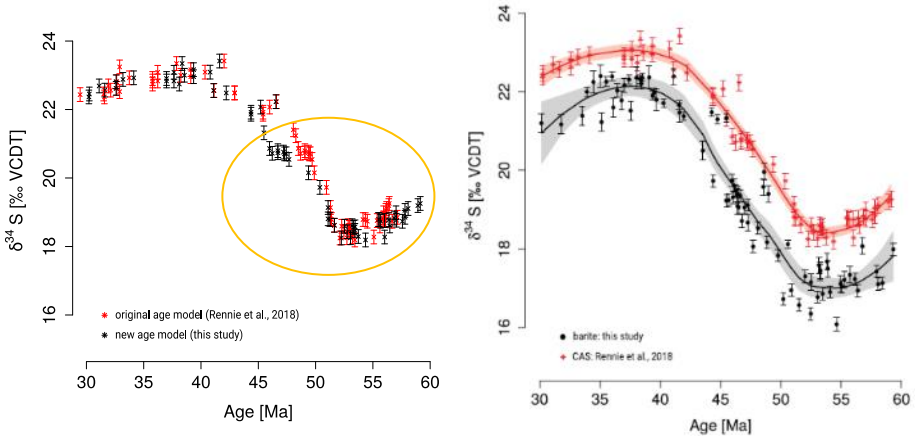

Figure 30. Plot of CAS data (Rennie et al., 2018) on the original timescale (red) versus that on the timescale used by Yao et al. (2020, black). Error bars are 1σ (figure from Yao et al., 2020).

Yao et al. (2020) also observed a few differences between their new data and the data by Paytan et al. (1998), which they attributed to a diagenetic overprint of some of the barite between 55 and 45 Ma, as some samples yielded values higher than the new data. Such diagenetic overprint could have happened in the sulfate depleted zone of sediments (see Chapter V) where barite could have dissolved and reprecipitated, incorporating isotopically modified sulfate (Yao et al., 2020a). However, once this modification performed, a roughly constant offset of 1 ‰ exists between both archives. A similar offset is then confirmed by a direct comparison between a bulk CAS record produced from the same samples from which additional barites are extracted (Toyama et al., 2020). Though this offset remains enigmatic, we can rule out various causes of modification of the $\delta^{34}S_{CAS}$ record. First, vital effects (see Chapter IV) were corrected in Rennie et al. (2018), so we assume that it is not the reason for the offset. It is intriguing however that the records are identical over the last 5 Myr of the Cenozoic. As a result, there is also the possibility that the Rennie record needs a better anchoring of data from site 926 to the modern values, as no actual overlap could be obtained between Site 758 (0-5 Ma) and Site 926.

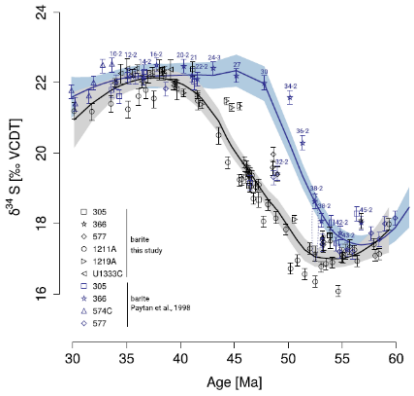

Figure 31. Plot of the older barite data (Paytan et al., 2020; blue) versus the new record (Yao et al. 2020; black). Error bars are 1σ (figure from Yao et al., 2020).

Overall, diagenetic alteration of the foraminifera is unlikely to be the cause of the offset. Indeed, the offset is constant with time and over diverse IODP cores. It would be extremely unlikely to imagine an offset identical between sites, especially considering how diverse diagenetic overprints can be for sulfur isotope ratios (Rennie and Turchyn, 2014). However, as shown in Yao et al. (2020) the barite record can be affected and heterogeneous at times, thus pointing to potential alteration of the barite record itself, which, combined to the complex history of pelagic barite, could also contribute to the offset.

5. A well-defined yet still debated Cenozoic $\delta^{34}S_{sw}$ trend.

In conclusion, barite and CAS share the difficulties inherent to the creation of composite cores, though CAS are more affected by various vital effects and is often considered to be more likely to be diagenetically overprint than barite. However, foraminifera have two advantages. The first one is that they bear the carbon and oxygen isotopic stratigraphy, allowing straightforward comparison between the different isotope ratios measured in calcitic tests (Fig. 1). They are also massively used to reconstruct seawater pH through boron isotope ratios, to measure other isotope ratios such as Li, Mg, Ca: they are an endless source of geochemical proxies. The second one is that foraminifera live in well-constrained and different parts of the water column, potentially allowing to investigate the evolution of $\delta^{34}S$ in different parts of the ocean, with a better depth and environment constraint than barite. At the beginning of the Cenozoic, the Cretaceous-Paleogene Boundary bears the largest discrepancies between CAS and barite, which led us to reexplore the sulfur isotopic composition of the ocean using both planktic and benthic foraminifera in order to understand possible variability within the ocean and/or within CAS archives precipitated in different locations of the ocean. This was at the heart of Arbia Jouini's PhD thesis (chapter VI).

III. Past evolution of the sulfur cycle.

Despite the difficulties inherent to each archive, the Cenozoic trends are now well described. However, their interpretation remains quite debated. In the following, we will present the main interpretations, non-necessarily mutually exclusive, that have been proposed over the last 25 years to explain this shift. The Cenozoic is used as an example of the various scenarios proposed to interpret $\delta^{34}S_{sw}$ throughout the Phanerozoic.

1. Pyrite (and reduced sulfur) burial.

Pyrite burial in sediments is ultimately the main control of $\delta^{34}S_{sw}$, because of the isotopic fractionation occurring during MSR. It seems virtually impossible to explain the major modifications of the Cenozoic $\delta^{34}S_{sw}$ shift without changing ε_{pyr} in addition to F_{pyr} (Rennie et al., 2018; Wortmann and Paytan, 2012; Yao and Paytan, 2020). Indeed, attributing the Eocene 5‰ change to the pyrite flux itself requires unrealistic variations (Paytan et al., 1998). A possible way to explain such a change in the pyrite depositional flux is to assume an occurrence of euxinic environments (Kurtz et al., 2003) where sulfur and carbon deposition become decoupled. However, the sulfur and carbon cycle might be coupled at times during the Cenozoic, especially at the onset of the Eocene shift.

For this reason, Rennie et al. (2018) suggested that the onset of the India-Asia collision (Bouilhol et al., 2013; Jagoutz et al., 2015) could have contributed to a shift in a major location of organic matter deposition from shallow to deep environments, where sulfate reduction rates could be lower and fractionation higher.

An alternate mechanism could come from deposition of highly fractionated pyrite in the Arctic ocean (Ogawa et al., 2009; Toyama et al., 2020; Yao and Paytan, 2020) that would have generated an isolated and isotopically heavy water mass. Its mixing with the rest of the ocean could have explained the Eocene shift. If similar deposition or enriched pyrite occurred on the Antarctic shelves, the onset of glaciation at the Eocene-Oligocene transition could explain the $\delta^{34}S$ decrease observed at ~33 Ma (Paytan et al., 1998; Rennie et al., 2018; Yao et al., 2021).

2. Variations in weathering and F_{in}.

The weathering flux in most models is assumed to bear an isotopic signature of +3 ‰. As mentioned in Chapter I, we decided to establish a database of $\delta^{34}S$ from the main rivers in the world (Burke et al., 2018b). This approach allowed us to establish that the average isotopic composition of sulfur delivered as sulfate is 4.8 ± 4.9 ‰, excluding the most polluted rivers. The exclusion is of importance as it is estimated than roughly on third of riverine sulfate due to anthropogenic pollution (Meybeck, 1987). As a result, most models prior to 2018 use an incorrect value for riverine inputs.

In addition, little constraints exist on past weathering. The only existing data-based approach to reconstruct the continental input flux through time comes from sulfur isotope analyses of coal through time, which reveal a roughly constant value that suggests no strong variation of $\delta^{34}S_{in}$ over the Phanerozoic (Canfield, 2013). F_{in} is thus rarely held responsible for the major changes observed in $\delta^{34}S_{sw}$.

3. Assessing the evaporite flux.

Evaporite formation is a flux that combines the sulfur and calcium cycles, with a major influence on oceanic alkalinity. It appears clearly that evaporite formation throughout Earth's history is not constant and different approaches have been used to reconstruct it. A mathematically simple yet unrealistic approach in different models is to assume that evaporite deposition is directly proportional to sulfate concentration in seawater (Rennie et al., 2018). However, evaporite deposition have been considered as the trigger of the Meso-Cenozoic variations observed in $\delta^{34}S$ values (Wortmann and Chernyavsky, 2007; Wortmann and Paytan, 2012). In this approach, the authors assume a depositional flux that increases suddenly 120 Myr ago. This flux would have decreased seawater sulfate concentration, which, assuming a global Michaelis-Menten relationship for both the pyrite flux and fractionation, would have decreased $\delta^{34}S_{sw}$. In return, evaporite dissolution during the Himalayan uplift would have rapidly increased seawater sulfate concentration and $\delta^{34}S_{sw}$ (Wortmann and Chernyavsky, 2011, 2007; Wortmann and Paytan, 2012).

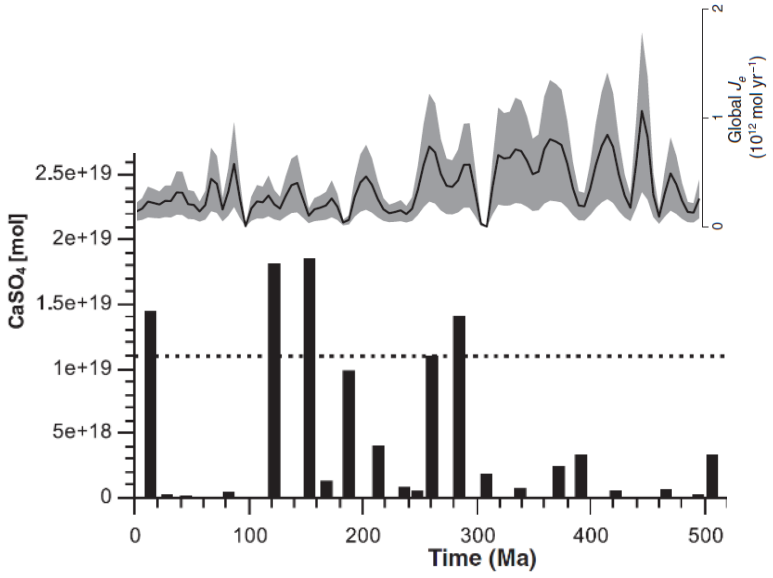

Figure 32. Evaporite deposition record used to match the $\delta^{34}S_{sw}$ record (left, Wortmann and Paytan, 2012) and flux based on the geological record (right, Halevy et al., 2012)

However, the underlying mechanism to change the isotopic composition of seawater sulfate is through a modification of the pyrite burial flux as well as of the fractionation between sulfate and pyrite. Another approach on the reconstruction of the evaporite flux come from a thorough

appraisal of evaporite formations in North America as a base for world gypsum deposition (Halevy et al., 2012). Using the geologically constrained evaporite burial flux as a direct in a sulfur cycle model, Halevy et al. (2012) suggested that pyrite burial and weathering dominate the long-term sulfur cycle and have remained roughly constant over the Phanerozoic, in contrast with the findings described previously. In addition, the evaporite flux used to match the $\delta^{34}S_{sw}$ record and the geologically constrained flux are very different from each other (Fig. 32).

In addition, evaporites bear the additional particularity of generating a fast recycling flux that might bias the weathering input (Halevy et al., 2012), and it has been recently demonstrated that a cryptic sulfur cycle was occurring during evaporite dissolution, generating a non-negligible flux of organic carbon remineralization (Guibourdenche et al., 2022).

IV. Conclusion: the importance of a proper archive and stratigraphy.

It is clear, however, that the sulfur cycle plays a role in the regulation of the carbon and oxygen cycles, even if the mechanisms that controlled the evolution of $\delta^{34}S_{sw}$ remain disputed. Additional information could be provided by minor isotopes measured in sulfate, such as $\Delta'^{17}O$, $\Delta^{33}S$ or $\Delta^{36}S$. The barite-based $\Delta^{33}S$ record shows that $\Delta^{33}S_{sw}$ remained constant to the first order over the last 130 Myr (Masterson et al., 2016). This additional information however is accompanied by modelling results that suggests that, except at low sulfate concentrations (<5 mmol/L) seawater $\Delta^{33}S_{sw}$ is mostly insensitive to the different scenarios assumed for explaining the changes in the $\delta^{34}S_{sw}$ record.

Oxygen isotopes from sulfate are more sensitive to the flux that add newly oxidized sulfur, which is the oxidation of pyrite on land and the reoxidation of sulfide in sediments (e.g. Turchyn and Schrag, 2004; Waldeck et al., 2022a; Yao et al., 2018). Additional constrains from the $\Delta^{17}O$ record of the last 130 Myr suggest that (Waldeck et al., 2022). This record suggests that the ratio between the flux of sulfate from rivers and from reoxidation of reduced sulfur has remained roughly constant over this period of time.

We must nonetheless consider the fact that significant progress on the stratigraphic record has been made since the first barite record of the Cenozoic (Paytan et al., 1998). In particular, the work of Vicky Rennie during her PhD has been essential to demonstrate that CAS is an archive that can be as reliable as barite in terms of signal fidelity, and with added benefits in terms of stratigraphy and comparison with other geochemical signals such as direct comparison with $\delta^{13}C$. In order to demonstrate the usefulness of CAS, a lot of work is necessary to understand how CAS acquires, and maintain, its $\delta^{34}S$ values. These two questions structure the articulation of the next two chapters.

Chapter IV. Carbonate Associated Sulfate (CAS): a work in progress.

As we described in Chapter III, the comparison between the different archives used to reconstruct past $\delta^{34}S_{sw}$ reveal that carbonate associated sulfate (CAS) tends to display a more pronounced variability than barite, and sometimes even more scattered than evaporites. Yet, carbonates are a critical archive for paleoenvironmental reconstructions, as many calcium carbonate-based paleoenvironmental proxies (e.g. $\delta^{13}C$, $\delta^{18}O$, Δ_{47}, $\delta^{11}B$, Mg/Ca) are critical to reconstruct past evolution of the Earth system processes and parameters such as oceanic pH and temperature, weathering, or organic carbon burial. In particular, as foraminifera can grow in different environments (e.g. benthic vs. planktic), they allow ideal age control through biostratigraphy and direct correlations to other fundamental proxies. Foraminifera constitute the backbone of geochemical stratigraphy for the last 130 Myr (see Fig. 1). In addition, the foraminifera-based $\delta^{34}S_{sw}$ record presented in Chapter III was able to reproduce the Cenozoic barite record, which demonstrates that CAS can be an archive as reliable as barite.

However, outstanding concerns remain about extracting information about sulfur cycling from carbonate archives. For example, the paths for sulfur incorporation into carbonate remain unknown. The question of sulfur/sulfate incorporation in biogenic carbonates in particular must be addressed for two reasons. First, the sulfate concentration of a solution is one of the parameters that affects the crystallography of the calcium carbonate that precipitates. At high sulfate concentrations, calcite precipitates less easily than aragonite (Bots et al., 2011; Kitano et al., 1975). Given that sulfate is very concentrated in today's ocean and that calcite is a naturally occurring biogenic carbonate, for instance in foraminifera, mechanisms might exist to control sulfate in the precipitating fluid of biomineralizing organisms. If such control exists and affects the sulfur isotopic composition or concentration of CAS, it must be understood and described both to improve the CAS proxy and our understanding of biomineralization. Second, sulfate plays also a key role in organic molecules that lead the biomineralization and it is actively debated whether sulfate groups substitute to carbonate ions, are linked to organic molecules, or both (Cuif et al., 2003; Paris et al., 2014b; Richardson et al., 2019a; Rose et al., 2019b; van Dijk et al., 2017). Sulfur overall plays many, insufficiently described, roles in biomineralization, a process itself fundamental in the carbon cycle.

This chapter is an extended introduction to work I have significantly contributed to during Yigal Barkan's PhD thesis under the supervision of Itay Halevy at the Weizmann Institute (Barkan et al., 2020; in prep.), the postdoctoral work of Caroline Thaler, whom I co-advised with

Annachiara Bartolini (Thaler et al., preprint), as well as my own work (Paris et al., 2014b; Paris et al., in prep.).

I. Where and what is sulfur in biogenic carbonates?

The nature of the sulfur present in carbonates is a matter of active discussion. In biogenic carbonates, how much of sulfur occurs respectively as inorganic (CAS) or organic sulfate or reduced sulfur is still a matter of debate (Cuif et al., 2003; Dauphin et al., 2003b, 2005; Erez, 2003; Richardson et al., 2019a).

Early investigations of travertines using Infra-Red and Raman spectroscopy first supported the idea that sulfate could substitute for carbonate (Takano, 1985; Takano et al., 1980). At the same time, growth experiments of the mussel *Mytilus edulis* revealed intra-shell variations of S/Ca ratios interpreted as variations in the organic matter content of the shell (Lorens and Bender, 1980) with sulfate bound to organic matter, rather than inorganically incorporated sulfate. Ever since, the question of the relative abundance of organic and inorganic sulfate in biogenic carbonates has remained an active field of research.

1. Substitution? A look into inorganic carbonates.

The structural integration of carbonate associated sulfate in the carbonate mineral lattice has been investigated first mostly in inorganically precipitated carbonate. Extended X-Ray Absorption Fine Structure (EXAFS) spectra of selenium showed that Se is incorporated as SeO_4^{2-} groups, connected to calcium atoms, instead of CO_3^{2-} (Reeder et al., 1994). Comparisons between sulfur and selenium are possible because the two elements have similar properties, although selenium is bigger than sulfur. In addition, sulfate is heterogeneously incorporated into the calcite crystal, preferentially along the c-axis (Staudt et al., 1994). X-ray Adsorption Near-Edge Spectroscopy (XANES) investigations of different types of organic and synthetic aragonites rules out fluid or $CaSO_4$ inclusions comparing both peak and post-peak features (Barkan et al., 2020; Pingitore, 1995). Only EXAFS could have directly proven the actual sulfate substitution for CO_3^{2-} as EXAFS is sensitive to the broader environment of the element of interest. However, EXAFS is not suitable for sulfur in carbonates (Pingitore et al., 1995). As a result, XANES spectroscopy is a widely used method to characterize sulfur in biomineral carbonate, as described below.

2. Foraminifera.

Early work revealed the occurrence of sulfate ions in the test of *Orbulina universa*, using infra-red spectroscopy (Tochon-Danguy et al., 1976). The presence of over-sulfated polysaccharid

molecules found during the investigation of *Heterostegina depressa* organic matrix led to the assumption that sulfate in foraminifera was organically-bound rather than inorganically incorporated (Weiner and Erez, 1984). XANES investigations of different foraminifera species (planktonic *Globorotalia* sp., benthic hyaline *Calcarina gaudichaudii* and porcelaneous *Amphisorus kudakajimensis*) all revealed the presence of sulfated organic molecules in the analyzed tests, despite the differences that can be seen in the biomineralization pathways of those foraminifera (Cuif et al., 2008; Yoshimura et al., 2019). This organic sulfate is described as chondroitin sulfate or glycosaminoglycan sulfate. Glycosaminoglycans are unbranched polysaccharide side-chains made of a sequence of amino sugars covalently attached to proteins (Langer, 1992), and thus chondroitin-, polysaccharid- and glycosaminoglycan-sulfates are the same thing. They overall constitute proteoglycans, which play critical roles in biomineralization that we will describe later. The organic matrix of the benthic foraminifera *Heterostegina depressa* or of the scleractinian corals *Hydnophora* and *Merulina* both contain sulfated glycosaminoglycans such as chondroitin sulfate in their organic matrix, in addition to sulfur in amino acids Dauphin et al., 2008).

However, Burdett (1989) suggested that at least some of the sulfate had to be inorganic by analogy with travertine and inorganic carbonates (Kitano et al., 1975; Takano, 1985; Takano et al., 1980) and the XANES data of Yoshimura et al. (2019) also confirmed the presence of inorganic sulfate in the tests.

Measurements of the trace element composition of foraminifera showed that sulfur covaries with magnesium within a test, and also across different bulk test shells grown in the same seawater conditions (Erez, 2003; Paris et al., 2014b; van Dijk et al., 2019). Overall, foraminifera rich in magnesium tend to be rich in sulfate as well, and clear differences appear between different species. Such observations suggested the possibility that sulfur either marks enrichment in organic matter, or that it displays inorganic incorporation behavior similarly to magnesium.

3. Brachiopods.

In brachiopods such as *Terebratalia transversa* sulfate concentrations tend to be higher in the primary layer compared to the fibrous secondary layer, co-incident with a higher magnesium concentration, though this is not observed in the high-Mg brachiopod *Novocrania anomala* (Cusack et al., 2008; England et al., 2007). In contrast, the sheaths surrounding the calcite fibers in *Terebratulina retusa* contain organic thiol-sulfur, while Micro-Raman spectroscopy confirmed that the sulfate within the fibers is structurally substituted (Cusack et al., 2008). A more recent XANES investigation of In *T. transversa* similarly revealed the occurrence of organic sulfate and diverse forms of reduced organic sulfur but suggested that the majority of

sulfate occurred as inorganic sulfate (Fig. 34; Richardson et al., 2019a). A sulfur banding due to varying concentration of inorganic sulfate is present in the shell of some brachiopods (and mollusks), and it can be preserved, still as inorganic sulfate, in specimens that are several hundreds of million years old (Johnson et al., 2020; Richardson et al., 2021; Tanaka et al., 2019; Fig. 33).

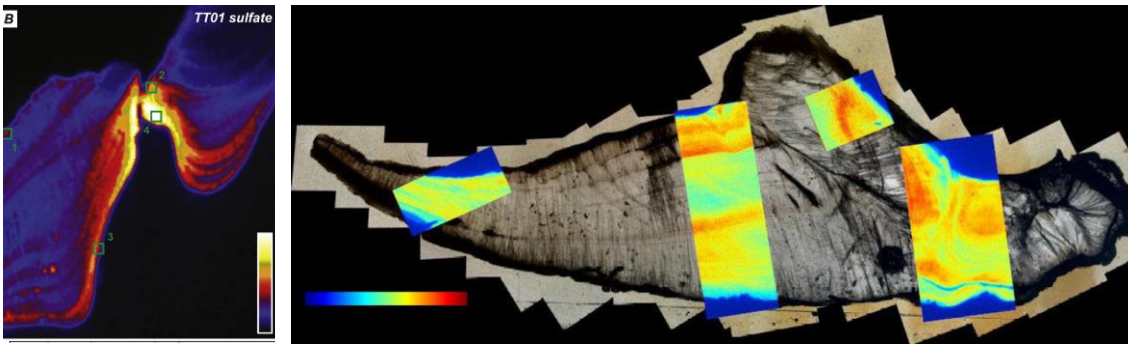

Figure 33. Examples of sulfur banding in modern Terebratalia transversa (Richardson et al., 2019a) as well as in the fossil Neospinifer dunbari (Carboniferous-Permian boundary; Johnson et al., 2020)

4. Mollusks

Amongst works that focus on the role played by organic matter in biomineralization, many studies focus solely on organic sulfur in the biomineral, and as result they do not provide information about inorganic sulfate incorporation. Within the shell of the *Crassostrea gigas* oyster, there appears to be more organic sulfate than amino acid sulfur in the intracrystalline matrices, whereas the relatively proportions are opposite in the organic envelopes of the prismatic layers. In addition, organic sulfate following the major growth phases of the prisms (Dauphin et al., 2013). For the calcitic prisms present in the outer prismatic layer of the shell of two other oysters, *Pinna nobilis* and *Pinctada margaritifera*, organic sulfate is similarly the most abundant species in both the intraprismatic organic matrices and the outer membranes, though the situation might be different for the interprismatic walls (Dauphin et al., 2003b, 2003a). The presence of sulfur in amino acids and organic sulfate is similarly observed in the aragonitic prismatic layer of *Unio pictorum* (Dauphin et al., 2018).

Additional work to collect µ-XRF and XANES spectra from the inner layer of different mollusk shells (the calcitic scallop *Mizuhopecten yessoensis* and the aragonitic giant clam shell *Hippopus hippopus,* as well as the freshwater calcitic pearl mussel *Hyriopsis* sp.) revealed the presence of inorganic sulfate in the marine aragonitic and calcitic bivalve shells but failed to discriminate between organic or inorganic sulfate in the freshwater shell (Yoshimura et al., 2014, 2013). However, a more recent study from another freshwater bivalve *Margaritifera laevis* revealed that the sulfate present in this organism is most likely organic (Tamenori and Yoshimura, 2018). Because sulfate concentrations in freshwater are usually lower than in

seawater, the inorganic incorporation of sulfate in freshwater shells can be expected to be lower.

Like in foraminifera tests, there is variability in sulfur concentrations in mollusk shells. The first-order fluctuations of sulfur in these shells may be connected to the biological activity or the growth rate of the shell and clear annual or daily fluctuations can sometimes be observed, with lower sulfur concentrations during periods of faster growth. Variations in the amount of sulfated molecules for instance occur with the daily rhythm of crystallization in the shell of the gastropod *Concholepas* (Cuif et al., 2008). Variations in trace sulfur from *H. hippopus* shells were interpreted as resulting from annual cyclic changes of shell growth related to insolation or some other environmental factors influencing shell growth (Yoshimura et al., 2014, 2013).

5. Corals.

In scleractinian corals, XANES spectra at the K-edge of sulfur led to the interpretation that sulfate occurs mostly as chondroitin-sulfate, with no reduced sulfur species detected (Cuif et al., 2003; Dauphin et al., 2008). However, in some of the studies presented here for corals, but also for mollusks (e.g. Cuif et al., 2003; Dauphin et al., 2003), the XANES spectra produced for sulfate lack the left shoulder peak observed in the C-SO_4 reference standard. Post-edge features differ for gypsum and organic sulfate (Fleet, 2005) but are quite similar for inorganic CAS and organic sulfate (Barkan et al., 2020). As a result, the shape of the peak is critical and a reinterpretation of XANES investigations published prior to Barkan et al.'s work could provide useful information. A more recent study revealed that inorganic sulfate and trace sulfite both exist in the skeleton of the red high-Mg calcitic coral *Corallium rubrum*, and inorganic sulfate exists in the organic tissues along with amino acids, sulfoxides and sulfonate groups (Perrin et al., 2017).

However, speciation mapping of the calcitic pink coral *Corallium elatius* using microscopic X-ray fluorescence and soft X-ray photo-absorption (µ-XRF/XAS) revealed that inorganic sulfate is the primary species in the calcitic coral skeleton, though minor amounts of organic sulfur are also present (Tamenori et al., 2014). This work also clarified that inorganic sulfate does substitute for the carbonate ions (Tamenori et al., 2014). The skeleton of the red coral *Paracorallium japonicum* displays a ratio of 1:20 for organic and inorganic sulfate, while overall S and Mg are anticorrelated with Mg being more concentrated in the light organic-poor yearly bands (Trong Nguyen et al., 2014), similarly to *Corallium rubrum*, which skeleton displays Mg-rich bands likely form during the warm season S-rich rings form immediately after (Vielzeuf et al., 2013).

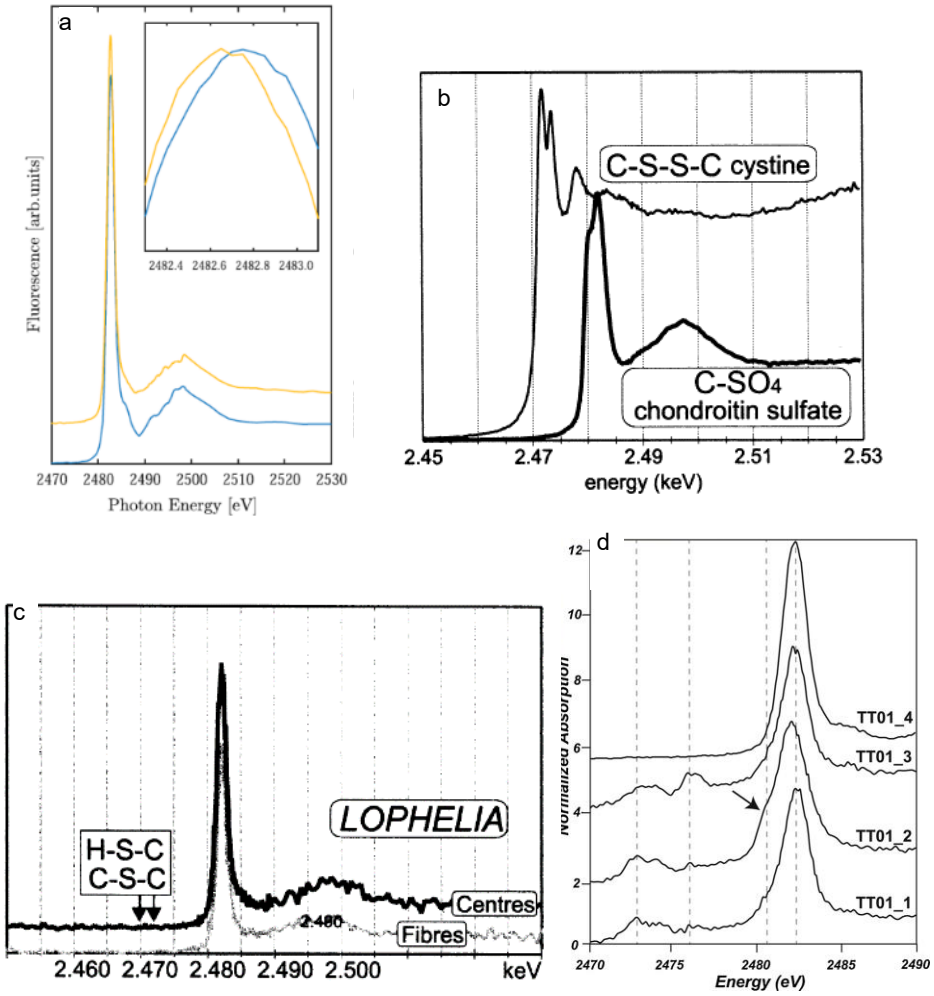

Figure 34. XANES spectra from CAS in inorganic calcite (a – Barkan e al., 2020), standards and the coral Lophelia pertusa (b, c – Cuif et al. 2003) showing that a peak looking like CAS rather than organic sulfate might have been incorrectly interpretated, and various spectra from a brachiopod showing the occurrence of both inorganic and organic sulfate (d - Richardson et al., 2019a)

6. Summary.

In all biogenic carbonates, the majority of sulfur is oxidized, some is reduced. Reduced sulfur occurs as sulfur in amino acids. Oxidized sulfur is almost only present as sulfate groups that can be either attached to organic molecules (organic sulfate) or incorporated into the mineral lattice. Inorganic calcite and aragonite XANES spectra we produced recently show that some of the past interpretations of sulfate groups as organic might need to be revisited. However, organic sulfate groups occur in all biogenic carbonates, though inorganic sulfate is likely the (vastly) dominant type of sulfate, the one exception being freshwater organisms.

II. Transport of ions and control of the composition of the biomineralizing fluid.

In the modern ocean, calcium carbonates can be found mostly as aragonite and high-Mg calcite (Mg/Ca > 30-40 mmol/mol) in shallow environments while low-Mg calcite dominate deep-water carbonates and the vast majority of those carbonates are secreted by marine organisms (Mackenzie et al., 1983; Stehli and Hower, 1961). As carbonates constitute a major carbon reservoir, this makes biomineralization a flux that is critical to understand the carbon cycle.

1. Calcium carbonates, a ubiquitous family of biominerals.

Biomineralization includes a variety of different processes generally related to the precipitation of minerals as a result of biological activity. In some cases, biomineralization can be induced in a fairly uncontrolled manner, as it is the case for stromatolites, or the process of mineralization can be highly orchestrated, as is the case for bones and shells (Lowenstam, 1981). Calcium is the cation of choice for most biomineralizing organisms, and calcium carbonates are the most abundantly produced amongst the – at least – 60 different biominerals. The capacity to biomineralize calcium carbonate is widely distributed among many different taxa (Lowenstam and Weiner, 1989). A proper review of biomineralization is not the end goal here, as many exist already (Cusack and Freer, 2008; de Nooijer et al., 2014; Drake et al., 2020; Erez, 2003; Gilbert et al., 2022; Spero, 1998; Weiner and Dove, 2003).

i. CaCO3 polymorphs.

$CaCO_3$ is usually secreted by organisms mostly as calcite (e.g. bivalves, foraminifera, coccolithophorids, echinoderms, mollusks), which can be classified as low or high-Mg calcite depending on the amount of magnesium, or aragonite (e.g. corals, mollusks; Fig. 35). Some organisms are even able to precipitate both (e.g. Bryozoans or mollusks such as the mussel *Mytilus edulis*). Calcite belongs to the trigonal system while aragonite belongs to the orthorhombic one. Under natural conditions at Earth's surface, low-Mg calcite is the most stable polymorph, which has led to many investigations regarding the common occurrence of aragonite as a biomineral. The common explanation for the ubiquity of aragonitic biominerals is that Mg^{2+} present in the modern ocean inhibits calcite nucleation and/or crystal growth, and, as a result, aragonite precipitates more rapidly and is thus kinetically stabilized (Berner, 1975; Bischoff, 1968; Bots et al., 2011; Morse et al., 1997; Sandberg, 1985). An additional explanation is that the incorporation of Mg in calcite makes calcite more soluble (Winland, 1969). Finally, a third $CaCO_3$ polymorph, the least stable, vaterite, has been observed, only in the planktonic foraminifera *Orbulina universa* and *Neogloboquadrina dutertrei* so far (Jacob et al., 2017).

Figure 35. Unit cells of the $CaCO_3$ polymorphs found in biocalcifiers. The blue circles represent the calcium atoms, the black spheres the carbon atoms and the red spheres the oxygen atoms.

ii. $CaCO_3$ polyamorphs.

$CaCO_3$ also occurs as Amorphous Calcium Carbonate (ACC; Fig. 36). ACC, rather than a specific amorphous structure, is actually an ensemble of polyamorphs, much like calcium carbonate is an ensemble of polymorphs, that can be hydrated or not (Cartwright et al., 2012). ACC is a metastable phase nonetheless observed in the shells of crustaceans, sponges, corals, some mollusks, sea sea-urchin spines or even earthworm granules (Addadi et al., 2003). It can be favored as a $CaCO_3$ precipitate when Mg inhibits calcite precipitation (Wang et al., 2012). Stabilization likely occurs through the interplay of ACC with Mg^{2+} , macromolecules or even small metabolites (Aizenberg et al., 2003, 1996; Akiva-Tal et al., 2011; Sato et al., 2011).

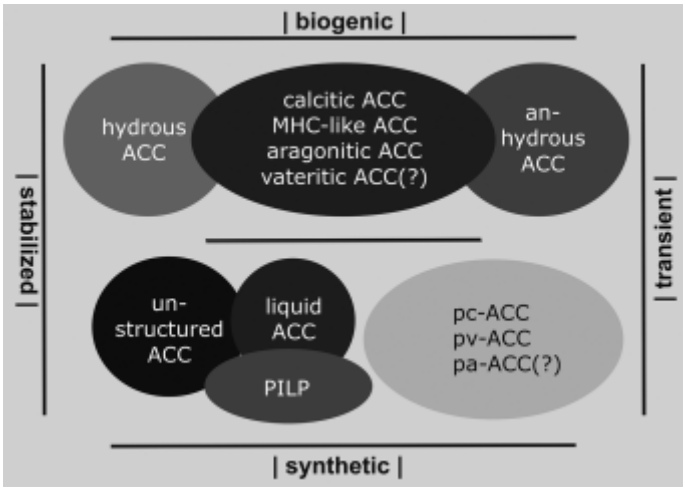

Figure 36. The different biogenic and synthetic calcium carbonate polyamorphs or ACC (Cartwright et al., 2012)

iii. Processes involved in biomineralization.

Organisms are able to precipitate calcium carbonate but also to control its composition and its mineralogy. Many organisms that produce biomineral carbonate, including foraminifera, do so by controlling the composition of a small volume of fluid, bounded by a membrane. Proteins allow the cell to transport ions passively or actively through the membrane, to and from the fluid from cells or from surrounding media. Diffusion of CO_2 and transport of cations into the fluid and transport of H^+ out of the fluid leads to an increase in the saturation state of the fluid with respect to calcium carbonate, encouraging calcification. Biomineralization also involves the interaction between this biomineralization fluid and an organic matrix or template, which also plays a role in facilitating the growth of calcium carbonate. This organic template is referred to as the Primary Organic Sheet (POS) or Membrane (POM) in foraminifera, the former being the preferred term, or the Extracellular Matrix in corals.

Overall, measurements of trace elements and isotopes in biocarbonates can help assess the processes that regulate the composition of the biomineralizing fluid, and the role played by organic molecules and provide constraints on models of biomineralization. Again, an exhaustive review is not the goal here, and extended discussions can be found elsewhere (Chen et al., 2018; Gagnon et al., 2012; Gothmann and Gagnon, 2021; Nehrke et al., 2013; Tambutté et al., 2007). Three non-mutually exclusive processes exist: seawater vacuolization, transmembrane transport, and precipitation of an amorphous precursor.

2. How are calcium and carbonate ions delivered to the site of calcification?

i. Ion transport: seawater vacuolization (SWV).

In most organisms except coccolithophorids, the fluid must originate from seawater, as revealed by staining experiments using calcein or other similar markers. Calcein is a fluorescent dye, which binds to calcium and is incorporated into growing calcium carbonate crystals. However, calcein doesn't go through membranes or pumps and thus indicates direct transport of seawater calcium to the site of calcification in most organisms with the exception of coccolithophorids (Baumgarten et al., 2014; Bentov et al., 2009; Bernhard et al., 2004; Evans et al., 2015; Fox et al., 2018; Jurikova et al., 2019; Moran, 2000; Tambutté et al., 2012).

A mechanism of seawater transportation has been described through the vacuolization of seawater (Bentov et al., 2009; Dellinger et al., 2018; Erez, 2003; Weiner and Addadi, 2011). In this SWV (seawater vacuolization) model, seawater is engulfed in a portion of the membrane that detaches itself from the rest of the membrane and is carried all the way to the site of calcification. By doing so, the vacuoles act as a transport system, bringing amongst other ions the calcium and DIC present in seawater to the site of calcification. An additional aspect of this

model is that the biomineralization site is isolated from seawater. In foraminifera, isolation occurs through an extension of the foraminifera pseudopodial network, itself a part of the cytoskeleton that protrudes out of the test (Erez, 2003). This protection from seawater has been suggested to be possibly 'leaky' (i.e. open to external seawater) at times (Nehrke et al., 2013). A limitation to this model is that the calcium flux represented by calcite precipitation in foraminifera requires a huge flux of vacuoles, roughly 75 times the cell's own volume in seawater to form a new chamber, within less than 6 hours (de Nooijer et al., 2009a, 2014; Nehrke et al., 2013; Yoshimura et al., 2019). The authors point out that the vesicles that can be observed at a given time (20) would be characterized by a much higher Ca content, up to 50 000 mol/L (compared to a seawater Ca concentration of ~10 mmol/L), and thus could not be simply engulfed seawater.

In multicellular organisms such as corals, the biomineralization fluid can be directly replenished by exchange with external seawater input (e.g. Chen et al., 2018; Gagnon et al., 2012; Gothmann and Gagnon, 2021), but active transport is also involved.

ii. Trans-membrane transport (TMT).

One way to increase the Ca content of the calcification site is to bring Ca ions from elsewhere in the cell (or from external seawater). As cell membranes are hydrophobic, they are impervious to direct ion transport, in all living organisms. As a result, ions can only cross a membrane through a channel (passive) or a pump (active), which are transmembrane proteins. Biomineralization relies heavily on the use of the Ca-ATPase, which uses ATP to catalyze the exchange of one Ca^{2+} for $2H^{+}$ (e.g. Adkins et al., 2003; Erez, 2003; McConnaughey and Whelan, 1997). Transport through pumps requires energy. Primary transporters such as proton pumps or Ca-ATPase requires the use of ATP to go against the transmembrane gradient of the ion, while secondary transport used an existing gradient to turn it to entropic energy used to transport the second ion against its gradient. The latter is, however, not involved in biomineralization processes.

To explain how calcium reaches the site of calcification, a second model exists, based on the transport of Ca through the cell's membranes, the TMT (trans-membrane transport). This model is suggested to be dominant for coccolithophorids, which are not sensitive to calcein, which suggests entirely an intracellular precipitation of the calcite (Gussone et al., 2006a; Langer et al., 2006, 2009; Nehrke et al., 2013). Control of the biomineralizing fluid by pumps and channels is also at play in brachiopods (e.g. Simonet Roda et al., 2019) and contributes to the control of the biomineralizing fluid in corals (e.g. Chen et al., 2018; Gagnon et al., 2012; Gothmann and Gagnon, 2021). In bivalves, Ca transport can occur through Ca-rich vesicles (Castro-Claros et al., 2021), but it might not be the dominant mechanism. Though vesicles

travel from the cells to the fluid and are thus different from the vacuoles that engulf seawater. In conclusion, this process could be a combination of SWV and TMT, depending on the origin of the calcium present in those vesicles.

3. Carbonate and other ion concentration regulation.

i. Carbonate and calcium.

Overall, biogeochemical mechanisms control the concentration, or the activity of the ions present at the site of calcification. For all organisms, the regulation of the fluid is aimed at a few goals that all contribute to facilitate calcium carbonate precipitation: to increase calcium carbonate saturation eventually increase Ca^{2+} or CO_3^{2-} concentration (Bentov and Erez, 2006; Castro-Claros et al., 2021; Chen et al., 2018; de Nooijer et al., 2009a, 2009b; Erez, 2003; Jurikova et al., 2019). The regulation of the fluid composition might occur directly at the site of calcification, in the cytosol or the surrounding cells (or of the cell in the case of foraminifera or coccolithophorids) or during seawater transport in vacuoles.

To increase CO_3^{2-}, two parameters can be tuned. The organism can either increase the DIC and/or the pH of the biomineralizing fluid (Gothmann and Gagnon, 2021; Liu et al., n.d.; Rollion-Bard et al., 2011, 2003; Rollion-Bard and Erez, 2010; ter Kuile et al., 1989; Ter Kuile and Erez, 1991; Toyofuku et al., 2017; Vigier et al., 2015). An increase of DIC can be produced by diffusion of CO_2, which can get across membranes as it is a non-charged molecule. Once CO_2 arrives near the site of calcification, interaction with the carbonic anhydrase enzyme catalyzes hydration and hydroxylation of CO_2 to HCO_3^-, which is otherwise a rate-limiting step (Chen et al., 2018; De Goeyse et al., 2021; Gutowska and Mitchell, 1945; Rollion-Bard et al., 2011; Tambutté et al., 2007; Uchikawa and Zeebe, 2012).

$$CO_2 \text{ hydration: } CO_2 + H_2O \leftrightarrow H_2CO_3 \leftrightarrow HCO_3^- + H^+$$

$$CO_2 \text{ hydroxylation: } CO_2 + HO^- \leftrightarrow HCO_3^-$$

An increase in pH can be accomplished using proton pumps that remove them from the site of biomineralization or from the seawater vacuole. As protons are removed, the alkalinity of the fluid increases as well. A common pump found in foraminifera is the Na^+-H^+ exchange pump. Another option for controlling the composition of the fluid is if the use of the coupled H^+-Ca^{2+} Ca-ATPase pump, which will both increase pH and Ca concentration of the fluid (e.g. Chen et al., 2018; de Nooijer et al., 2014; Erez, 2003).

As a result, Ca concentration can be increased by pumping or Ca-delivery from seawater vacuoles or calcium rich vacuoles, CO_3^{2-} concentration can increase through DIC-delivery from seawater vacuoles or CO_2 diffusion towards a fluid with an elevated pH (Fig. 37).

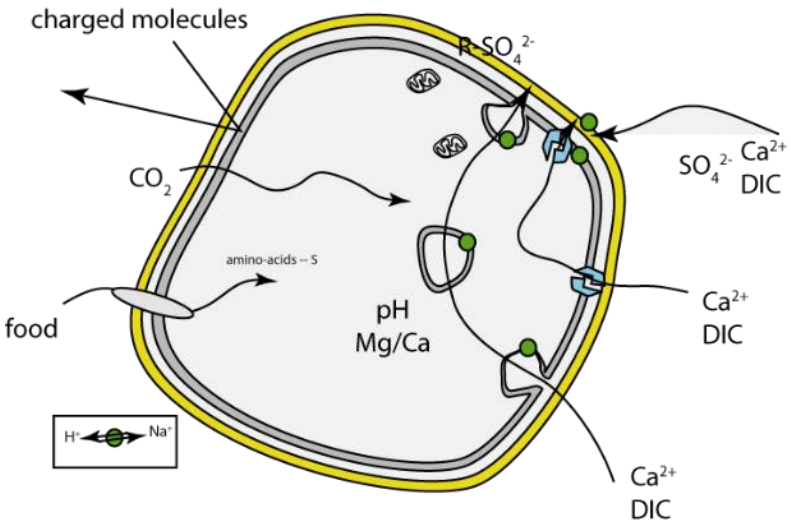

Figure 37. Schematic view of the nature of sulfur and origin of ions in a foraminifera

ii. Control of magnesium concentration.

Another common goal of the control of the fluid composition is to reduce and regulate Mg^{2+} because of its impact on calcium carbonate polymorphism and solubility. Active biological control has been evidenced in many biocalcifiers (Bentov et al., 2009; Bentov and Erez, 2006; England et al., 2007; Evans et al., 2018; Khalifa et al., 2016; Pérez-Huerta et al., 2008; Purton et al., 1999; Saulnier et al., 2012). An alternate strategy to Mg-removal is H^+ removal (and thus pH and/or CO_3^{2-} concentration increase). Different strategies have been proposed.

Active biological exclusion has been suggested in different organisms (Bentov and Erez, 2006; Lorens and Bender, 1980; Saulnier et al., 2012), which in foraminifera at least is supported by the observation of Mg-rich particles in the cytosol (Khalifa et al., 2016). Another strategy to facilitate calcite precipitation despite elevated Mg concentrations is to increase the saturation state at the site of calcification. This strategy has been suggested to be more efficient than active Mg-removal, especially under conditions stressful for calcification (Evans et al., 2016; Zeebe and Sanyal, 2002).

In the case of coccoliths, as well as possibly some foraminifera, the TMT offers another strategy. Coccolithophorids produce low-Mg calcite, which can be explained by preferential uptake of Ca compared to Mg across the cell membrane. If organisms pump actively Ca^{2+} out of seawater and into the calcifying fluid, Mg^{2+} ions do not need to be excluded and low-Mg calcite could result from the omnipresence of such a TMT endmember (e.g. Nehrke et al., 2013, van Dijk et al., 2019). However, Mg isotope ratios reveal that the low Mg/Ca ratios in foraminifera, echinoids and coccoliths are explained by different mechanisms as they are characterized by very different $\delta^{26}Mg$ values despite similar Mg contents (Saulnier et al., 2012).

As a result, TMT is unlikely to be the only mechanism at the origin of the low Mg/Ca ratios in foraminifera.

iii. A role for mitochondria?

At least in foraminifera, mitochondria might also play a role in calcite precipitation (Bé et al., 1979; Bentov et al., 2009; Spero, 1988). Mitochondria are associated with the glycosaminoglycan and organic network in the cytoskeleton (Langer, 1992). In *O. universa* and possibly in *G. truncatulinoides*, calcification near the POS occurs in association with the cytoskeleton and pseudopodia containing mitochondria. Besides their fundamental role in respiration, mitochondria pump Ca^{2+} and Mg^{2+} from the cytosol, and therefore can store and modulate the activity of those ions in the cell (e.g. Gout et al., 2014; Gunter et al., 2004; Szanda et al., 2009). As a result, these mitochondria may possibly play a role in modulating the Mg^{2+} concentration at the site of calcification (Bé et al., 1979; Spero, 1988; Spero et al., 2015). Additionally, the observation that high-Mg bands are precipitated at night (Fehrenbacher et al., 2017), suggests that there may be a diurnal change in mitochondrial activity in foraminifera. Finally, mitochondrial production of metabolic CO_2 might contribute to DIC accumulation in biomineralizing fluid (Bentov et al., 2009).

iv. Implications for geochemical models.

In the SWV or direct seawater input models, the fluid that reaches the biomineralization site is sourced from seawater. However, in this model, the seawater can be manipulated through specific pumps, which can, for example, remove Mg (e.g. Bentov and Erez, 2006) or add Ca. The occurrence of other pumps like the Na-H exchange pump can also impact Li content and Li isotopes in carbonates (e.g. Dellinger et al., 2018; Erez, 2003; Vigier et al., 2015). In the SWV model, as the calcium carbonate precipitates and as elements are incorporated in the solid, the fluid evolves according to a Rayleigh distillation process (e.g. Adkins et al., 2003; Chen et al., 2018; Evans et al., 2018; Gagnon et al., 2007; Gothmann and Gagnon, 2021). By contrast, in the case of a purely TMT model, all trace elements are discriminated against except calcium, leading to a biomineralizing fluid much enriched in Ca and poor in Mg. To this intracellular fluid, some seawater may be added by passive transport – either vacuoles or leaks at the biomineralization site (Nehrke et al., 2013). However, none of those models so far take into account sulfate incorporation and they all rely on inorganically controlled precipitation, while the organic matrix plays a key role in biomineralization. In particular, we will focus next on the role of sulfated glycosaminoglycans.

4. Role of sulfur in the organic matrix, notably sulfated glycosaminoglycans.

The organic matrix plays many critical roles in biomineralizing organisms. The organic matrix act as a template for the precipitating mineral, contributes to controlling which $CaCO_3$ polymorph precipitates and to induce nucleation (e.g. Falini et al., 1996). In foraminifera, the POS acts as the template on which precipitation occurs. In pluricellular organisms, the structuration of the organic matrix is very complex but interactions between calcium carbonate and organic matter is intricate and the matrix also acts as a template (e.g. Addadi et al., 1987; Castro-Claros et al., 2021; Dauphin, 2006; Dauphin et al., 2003a; Falini et al., 2015, 1996; Mass et al., 2013).

In this regard, sulfate plays a central role. Sulfate is present in the sulfated glycosaminoglycans found on the organic linings at the site of calcification in various groups of organisms (Fig. 38; Angell, 1967; Bé et al., 1979; Dauphin et al., 2008; Hemleben et al., 1986; Spero, 1998; Weiner and Erez, 1984). Sulfate (and sulfur) can also occur in coral acid-rich proteins, or CARPs (Addadi et al., 1987; Falini et al., 2015; Mass et al., 2013). In all those molecules, the sulfate groups interact with Ca^{2+} and create a locally enriched environment. By doing so, sulfate-containing molecules contribute to create a very local interactions between the Ca^{2+} and the CO_3^{2-} (or HCO_3^-) ions and thus induce the biomineral nucleation (Falini et al., 1996). A detailed description of the organic matrix in the coral *Stylophora pistillata* reveals that acid-rich proteins are invariably associated with carbonic anhydrase and calcium-binding proteins where spatial arrangements allow highly coordinated interactions that are key to understanding the formation of the aragonitic skeleton (Mummadisetti et al., 2021). Such nucleation has been shown through the in vitro culture of coral or mollusks cells, that produced an extracellular matrix containing sulfated glycosaminoglycans on which aragonite precipitated (Addadi et al., 1987; Helman et al., 2008). Overall, the presence of regularly spaced negatively charged groups able to bind calcium, nucleate $CaCO_3$ precipitation, and thus form a part of the carbonate structure likely contribute to biomineralization in many organisms.

Organic matter may play a role in banding for various organisms, as sulfur banding is often interpreted as reflecting the occurrence of variable amounts of organic matter. However, sulfur and magnesium banding are often associated, and magnesium is usually interpretated as reflecting an inorganic process (e.g. Lorens and Bender, 1980; Paris et al., 2014; Richardson et al., 2019a; Spero et al., 2015; Tanaka et al., 2019; van Dijk et al., 2017).

Proteins containing reduced sulfur are also identified in all calcifying organisms though their role in biomineralization might be less ubiquitous, since they are not as abundant as sulfated molecules in the organic matrix associated to (Cuif et al., 2008; Dauphin, 2006; Dauphin et al., 2005; Perrin et al., 2017; Richardson et al., 2019a; Tamenori and Yoshimura, 2018). For

instance, in avian eggshells, the nucleation sites are spherulitic protein masses organized on the disulfide-linked proteins of the inner shell membrane (Mann, 1988).

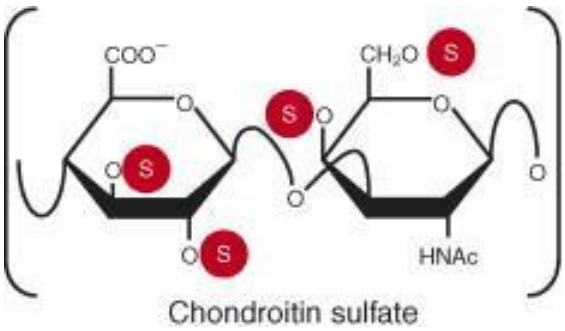

Figure 38. Chondroitin sulfate, an example of sulfated glycosaminoglycan (Uyama et al., 2007)

5. Mineral precursors.

i. "Non-classical" biomineralization.

Most calcitic skeletons are aragonite or calcite, though transient phases have been suggested or observed, such as vaterite or ACC (Amorphous Calcium Carbonate). Under ambient conditions, ACC is kinetically and thermodynamically unstable and easily dissolved (Clarkson et al., 1992), and stable hydrated ACC can be found only in Crustaceans (Addadi et al., 2003). Instead, ACC is usually considered as a way for organisms to store and transport calcium and carbonate ions and as a precursor phase to the final calcium carbonate (Addadi et al., 2003; Baronnet et al., 2008; de Nooijer et al., 2009a; De Yoreo et al., 2015; Gilbert et al., 2022; Jacob et al., 2017; Lowenstam and Weiner, 1989; Mass et al., 2017; Raz et al., 2003). In foraminifera, ACC has been suspected to occur in calcium-rich vesicles as a calcium and DIC storage (de Nooijer et al., 2014, 2009a) and likely occurs as a precursor (Jacob et al., 2017). In corals, hydrated and dehydrated ACC precursors are formed inside the polyp organic tissue as nanoparticles (~400-nm) that later attach to the surface of the skeleton. There, ACC remains amorphous for hours before crystallizing into aragonite (Mass et al., 2017). High-Mg calcite of sea urchin larvae spicules and aragonite of mollusk larvae also precipitate from an ACC precursor inside vesicles before being delivered to the site of calcification (Beniash et al., 1999, 1997; Raz et al., 2003; Weiner et al., 2003).

The existence of precursors has contributed to the development of the "non-classical" biomineralization pathways, where Ca et CO_3^{2-} first interact to form ACC instead of a pathway where calcite or aragonite precipitates directly (Fig. 39; Bots et al., 2012; De Yoreo et al., 2015; Gilbert et al., 2022; Jacob et al., 2008; Mass et al., 2017). The solid can grow through oriented attachment or spherulitic growth and/or dissolution-reprecipitation, ACC evolves first to vaterite or directly to calcite or aragonite and transformation mechanisms can be solid-solid recrystallization or, again, dissolution-reprecipitation (Bots et al., 2012; Giuffre et al., 2015).

The crystal phase is sometimes described to grow through either spherulitic growth or Ostwald ripening but many mechanisms exist (De Yoreo et al., 2015; Gilbert et al., 2022; Jacob et al., 2008).

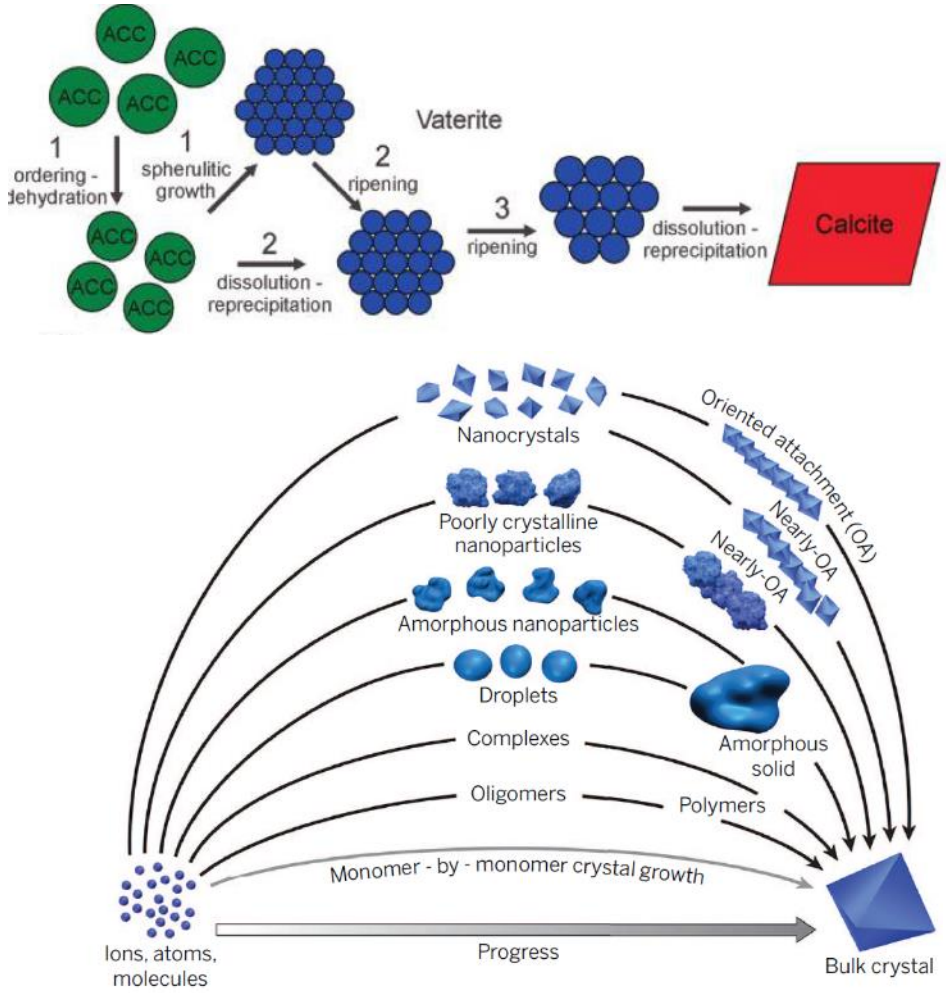

Figure 39. Non-classical (bio)mineralization pathways. Upper panel, the fate of ACC through vaterite formation and ultimate calcite precipitation (Bots et al., 2012). Lower panel: schematic view of possible pathways leading to formation of a mineral (De Yoreo et al., 2015)

III. Carbonate associate sulfate: nature and control.

1. Inorganic experiments.

i. Sulfate incorporation.

As previously presented, CAS are the inorganic sulfate groups that replace CO_3^{2-}, both into inorganic and biogenic $CaCO_3$ minerals as CAS within the growing mineral structure, the larger tetrahedral sulfate substituting to the smaller trigonal-planar carbonate ion (Busenberg and Plummer, 1985; Kontrec et al. 2004; Balan et al., 2014; Tamenori et al. 2014; Perrin et al. 2017; Tamenori and Yoshimura 2018).

Three experiments have been focusing on sulfate concentration in inorganic calcium carbonate minerals with different sulfate concentrations of the solution (Barkan et al., 2020; Busenberg and Plummer, 1985; Fernández-Díaz et al., 2010). Overall, a detailed comparison proves difficult as ion content can be reported as activity (Barkan et al; 2020) or concentration (other studies in Fig. 40) and that the experimental set-ups vary. Nonetheless, general conclusions can be drawn. For each experiment, in inorganic carbonates, the CAS content increases with either $[SO_4^{2-}]$, $[SO_4^{2-}]/[CO_3^{2-}]$ or even $[SO_4^{2-}]/[Ca^{2+}]$. As no experiment decoupling these parameters currently exists, it is difficult to say which one truly dominates the control of sulfate incorporation. Incorporation of sulfate depends on the carbonate polymorph, as has been shown in many inorganic experiments. In similar conditions (experimental set-up, precipitation rate, saturation state) and for a given SO_4^{2-}/Ca^{2+} or SO_4^{2-}/CO_3^{2-} ratio, calcite contains more sulfate than vaterite and aragonite (Barkan et al., 2020; Busenberg and Plummer, 1985; Fernández-Díaz et al., 2010). In addition, for a similar ion activity ratio, the lower the precipitation rate, the less sulfate is incorporated (Barkan et al., 2020; in prep). Because of its actual incorporation in the mineral lattice, sulfate plays many roles in calcium carbonate precipitation.

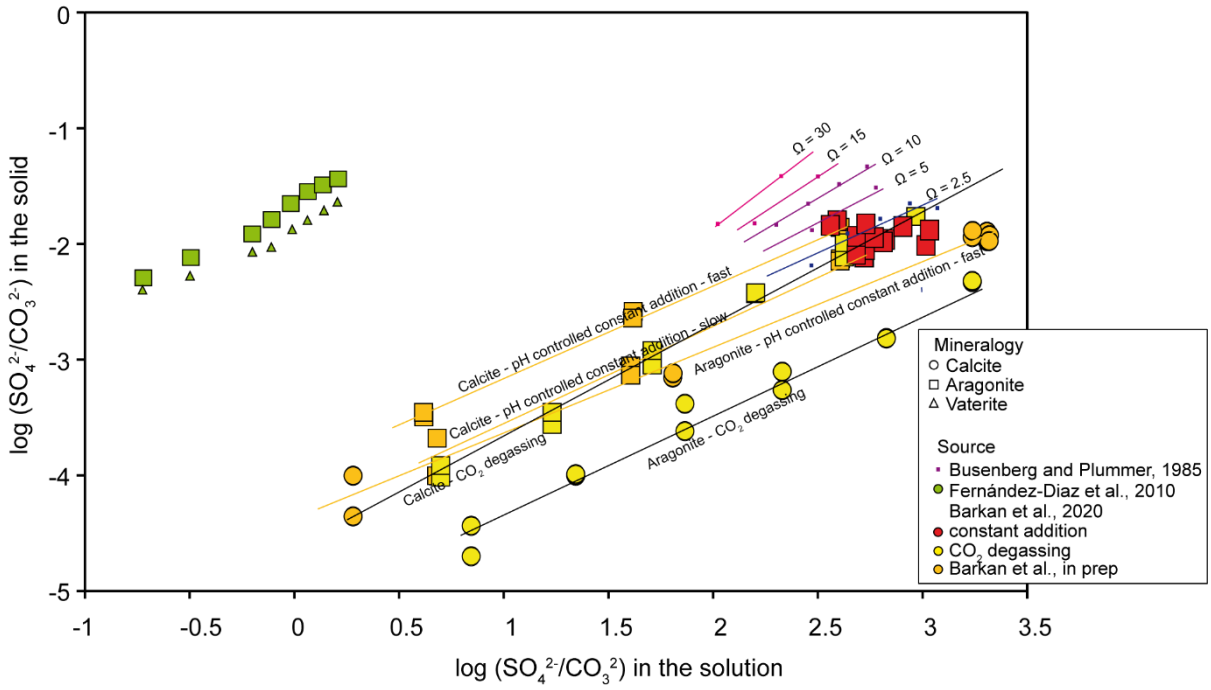

Figure 40. Compilation of different inorganic precipitation experiments, as a function of SO_4^{2-}/CO_3^{2-} ratios, mineralogy, and other experimental parameters, such a saturation state Ω, method of precipitation, and precipitation rate.

ii. Control of sulfate on crystal growth and polymorphism.

The presence of sulfate can impact the type of $CaCO_3$ polymorph grown from a solution. For instance, high sulfate concentrations inhibit calcite formation and lead to aragonite precipitation (Barkan et al., 2020; Bots et al., 2011; Fernández-Díaz et al., 2010; Wang et al., 2012), though sulfate might also inhibit aragonite growth (Mucci et al., 1989). Part of the reason sulfate poisons the growth of calcite might be linked to the change of structure of calcite with sulfate incorporation. The more sulfate is incorporated, the longer of the c-axis of the calcite becomes, and thus distortion of the mineral structure, with bigger cell size (Fig. 41; Barkan et al., 2020; Busenberg and Plummer, 1985; Goetschl et al., 2019; Kontrec et al., 2004) and higher free energy. Calcite becomes more soluble, less stable, and the growth rate decreases with sulfate concentrations above 5 mM in the precipitating solution, suggesting that sulfate also poisons the growth sites (Vavouraki et al., 2008). Finally, a combined effect of both Mg and sulfate has been documented: Mg would inhibit calcite growth more effectively in the presence of SO_4^{2-}, possibly as the result of $MgSO_4$ ion pair formation (Nielsen et al., 2016). Possible explanations are that sulfate promotes Mg^{2+} dehydration, which facilitates Mg uptake by calcite and that the incorporation of the pair is energetically favored compared to Mg^{2+} alone (Nielsen et al., 2016; Sakuma et al., 2014).

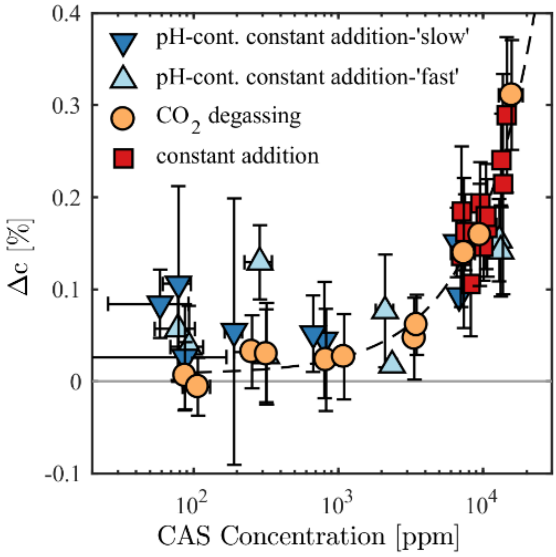

Figure 41. Change in calcite c axis relative to the low-[CAS] CO_2 degassing samples (∆c) as extracted from X-ray diffractograms. The c axis length grows linearly with CAS concentration in the CO_2 degassing and constant addition samples (Barkan et al., in prep).

iii. Sulfate and vaterite.

Sulfate has a contrasting effect on vaterite precipitation since both poisoning of the polymorph and its stabilization have been described (Bots et al., 2012; Fernández-Díaz et al., 2010).

Fernandez-Diaz et al. (2010) investigated the influence of sulfate on vaterite precipitation and stabilization. Vaterite precipitation appears to be favored by increasing SO_4^{2-}/CO_3^{2-} ratios. In addition, despite being unstable, vaterite appears to be stable for a longer time in solutions with SO_4^{2-}/CO_3^{2-} ratios above one. This occurs alongside an increase in the free energy of the crystal lattices of each polymorph (calcite, aragonite, vaterite) with increasing sulfate content. This increase is higher for aragonite than for calcite, suggesting that the substitution of a carbonate by a sulfate group is less favorable in aragonite than in calcite. This substitution is easier in the low-density vaterite and vaterite even appears to be stabilized at sulfate contents smaller than 2.5 mol%. As a result, initial behavior during precipitation of the initial polymorph might be related to kinetic effects due to the high supersaturation state used in this experimental study, but the longer term evolution of the solids is explained by the higher energy difference between vaterite and calcite at higher SO_4^{2-}/CO_3^{2-} ratios (Fernández-Díaz et al., 2010).

Yet, the presence of sulfate leads to the formation of smaller vaterite grains, supporting the idea that sulfate negatively affects vaterite precipitation (Bots et al., 2012). To explain the contrast with results of Fernández-Diaz et al. (2010), the authors suggest that it might not be the result of bulk thermodynamic changes caused by the presence of sulfate but rather due to the adsorption of sulfate. This adsorption would poison the nucleation site, similarly to hat is observed in calcite (Vavouraki et al., 2008)

iv. $CaCO_3$ polyamorphs.

To this day, very little is known about sulfate incorporation in ACC. In organic ACC, with up to almost 6 mol % Mg, the presence of sulfate is possible and interpreted either as organic-bound sulfate associated to the macromolecules of the organic sheath (Aizenberg et al., 2002) or as inorganic sulfate incorporation (Fichtner et al., 2018). Inorganic ACC precipitation experiments reveal that the Mg and CO_3^{2-} activities of the solution plays a role in the nature and stability of the ACC that precipitates, as well as in the determination of the subsequent polymorph that forms (e.g. Blue et al., 2017; Loste et al., 2003). Nevertheless, the nature of the subsequent polymorph cannot be predicted based on the nature of the ACC alone (Cartwright et al., 2012). The role of sulfate ions remains an understudied question, though existing investigations suggest that ACC formation and stability is not influenced by sulfate (Aizenberg et al., 2002; Bots et al., 2012).

2. CAS content and control in biogenic carbonates.

i. CAS content in biogenic carbonates.

We recently submitted a manuscript for publication in Biogeosciences to investigate the question of sulfate incorporation in biogenic carbonates, investigating the case of a benthic foraminifera (Thaler et al., preprint). Part of the data in this manuscript also comes from an ongoing survey study of S and Ca isotopes from carbonates we previously investigated for lithium isotopes during Matthieu Dellinger's postdoctoral work at USC (Dellinger et al., 2018). S isotope samples were analyzed at CRPG using the Neptune + MC- ICP-MS, while Mg/Ca and SO_4/Ca ratios were measured on a X-series II MC- ICP-MS and a Metrohm ICS 300, respectively (see Jouini et al., 2023 for more details). For the samples presented in Fig. 42, which include new and previously published data, different cleaning protocols have been applied. Samples from this study were cleaned for 24h in high purity water with 10 % NaCl and regularly sonicated to remove water-soluble phases, and then rinsed two times with the NaCl solution and three with HPW, using a cleaning after simplified after Present et al. (2015). Kampschulte et al. (2001) added a 15 min leach in H_2O_2 to the NaCl cleaning and no cleaning is mentioned by Busenberg and Plummer (1985). As a result, except for Busenberg and Plummer's data, all samples had water-soluble sulfate removed.

In biogenic carbonates, there is a first order control of the polymorph precipitated by the organism (Fig. 42). Calcite is usually more concentrated in sulfate than aragonite, in agreement with inorganic experiments. The highest sulfate concentrations are found in high-Mg calcite such as echinoderms and some foraminifera species, while organisms susceptible to precipitate both calcite and aragonite, such as the mollusks *Chione californiensis*, *C. subrugosa*, *C. subimbricata*, *Mytilus californianus*, *Chlamys squamosus* and *Tridacna maxima* tend to be characterized by low sulfate contents, even if they mostly precipitate calcite.

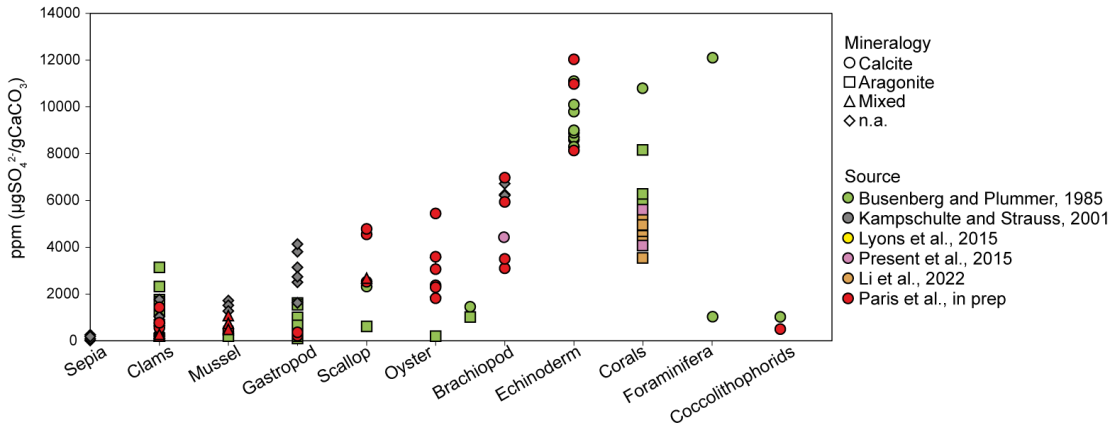

Figure 42. CAS content measurement in different publications by groups of organisms, as a function of mineralogy.

Despite the ion concentration of sulfate in the modern ocean, ~28 mmol/L, that inhibits calcite growth in inorganic calcium carbonate experiments, many organisms are able to biomineralize calcite. Moreover, the calcite they precipitate is significantly less concentrated in sulfate than its inorganic counterpart at 28 mmol/L of sulfate in seawater (e.g. Barkan et al., 2020; Busenberg and Plummer, 1985). However, this conundrum can be explained partly by a seawater SO_4^{2-}/CO_3^{2-} ratio near 315 (Barkan et al., 2020), which allows calcite precipitation, with CAS content between 6000 and 8000 ppm.

Coccoliths, the calcite plate secreted by coccolithophorids, are a clear exception, with very low sulfate concentration. This exception might be linked to the specific biomineralization pathway of those algae, possibly the only organism studied here with intracellular biomineralization, assumed to rely entirely on the TMT model.

ii. SO_4^{2-}/Ca ratios in calcite: carbonate ion control?

The sulfate concentration of foraminifera has been proposed as a proxy for the carbonate ion concentration in seawater, based on the substitution of CO_3^{2-} by SO_4^{2-} groups (Boyle et al., 2002). While recent culture experiments with foraminifera support this idea, it also appears that sulfate concentrations in foraminifera are sensitive to other seawater parameters. For example, two culture experiments focused on variations of sulfate concentrations in artificial seawater solutions, showed that to the first order, CAS content of foraminifera tests follows the sulfate concentration of seawater, or the SO_4^{2-}/Ca ratio (Paris et al., 2014b; Thaler et al., preprint; Fig. 43). On the other hand, experiments in which seawater CO_3^{2-} was varied found that the CAS content of the foraminiferal calcite follows the SO_4^{2-}/CO_3^{2-} ratio of the seawater at a given sulfate concentration of seawater (van Dijk et al., 2017).

Indeed, part of the reason why foraminifera may be able to readily precipitate calcite despite the high sulfate concentration of seawater could be the organism ability to increase the CO_3^{2-} concentration of the biomineralization fluid, thus reducing the SO_4^{2-}/CO_3^{2-} ratio of the solution (e.g. Yoshimura et al., 2014). Calcite is then more likely to precipitate despite high sulfate concentrations (Barkan et al., 2020).

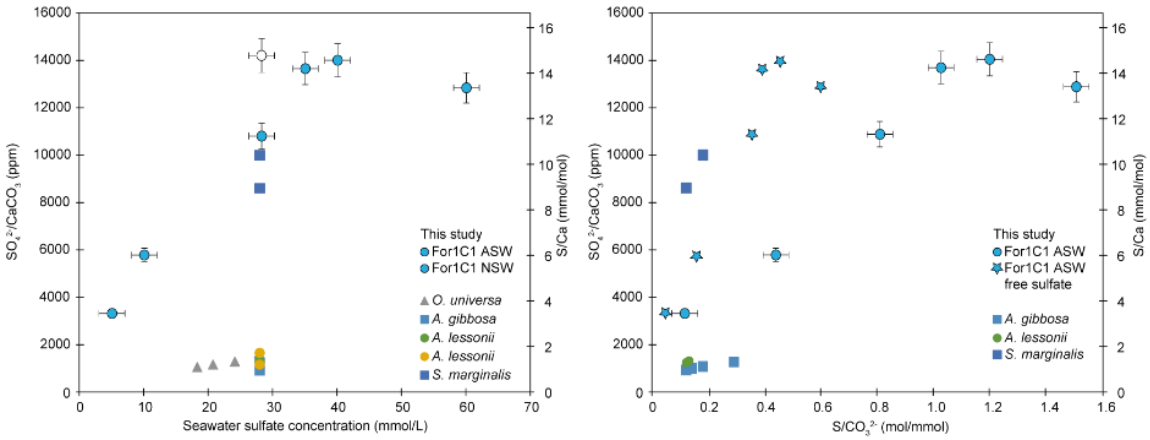

Figure 43. Left panel: $SO_4^{2-}/CaCO_3$ and S/Ca ratios on tests of the For1C1 strain at the end of SET1 and SET2 experiments, as a function of seawater [SO_4^{2-}]. Right panel: $SO_4^{2-}/CaCO_3$ and S/Ca ratios on tests of the For1C1 strain at the end of SET1 and SET2 experiments, as a function of seawater S/CO_3^{2-} . For our experimental results, we report the values using both S as the sum of free and complexed sulfate based on our model results (circles), and as free sulfate only (stars). Values are compared to other culture experiments (Paris et al., 2014: van Dijk et al., 2017; 2019).

A growth experiment of the coral *Pocillopora damicornis* was performed at different SO_4^{2-}, Ca^{2+} and Mg^{2+} revealed that the incorporation of sulfate in the skeleton of this organism was related not only to the sulfate concentration, but also to that of calcium and magnesium of seawater (Giri and Swart, 2019; Fig. 44). The authors related this co-influence of calcium on the need for the coral to pump less calcium into the biomineralizing fluid, with less protons being pumped out in return, and thus a lower pH and carbonate ion increase for a similar saturation state at the time of precipitation. This result however reveals that the control by the SO_4^{2-}/CO_3^{2-} ratio of seawater is only modulated by the biological activity of the organism to induce or control calcium carbonate precipitation. It must be noted however that the distribution coefficient of sulfur in this study is normalized to the calcium concentration of the skeleton and the seawater and not the carbonate ion concentration.

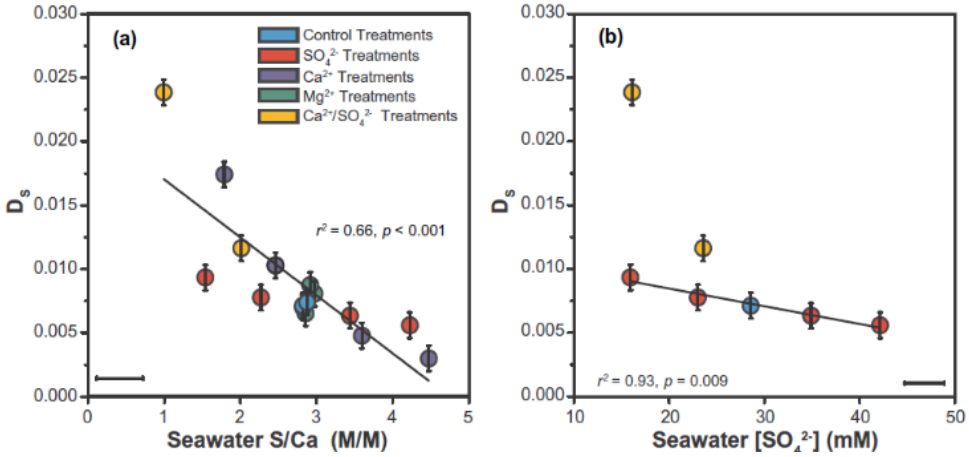

Figure 44. Experimental results for corals grown in artificial seawater with different Mg, Ca, and sulfate concentrations (Giri and Swart, 2019)

iii. Small scale variations and interaction with Mg.

In addition to the control linked to the (biologically controlled) fluid chemistry, there is likely a biological control on sulfate incorporation as Mg and S correlate both at small and bulk scale in biogenic calcium carbonates (Fig. 45 and 46). Overall, many biocalcifiers (including mollusks, brachiopods and foraminifera) display variations in sulfur content at the micron-scale (Cusack et al., 2008; Dauphin et al., 2003a; Erez, 2003; Fichtner et al., 2018; Lorens and Bender, 1980; Paris et al., 2014b; Tanaka et al., 2019; van Dijk et al., 2019, 2017; Fig. 45).

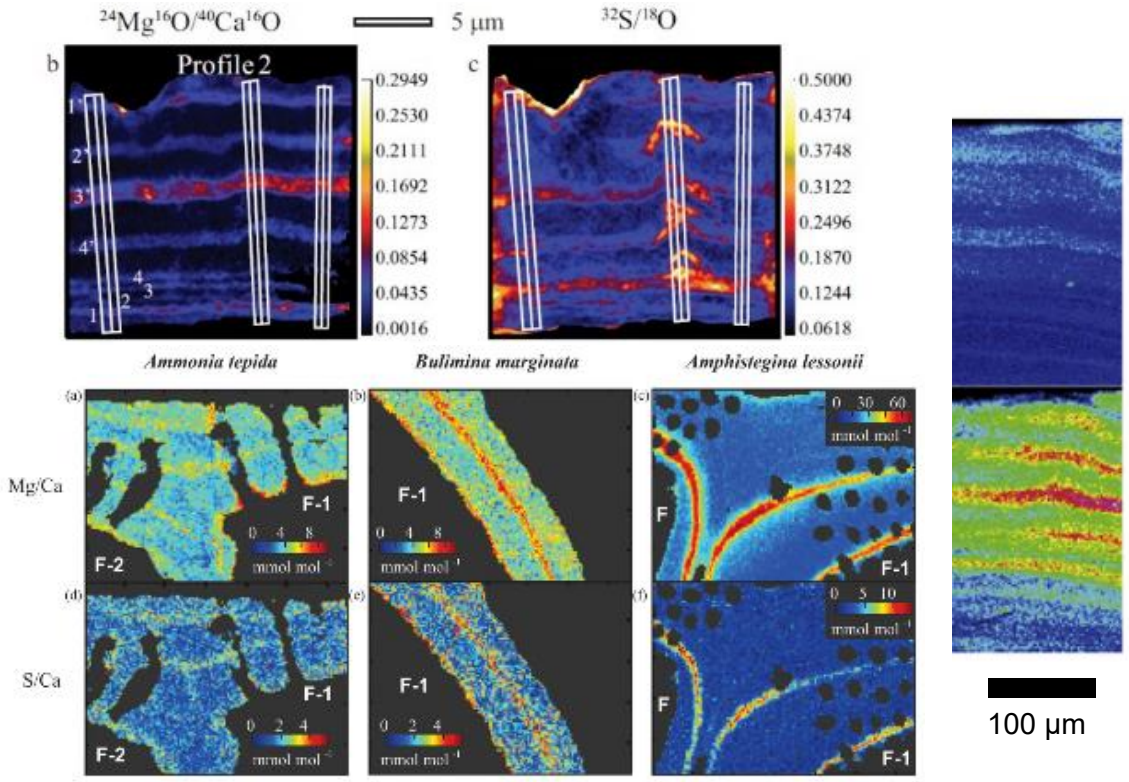

Figure 45. examples of small scales covariation of S and Mg in foraminifera and brachiopods. Upper left: O. universa (Paris et al., 2014), bottom left: three different benthic foraminifera (van Dijk et al., 2017), right: Mytilus galloprovincialis (Tanaka et al., 2009)

In some cases, these variations are interpreted as the occurrence of S-rich organic matter in association with higher inorganic Mg content, or even with organic-associated Mg, while other authors interpret the variations as a co-occurrence of sulfate and magnesium in the mineral lattice.

The correlation is also observed at the bulk scale (Fig. 46). Indeed, there is an overall relationship between the sulfate and the magnesium content of biogenic carbonates. Calcite rich in magnesium is also rich in sulfate. A crystal lattice distortion effect could explain this correlation. Indeed, the presence of Mg in the crystal lattice encourages the incorporation of more trace elements (such as Sr) in the calcite (Mucci and Morse, 1983). Similarly, more Na

is included in calcite with more SO_4^{2-} groups (Busenberg and Plummer, 1985). This could suggest that the presence of Mg allows calcite to accommodate more SO_4^{2-} or the opposite (Burdett et al., 1989; Nielsen et al., 2016; van Dijk et al., 2019). However, this hypothesis seems to not hold for low-Mg calcite. Indeed, synthetic calcite experiments revealed that the c-axis extension induced by SO_4^{2-} incorporation produces calcite with a larger unit cell, unfavorable for incorporating smaller Mg ions substituting for Ca (Goetschl et al., 2019).

Without invoking distortion effects, concomitant changes in precipitation rates and temperature could explain the increased incorporation of both Mg and sulfate as the former is more readily incorporated at lower temperature and the latter is more concentrated in carbonates precipitated at higher precipitation rates (Barkan et al., 2020; Busenberg and Plummer, 1985). Mg/Ca banding is also related to the diurnal activity of the foraminifera and high Mg/Ca bands form at night in *Neogloboquadrina dutertrei*, even at constant temperature and pH (Fehrenbacher et al., 2017). As mentioned previously, physiological control may drive variations of Mg/Ca, but it has not yet been investigated whether this same physiological control can explain the observed sulfate banding.

There are situations where the correlation between Mg and SO_4^{2-} breaks down. For example, the SO_4^{2-}/Ca ratio of the cultured benthic foraminifera *Amphistegina lessonii* is not sensitive to temperature, whereas the Mg/Ca ratio does display a temperature sensitivity (van Dijk et al., 2019). Such differing behaviors indicate independent controls for Mg and sulfate. The different temperature sensitivities may be explained if the reactive Mg species in the solution is $MgCO_3$, whose activity changes with temperature and pH, unlike SO_4^{2-} (van Dijk et al., 2019). However, sulfate also makes different complexes in solution and free sulfate is not necessarily the dominant species, especially in the presence of Mg (Barkan et al., 2020; Thaler et al., preprint). It is however so far unclear if ion pairs or only ions are incorporated, and if incorporation of ion is sensitivity to only the activity of the free ion in solution or that of the ionic complex or pair.

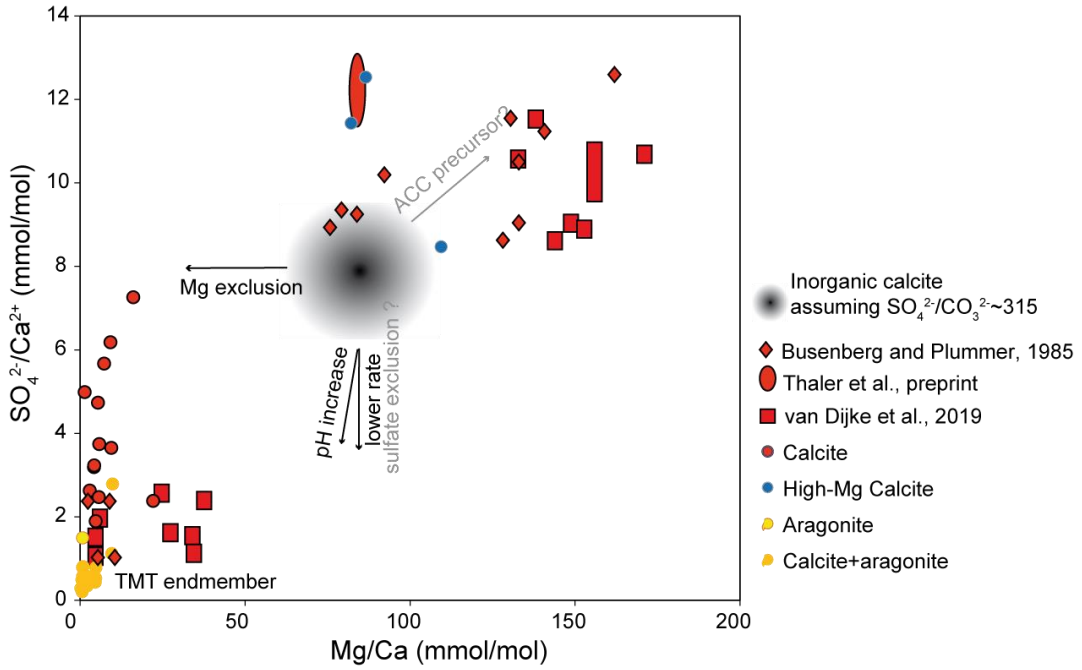

Figure 46. Relationship between SO4/Ca (mmol/mol) and Mg/Ca (mmol/mol) ratios for different organisms.

3. Models for CAS content control in biogenic carbonates

It might be possible to think about the controls of each element based on the SWV and TMT models, as well as the local control of the fluid composition at the site of calcification. Revisiting the model of van Dijk et al. (2019) for sulfate and magnesium incorporation, three scenarios can be outlined (Fig. 46).

i. *SWV dominated scenario*. In the course of a seawater vesicle's journey inside the cell, its Mg/Ca ratio will be actively lowered, and SO_4^{2-}/CO_3^{2-} is lowered due to an increase in pH in the vacuoles. Little is known about active SO_4^{2-} control by ion pumps or channels, though it has been suggested as a possibility (Thaler et al., preprint). The SWV dominated control would then lead to covariations of S and Mg content of the shell, though the exact trend would depend on the respective rates of Mg and proton pumping.

ii. *TMT dominated scenario* In the TMT model, the transport of Ca^{2+} through Ca channels to the site of calcification, only the Mg/Ca would be lowered, according to van Dijk et al. (2019). Mg might occasionally be accidentally pumped through the Ca channels (Nehrke et al., 2013). As a result, no effect on the SO_4^{2-}/CO_3^{2-} of the solution is expected. However, the SO_4^{2-}/Ca ratio would be lowered, and as mentioned previously, no experiments tried to decouple the influence of the variation of either. SO_4^{2-}/CO_3^{2-} or SO_4^{2-}/Ca^{2+}. In addition, if Mg and sulfate are incorporated in calcite through seawater leaks at the site of calcification, as both ions are present in seawater, a covariation of Mg and S would be expected (Nehrke et al., 2013). Finally, Ca and proton pumping can be coupled in a single pump. As a result, Ca-pumping

would also lead to an increase in alkalinity and to a decrease in the SO_4^{2-}/CO_3^{2-}ratio of the biomineralizing fluid. Therefore, there could even be an anticorrelation in Mg/Ca and SO_4^{2-}/CO_3^{2-}ratios of the precipitating calcium carbonate.

iii. Proton pumping scenario. Pumping protons out of the site of calcification (Toyofuku et al., 2017) will increase the fluid alkalinity and thus its pH and CO_3^{2-} concentration. According to van Dijk et al. (2019), the following increase in $[CO_3^{2-}]$ will lower SO_4^{2-}/CO_3^{2-} values in the site of calcification and lead to less sulfate incorporation. However, it could also lead to lower Mg/Ca ratios, as higher pH sometimes (but not always) leads to less Mg incorporation (Dissard et al., 2010; Russell et al., 2004; Spero et al., 2015). In a proton pumping scenario, both sulfate and Mg could also covary, and a diminution of the carbonate ion concentration from 300 to 150 µmol/L would lead to a Mg/Ca multiplied by two or less and a SO_4^{2-}/Ca multiplied by up to 1.5 (Russel et al., 2004; van Dijk et al., 2019).

As can be seen in Fig. 46, some foraminifera, and echinoderms, produce high Mg and high sulfate calcite, while coccoliths produce low-Mg and low-sulfate calcite, and the scenarios above don't seem to explain all the possible variations observed in nature, compared to a hypothetic synthetic calcite. This endmember is based on the results from Mucci and Morse (1983) and Barkan et al. (2020), assuming that the ambient SO_4^{2-}/CO_3^{2-} is around 315. However, this is only hypothetical as the sulfate incorporation during inorganic experiments occurred in synthetic solutions different from seawater. Calcitic mollusks and low-Mg foraminifera on the other hand, produce a relatively low-Mg calcite in which sulfate concentrations increase faster than Mg. based on the above scenarios, this could be explained by the SWV model in which Mg is more efficiently removed than sulfate, or in which Mg removal is less fast than carbonate ion increase.

As a result, additional mechanisms could be invoked, such as differences in precipitations rates, given that lower rates result in lower sulfate incorporation (Barkan et al., 2020, in prep; Busenberg and Plummer, 1985). Additionally, although hypothetical thus far, sulfate may be excluded from SWVs (Thaler et al., preprint). Finally, there may be a yet underappreciated role of ACC precursors. ACC is rich in trace elements and Mg and when it evolves into calcite, even through dissolution-reprecipitation, the final calcite is richer in Mg than if it had precipitated directly from seawater (Blue et al., 2017; Blue and Dove, 2015; Evans et al., 2020; Han et al., 2013; Wang et al., 2012). Yet sulfate in ACC remains to be investigated. If we assume however that ACC is also rich in sulfate, then incorporation of some ACC or crystallization of calcite from an ACC precursor might generate a Mg and sulfate rich calcite.

4. Conclusion

Sulfate plays many roles in calcium carbonate precipitation. It is incorporated as sulfate groups that substitute for carbonate ions in the mineral lattice. Sulfate is more readily incorporated in calcite than vaterite or aragonite and increases the length of the c-axis and the size of calcite cell. As a result, it is an anion that contributes to inhibit calcite precipitation, and to favor aragonite, vaterite or even ACC precipitation. Sulfate concentrations in inorganic calcite depend on the SO_4^{2-}/CO_3^{2-} ratio of the solution as well as the precipitation rates, to a lesser extent.

We haven't sufficiently explored and understood sulfate incorporation in ACC yet and we need to better test whether sulfate incorporation is controlled by SO_4^{2-} activity itself, solution SO_4^{2-}/Ca^{2+} ratios, and/or SO_4^{2-}/CO_3^{2-} ratios. Further work on sulfur in inorganic calcium carbonate should thus focus on these questions.

In biogenic carbonate, polymorphism controls the CAS content. Further control is related to biogenic control of the biomineralizing fluid. Increase of $[CO_3^{2-}]$ is likely to decrease the CAS content of the biocarbonate as it decreases the SO_4^{2-}/CO_3^{2-} of the fluid. However, similarly, to control of the Mg content of the fluid through active Mg-exclusion could suggest that by analogy, sulfate is also actively excluded.

In order to further explore sulfate behavior during biomineralization, and to understand the role CAS can play as an archive of past $\delta^{34}S_{sw}$, the $\delta^{34}S$ of CAS must also be explored, both in abiotic and biogenic carbonates.

IV. Sulfur isotope composition of carbonates.

We established that sulfate concentration in biogenic carbonates results from a combination of inorganic and organic processes. Sulfur isotope fractionation between seawater and carbonate is an equally critical question to understand the reliability of CAS as a past seawater archive and to understand if vital effects explain the variability of CAS compared to barite or evaporite, as detailed in Chapter III. If the behavior of sulfur isotopes is also a combination of inorganic and organic processes, they can help us better understand the mechanisms of S incorporation in biominerals and in return, this improved understanding will allow us to make CAS a more reliable archive.

1. Sulfur isotopes in inorganic carbonates.

Barkan et al. (2020; in prep) provide the only documentation thus far of sulfur isotope fractionation measured in inorganic calcium carbonate precipitation experiments (with both calcite and aragonite). Both polymorphs show positive S fractionations relative to seawater. Additionally, for calcite only, the magnitude of this fractionation is related to the amount of

sulfate incorporated in the mineral, itself reflecting the sulfate concentration of seawater. Over almost three orders of magnitude of sulfate concentrations in the solution as well as in the carbonate, the fractionation decreases by 1.5 ‰ (Fig. 47).

In addition, the fractionation between calcite and aragonite depends on calcite precipitation rate, with a 0.5 ‰ change in fractionation over two orders of magnitude of rate changes.

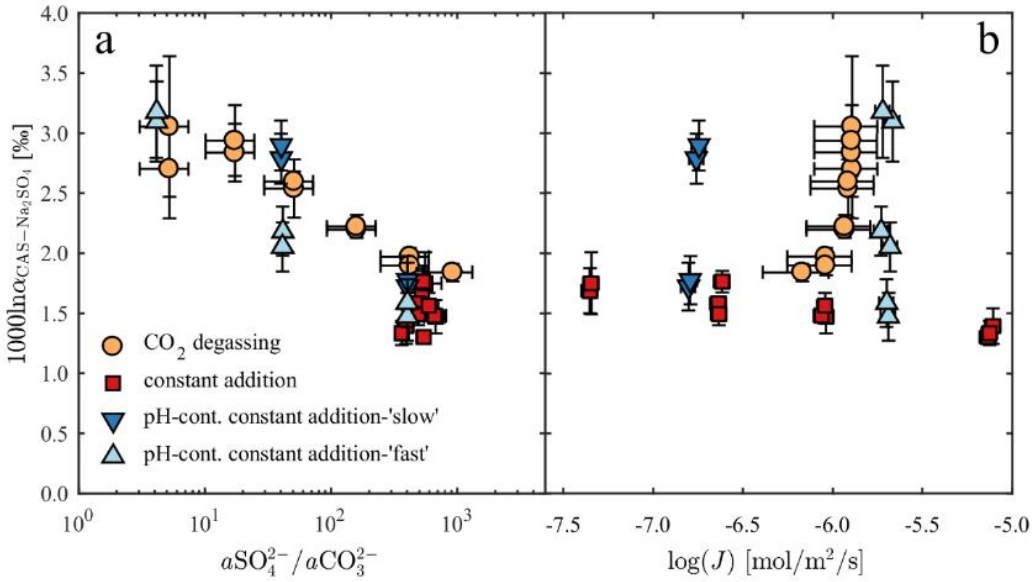

Figure 47. Fractionation between CAS and seawater sulfate ($1000\ln\alpha_{CAS\text{-}Na_2SO_4}$) of inorganic calcite samples versus (a) aSO_4^{2-}/aCO_3^{2-} and (b) log(J) (with J the surface specific rate) of the three experimental methods. The results of the CO_2 degassing and constant addition experiments are from (Barkan et al., 2020) while the pH controlled constant addition are from Barkan et al. (in prep). Figure from Barkan et al. (in prep).

Very little estimates of biogenic carbonate precipitation rates exist. For instance, based on the observations of de Noojier et al. (2009a), 3.6×10^{-10} mol of $CaCO_3$ precipitate in less than 3 hours on a sphere with a ~25 µm radius. The calculated rate is $\sim 5.5 \times 10^{-6}$ mol/m^2/s, comparable to the highest rates in our experiments. In the lack of additional constraints, we use nonetheless the equilibrium fractionation value as the inorganic endmember for calcite, for an aSO_4^{2-}/aCO_3^{2-} ratio within the range of modern seawater values. Though the range of experimental rate values in our study makes it delicate to fully constrain the kinetic isotopic fractionation endmember, we suggested an equilibrium fractionation factor close to 1.7 ± 0.2 ‰ (Barkan et al., 2020). The proposed equilibrium fractionation factor measured for aragonite is slightly lower, with a value of 1.0 ± 0.2 ‰.

2. Biogenic carbonates.

i. Survey of various organisms.

Many studies have focused on measuring sulfur isotopes in carbonates to reconstruct past seawater $\delta^{34}S$ values. Overall, modern biogenic carbonates (including calcites and aragonites) record the seawater isotope ratio of sulfate-sulfur, within 2 ‰. The range is even narrower considering only the most recent investigations. We extended the range of carbonates studied using the samples previously analyzed by Dellinger et al. (2017) and cleaning them overnight in a 10 ‰ NaCl solution, thus following a slightly modified protocol compared to Present et al. (2015). The results are presented in Fig. 48.

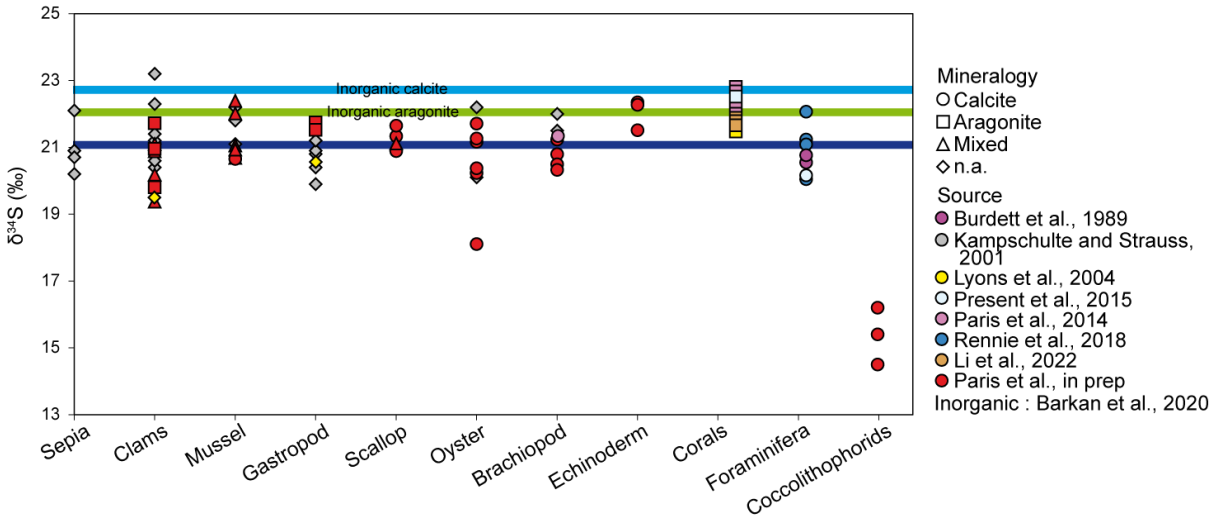

Figure 48. Values of $\delta^{34}S_{CAS}$ measured in different biogenic carbonates (Paris et al., in prep)

Most organisms had $\delta^{34}S$ compositions that are close to the value of seawater and most of them are less fractionated than their inorganic equivalent. Aragonitic samples tend to be close to the inorganic aragonite value whereas some calcitic biomineral samples display much lower isotopic compositions than their inorganic counterpart. In the case of coccolith calcite, the low $\delta^{34}S$ observed is likely a result of the coccolithophore's intracellular biomineralization pathway, which causes sulfur present in carbonate to be derived from an intracellular pool of sulfur rather than from vacuolized seawater. The oyster sample with a much lower isotopic composition (*Crassostrea gigas*) grew in seawater with a salinity of 21. As a result, it is possible that the sulfate bears a $\delta^{34}S$ value different from the global ocean.

Sulfur isotopes can be expressed in terms of fractionation from the inorganic mineral that would have precipitated We can calculate a vital effect fractionation, hereafter ε_{vital}, after Dellinger et al. (2017), defined as follow:

$$\varepsilon_{vital} = \delta^{34}S_{carb} - (\delta^{34}S_{sw} + \varepsilon_{ara} \times \%ara + \varepsilon_{cal} \times \%cal),$$

where $\delta^{34}S_{carb}$ is the sample $\delta^{34}S$ value, %ara and %cal the relative fractions of calcite and aragonite measured by XRD, ε_{ara} is + 1.0 ‰, the fractionation between seawater and inorganic aragonite and ε_{cal} is + 1.7 ‰, the fractionation between seawater and inorganic aragonite (Fig. 49).

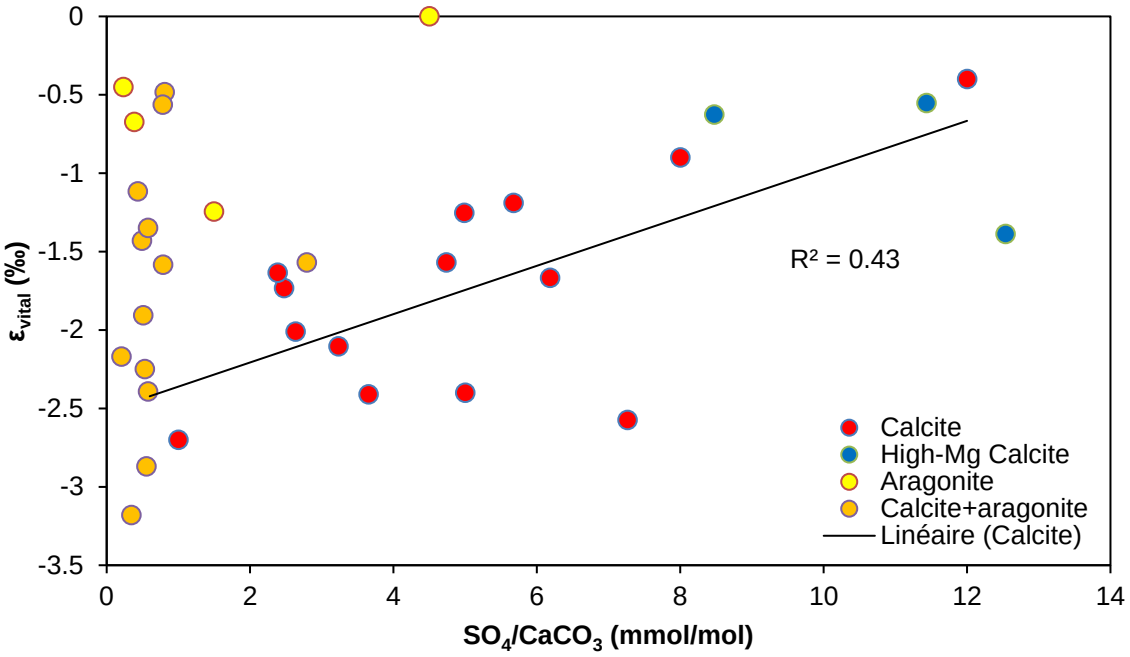

Figure 49. Relationship between ε_{vital} and CAS content as a function of mineralogy in different biogenic carbonates (Paris et al., in prep)

ii. Determination of vital effects, implications for paleoenvironmental reconstructions.

In order to understand organism-specific fractionations for foraminifera, I have played a key role in developing two different calibrations. One calibration consisted of measuring $\delta^{34}S$ in the planktic foraminifera *Orbulina universa* grown in artificial seawater (Paris et al., 2014b). Another focused on benthic foraminifera, also grown in artificial and natural seawater (Thaler et al., preprint). In both cases, a constant fractionation was observed as either a function of $\delta^{34}S_{sw}$, of ~- 1 ‰ for the former and +1.5 ‰ for the latter, at different either SO_4^{2-}/Ca^{2+} or SO_4^{2-}/CO_3^{2-} ratios; Fig. 50).

These results are important for paleoenvironmental reconstructions as they suggest that despite variability in the fractionation factor across different organisms, a given organism has a constant vital effect, regardless of the pH and sulfate concentration of the ocean. For this reason, reconstruction of seawater $\delta^{34}S$ should rely on species-specific carbonate samples.

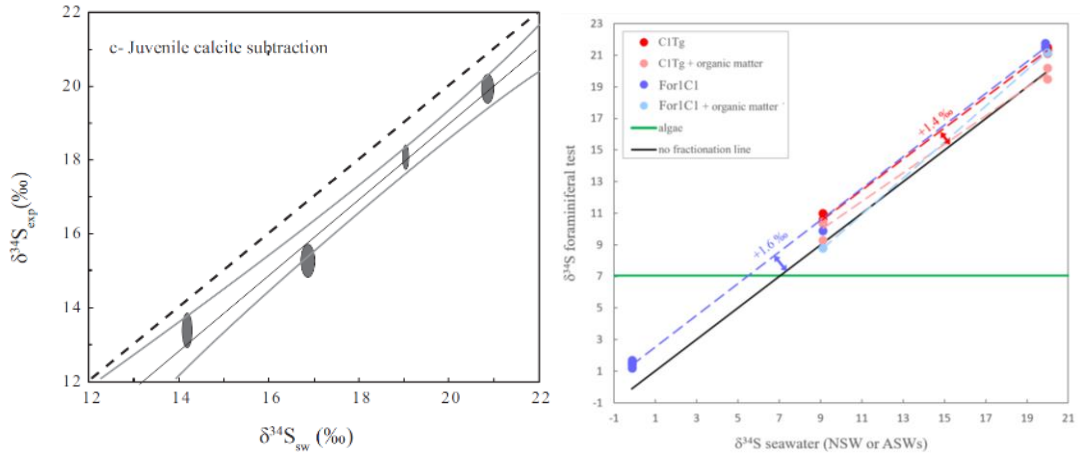

Figure 50. Species-specific calibration of vital effect for sulfur isotopes in O. universa (left, Paris et al., 2014) and Rosalina species (right, Thaler et al., preprint)

Whether considering biogenic calcium carbonates produced by different genera or species-specific vital effects, biogenic calcium carbonates usually demonstrate isotopically lighter $\delta^{34}S$ than what is expected based on inorganic precipitation experiments. Additionally, the range of $\delta^{34}S$ values in biocarbonates is far too big to be explained by changes in precipitations rates, which could explain at best variations of the order of ~0.5 ‰. In addition, lower rates would generate calcite with both less sulfate and with more positive sulfur isotope fractionation, the opposite trend to that observed in Fig. 49. The range in $\delta^{34}S$ is also unlikely to be explained by changes in the SO_4^{2-}/CO_3^{2-} ratio of the solution, as lower ratios would generate calcite with even more positive values (Barkan et al., 2020), much like lower rates. In this case, if the isotopic control is different from what happens in inorganic calcite, and too big to be explained by kinetic effects, how can we explain this difference?

3. Control of the sulfur isotope ratio of biogenic carbonates.

i. Contribution of organic matter?

In most studies of sulfur in biogenic carbonates, the authors attempt to remove all contaminating organic matter. For example, in studies of *O. universa* and *Rosalina* sp., Paris et al. (2014) and Thaler et al. (preprint) performed a NaOCl cleaning step, after having cracked open the tests of *O. universa*. In Thaler et al. (preprint), we also attempted to oxidize all organic matter so that organic-associated sulfur could be collected and analyzed as sulfate. The results showed that overall, the sulfur isotope ratio measured was lowered, suggesting the oxidized organic sulfur was isotopically lower than seawater.

This result is consistent with the processes related to sulfur incorporation in amino acids. Indeed, this assimilatory sulfate reduction, similarly to MSR, generates a reduced sulfur with lower isotope ratios, fractioned by up to -5.5 ‰ compared to the initial sulfate (Fichtner et al.,

2018; Kaplan and Rittenberg, 1964). Reduced sulfur thus likely bears a lower isotopic composition than seawater, which is coherent with our own observations. Fichtner et al. (2018) also analyzed the sulfur isotope ratio of water-soluble sulfate extracted from the shell of the bivalve *Arctica islandica* and found a $\delta^{34}S$ value of ~17‰, lower than the CAS value of ~21 ‰. This observation would suggest that water-leachable sulfate represents the sulfate from the glycosaminoglycans previously described is fractionated compared to seawater, but easily removed from the carbonate before isotopic analyses. Indeed, aqua regia digestion of NaCl-cleaned *Terebratulina transversa* revealed no difference with HCl digested shell parts (Present et al., 2015). This can be explained by a thorough removal of water-soluble sulfate by the cleaning process and a very low contribution of reduced sulfur present in organic matter, either because it is present in low amounts, or because even aqua regia did not manage to dissolve and oxidize it. On the other hand, acid-insoluble organic matter is harder to remove, but would not be dissolved during acid digestion of the sample.

ii. A role for mineral precursors?

Another possibility to explain the variability in biogenic carbonate $\delta^{34}S$ is the incorporation of sulfate within ACC before crystallization of calcite or aragonite. This is however impossible to determine, as no data exist so far for sulfate incorporation in ACC or vaterite.

Figure 51. An example of geochemical differences between calcite precipitated directly from the fluid, or through an ACC precursor (Mavromatis et al., 2017)

A possible analogy can be made with the measurement of Mg isotope fractionation over the course of ACC precipitation and transformation into calcite (Mavromatis et al., 2017; Fig. 51). These experiments reveal that the final signature of calcite depends on whether it is directly precipitated as calcite (-2 ‰ kinetic fractionation) or precipitated first as ACC that evolved to calcite (-3.6 ‰ total fractionation). In the second case, the fractionation is dominated by the equilibrium value for Mg isotope fractionation between calcite and the fluid at high Mg concentrations, the isotopic signature acquired during ACC formation is not preserved (Mavromatis et al., 2017). This observation is consistent with a mechanism of dissolution-

reprecipitation to explain the transformation from ACC to calcite (Blue et al., 2017; Giuffre et al., 2015). As a result, if we assume that the same is true for sulfate, organisms relying on ACC precursor, such organisms could be much closer to the -1.7 ‰ fractionation value that possibly represents equilibrium for inorganic calcite (Barkan et al., 2020), or even more fractionated if ACC precipitation involves an additional fractionation step.

iii. A role for sulfate exclusion?

The calcitic organisms do appear to evolve between a low sulfate endmember that is more fractionated compared to the expected inorganic calcite, and a sulfate rich endmember that appears to be closer to the equilibrium value. The fractionated endmember reaches approximately ε_{vit} = - 3 ‰. Organisms with mixed mineralogy, mostly mussels and oysters, follow a different trend, though the range of fractionation is identical. Only aragonitic samples seem to be overall closer to the inorganic endmember independently of the sulfate content.

Focusing solely on calcitic biomineralizers (and in particular foraminifera), if we assume that the sulfate content of the carbonate depends only on the SO_4^{2-}/CO_3^{2-} ratio, the range of CAS content would call for major differences in carbonate ion concentrations in the biomineralization fluid, even between foraminifera. However, a change in sulfate concentration could also be at play. An intriguing observation is the ~ - 2.5 ‰ ε_{vit} value for calcite incorporating the least sulfate, which is actually very close to the fractionation associated to the sulfate pumping that occurs in MSR organisms (e.g. Rees et al., 1973). Sulfur isotopes in CAS could provide an indirect observation constraining the existence of a biological control of sulfate concentration in the biomineralizing fluid.

V. Conclusion.

Sulfur is a key element in biomineralization. It is present mostly as inorganic sulfate but also occurs as sulfate bound to glycosaminoglycans that play a major role during biomineralization. Organic sulfur molecules can locally increase the saturation state of a solution with respect to calcite and/or aragonite, can act as a template for Ca^{2+} and CO_3^{2-} ions, and contribute to facilitate and control aragonite and calcite precipitation. Reduced sulfur is also present in amino acids but is usually much less abundant than organic sulfate in XANES investigations.

Inorganic sulfate content is controlled first by the SO_4^{2-}/CO_3^{2-} activity ratio of the solution, though it has not been demonstrated that the SO_4^{2-}/Ca^{2+} activity ratio is without influence. S content is also controlled by precipitation rate. Finally, solution sulfate concentrations govern the nature of the polymorph that precipitates and contributes to stabilizing vaterite.

Overall, variations of sulfate content from one species of biomineral carbonate to the other could be explained by inorganic processes following physiologically induced changes in CO_3^{2-}

concentrations in the biomineralizing fluid, but also by the precipitation of ACC precursor, or active sulfate exclusion.

Modern biogenic carbonates are characterized by sulfur isotope ratios close to that of seawater. They are thus a potentially good archive for reconstructing past changes of seawater $\delta^{34}S$, provided that the samples that are used are monospecific. However, the isotope ratios of biogenic calcite are different from inorganic calcite, which is unlikely to be explained by a contribution of the isotopically lower water-soluble organic bound sulfate but could maybe result from varying levels of active sulfate exclusion.

In conclusion, vital effects affect the sulfur isotope ratios of biogenic carbonates, but we produced calibrations revealing that the fractionation between seawater sulfate and CAS is constant for a given species, at least for the two foraminifera investigated. Therefore, in order to use CAS as an archive, monospecific samples are necessary, which is what we targeted for the Cenozoic record produced by Vicky Rennie (Rennie et al., 2018). Biogenic carbonates are also the target of main of the investigations we led over the years, as will be further detailed in the next chapters.

Chapter V. Why are CAS so often different from other records? A history of diagenesis, and of new information to be extracted from the sedimentary record.

We previously detailed the different sedimentary archives for the reconstruction of past seawater $\delta^{34}S$ values. Amongst those archives, CAS are strongly used but tend to display a variability at times higher than other archives from the era (Present et al., 2020), while we know that CAS has the ability to record the actual value of seawater. This variability is intrinsic to the carbonate archive and must be explained in order to understand its nature and to be able to exploit it in order to be able to reconstruct not only past seawater $\delta^{34}S$ values but also to extract additional information from the sedimentary record that are so far hidden from us. It is within this framework that the work of Ted Present, Vicky Rennie and Arbia Jouini took place. In the following chapter, after presenting a literature review on carbonate rocks and diagenetic processes, I will develop how Ted Present's PhD work, as well as Dan Johnson's, though I wasn't directly involved, helped us rethink about carbonate diagenesis and sulfur isotopes, as well as microbial processes.

I. Post-depositional processes.

1. Carbonate rock classifications.

CAS are mostly analyzed from bulk and/or micritic rocks and biogenic carbonates, on which we will focus this presentation. If biogenic carbonates used in paleoenvironmental reconstructions are usually well identified (mostly bivalves, foraminifera or mollusks such as brachiopods), micrite or bulk rocks can encompass different types of rocks. Two main classifications (or versions of) have been used to describe carbonate rocks over the last 60 years, the Folk and Dunham classifications (Dunham, 1962; Folk, 1959).

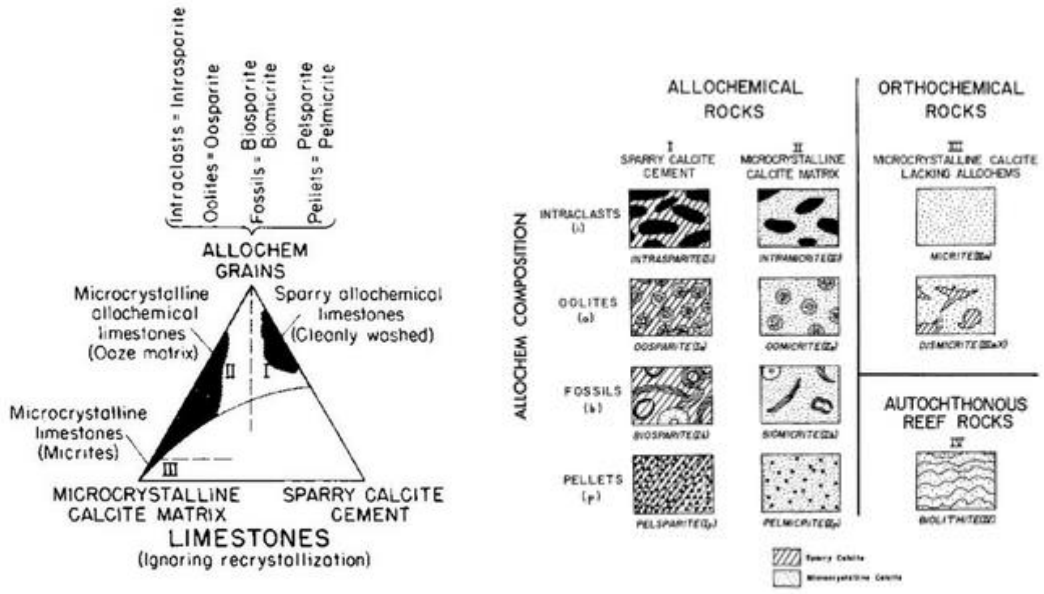

Figure 52. The Folk classification for carbonate rocks

Folk classification (Fig. 52) is first based on a subdivision between rocks containing foreign elements (allochems, i.e. intraclasts, oolites, fossils, and pellets, Family I and II), precipitated in-situ (orthochems, Family III) and reefs (family IV). In this classification, micrite, or MICRocrystalline calcITE (Family III) consists of less than 10 % allochem sediments in a carbonaceous mud, the matrix component of the rock with elements smaller than 4 µm in size (Folk, 1959). Unlike the sparry calcite cement that binds the rock together in family I, the micritic matrix is constituted of extremely small pieces of carbonate of unknown origin or precipitation conditions.

Dunham proposed a different approach with a classification based on whether the rock is constituted of grains originally bound or not during deposition (Fig. 53; Dunham, 1962). If the components are not bound at the time of deposition, the rocks can be composed of loose grains in a matrix, or mud (Mud- and Wackestone) or the opposite (Packstone). In the absence of mud, cement binds the rock (Grainstone). The two other categories are Boundstone (original elements are bound together, like a reef) and Crystalline (the original texture cannot be recognized). An extended version of the classification exists for different types of boundstones, depending on the nature of the bound (organic or not). In the Dunham classification, micrite would be equivalent to mudstone.

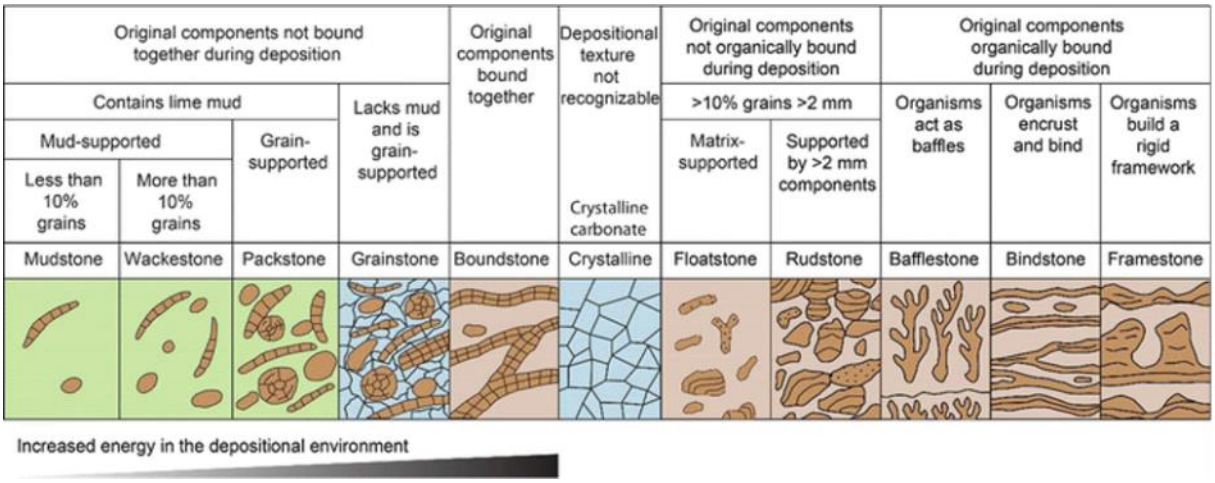

Figure 53. The Dunham classification for carbonates

Very different levels of details can be found in published investigations of sulfur isotope ratios in carbonates rocks. Sometimes very little description is provided, except generic terms such as whole rocks (Kampschulte and Strauss, 2004), limestone or calcareous shale (e.g. Ohkouchi et al., 1999; Adams et al., 2010) or “carbonate lithologies with abundant microfossils, along with some macrofossils” (Owens et al., 2013). As a result, investigations that are not based on biogenic carbonates can be based on a wide range of carbonate rocks, which by itself could be a source of variability. Though prior to the Phanerozoic, or even in parts of the Paleozoic or later, organic debris are virtually absent or unavailable in sufficient amount, one must turn to other type of carbonate sediments (Kah et al., 2004; Planavsky et al., 2012). However, careful description of the lithology remains necessary in order to provide a first sense of a possible source of sulfur isotope variability, and some studies carefully detail the investigated lithologies (e.g. Gill et al., 2011; Jones and Fike, 2013; Osburn et al., 2015; Paris et al., 2020, 2014a; Present et al., 2020). As will be detailed below, this lithological description is the first step of a careful appraisal of the meaning of the $\delta^{34}S_{CAS}$ values of a sample (Present et al., 2015, 2019).

2. Cleaning protocols.

In addition to the mixing of different phases, especially critical in bulk rock analyses, another source of variability of sulfur isotopes during CAS extraction can be improper cleaning of the samples. This aspect has received extensive attention.

One of the main risks in the incorporation of sulfate coming from the oxidation of pyrite in the lab, as pyrite is a frequent component of sedimentary rocks. Most protocols rely at least on a NaCl leaching of the rocks, which has been shown to remove an isotopically lighter phase, which can represent a combination of soluble organic matter and already oxidized pyrite that produced labile sulfate (Fichtner et al., 2018; Loyd et al., 2012; Wotte et al., 2012). Most

cleaning methods imply an oxidative cleaning step, either with H_2O_2 or NaOCl. In the lack of a NaCl step, $\delta^{34}S_{CAS}$ values produced for the same rocks remains isotopically low, suggesting that the NaCl step is mandatory to remove those secondary sulfates (e.g. Wotte et al., 2012). However, the requirement of the oxidative step can be questioned, especially in the smaller samples used for MC-ICP-MS method. Present et al. (2015) added pyrite to a carbonate sample and showed that three successive NaCl cleaning were suitable for geological CAS analyses, in agreement with tests later performed on other Ordovician or more recent carbonates (Edwards et al., 2019; Li et al., 2022). It has been suggested that Fe(III) was a more efficient oxidative agent than O_2 in the contamination process (Marenco et al., 2008a; Mazumdar et al., 2008). For this reason, we also tested the influence of the presence of Fe(III) by leaving iron oxides present in the test carbonate and found no difference (Present et al., 2015). As a result, the three NaCl cleaning steps might be the most effective to clean carbonate samples prior to sulfur isotope and CAS concentration analysis.

A different protocol had been used by Rennie et al. (2018) who worked on hand-picked foraminifera. As the hand-picking allowed ensuring the absence of pyrite, the priorities of the cleaning were different. However, foraminifera picked from oceanic cores present a different diagenetic history that require a suited protocol. Cleaning tests based on typical trace metal foraminifera cleaning steps helped to establish a protocol producing the most reproducible results. First, as oceanic core samples are less lithified and cemented than Paleozoic carbonates, clay removal is required, as well as cracking the foraminifera open. This is followed by oxidative (H_2O_2 + NaOCl solution) and reducing (hydrazine) steps, both of which appear necessary to ensure reliable data (Rennie et al., 2018). In any case, a final leaching step in diluted acid is required. It should be noted however that variability between tests is very small, 1 ‰ at worst.

3. Diagenesis: a brief overview.

After their deposition, sediments undergo diagenetic processes likely to alter their mineralogy and geochemical characteristics. In the case of the lithologies of interest here, diagenesis will affect the composition of the biological allochems, the grains of the matrix, and be associated to dissolution-reprecipitation process and authigenic carbonate and cement precipitation (Fig. 54). Diagenetic processes are of primary importance as they contribute to the biogeochemical processes that control the composition of the ocean-atmosphere and imply a wide variety of biological metabolisms (e.g. Froelich et al., 1979).

Diverse processes happen to carbonates, including mineralogical transformation, dissolution, dissolution-reprecipitation, authigenic carbonate precipitation. Aragonite tends to evolve to (low-Mg) calcite, high-Mg calcite to low-Mg calcite (Brand and Veizer, 1980; Land, 1967), which

has led to suggest that low-Mg calcite is the most stable and diagenesis-resistant biocarbonate (Ullmann and Korte, 2015). Authigenic carbonates can precipitate in the sediments, as alkalinity and/or DIC evolves in the pore fluid with depth (Fantle and Ridgwell, 2020; Schrag et al., 2013; Turchyn et al., 2021). And, especially in sediments older than 40 Ma, dolomitization can occur (e.g. Holland and Zimmermann, 2000).

Geochemical aspects of diagenesis were first based on petrographic observations with carbon and oxygen isotope ratios measured in carbonates (e.g. Gross, 1964; Hudson, 1977; Land, 1967). They correspond to the processes happening to carbonates described previously as well as isotopic and elemental exchange, diffusion or equilibration (Adams et al., 2023; Ahm et al., 2018; Cisneros-Lazaro et al., 2022; Fantle and DePaolo, 2007; Higgins et al., 2018; Rennie and Turchyn, 2014). Early work first established the trends of trace elements such as Mg, Sr, Mn, or $^{87}Sr/^{86}Sr$ during diagenetic processes in order to not only understand the original signature of the components of the rock but also to better constrain diagenesis and its multiple processes (Banner and Hanson, 1990; Brand and Veizer, 1981, 1980), and many new isotopic systems have since been applied to explore diagenesis in different environments, including Li, B, S, Ca or Mg and “clumped” isotopes (e.g. Ahm et al., 2018; Blättler et al., 2015; Fantle, 2015; Fantle and Higgins, 2014; Higgins et al., 2018; Paris et al., 2010; Smith et al., 2022; Stolper et al., 2018; Ullmann et al., 2013).

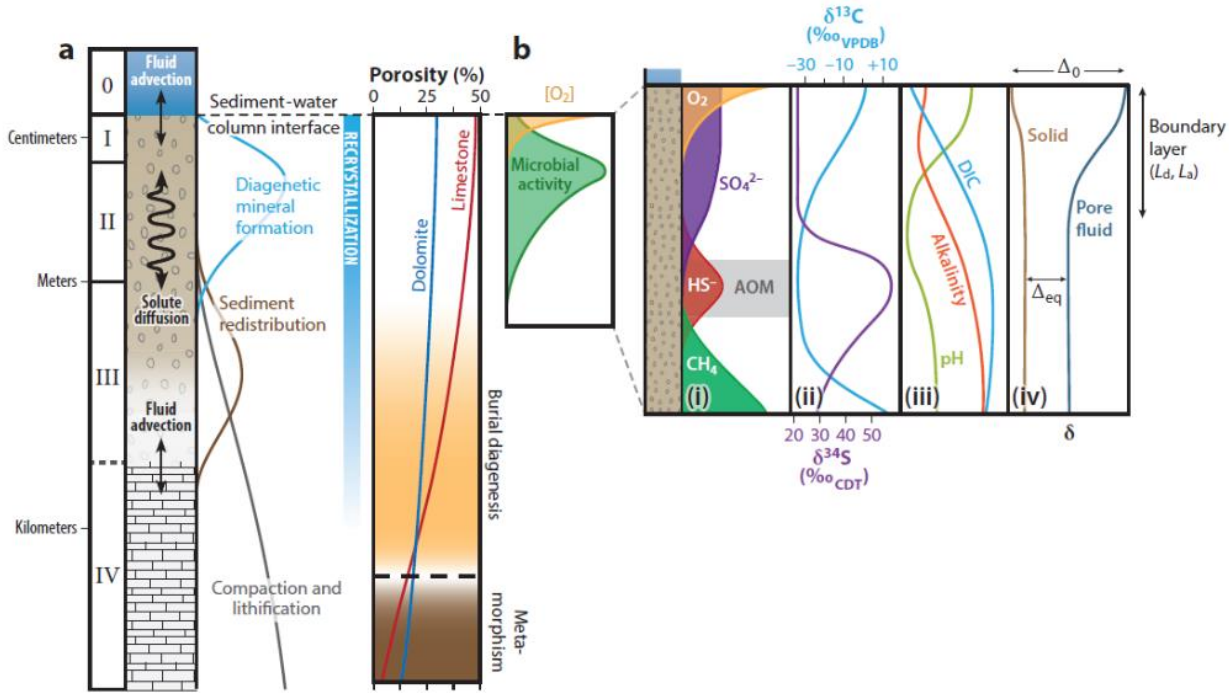

Figure 54. Schematic description of the processes occurring in sediments, from burial to metamorphism (a) with a focus on the biogeochemical processes that occur in the upper part of the sedimentary pile. Figure from Fantle et al. (2020)

It is virtually impossible to summarize all the effects of diagenetic processes. Many reviews exist (e.g. Fantle et al., 2020; Swart, 2015). In marine environments, diagenesis can happen in shallow environments with influence of meteoric water, in tidal environments or in the deep ocean, in organic matter rich or poor sediments, and each will be likely to respond differently depending on the composition of the sediments and of the fluid. However, every diagenetic setting is different, and diagenesis should not be seen as a toolbox or a checklist, but rather as a highly complex and still at times unpredictable combination of processes.

Diagenesis will be strongly influenced by the local conditions and some of the controlling parameters are the openness of the system and the water/rock ratio (Ahm et al., 2018; Brand and Veizer, 1981, 1980; Higgins et al., 2018). For instance, in an open system, under fluid-buffered conditions, if alteration involves seawater or seawater-derived fluids, the recrystallization of carbonate minerals is expected to tend to get closer to the equilibrium value of a carbonate precipitated in seawater. By contrast, in a sediment-buffered setting, the recrystallization of carbonate will start from a solution with a composition different from that of seawater. In any case, if the fluid composition has evolved during diagenesis, the carbonate will precipitate in equilibrium with the new fluid (e.g. Higgins et al., 2018). As the composition of the new fluid is usually lower than seawater for Sr and Mg and that the carbonates that reprecipitate are no longer controlled by biological activity, carbonate sediments that undergo open-system diagenetic alteration are characterized by lower Sr/Ca ratios, $\delta^{13}C$ and $\delta^{18}O$ (Brand and Veizer, 1981, 1980; Dickson and Coleman, 1990; Dutton et al., 2005; Regenberg et al., 2007). For instance, Mg behavior is more complex as carbonate that are high-Mg calcite will tend to lose Mg, and the opposite is true for low-Mg calcite even if porewater becomes less concentrated in Mg (e.g. Higgins and Schrag, 2012), but dolomitization, when it occurs, is a clear Mg enrichment of the rock (Berner, 1966; Land, 1967). Elements like Mn can have a very complex behavior. For instance, during the transformation from aragonite to calcite, Mn concentration is higher in reprecipitated carbonate, but this requires a Mn supply to replenish the fluid. As a result, in a closed system, Mn-depletion will end up resulting in calcite with no Mn, while an open-system would be able to continuously provide Mn (Pingitore, 1978). Those are only a few examples of processes occurring. We detail below the behavior of sulfur during diagenesis.

II. Diagenetic processes affecting sulfur isotopes.

Because sulfate is a highly concentrated ion in seawater, pore-fluids, at least near the water-sediment interface, are also rich in sulfate. Diagenetic processes in connection with sulfur thus depend on the nature of the fluid (seawater vs. meteoric water) and of the redox state of the locus of recrystallization of the carbonate.

1. Microbial sulfate reduction, a key player in diagenetic processes.

i. MSR, $\delta^{34}S$, DIC and alkalinity.

In sediments, the succession or redox reactions leads to the occurrence of microbial sulfate reduction, once O_2, NO_3^{2-}, Mn and Fe have been consumed (Froelich et al., 1979). As we detailed previously, MSR consumes sulfate and produces reduced sulfur enriched in ^{32}S, leaving the residual sulfate pool enriched in ^{34}S. Part of the reduced sulfur can precipitate as pyrite, part of it can be reoxidized anaerobically, or move toward the surface by diffusion-advection and be oxidized aerobically. Overall the most common result is that, as we go deeper into the sediment pile, the $\delta^{34}S$ value of porewater increases and the sulfate concentration diminishes, and pyrite forms, bearing lower or even negative $\delta^{34}S$ values (e.g. Fike et al., 2015; Jørgensen, 1979; Rennie and Turchyn, 2014; Richardson et al., 2019; Fig. 55).

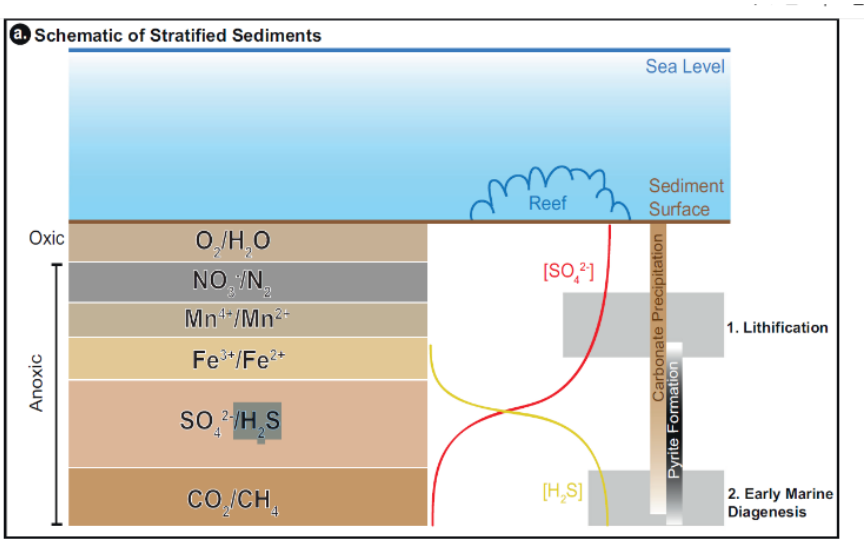

Figure 55. Redox couple used in microbial metabolisms in the upper part of the sedimentary pile with schematic depth evolution of sulfate and H_2S concentrations. Figure from Richardson et al. (2019b).

Because organic matter becomes oxidized, MSR usually increases DIC and can increase alkalinity (e.g. Baumgartner et al., 2006; Turchyn et al., 2021), though this depends on the nature of the organic substrate used by the microbes (Gallagher et al., 2012). A the global scale, compilation of porewater data reveals that porewater alkalinity and sulfate concentration are anticorrelated (Turchyn et al., 2021), which means that the saturation state of porewaters influenced by MSR increases with depth and favor carbonate precipitation in the sediment (Baumgartner et al., 2006; Berner et al., 1970; Richardson et al., 2019b). Therefore, both saturation and $[CO_3^{2-}]$ are likely to increase in porewater as sulfate decrease and $\delta^{34}S$ increases. As a result, newly precipitated calcite could be expected to incorporate less sulfate (lower SO_4^{2-}/CO_3^{2-}) with higher $\delta^{34}S$, the high value of porewater being possibly reinforced by higher fractionation at low SO_4^{2-}/CO_3^{2-}. However, if increased carbonate supersaturation

increases the rate of carbonate precipitation (Langdon et al., 2000), though calcium carbonate precipitation in sediments is occurring mainly where sulfate reduction is coupled with anaerobic methane (Turchyn et al., 2021). In this case, faster rates are due to steeper gradients and faster diffusion rates. In the case of faster rates, sulfate incorporation in inorganic calcite is anticipated to increase (Barkan et al., 2020, in prep; Busenberg and Plummer, 1985).

ii. MSR and AOM.

Another crucial metabolism in anaerobic environments is anaerobic methane oxidation (AMO), that leads to up to 90 % of the oceanic methane production to be recycled in anaerobic marine sediments Methanogenesis is a metabolism that occurs the deepest in the sediments, when O_2, nitrate, manganese, iron and sulfate are consumed (Froelich et al., 1979; Jørgensen and Kasten, 2006). As MSR is energetically more interesting than methanogenesis, always though this is not always true, at least on land (Wieder et al., 1990), MSR and methanogenesis are often considered to be mutually exclusive, with MSR possibly outcompeting methanogenesis when sulfate is available. As methane is a gas with a greenhouse effect much more potent than CO_2, methane oxidation is a process of interest, whether in the ocean or in wetlands, the main natural source of methane today (Gauci et al., 2004; Orphan et al., 2001).

Below the MSR zone is the sulfate-methane transition zone and anaerobic methane oxidation occurs as methane diffuses upwards (Turchyn et al., 2021). However, the capacity of methanogens to use non-competitive substrates, i.e. not used by sulfate-reducing microorganisms, can lead to the overlap of sulfate reduction and methane consumption and to the absence of a transition zone (Mitterer, 2010). The oxidation is mediated by a consortium of methanotroph archaea that lead to the oxidation of methane and the production of CO_2 and sulfate-reducing bacteria (Boetius et al., 2000; Knittel and Boetius, 2009; Orphan et al., 2002, 2001; Schubert et al., 2011). In those consortia, electrons are directly transferred between the anaerobic methanotrophic archaea (ANME) and the sulfate-reducing bacteria (SRB, Fig. 56; McGlynn et al., 2015; Wegener et al., 2015).

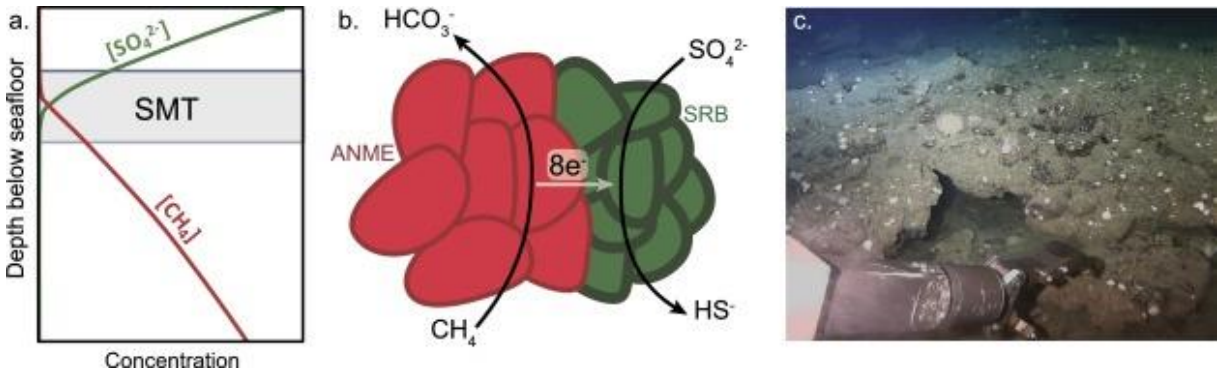

Figure 56. Schematic pore fluid profile of the sulfate-methane transition (SMT). b. Model for AOM coupled to MSR (after McGlynn et al., 2015; Wegener et al., 2015). c. Carbonate crusts covering the seafloor at the methane seep in the Barents Sea (caption and figure from Crémière et al., 2020).

As sulfate reduction increases DIC and tends to increase alkalinity, the sulfate-methane transition zone can be a place of authigenic carbonate production (Naehr et al., 2007; Turchyn et al., 2021). Such carbonates tend to be characterized by very low $\delta^{13}C$ values, as methanogenesis produces CO_2 with low $\delta^{13}C$ values, combined with positive to extremely positive $\delta^{34}S$ values and low CAS content, reflecting the evolution of pore fluid sulfate down to the sulfate-methane transition zone (Crémière et al., 2020; Loyd et al., 2012).

iii. MSR and dolomitization.

Dolomitization is a complicated process hard to reproduce in laboratory conditions that constitutes one of the main sinks of magnesium in the ocean (Holland and Zimmermann, 2000). Dolomite is a magnesium-rich double carbonate mineral. Its abundance in fossil carbonate reef platforms despite its paucity in modern sedimentary environments is a the heart of a conundrum described as the "Dolomite Problem", with important implications for the Mg concentration of the modern ocean (Arvidson and Mackenzie, 1999; Holland and Zimmermann, 2000). The post-depositional diagenetic process at the origin of marine dolomite precipitation remains misunderstood, with minimal experimental success in reproducing dolomitization in laboratory, room temperature conditions (Baldermann et al., 2015; Gregg et al., 2015; Montes-Hernandez et al., 2016), except through interaction with amorphous calcium-magnesium carbonate (Montes-Hernandez et al., 2020), which suggests that dolomitization might be a very slow process (Pina et al., 2022). A growing body of evidence suggest a role for biological activity of organisms such as the crustose coralline alga, *Hydrolithon onkodes* (Baldermann et al., 2015; Nash et al., 2011).

Dolomitization mostly takes place in marine anoxic organic rich sediments where MSR occurs (Warren, 2000). As MSR consumes sulfate, an inhibitor of dolomite nucleation, and increase alkalinity and carbonate ion concentration, it might directly contribute to facilitate dolomitization (Loyd et al., 2012; Vasconcelos et al., 1995). In addition, the CAS content also plays a role in the control of the degree of cation order. The least amount of CAS is incorporated in the dolomite, the most ordered and least soluble it is (Baldermann et al., 2015). As a result, MSR does not only contribute to favor dolomite formation, but it also contributes to the precipitation of a more stable dolomite. In this interpretative framework, dolomite is characterized by $\delta^{34}S_{CAS}$ distilled by MSR and thus heavier than expected from precipitation from seawater (e.g. Baldermann et al., 2015; Loyd et al., 2012), even though the lower $\delta^{34}S$ has been documented as well (e.g. Marenco et al., 2008b, Present et al., 2015) and even possibly dolomite that records $\delta^{34}S_{sw}$ values (Present et al., 2019), as will be detailed in section III.

2. The behavior of sulfate during recent subaerial and platform diagenesis.

A few studies have focused on how the impact of diagenesis on carbonate platforms affect sulfate content and sulfur isotopes.

The carbonate sediments of the Florida Keys shallow platform are often characterized by appreciable early diagenetic aragonite dissolution and active MSR (Hoffmeister and Multer, 1968; Lyons et al., 2004). In subaerial deposits, Gill et al. (2008) produced a high-resolution profile of the CAS content and $\delta^{34}S$ values across a transect of aragonite evolving to calcite in the Pleistocene Key Largo limestone (Florida, USA; Fig. 57). This transect is going through a recrystallization front from the original coralline aragonite to the replacement low-Mg calcite.

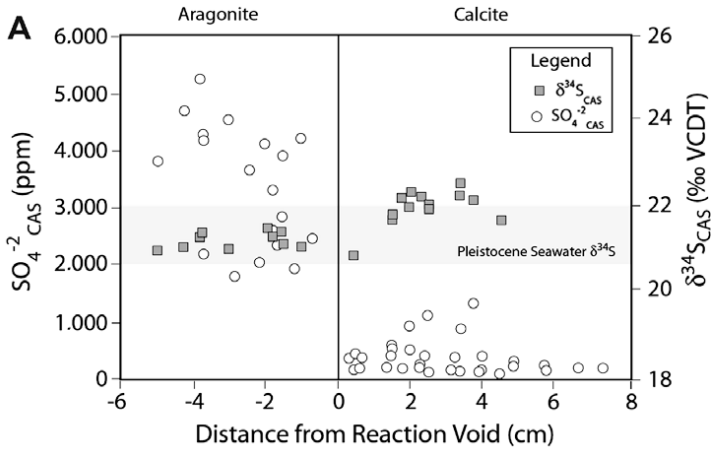

Figure 57. Composite profiles of sulfate concentrations and $\delta^{34}S$ measured across the transition between pristine aragonite and recrystallized calcite (figure from Gill et al., 2008).

In this environment, the diagenetic fluid is most likely sulfate poor-meteoric water and the replacement calcite is much poorer in sulfate that the initial aragonite, while the $\delta^{34}S$ value of the carbonate does not evolve by more than 1‰. However, the mineralogical contrast is very stark as the CAS and $\delta^{34}S$ gradient occurs within a few centimeters. At depth, the situation is different as pore fluid is impacted by MSR. And yet, despite ^{34}S enrichments in the pore fluid sulfate and clear evidence for diagenetic calcium carbonate precipitation, the CAS from the bulk calcareous mud preserve the $\delta^{34}S$ of seawater sulfate (Lyons et al., 2004). The combination of these two studies led to the sense that diagenetic overprint of CAS was low. Similarly, $\delta^{34}S_{CAS}$ values measured in core-top unlithified carbonate sediments from shallow waters of the South China sea near the Nansha Islands revealed no discernable sulfur isotope ratio variations (Li et al., 2022).

Similar results have been provided by the investigations of the Enewetak Atoll (equatorial Pacific Ocean) and of the Meiji Atoll (South China Sea) that both underwent episodes of subaerial exposures and were affected by meteoric and marine diagenesis, including dolomitization, more pervasive in the Meiji Atoll than at Enewetak (Fig. 58; Di et al., 2023;

Smith et al., 2022). In the Meiji Atoll, dolomitization most likely occurred by interaction with a dolomitizing fluid composed of a fresh- and seawater mix, or the reflux of evaporative brines evolved from seawater (Guo et al., 2021).

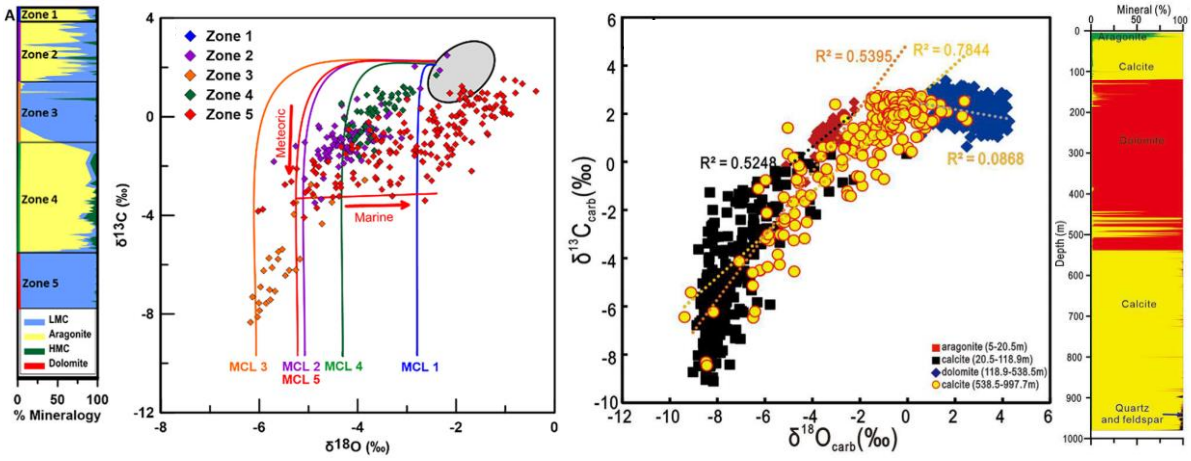

Figure 58. $\delta^{13}C_{carb}$ combined to $\delta^{18}O_{carb}$ for Enewetak (left) and Meiji (right) atolls. At Enewetak, the pristine endmember (grey oval) comes from modern sediment values (Weber and Schmalz, 1968). In the left panel, the solid lines represent diagenetic trends following the meteoric calcite line (MCL) for each zone of core KAR-1 (figures from Di et al., 2023 and Smith et al., 2022).

$\delta^{13}C_{carb}$ combined to $\delta^{18}O_{carb}$ reveal the global trends of the diagenetic history of the samples. The initial aragonite and modern sediments represent the highest $\delta^{13}C_{carb}$ values and, except for dolomite at Meiji, the highest $\delta^{18}O_{carb}$ values. At Enewetak, combining clumped isotopes and carbonate $\delta^{18}O_{carb}$ measurements, Smith et al. (2022) were able to propose a reconstruction of the $\delta^{18}O$ of the diagenetic fluid, showing an influence of meteoric waters in the diagenetic processes for the different zones of the core, but also the influence of marine diagenesis in zone 5, the deepest. At Meiji, Guo et al. (2021) reveal a mostly meteoric diagenesis, with a dolomitizing fluid involving seawater or seawater-derived brines.

Di et al. (2023) combined their sulfur isotope analyses to the oxygen composition of CAS to explore the diagenetic processes at play. They found the $\delta^{18}O_{CAS}$ values to be different from the barite $\delta^{18}O$ record (Turchyn and Schrag, 2006), especially in the dolomitized portion of the sediments. (Di et al., 2023). The corresponding $\delta^{34}S_{CAS}$ values vary within a range from 18.9 ‰ (core OOR-17) to 24.4 ‰ (core KBZ-4) in the Enewetak Atoll and they vary between 21.5 and 24.1‰ in the Meiji Atoll (Di et al., 2023; Smith et al., 2022). In the Meiji atoll, CAS contents were found to decrease rapidly during meteoric and marine diagenesis, Those results are interpreted to suggest minimum diagenetic overprint of $\delta^{34}S$, even during dolomitization and stronger modification of $\delta^{18}O_{CAS}$ values (Di et al., 2023; Smith et al., 2022). The original $\delta_{34}S_{CAS}$ values from the Enewetak Atoll samples are mostly preserved and seem unaffected by recrystallization There again, the alternation between sulfate rich and poor carbonates can reflect the occurrence of recrystallization in a fluid dominated by meteoric waters, poor in

sulfate, with moderate impact on the $\delta^{34}S$ values (Smith et al., 2020). The observed deviations from $\delta^{34}S_{sw}$ values are interpreted as local occurrences of MSR, or recrystallization of reduced sulfur.

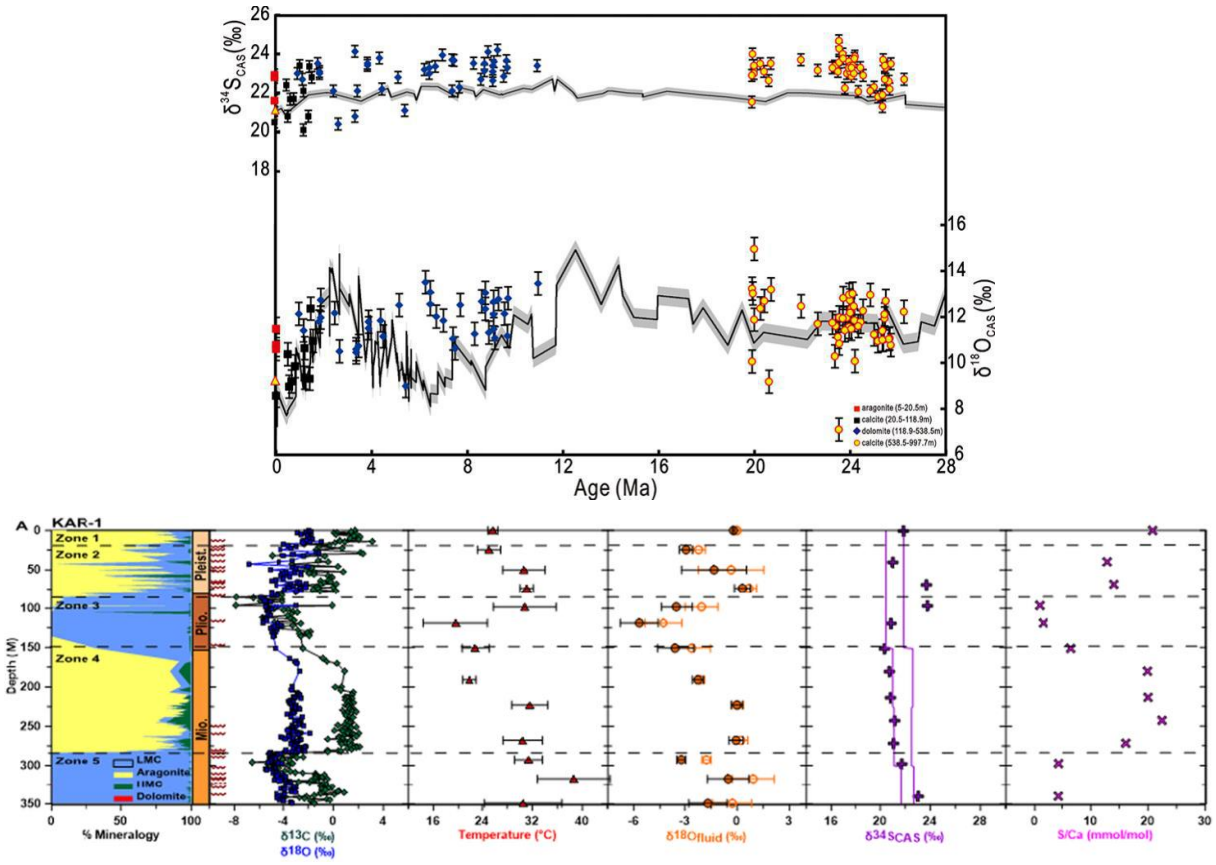

Figure 59. $\delta^{13}C_{carb}$ combined to $\delta^{18}O_{carb}$ for Enewetak (left) and Meiji (right) atolls. At Enewetak, the pristine endmember (grey oval) comes from modern sediment values (Weber and Schmalz, 1968). In the left panel, the solid lines represent diagenetic trends following the meteoric calcite line (MCL) for each zone of core KAR-1 (figures from Di et al., 2023 and Smith et al., 2022).

Nevertheless, even though diagenesis is dominated by meteoric processes, the isotopic variability of those records is stronger than that of barite.

3. Deep ocean diagenesis.

Rennie and Turchyn explored diagenetic processes across a series of IODP sites (807, 821 and 1003). Site 807 (Ontong-Java) is the deepest (2815 m) and the sediments are 90 wt% carbonate, with 0.02 to 0.6 ‰ of organic carbon (Fig. 60). Analyzed samples are made of nannofossil and foraminiferal ooze above nannofossil chalk at 293 m below the seafloor (mbsf). Sedimentation rates in the uppermost 600 m average at least 15m/Ma. Pore fluid sulfate concentrations drop from seawater values (28 mmol/L) to 22 mmol/L in the top first 100 m (Shipboard Scientific Party, 1991a). Site 1003 (Bahama Bank) is much shallower, with a water depth of 490 m. The uppermost 200 m of sediments are also 90 wt% carbonate, with usually less than 1 wt% organic carbon, and consist of predominantly unlithified packstones with

unlithified and bioturbated mudstones. Carbonates are mostly high-Mg calcite and come from both mixed pelagic and bank-derived carbonates. Finally, site 821, located and the Eastern Australian continental slope is the shallowest one (water depth 212 m). It is the least carbonate-rich core (40-70 %) and contains between 0.15 and 0.45 % organic carbon. The sediment consists of siliciclastic sands and muds interbedded with calcareous clays. This site also represents the highest sedimentation rate (from 100 to 200 m/Ma). Comparison of the $\delta^{34}S_{CAS}$ from these three cores reveals contrasting behaviors, with site 807 yielding values very similar to the barite record, while site 821 offers the most modifies $\delta^{34}S_{CAS}$ values, while all of them display $\delta^{18}O_{CAS}$ data distinct from the barite record. It is also worth noting that $\delta^{18}O_{CAS}$ record from Rennie and Turchyn (2014) is very similar to that of Di et al. (2023).

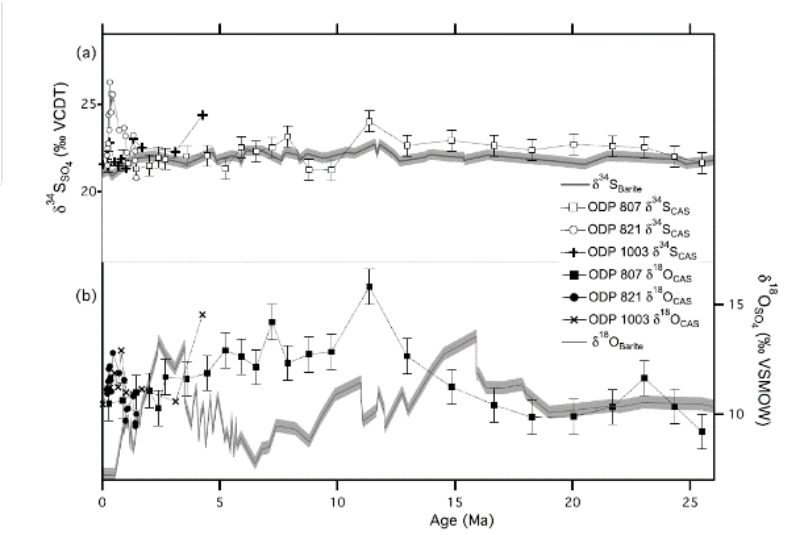

Figure 60. Sulfur and oxygen isotope ratios of CAS collected from 3 different IODP sites analyzed to explore the influence of diagenesis reported as a function of the age of the samples (Rennie and Turchyn, 2014)

In order to describe the evolution of the $\delta^{34}S_{CAS}$ values in their data, Rennie and Turchyn (2014) ran a model in which they test the influence of the sedimentation and recrystallization rates (Fig. 61). In this model, the recrystallization rate is time dependent and set at $R = 0.4 \times e^{(-t/0.875)}$ (Fantle and DePaolo, 2007) and lead to precipitation of carbonate with the δ34S value of the pore fluid at that depth.

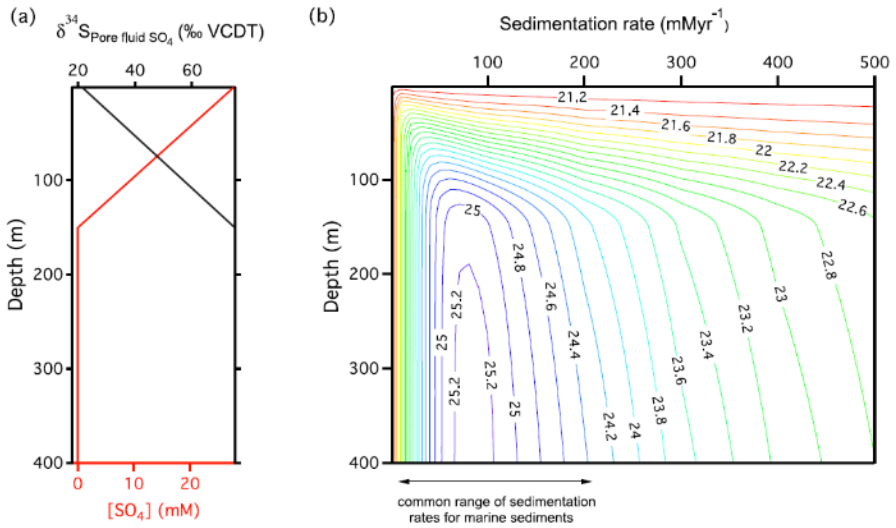

Figure 61. Diagenetic model of Rennie and Turchyn with (a) synthetic pore fluid profile with the evolution of sulfate concentration and $\delta^{34}S$ values and (b) isolines of $\delta^{34}S_{CAS}$ of recrystallized calcite as a function of depth and sedimentation rate evolution for a given recrystallization rate $R = 0.4 \times e^{(-t/0.875)}$. Figure from Rennie and Turchyn (2014).

As a result, in this model, the youngest sediments will incorporate the most pore fluid sulfate. If MSR occurs close to the water-sediment interface, then the most recrystallization will occur with the most modified sulfate, and the $\delta^{34}S_{CAS}$ value will be the furthest from the initial seawater value. On the other hand, in slow sedimentation locations, with little evolution of the pore fluid $\delta^{34}S$ value, then recrystallization will not have a perceptible effect on $\delta^{34}S_{CAS}$ (Rennie et al., 2014). As a result, deeper ocean sites, with less organic matter and lower sedimentation rates are possibly better targets to reconstruct past seawater $\delta^{34}S$ values.

4. Late diagenesis and metamorphism.

Further modification of the $\delta^{34}S_{CAS}$ values can also occur during deeper burial of the sediments, all the way up to the metamorphic window. Carbonates from the Hauptdolomit in the Eastern Alps underwent burial and metamorphic overprint due to intense tectonic deformation (Fichtner et al., 2017 citing Zorlu, 2007). It is composed of early diagenetic dolomite with limestone and calcite cements with bituminous carbonates, originally deposited in sub- to supra-tidal environments (Fichtner et al., 2017; Ziegler, 1988).

The samples come from different parts of the platform, with different sedimentological and burial histories and exhibit contrasted isotopic behaviors (Fig. 62). The lowest temperatures were experienced by samples from the Osterhorn Block and Sella locations (100 °C), followed by the Rellstal (200 °C) and the Piz Lad (300 °C) samples. Finally, samples from the Kalkkögel location underwent the highest temperatures.

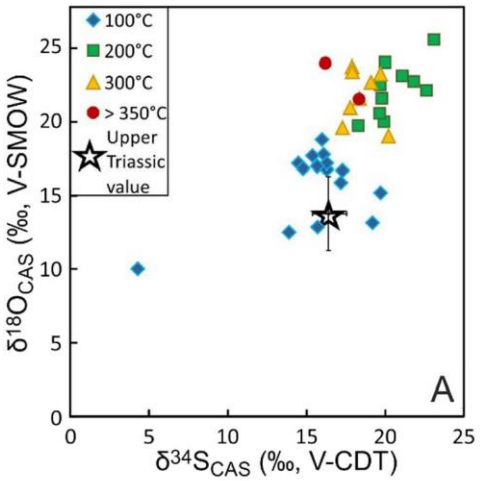

Figure 62. Sulfur and oxygen isotope compositions of CAS in Hauptdolomit samples that experienced burial temperatures of 100 °C (blue diamonds; Osterhorn Block and Sella locations), 200 °C (green squares; Rellstal location), 300 °C (yellow triangles; Piz Lad location) and > 350 °C (red circles; Kalkkögel location). The Upper Triassic values (marked with a black star) for sulfur and oxygen isotope compositions of seawater sulfate are mean values from both CAS and evaporite data (figure and caption from Fichtner et al., 2017).

Sulfur isotopic analyzes of the CAS extracted from the Hauptdolomit carbonates reveal a complicated history where no discernable trend exist between burial temperature and evolution from the Upper Triassic seawater value reconstructed from CAS (Kampschulte et al., 2001; Kampschulte and Strauss, 2004) and evaporite data compiled by Fichtner et al. (2017). By contrast, the increase observed in $\delta^{18}O_{CAS}$ values could reflect either sulfate modified by MSR or recrystallization in a deep fluid at ~200 °C where an exchange of the oxygen isotopes between CAS and carbonate could be made possible. However, the reason for the increased $\delta^{34}S_{CAS}$ values is more puzzling. Thermal sulfate reduction could be the cause for enriched $\delta^{34}S$ values of the fluid, but the evolution of the $\delta^{13}C$ values does not support this hypothesis. Alternatively, the highest $\delta^{34}S_{CAS}$ values could reflect early diagenesis during dolomite precipitation in a partially confined sabkha environment. However, such a trend would likely be supported by lowest CAS content for the highest $\delta^{34}S_{CAS}$ values, which is not the case. The reason for the $\delta^{34}S_{CAS}$ values from the Piz Lad location to be lower than those from Rellstal despite having been submitted to higher temperature could be lower initial $\delta^{34}S_{CAS}$ values due to early sulfide oxidation and lowering of the dolomitizing fluid $\delta^{34}S$ value. In this scenario, despite burial possibly affecting the $\delta^{18}O$ value of CAS, $\delta^{34}S_{CAS}$ values would retain the early diagenetic value acquired before burial (Fichtner et al., 2017).

5. Conclusion.

There is thus, in modern environments, a broad variety of diagenetic processes and it cannot be easily predicted how a carbonate sample would behave. Reconstructing past $\delta^{34}S_{sw}$ requires a thorough investigation and description of the samples selected for analyses as

diagenesis will depend on the nature of the fluid that interacts with the rock, as well as the sedimentation rate, the supply of organic matter and MSR intensity as well as the nature of the carbonate.

Diagenesis can increase or decrease $\delta^{34}S_{CAS}$ values, depending on the dominating process. Incorporation of sulfate affected by MSR will generate heavier $\delta^{34}S$ values, while the opposite is true in case of incorporation of sulfate produced by reoxidation of sulfide.

The samples can undergo significant modifications of their isotopic composition (at least 5 ‰ in the cases introduced for the Cenozoic, and up to 10 ‰ for the Triassic example). It is therefore critical to explore the effects of diagenesis on ancient carbonates to understand how much of the $\delta^{34}S$ signal comes from seawater variations instead of diagenesis.

III. Revisiting $\delta^{34}S_{CAS}$ variations under the prism of diagenesis.

As exposed previously, CAS is an archive with a variability beyond that of the other archives used to reconstruct past $\delta^{34}S_{sw}$ values (Present et al., 2020; Fig. 63). Despite this constatation, $\delta^{34}S_{CAS}$ are often used to reconstruct global $\delta^{34}S_{sw}$ values. In the following section, we will explore how diagenesis can generate signals that can be of huge amplitude, even at the small scale of a sample, which casts doubt on the way we perceive the Phanerozoic $\delta^{34}S_{sw}$ curve based on CAS.

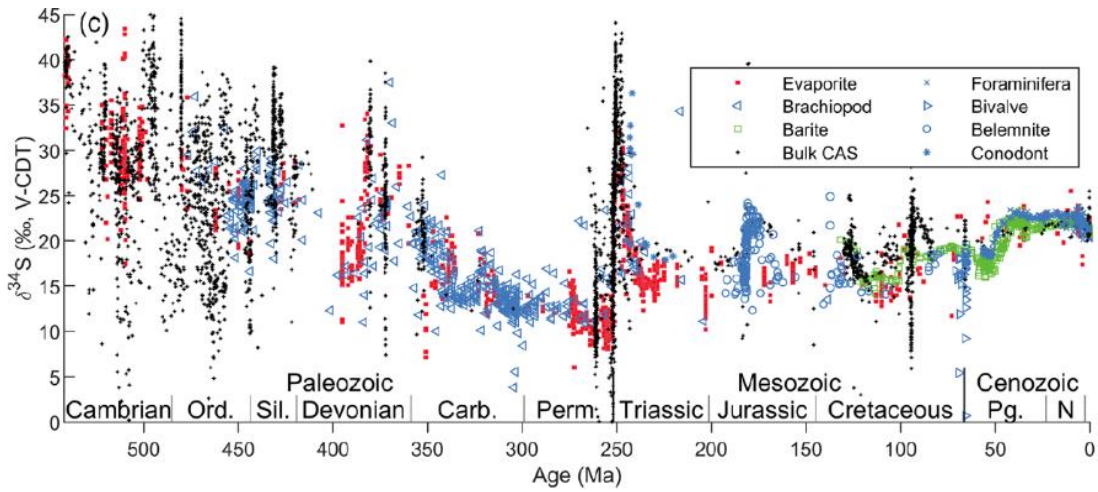

Figure 63. The Phanerozoic CAS record compilation of Present et al. (2020)

In order to understand the source of extra-variability in the CAS record compared to other contemporaneous archives, the discussion will focus on some events and period of times that we revisited over the last years: the Permian (Present et al., 2019), the Ordovician-Silurian boundary (Present et al., 2015), the Cenozoic (Rennie et al., 2018). We will also present data from the Archean and from the Permian-Triassic boundary, the most recent wildest $\delta^{34}S_{CAS}$

variations recorded through the Phanerozoic. The latter is the only investigation to which I did not contribute directly. The Cretaceous-Paleogene boundary will be the focus of Chapter VI.

Gill et al. (2008) showed that diagenesis can occur at a very small scale. For this reason, it appears necessary to assess variability of sulfur evolution isotopes at a small scale in ancient sediments. This makes the MC-ICP-MS method particularly suited for such studies as it allows us to analyze samples of small sizes.

1. Intra-sample variability of diagenesis in samples without biogenic carbonates.

i. The example of Archean carbonates.

The speciation of sulfur within complicated rocks can help understand how sulfur is preserved, and if it is present as CAS. For instance, Paris et al. (2014, 2020) tried to assess the sulfur isotopic variability within a hand sample in order to understand the $\delta^{34}S$ and $\Delta^{33}S$ variability in the Neoarchean Campbellrand basin (South Africa) seawater sulfate. They explored sulfur speciation using sulfur K-edge XANES spectroscopy and were able to show that Archean carbonates contains trace amount of sulfate, even though they had been deposited in a reducing ocean, alongside with organic and mineral reduced sulfur. As such rocks do not offer biogenic carbonates, in order to understand the sulfur isotopic composition of seawater, the study was designed to target different fabrics to understand the history of sulfur isotopes in the rock. A comparison between well-preserved fabrics (stromatolites, aragonite fans, ooids) and later precipitated spar cements helped supporting that in the aragonitic phases the sulfate was coeval of the rock deposition, or at least from the early diagenesis (Paris et al., 2014a). The Archean origin of the sulfur was confirmed by sulfur isotopic analyses, as the sulfate extracted from those rocks bears a very positive $\Delta^{33}S$ (up to +12 ‰), a signature found only in Archean sediments. The complete lack of negative values in the series of samples that were analyzed, and the demonstration that later successive geochemical overprints mostly led to loss of sulfate rather than creation of a post-depositional positive $\Delta^{33}S$ values supports the interpretation of this positive $\Delta^{33}S$ has being originally that of sulfate (Paris et al., 2020). Those results were in contradiction with the commonly accepted idea that Archean sulfate carried a negative $\Delta^{33}S$ value, at least for the Campbellrand basin during the Neoarchean.

ii. The End Permian Mass Extinction.

The End Permian Mass Extinction (EPME) is a well-studied mass extinction with CAS data interpreted as extreme $\delta^{34}S_{sw}$ variability across the extinction event (e.g. Kaiho et al., 2006, 2001; Kampschulte and Strauss, 2004; Li et al., 2009; Luo et al., 2010; Riccardi et al., 2006; Schobben et al., 2015; Song et al., 2019), while evaporite data suggest on the contrary very little change (Bernasconi et al., 2017). Though the Permian is usually rich in fossils, the lack

of biogenic carbonate suitable for CAS analyses in three sections analyzed in China across the Permian-Triassic boundary prevents from using fossils to understand past $\delta^{34}S$ values (Johnson et al., 2021). Instead of targeting different identified fabrics, the authors resorted to bulk rock analyses, but on a small scale, in order to assess the intra-sample variability (Fig. 64).

The Meishan section is the Global Stratotype Section and Point (GSSP) for the PT boundary (Hongfu et al., 2001) and was deposited on a carbonate ramp within a local topographic depression above the storm wave limit, with low sedimentation rates. In this section, facies include bioclastic micrite, wackestones, packstones, and grainstones with abundant pyrite. Different fossils occur in the grainstones, such as brachiopods, crinoids, conodonts or foraminifera. The Yudongzi section represents a continental shelf environment with skeletal grainstones, thrombolytic microbialites, lime mudstones and grainstones and the Penglaitan section was deposited near the carbonate platform with higher sedimentation rates, up to 690 m/Ma (Shen et al., 2019).

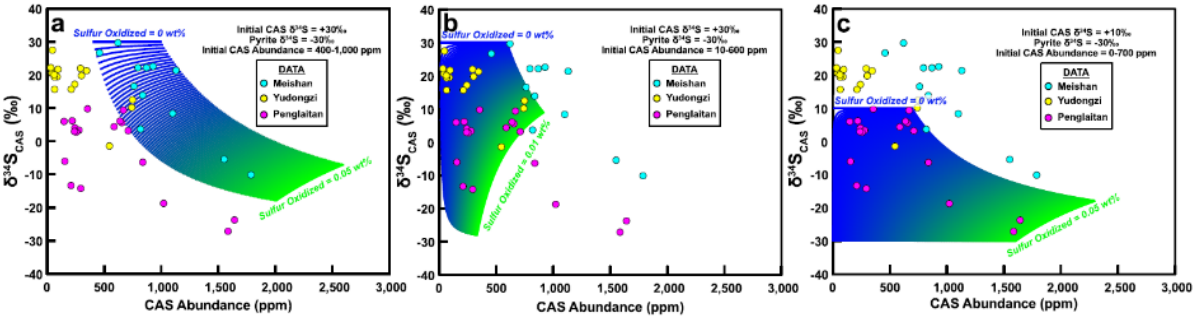

Figure 64. $\delta^{34}S_{CAS}$ value vs. CAS abundance for (A) Meishan, (B) Yudongzi, and (C) Penglaitan. The data are plotted against the model results where various amounts of pyrite ($\delta^{34}S$ =−30 ‰) were oxidized and incorporated as CAS. Colors represent different the increasing amount of oxidized S, with dark blue (top left) denoting no oxidation and lime green (lower right) denoting 0.05 wt% (or 0.01 wt% in panel B) oxidized S (figure from Johnson et al., 2021).

This approach allowed them to understand the diversity of diagenetic influence on those three sections. Analyzes revealed an intra-sample variability of up to 20 ‰ within a single hand sample. The sections with the highest sedimentation rates, such as Penglaitan, do not reach $\delta^{34}S$ values higher than that of evaporites and display some very negative values, down to *ca.* - 25 ‰. Sections with lower sedimentation rates such as Meishan and Yudongzi, from shallower environments, tend to display values more positive than evaporites, up to + 30 ‰, with rare values lower than evaporites. In Penglaitan, the initial CAS value of 10 ‰, in agreement with Permian seawater estimates from evaporites, can be explained by the high sedimentation rate (Rennie and Turchyn, 2014). The variability towards lower values reflects oxidation of reduced sulfur with low $\delta^{34}S$ values. In the shallow, fast-deposing environments, lower ODP likely means greater influence of MSR on the porewater $\delta^{34}S$ and thus highest

likeliness of recrystallization of calcium carbonates in a fluid with a $\delta^{34}S$ values higher than that of Permian seawater.

In conclusion, part of the Permian-Triassic $\delta^{34}S$ variability in the different sections that have been explored can be explained by differences in sedimentation rates and oxygen penetration rather than redox oscillations of the whole ocean.

iii. The late Permian Capitan reef.

The previous case study revealed that intra basin variability can be a source of information regarding diagenetic processes. This observation led us to lead a thorough investigation of the Permian Capitan Reef in west Texas (~260 Ma; Present et al., 2019). The shallowest carbonate rocks representing peritidal facies in the Yates and Tansill formations preserve the $\delta^{34}S$ composition of the coeval seawater sulfate despite alteration of the carbon and oxygen isotopic compositions by meteoric and dolomitizing diagenetic processes. This unexpected observation reveals that diagenesis can also occur in an oxic, dynamic environment in which it might be able to preserve the initial composition of seawater, defined from contemporaneous evaporites, if the proper phase is targeted. Unlike most description of dolomitization in a fluid influence my MSR that reduces sulfate concentration an increase the $\delta^{34}S$ of the fluid (Baldermann et al., 20&5; Loyd et al., 2012), we observe here dolomitization that occurs mainly through seawater advection (Present et al., 2019: Bryant et al., 2022).

By contrast, sulfur isotopic data from the limestones deposited in the deeper, more distal reef and slope facies in the Capitan and Bell Canyon formations largely incorporate sulphate from anoxic marine-phreatic pore fluids isotopically modified from seawater by MSR, even though the $\delta^{13}C$ and $\delta^{18}O$ values appear more pristine. Interestingly, when all carbonate phases are compared, the variability is the same in the different parts of the basins. On the shelf, the $\delta^{34}S_{CAS}$ values are that of the pore fluid composition during early cementation and neomorphism of aragonite and high-Mg calcite to low-Mg calcite. The pore fluid value remained close to seawater value on the shelf crest and outer shelf facies but evolved under the effect of MSR in the margin and slope facies. This interpretation is based on the higher $\delta^{34}S$ values recorded in equant calcite spars that precipitated during lowstands after deposition of the carbonate rocks and was later confirmed through Ca isotope measurement (Bryant et al., 2022).

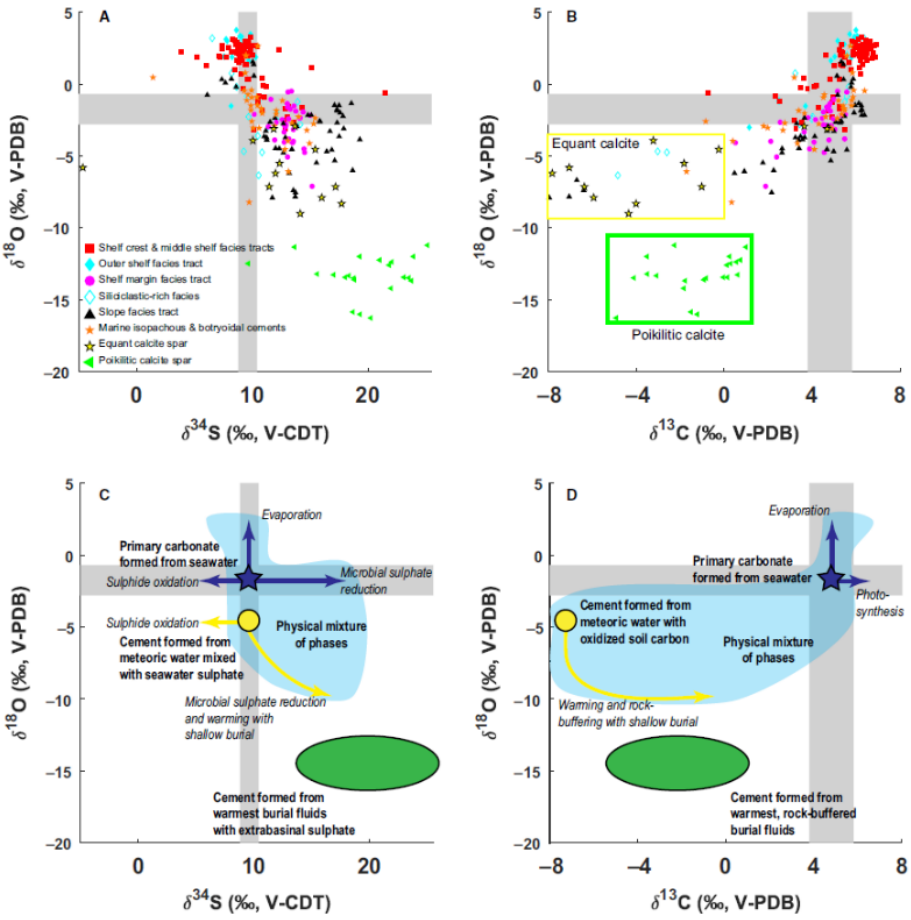

Figure 65. Comparison of $\delta^{18}O$ values of the carbonates collected along the Capitan Reef with $\delta^{34}S$ from CAS with (A) and $\delta^{13}C$ values of the carbonates and various diagenetic pathways explaining the data and detailed in the text (figure from Present et al., 2019).

Overall, in contrast with the observations by Gill et al. (2008) and Smith et al. (2022), some early and all late meteoric calcite cements display $\delta^{34}S_{CAS}$ values with a sulfur isotopic composition distinct from that of Permian seawater. The lower $\delta^{34}S$ values associated in some of the later equant calcite cements suggest meteoric oxidative processes close to the time of deposition, turning the isotopically low sulfide in sulfate incorporated in the cements. In addition, the Guadalupe Mountains record also show that the connection between sulfur behavior and dolomitization is not unique.

2. Variability within samples with biogenic carbonates.

The Ordovician-Silurian boundary (~-444 Ma) is recorded in different places including from Gotland (Sweden) and Anticosti Island (Canada). Bulk rock investigations of paired CAS-pyrite based on bulk rock samples of different carbonates (mudstone, wackestone, packstone, oncolytic and skeletal grainstones and bioherm) produced CAS sulfur isotopic records with a scatter bigger than 5 ‰ (Jones and Fike, 2013; Rose et al., 2019a). In order to document the sulfur isotopic composition of seawater itself, we focused on well-preserved brachiopods that

retained the original mineralogical texture of the low-Mg fibrous calcite secondary layer, which Ted collected using tweezers to pick individual flakes of pieces of the shell secondary layers (Fig. 66; Present et al., 2015). Using microdrill, or tweezers again, to physically separate different components of the rocks, we also analyzed micrite, bryozoan, rugose corals or trilobites (Present et al., 2015).

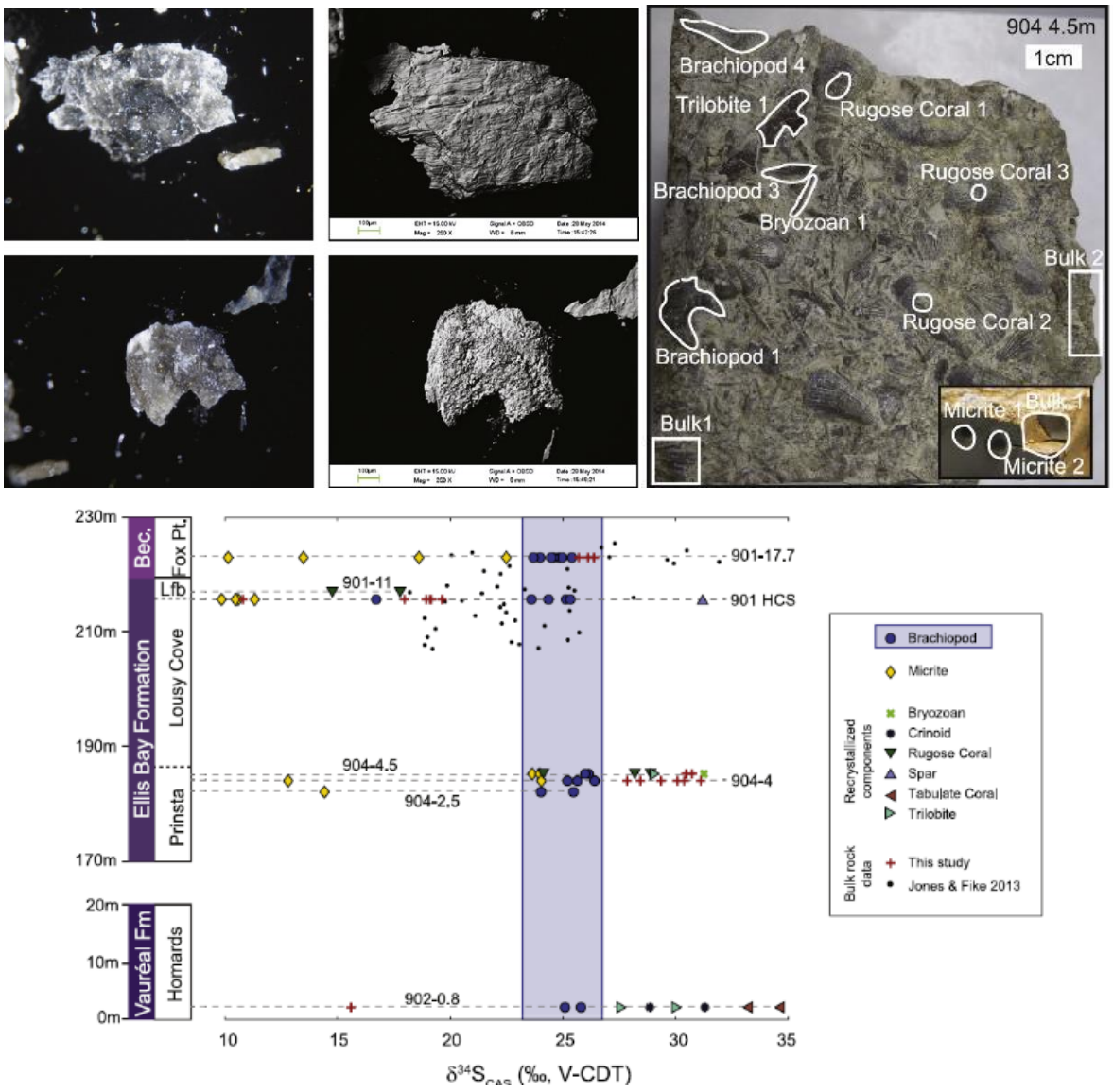

Figure 66. The upper left panel represents binocular and electron microscope backscatter views of brachiopod flakes picked from sample 904-2.5m with an example of well and poorly preserved flakes (the latter was excluded from later analysis. The upper right panel represents an example of hand sample (904-4.5m) with the different phases that were targeted. The lower panel represents the $\delta^{34}S_{CAS}$ values of the different phases as a function of age (figures from Present et al., 2015).

Our results revealed that the best preserved brachiopod shells yielded a sulfur isotopic composition of ~25 ‰ with a much narrower scatter than the previously published bulk analyses (Jones and Fike, 2013). Other phases however displayed a greater variability, beyond that of the bulk rock record, with values either lower or higher than the $\delta^{34}S$ of the

brachiopods. Our results agree with a more recent exploration of sulfur speciation in the same complex Upper Ordovician and lower Silurian carbonates of Anticosti Island, as well as those from Gotland. Interestingly, Richardson et al. (2019) confirmed that CAS constituted the vast majority of sulfur present in the different fossils, with concentrations in agreement with the anticipated contents, especially for brachiopods that appear unaltered. As the secondary fibrous layer of brachiopods, made of low-Mg calcite, is often a target of choice for paleoenvironmental reconstructions, this is of particular interest. Those observations show that well-preserved brachiopods constitute a solid archive for seawater $\delta^{34}S$, and that in those organisms, sulfur is preserved as inorganic sulfate where even the original sulfate banding can be preserved (Richardson et al., 2019b).

In micritized rugose corals, XANES evaluated sulfate concentration is higher than in the recrystallized calcite, while brachiopods have the highest concentrations, followed by bryozoans, which is roughly in agreement with Present et al. (2015). Rose et al. (2019b) also found preserved organic sulfate groups possibly from dissolved and recrystallized gastropod shells in Anticosti Island samples. Richardson et al. (2019b) however found sulfate concentrations to be low in micrite, and usually linked to the oxidation of sulfide minerals, which is in agreement with the low $\delta^{34}S$ values we found in micrite, in which Richardson et al. (2019) observed both sulfide and sulfate.

However, the micrite samples we analyzed were richer in sulfate than those studied by Richardson et al. (2019), which could be explained partly if Richardson et al. (2019) included micritized corals. In Present et al. (2015), we interpreted the micrite signature as that of microbially-mediated reduced sulfide oxidation and incorporation during diagenesis. Alternatively, fluids with low $\delta^{34}S$ values could have migrated from a separate location, such as a dolomitizing fluid strongly influenced by pyrite oxidation (Marenco et al., 2008b). This interpretation is supported by the fact that the lightest $\delta^{34}S$ value measured comes from the only dolomite-containing sample. The last hypothesis is that pyrite oxidation occurred during surficial exposure, which is supported by the occurrence of iron oxides in the samples. Most other fossils, likely initially high-Mg calcite, were strongly recrystallized and likely incorporated ^{34}S-rich sulfate residual of MSR, generating heavier $\delta^{34}S$ values. If Rose et al. (2019a), unlike Jones and Fike (2013), observed a trend in $\delta^{34}S_{CAS}$, they accordingly interpret their signal as the result of carbonate precipitation in porewaters influenced by MSR and local changes in the sulfur cycle as the basin becomes shallower and more restricted, which allows sulfate to be more distillated during MSR.

IV. Conclusion.

Diagenesis can affect sulfur concentrations and sulfur isotope ratios in carbonates mostly through the effect of recrystallization in pore fluids with a composition modified by MSR. Incorporation of sulfate with higher $\delta^{34}S$ in reprecipitated carbonates will lead to an alteration of the original signal by increasing the $\delta^{34}S_{CAS}$ value of the sample. Other effects can come into play.

First, transformation of aragonite to low-Mg calcite in contact with meteoric fluid tends to decrease the CAS content and only has a minor, but measurable, effect on $\delta^{34}S_{CAS}$. When redox levels oscillate, reoxidation of reduced sulfur can generate sulfate with lower isotope ratios than ambient seawater, which can thus decrease the $\delta^{34}S_{CAS}$ value of the sample.

We showed that diagenesis can alter differentially the various phases of a rock and that samples should be carefully appraised before analyses (Present et al., 2015, 2019). The advantage of this situation is that a single rock can reveal many elements about its history, from precipitation of the calcium carbonate in seawater to the different phases of diagenesis. The $\delta^{34}S_{CAS}$ values can thus document the interplay between the redox state of the sediment and the supply of material.

We also demonstrated that localized analyses of samples like the ones enabled by the MC-ICPS-MS, much like what is more and more frequently done for pyrite by SIMS (e.g. Pasquier et al., 2020), reveals more and more information about the sediment history and the processes happening in the sediment pile, that also affect the carbon and oxygen budgets of the ocean, and even influence methane emissions (Present et al., 2015).

Though biogenic carbonates are the favored target for CAS extraction, they're not always available or not always well-preserved enough. In such situations, MC-ICP-MS analyses still allow us to extract information from the samples by drilling localized area and revealing small scale variations related to the diagenetic history of the sediment (Present et al., 2019).

Carefully accounting for vital effects and diagenesis has allowed us to produce $\delta^{34}S_{CAS}$ record that unambiguously document $\delta^{34}S_{sw}$ for the Cenozoic. As a result, I decided to apply the same approach to the K-Pg boundary, which was the main goal of Arbia Jouini's PhD work and presented in the next Chapter.

Chapter VI. Reconstructing past $\delta^{34}S_{sw}$ and diagenetic processes across the K-Pg boundary.

The precedent works allowed us to demonstrate that CAS can provide reliable reconstructions of past seawater $\delta^{34}S$ if the (1) the right phase is targeted and (2) the right cleaning protocol is applied and (3) the diagenetic history of the rock can be reconstructed. In return, if the diagenetic history of the rock is not fully constrained, sulfur isotopes can provide essential information on diagenetic processes. By doing so, we are able not only to access information about the global ocean and biogeochemical cycles, but also able to provide additional insights into the diagenetic history of the sediments.

Both Present et al. (2015, 2019) and Rennie et al. (2018) were able to demonstrate that CAS can have a variability no bigger than evaporites or barite, if the right samples are used. Over the Cenozoic, bulk CAS from oceanic cores can also provide $\delta^{34}S$ records with a variability and a signal equivalent to barite (Toyama et al., 2020; Turchyn et al., 2009). As existing $\delta^{34}S_{CAS}$ records for the K-Pg are very different from the barite record, it is necessary to produce a new record to reconcile the different archives and properly reconstruct $\delta^{34}S_{sw}$.

I. Oceanic carbon and sulfur cycle of the K-Pg boundary.

1. The K-Pg boundary, a short introduction.

A succession of major environmental and geological perturbations occurred through the transition from the late Maastrichtian to the Paleogene. During the Late Maastrichtian, a period of global warming known as the Late Maastrichtian Warming Even (Li and Keller, 1998) preceded the Cretaceous-Paleogene (K-Pg) boundary (66.038 Ma, e.g. (Renne et al., 2013) by ~100 – 300 kyr and is attributed to the main phase of Deccan volcanism (Barnet, 2018; Hull et al., 2020; O'Hora et al., 2022). A cooling then took place over the next 100 - 200 kyr and terminated at the K-Pg boundary. Just after the K-Pg boundary, rapid ocean acidification is attributed to the Chicxulub impact that starts and a transient period of ocean acidification, attributed to the onset of Deccan volcanism (Henehan et al., 2019). These environmental disruptions might have cause the K-Pg boundary crisis, one of the five biggest mass extinctions of the Phanerozoic (e.g. Sepkoski, 1996). The K-Pg mass extinction is characterized by an oceanic carbonate production crisis that preferentially impacted planktonic biocalcifiers (foraminifera and calcareous nannofossils), drastically reducing the export of pelagic calcite and organic matter to the deep ocean (Abramovich and Keller, 2003; Alegret et al., 2021, 2012; Alegret and Thomas, 2009, 2004; Barnet, 2018; Barrera and Keller, 1994; D'Hondt, 2005; D'Hondt and Keller, 1991; Hull and Norris, 2011; Kaneoka, 1980; Keller et al., 2012, 1993;

Pardo and Keller, 2008; Punekar et al., 2016; Renne et al., 2013; Vellekoop et al., 2017; Zachos et al., 1989). The ultimate trigger and the sequence of events that led to the K-Pg crisis remain heavily disputed since two major geological events occurred that could have likely contributed to the mechanisms that led to the mass extinction: the Chixculub impact, that marks stratigraphically the K-Pg boundary with the imprint of an enriched iridium layer, as well as a peak of paroxysmal activity of the Deccan, whose age is likely to be extremely close to the K-Pg boundary (Abramovich and Keller, 2003; Alvarez et al., 1980; Archibald et al., 2010; Arenillas et al., 2016, 2006; Font et al., 2016; Henehan et al., 2019; Hildebrand et al., 1991; Hull et al., 2020; Keller et al., 2020, 2018, 2010; Renne et al., 2015; Richards et al., 2015; Schoene et al., 2019; Schulte et al., 2010; Smit and Hertogen, 1980; Sprain et al., 2019). The bolide impact created a dust cloud that blocked photosynthesis and vaporized the surrounding oceanic sediments made of carbonate and evaporite, instantaneously releasing massive amounts of CO_2 and SO_2 (Artemieva et al., 2017; Pope et al., 1997). On the other hand, the Deccan volcanism emitted CO_2 and SO_2 on a time scale of tens of thousands of years in amounts orders of magnitude above impact-induced emissions (Beerling et al., 2002; Chenet et al., 2009; Courtillot and Fluteau, 2014; Nordt et al., 2003).

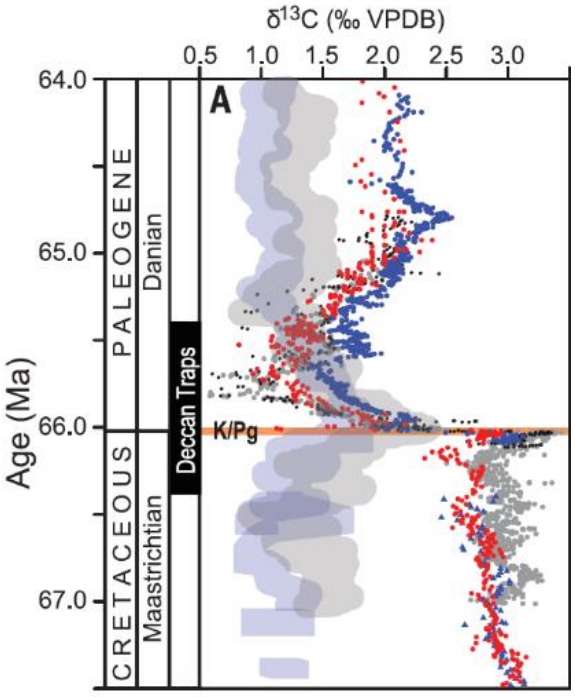

Figure 67. Data compilation from different IODP sites showing how surface $\delta^{13}C$ values (dots) collapsed onto the benthic values right at and after the boundary (figure from Hull et al., 2020).

One of the main geochemical characteristics of the carbon cycle disruptions at the K-Pg is the collapse of the gradient between the $\delta^{13}C$ values of the surface and deep ocean (e.g. Hull et al., 2020; Fig. 67). As this gradient is maintained by primary productivity in the photic zone and

export towards the deep ocean, this signal was first interpreted as a full disappearance of primary productivity in a “Strangelove Ocean” (Kump, 1991). Alternatively, the 'Living Ocean' scenario predicted that, primary productivity persisted, but a reduction in abundance and size of the calcareous plankton would have affected the export production and consequently induced greater remineralization of organic matter in the water column and muted the efficiency of the biological pump (D’Hondt et al., 1998). Finally, the fact that the collapse of the biological did not seem to be a global event led to the “Heterogeneous Ocean” scenario (Alegret et al., 2012; Hull and Norris, 2011). Recent modelling results based on seawater pH reconstructions seem to support the “Living Ocean” theory, which is the only scenario susceptible to produce flat $\delta^{13}C$ and pH gradients (Henehan et al., 2019). In all scenarios however, the export of organic and inorganic carbon to the bottom of the ocean is impacted and reduced at the boundary and remain low during the couple million years that follow (D’Hondt et al., 1998).

2. Existing sulfur records.

Disturbances of the sulfur cycle at the Cretaceous-Paleogene transition have been poorly documented. The low time resolution of the existing long-term $\delta^{34}S$ records covering the Cretaceous-Paleogene transition (Paytan et al, 2004, 1998) unfortunately do not allow the extraction of information on possible short-term (< 1 Myr) disturbances of the sulfur cycle across the K-Pg boundary. To date, only two studies have focused on disruptions of the sulfur cycle through the K-Pg transition through the reconstruction of $\delta^{34}S_{sw}$ (Kaiho et al., 1999; Witts et al., 2018).

The first CAS record ever produced across the K-Pg boundary is a very high-resolution bulk rock record from sediments collected at the marl section of Caravaca (Spain; Kaiho et al., 1999; Fig. 68). The authors collected sediments on the 80 cm thick interval centered around the boundary defined by a layer enriched in iridium (e.g. Nichols et al., 1986; Orth et al., 1981; Smit and Hertogen, 1980), the global marker of the Chixculub impact. The record was established on samples of 50 g of sediments treated with hydrogen peroxide and sieved above 63 µm to recover foraminifera tests described as filled by diagenetic calcite. No details are provided about the part of the sediments analyzed for $\delta^{34}S_{CAS}$ though the CAS content of the sediments is very low (100 to 200 ppm). The record presents an instantaneous 6 ‰ jump across the boundary. However, the high sulfide content of the Maastrichtian part of the record compared to the low CAS concentration could indicate a contribution of pyrite oxidation to the measured CAS, especially regarding the size of the samples required.

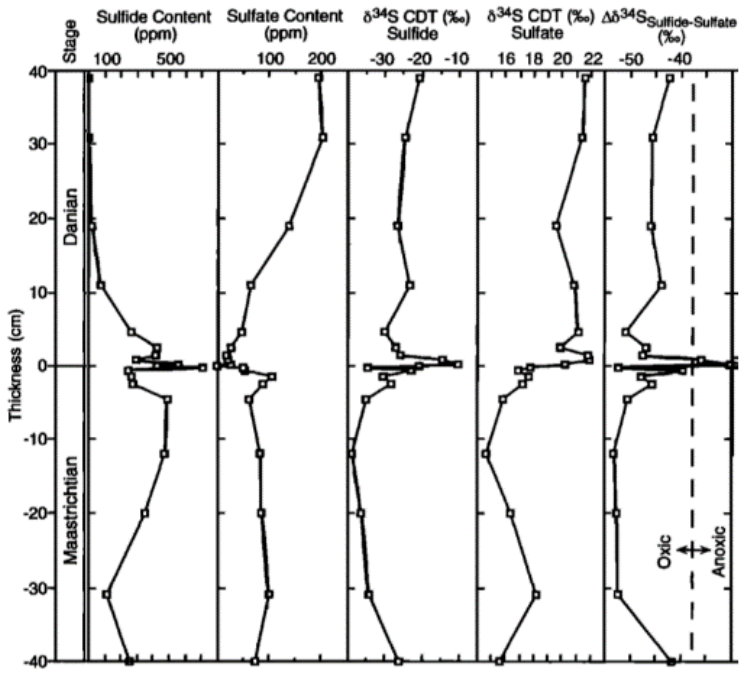

Figure 68. First K-Pg boundary record of $\delta^{34}S_{CAS}$ values used to reconstruct $\delta^{34}S_{sw}$, Caravaca section, Spain (figure from Kaiho et al., 1999).

Witts et al. (2018) extracted CAS from bivalves collected of Seymour Island (Antarctica). The shallow marine López de Bertodano consists of mudstone sediments deposited in inner to mid shelf conditions (Olivero, 2012). Witts et al. (2018) collected well-preserved mollusk shells of six different genera from the unlithified silty clays to extract CAS and measured both $\delta^{34}S_{CAS}$ and $\delta^{18}O_{CAS}$. Correlations between the two isotopic systems were used to assess the impact of diagenesis, and the most abnormal values were interpreted as the result of either laboratory pyrite oxidation or recrystallization in the MSR zone (Fig. 69; Witts et al., 2018).

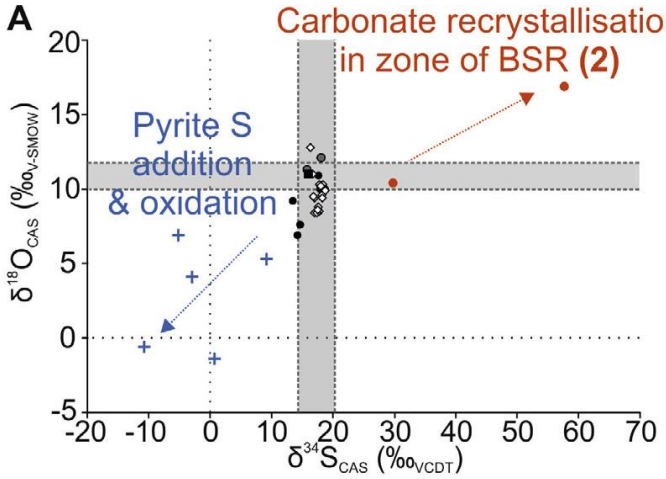

Figure 69. Crossplot of the $\delta^{34}S_{CAS}$ and $\delta^{18}O_{CAS}$ values from the bivalves of Seymour Island along with the possible trends for diagenesis and pyrite oxidation (figure from Witts et al. 2018).

Once this check performed, they produce a $\delta^{34}S_{CAS}$ record through the late Maastrichtian and the early Danian, revealing oscillations interpreted in terms of global $\delta^{34}S_{sw}$ variations (Witts et al., 2018; Fig. 70). In particular, the one datapoint with a more positive $\delta^{34}S_{CAS}$ value is interpreted as the marker of oceanic anoxia leading to increased pyrite burial and the marked negative excursion that follows the boundary is interpreted as the result of a significant decrease in pyrite burial associated with the large decrease in carbon burial, suggested by the weakening of the biological pump observed at the K-Pg boundary (Henehan et al., 2019; Kump, 1991).

In order to interpret their data in terms of global ocean $\delta^{34}S_{sw}$ values, Witts et al. (2018) calculate that the sulfate concentration of seawater must have been 2-3 mmol/L (Fig. 70). This is much lower than estimates based on fluid inclusions from evaporites, that suggest values between 10 and 23 mmol/L for the Cretaceous (Horita et al., 2002; Lowenstein et al., 2001; Timofeeff et al., 2006). It is also lower than estimates based on calculations derived from the barite record that suggests sulfate concentrations down to 5 mmol/L (Wortmann and Chernyavsky, 2007; Wortmann and Paytan, 2012). One could assume that to reproduce the data collected by Kaiho et al. (1999), the sulfate concentration would have to be even lower.

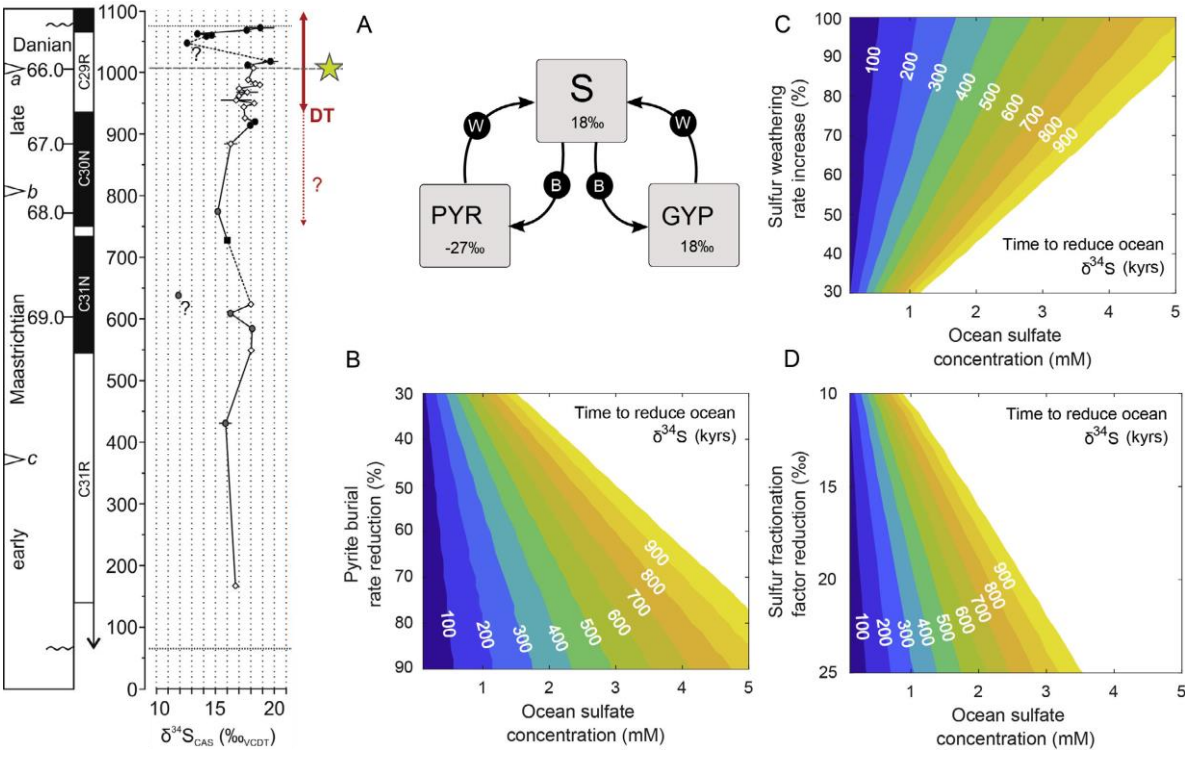

Figure 70. The left panel represents the stratigraphic age of the sediments analyzed across the K-Pg transition at Seymour Island, the $\delta^{34}S_{CAS}$ data the iridium anomaly used to locate the K-Pg boundary (Elliot et al., 1994), the red arrow represents the main phase of the Deccan (Schoene et al., 2015; Renne et al., 2015). The right panel presents numerical modeling calculations to assess the sulfur cycle changes inferred from the $\delta^{34}S_{CAS}$ record as a function of ocean sulfate concentration. The colors represent the time required to reduced $\delta^{34}S_{sw}$ by 3 ‰ (figures from Witts et al., 2018).

Overall, these K-Pg records show rapid and marked variations that barite does not, and variations different from each other, while each of these records is interpreted as that of the global ocean. In order to better understand and thus constrain the sulfur cycle over the Meso-Cenozoic transition, we produced a continuous high resolution $\delta^{34}S_{CAS}$ record using both planktic and benthic foraminifera from the open Pacific Ocean, in the framework of Arbia Jouini's PhD (Jouini, 2023), from the same samples used to analyze $\delta^{44/40}Ca$ (Jouini et al., 2023, Annex II).

II. A new combined sulfur record from benthic and planktic foraminifera.

1. New records from the Pacific equatorial ocean.

i. Material and methods.

The same foraminifera collected from Sites 1209 A and C from Shatsky Rise (Pacific Ocean) were treated to measure sulfur isotopes using the same cleaning protocol as the one established by Rennie et al. (2018). Different species were used for the planktic record (*Chiloguembelina Morsei, Praemurica inconstens, Woodringina claytonensis* and *Pseudoguembelina costulata*). One species was used for the benthic record (*Oridorsalis umbonatus*), which lives in the first 4 cm of the sedimentary pile (Rathburn and Corliss, 1994). Foraminifera were collected in the coarse fraction (> 125 µm) with the exception of *W. claytonesis* (> 63 µm). The age model of our core was discussed at length in Jouini et al. (2023) and the planktonic foraminiferal record reveals in a limited interval some Danian contamination in the Uppermost Maastrichtian sediments, probably due to drilling disturbances as already discussed in Dameron et al. (2017).

Samples were carefully picked and visually checked before and after cracking to remove foraminifera containing pyrite or filled with secondary calcite. Foraminifera, especially benthic, often had coccoliths aggregated to them, which we believe were removed during cleaning and final acid leaching. The cleaning steps were the same as Rennie et al. (2018).

Upon picking and cleaning, samples were dissolved and after saving an aliquot for trace elements by ICP-MS (X-series II Thermo Scientific) and an aliquot for sulfate measurements by Ion Chromatography (Metrohm ICS 300), samples were processed depending on the amount of sulfate available. For samples with sufficient sulfate to allow us to take an aliquot for Ca isotopic analyses, we did so. For the smallest samples, we spiked the samples for Ca isotopic analyses before introduction on the column, and the cation cleaning fraction was collected for later measurements of Ca isotopes (Jouini et al., 2023).

ii. Results and vital effect correction.

Data are presented against depth after vital effect correction (rmcd – revised meters composite depth Fig. 71).

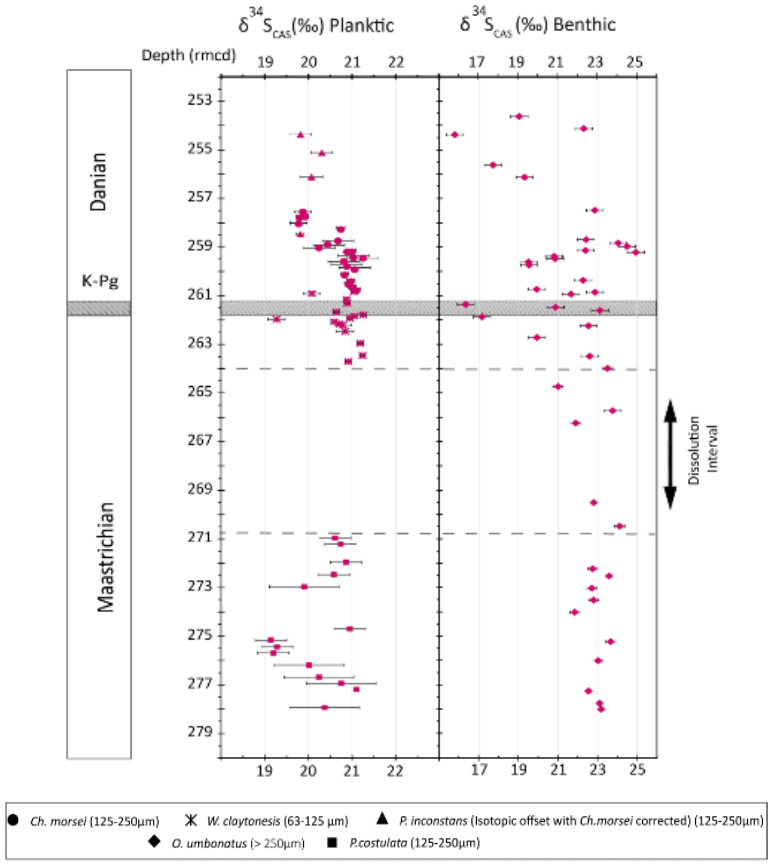

Figure 71. $\delta^{34}S_{CAS}$ measured in the planktic and benthic foraminifera collected from site 1209 A and C across the K-Pg transition, as a function of depth (stratigraphic information detailed in Jouini et al., 2023, figure from Jouini, 2023).

The $\delta^{34}S_{CAS}$ offset between the different planktonic species was corrected where possible. This offset was corrected between the two species *Ch. morsei* and *P. inconstens* from 253.13 to 253.63 rmcd based on the measurements of $\delta^{34}S_{CAS}$ (n=3) within the same sample and giving an isotopic shift of the order of - 1 ± 0.2‰. However, the very low abundance of the species *Ch. morsei*, between 263.74 and 260.94 rmcd, both in the two size fractions 250-125 µm and 125-63 µm did not allow us to correct the isotopic difference between *W. claytonensis* and *Ch. morsei*. The carbonate dissolution interval highlighted in the studied core between 270.73 and 264.24 rmcd (Dameron et al., 2017)also prevented us from comparing *W. claytonensis* and *P. costulata*. The difference in vital effect is assumed to be zero in both cases though the differences in $\delta^{34}S_{CAS}$ linked to vital effects can be up to 2 ‰ between foraminiferal species (e.g. Rennie et al., 2018).

Overall, planktic and benthic foraminifera are characterized by distinct values, with planktic foraminifera values between 19 ‰ and 21.5 ‰ while benthic foraminifera values range from 16.5 ‰ to 25 ‰. The datasets reveal no significant stratigraphic trends, except a decrease of $\delta^{34}S_{CASplanktic}$ over the Danian and in the upper Maastrichtian.

2. Diagenetic overprint and lab contamination?

The difference between benthic and planktic foraminifera is striking and must be elucidated. It is very unlikely to be due to vital effects as such a range has never been documented (see Chapter IV). In the following, we assess possible diagenetic overprint and lab contamination.

CAS concentrations of the planktic foraminifera varied between 700 and 1400 ppm. They were slightly lower for the benthic foraminifera (between 400 and 1200 ppm). The combination of careful visual screening during the picking as well as the lack of correlation between $\delta^{34}S_{carb}$ and the CAS content or the Fe/Ca ratio is consistent with no contribution of pyrite oxidation to our $\delta^{34}S_{carb}$ record. Coccolith contribution is unlikely as they tend to be much less concentrated in CAS than foraminifera in the first place and fractionated towards much lower $\delta^{34}S_{carb}$ values (Fig. 42 and 72).

The studied planktonic foraminifera from cores 1209 A and C visually appeared to have recrystallized to some extent, with a typical frosty appearance generally observed in the chalky sediments of deep marine cores (Sexton et al., 2006). And yet they retained trace metal and $\delta^{44/40}Ca$ ratios consistent with minimum diagenetic overprint in a sediment-buffered setting (Jouini et al., 2023). The Mg/Ca of the two populations of foraminifera are different. *O. umbonatus* reveals lower Mg/Ca values, between 3 and 5 mmol/mol, similar to or slightly higher than values measured in PETM or modern sediments (Rathmann et al., 2004; Rathmann and Kuhnert, 2008). The planktic foraminifera Mg/Ca ratios are mostly ranging from 6 to 8 mmol/mol with Sr/Ca ratios between 1 and 1.1 mmol/mol both in agreement with bulk and SIMS microanalyses of PETM foraminifera from the same core (Dutton et al., 2005; Kozdon et al., 2013).

The only possible diagenetic trend that appears in our dataset could be the relationship between CAS and $\delta^{34}S_{CAS}$ for data from the benthic foraminifera *O. umbonatus*. As discussed above, this trend might reveal a contribution of recrystallized calcite. As a result, even though benthic foraminifera are bigger and thicker than planktonic foraminifera, they seem to have been more influenced by pore fluid sulfate modified by MSR. For this reason, we first discuss the planktic record in terms of $\delta^{34}S_{sw}$ reconstruction.

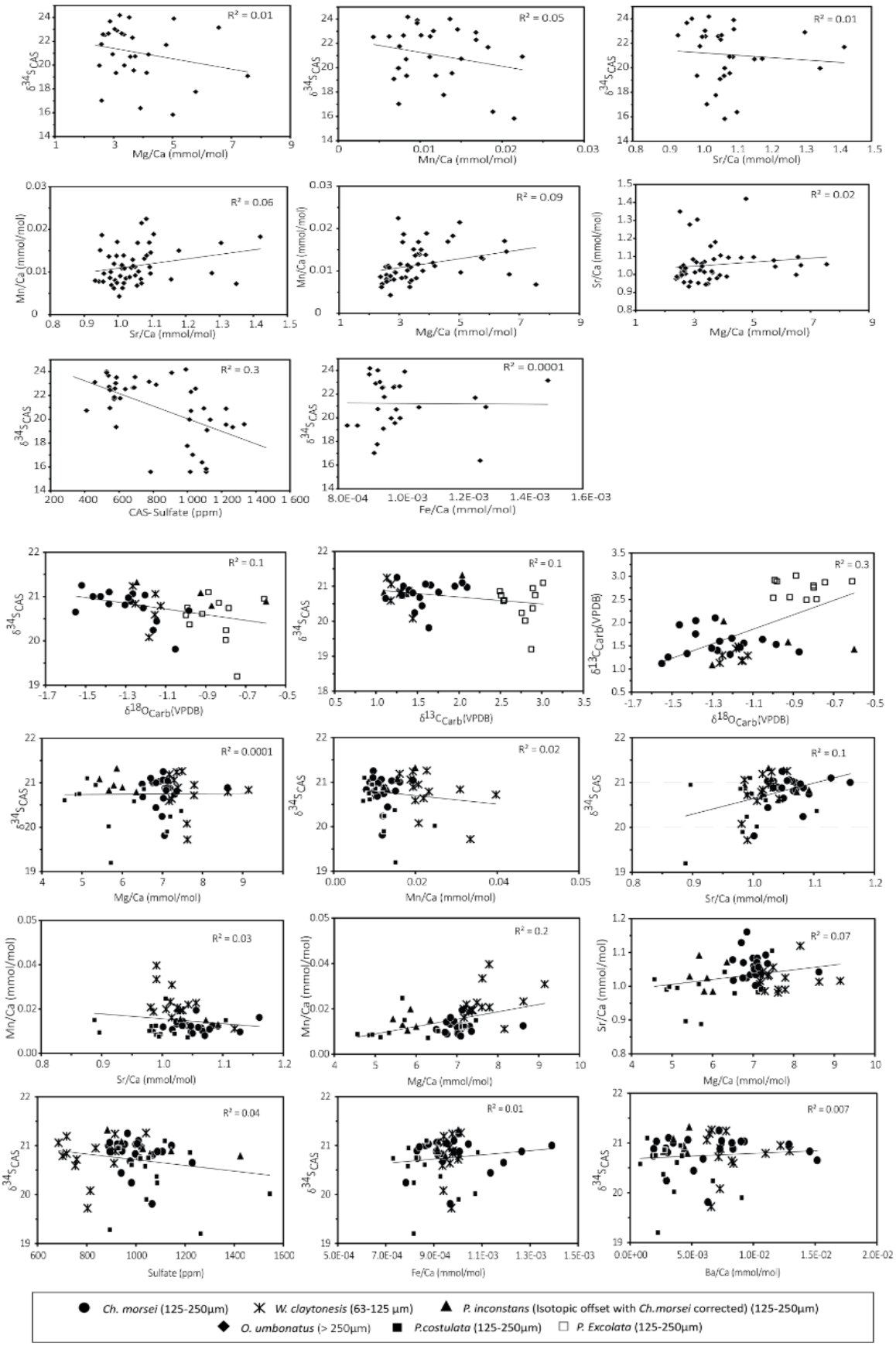

Figure 72. Trace element and stable isotope data measured in the foraminifera collected from site 1209 A and C across the K-Pg transition (figure from Jouini, 2023).

III. Reconstruction of the sulfur cycle.

1. Comparison of the planktic signal to other records.

Fig. 73 represents a compilation of the records covering the Meso-Cenozoic transition from -75 to -55 Ma. This compilation reveals that, similarly to what can be observed over the Cenozoic, the single-species foraminifera record proves to be the most consistent with the barite record.

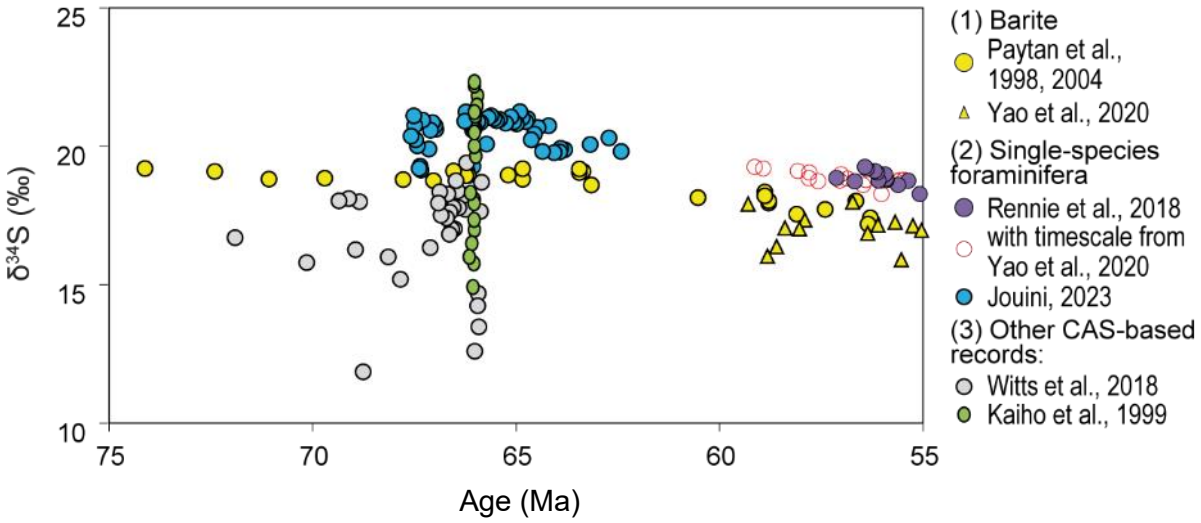

Figure 73. Compilation of different $\delta^{34}S$ records interpreted as global seawater signals. The CAS record from single-species foraminifera samples of Rennie et al. (2018) is presented with both the initial and Yao et al. (2020)'s revisited age models. Data from Paytan et al. (1998) are plotted using the age model from Kurz et al. (2003) and associating a K-Pg boundary age of 66.04 Ma.

Our $\delta^{34}S_{CAS}$ reveals very little change across the boundary unlike the previous CAS records (Kaiho et al., 1999; Witts et al., 2018). These records are characterized by different time resolution. Though we are far from the high time-resolution achieved by Kaiho et al. (1999), the level of variability observed in their record is delicate to explain based on our knowledge of the sulfur cycle, and insufficient characterization of their samples makes it hard to assess whether their signal reflects global changes or not. We also observe that most data by Witts et al. (2018) are trending towards negative values to an extent that is reproduced neither in the barite nor the planktonic foraminifera records. Three scenarios could explain the difference: ocean heterogeneity, vital effects, or diagenesis.

Ocean heterogeneity is unlikely to be the origin of the difference observed here as the residence time of sulfate, even with a concentration of 2-3 mmol/L is probably at least 1 Ma, which suggest that the open ocean is well mixed with respect to sulfate. Vital effects in mollusks living in the open ocean is unlikely to explain such a variability (see Chapter IV). It should be noted that in bivalves, CAS can be characterized by low $\delta^{34}S_{CAS}$ values. A recent investigation of lucinids infaunal bivalves revealed that the sulfur isotopic composition of their CAS was

much lower than seawater values (Bryant et al., 2023). This observation was interpreted as the result of incorporation of sulfate with low $\delta^{34}S$ value produced by the sulfur-oxidizing symbionts hosted by lucinids. However, most of the record by Witts et al. (2018) is based on epifaunal Pycnodonts, in which no such association has been documented. Vital effects are unlikely to be the cause of the variability observed.

Witts et al. (2018) excluded that diagenesis was at the source of the variability they observe, because of the lack of correlation between $\delta^{34}S_{CAS}$ and $\delta^{18}O_{CAS}$. Though the authors have no barite record to compare their data to in order to ensure that the $\delta^{18}O_{CAS}$ signal is of seawater origin. Since 2018, the resolution of the $\delta^{18}O_{barite}$ curve covering the last 130 Ma improved and supports a value for $\delta^{18}O_{SO4}$ around 13 ‰ for the K-Pg boundary (Waldeck et al., 2022), higher that the values centered around 10 ‰ from the Seymour Island bivalve CAS. In addition, a $\delta^{34}S_{CAS}$ vs. $\delta^{18}O_{CAS}$ correlation is not necessarily observed, though in those cases, $\delta^{18}O_{CAS}$ values are more affected than $\delta^{34}S_{CAS}$ (Di et al., 2023; Rennie and Turchyn, 2014; Turchyn et al., 2009). Therefore, diagenesis cannot be fully excluded, at least for sulfate.

Our planktic record, in agreement with barite data, thus seems to suggest that the K-Pg mass extinction was of little influence on the global sulfur cycle in the short term. Alternatively, this may be due to the fact that for both the barite record and our foraminiferal record, the sampling resolution step did not enable us to capture the sulfur cycle disruptions associated to the mass extinction, but rather the evolution before and after. In the core studied, this could be due to the presence of a gap as the iridium-enriched clay layer, the main marker of the K/Pg boundary, was not detected here. Regardless, our data do not reproduce the trends observed by Witts et al. (2018) and the K-Pg transition appears mostly as a point at which $\delta^{34}S$ values start to decrease towards the Cenozoic $\delta^{34}S$ minimum at ~52 Ma.

2. The long-term sulfur cycle.

Despite the offset between the CAS and barite records, both provide the same stratigraphic evolutions and draw the possibility of more connections between the carbon and sulfur cycle evolution over the Cenozoic than what could have been previously described. First, the K-Pg boundary (~66.04 Ma) does appear to be the onset of a long-term $\delta^{34}S_{sw}$ decrease from the late Mesozoic value, as a long-term decrease of the $\delta^{13}C$ signal starts as well.

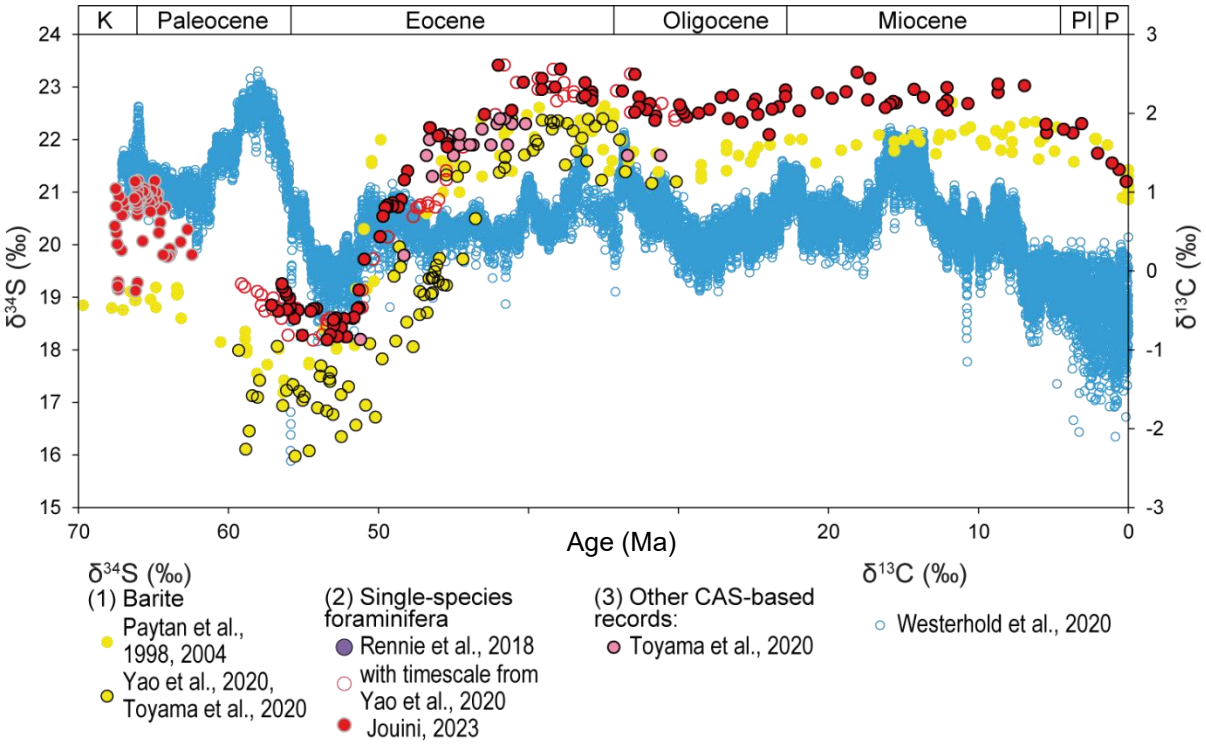

Figure 74. Cenozoic record of $\delta^{34}S_{sw}$ values against Westerhold et al.'s $\delta^{13}C$ (2020) compilation. Data from Paytan et al. (1998) are plotted using the age model from Kurz et al. (2003) and associating a K-Pg boundary age of 66.04 Ma. K: Cretaceous. Pl: Pliocene. P: Pleistocene.

As previously pointed out by Kurtz et al. (2003), the Paleocene positive $\delta^{13}C$ excursion is not reflected in $\delta^{34}S_{sw}$ values and yet, the value reached by $\delta^{13}C$ after the excursion is much lower than at the beginning of the Paleocene, similar to the long-term decrease of $\delta^{34}S_{sw}$. At ~52 Ma, both curves start evolving towards heavier values at the same time (Rennie et al., 2018), and both curves display decreasing values near the Eocene-Oligocene transition (~33.9 Ma). Further constraints are thus overall required to fully describe the possible connections between the carbon and sulfur cycles. First, the foraminifera record is uncomplete and the Rennie and Jouini records must be connected. Second, age models must be reconciled. And finally, a careful $\delta^{13}C$-$\delta^{34}S$ crossplot must be established for the Cenozoic to determine how much the sulfur and carbon cycles are directly correlated or not.

3. The difference between benthic and planktic foraminifera.

Regardless of whether we assume that planktic foraminifera record the value of seawater or not, the benthic-planktic difference remains, and benthic foraminifera exhibits signs of $\delta^{34}S_{CAS}$ affected by MSR-induced sulfate distillation in pore fluids. In Fig. 75, we present the evolution of $\delta^{34}S_{CAS}$ and that of the benthic-planktic difference as a function of age following our age model (Jouini et al., 2023).

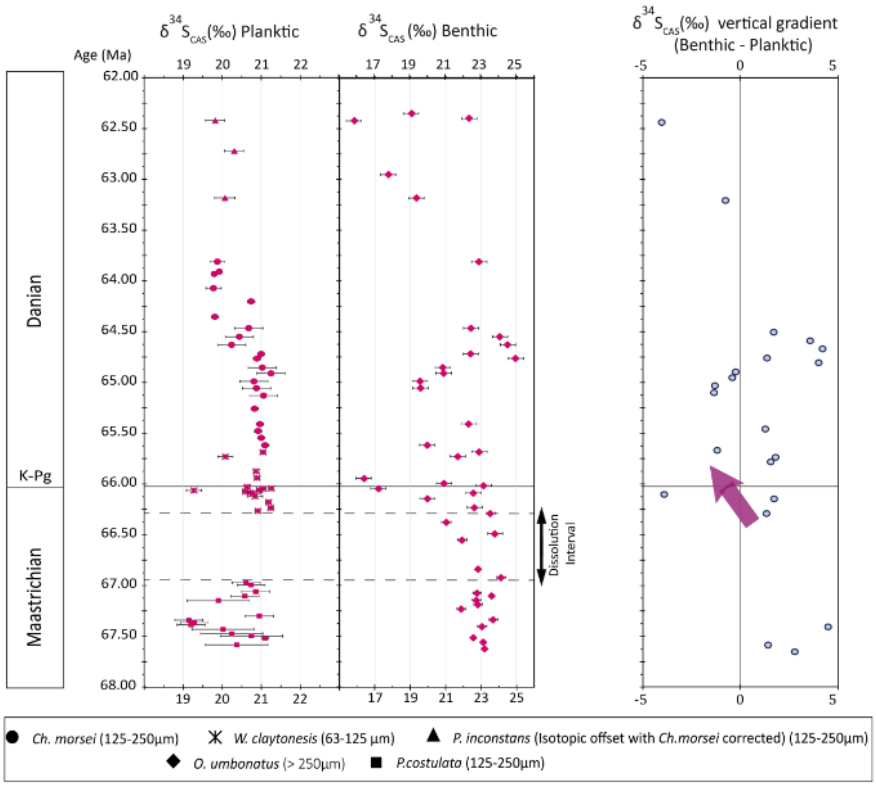

Figure 75. Age model of the benthic and foraminifera records and calculated difference between them. Age model and data from (Jouini, 2023)

Three scenarios can explain this difference between benthic and planktic: (1) oceanic sulfur isotope stratification, (2) a pore fluid $\delta^{34}S$ composition at the sediment-water interface where *O. umbonatus* resides and (3) a stronger diagenetic overprint of benthic foraminifera (Fig. 76).

(1) Oceanic stratification has never been observed in the Mesozoic or Cenozoic oceans, even though it has been suggested that some water masses such as a partially connected Eocene Arctic ocean could have different sulfur isotopic composition (Yao et al., 2021; Yao and Paytan, 2020) or that stratification could have occurred in earlier times of the Phanerozoic (e.g. Kajiwara et al., 1994).

(2) A pore fluid $\delta^{34}S$ composition that evolved in the first few centimeters of the sediment water interface is possible, but to the best of our knowledge it has never been observed in the deep ocean. It would however reconcile the trace element composition with the calcium and sulfur isotope signals, as the benthic foraminifera would thus record a $\delta^{34}S$ value that increased due to MSR. However, *O. umbonatus* has been documented to live in modern methane seeps and to be able to live in dysoxic environments. As MSR is not necessarily mutually exclusive with aerobic respiration (Martin et al., 2010; Rathburn and Corliss, 1994), it is at least possible to assume that MSR occurred close to the sediment-water interface. However, in that case, recrystallization of the planktic foraminifera would have likely been influenced by MSR as well. An alternative

exploratory scenario would be that the higher $\delta^{34}S$ values measured in benthic reflect MSR occurring in anaerobic microniches enriched in organic matter in the sediments (Jørgensen, 1977) and that they reflect very local MSR and redox processes.

(3) A stronger diagenetic overprint of *O. umbonatus* would suggest that the recrystallization rate of the benthic foraminifera is slower than that of the planktic. This hypothesis is consistent with the heterogeneity of diagenetic overprint previously documented (e.g. Present et al., 2015). *O. umbonatus* is poorer in Mg and SO_4^{2-} than the planktic foraminifera we analyzed, which suggests that their tests are more resistant to recrystallization. If the planktic recrystallize faster, they would do so in a seawater-like pore fluid, while the benthic foraminifera, more resistant, would recrystallize slower and deeper in the sediment column.

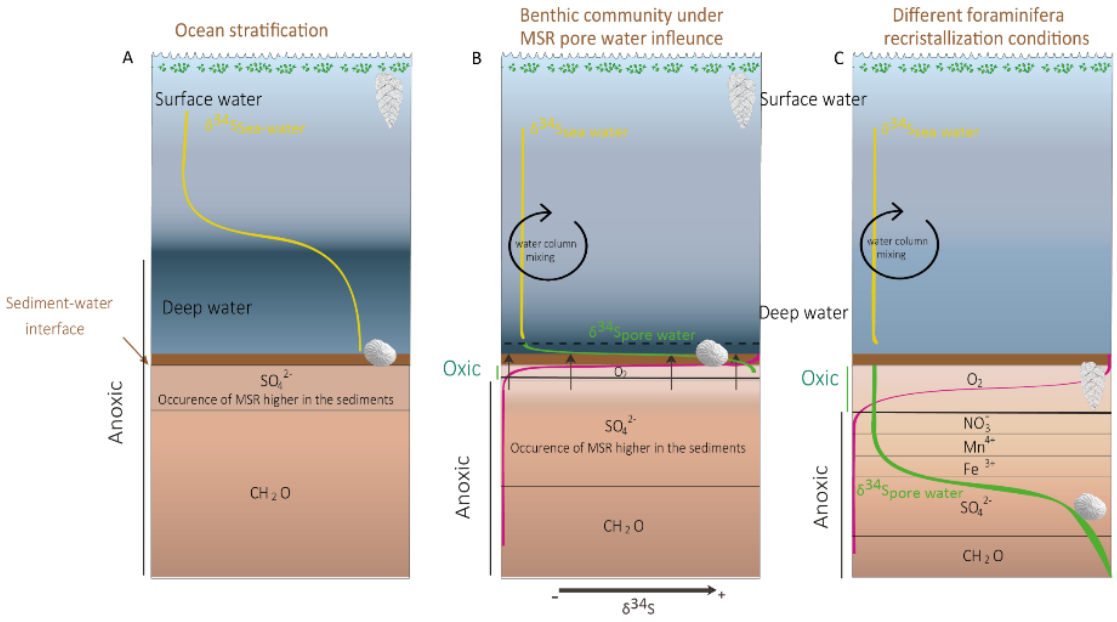

Figure 76. Different models of possible source of the $\delta^{34}S_{CAS}$ difference between benthic and planktic foraminifera. (A) Ocean stratification, (B) sharp pore fluid evolution with water-sediment interface influenced by MSR, (C) different of recrystallization depths between benthic and planktic foraminifera as the results of different recrystallization speeds (figure from Jouini, 2023).

4. An oscillating MSR zone around the K-Pg boundary?

As a result, the difference between benthic and planktic foraminifera, if we assume a different time-dependent recrystallization rate for each of them, could be translated into a variation of the MSR zone position. When the difference is more positive, MSR occurs closer to the water-sediment interface. Alternatively, it could also mean that MSR is characterized by a greater fractionation between sulfate and sulfide, hereby suggesting higher MSR rates. When the difference is closer to zero, or becomes negative, it can be assumed that the MSR zone moves down in the sediments and that porewater sulfate becomes isotopically similar to seawater

sulfate. Pore fluid sulfate could also possibly become isotopically lower if reoxidation of sulfide occurs in the sediments, which could be expected if the pile is more oxic. The redox level is related to the Depth Penetration of Oxygen, itself following the sedimentation rates and organic matter availability (e.g. Berner, 1984; Johnson et al., 2021). If we assume that scenario 2 occurs, the interpretation is similar.

Since sulfate is abundant in seawater and most likely constant over the K-Pg boundary, the availability and nature of the organic matter, and not sulfate, is likely to be the key parameter that controls the presence and rate of RMS (e.g. Berner and Raiswell, 1983; Sim et al., 2011). However, during the Cretaceous-Paleogene transition, a drastic reduction in the flux of calcareous pelagic sedimentation occurred in oceanic sites that followed the mass extinction of calcareous plankton. It induced a strong condensation at the K-Pg boundary, or even a hiatus (Alvarez et al., 1980). The sedimentary expression of condensation is the level of iridium-enriched clay, and the P0 zone is often very condensed or absent, similarly to what can be observed at Site 1209 (Fig. 77; Bralower et al., 2002).

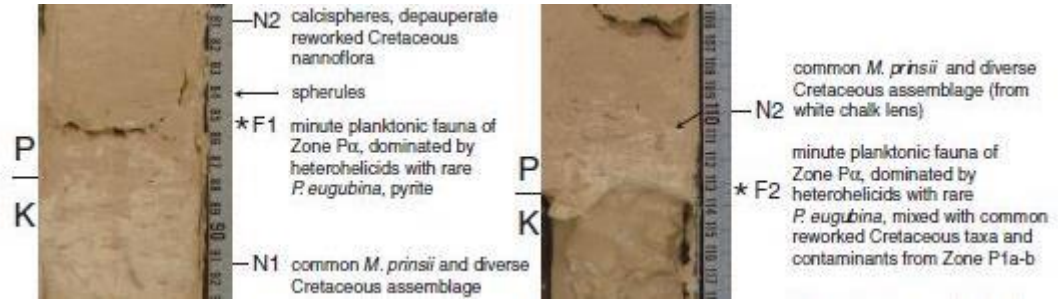

Figure 77. The K-Pg boundary at Shatsky Rise (figure from Bralower et al., 2002)

In addition to the reduction in diversity, the reduction in the size of calcareous plankton has contributed the export of organic matter to the ocean floor (Birch et al., 2016). As detailed previously, whether due to lower productivity, lower export or higher remineralization in the water column, less organic matter reached the bottom of the ocean (Henehan et al., 2019). It is plausible to assume that it induced a migration of the redox stages of the sedimentary column, and therefore of RMS, towards greater depth. Such deepening is consistent with the presence of bioturbation and a reddish color change in sediments at the K-Pg boundary at Shatsky Rise (Fig. 7), which reflect a well-oxygenated ocean floor.

For all the reasons listed above, the variations of the difference between benthic and planktic $\delta^{34}S_{CAS}$ values could be interpreted as redox oscillations in the deep ocean sediments. This interpretation is supported by the disappearance of the $\delta^{34}S_{CAS}$ difference at the same time as the $\delta^{13}C$ gradient collapses. Hence, MSR deepens as organic matter export is reduced. It is more puzzling, however, that the signals appear simultaneous, as recrystallization is an asynchronous post-depositional signal (Fig. 78). If, however, a version of scenario 2 is at the

origin of the measured signal, then the signals can be synchronous as the benthic foraminifera would then acquire their $\delta^{34}S_{CAS}$ in their lifespan.

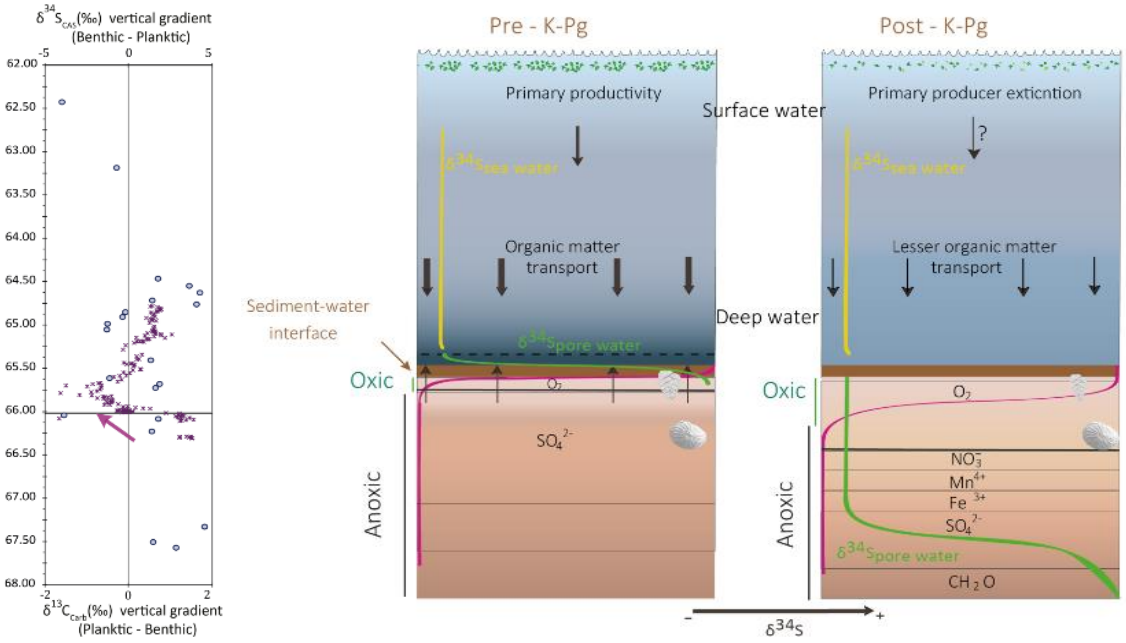

Figure 78. Left panel: evolution of the benthic-planktic $\delta^{34}S$ difference in comparison to the evolution of the $\delta^{13}C$ gradient (Hull et al., 2020) as a function of age (Ma). Right panel: pre and post K-Pg situation showing the difference between a shallow MSR zone before the boundary and its deepening after the boundary (figures from Jouini, 2023).

IV. Conclusion.

We produced a new combined record of $\delta^{34}S_{CAS}$ based on planktic and benthic foraminifera picked from IODP cores 1209 A and C cored in the equatorial Pacific at Shatsky rise. Our new record reveals that planktic foraminifera and benthic foraminifera did not recrystallize at the same depths and that planktic foraminifera are more likely to have preserved their original values due to a faster recrystallization.

Consequently, we use the planktic foraminifera record as a proxy to reconstruct $\delta^{34}S_{sw}$ during the Meso-Cenozoic transition and show that, in agreement with the barite record, no major change occurs. In this regard, our results contradict previously published CAS records.

The benthic foraminifera record is best interpreted in comparison to the planktic record, and we calculate the difference between the benthic and planktic foraminifera. The difference is not constant through time and reveals an oscillating trend in agreement with the gradient calculated between surface and deep ocean $\delta^{13}C$ values reconstructed across the K-Pg boundary.

We interpret this signal as the result of the decrease organic matter export documented at the K-Pg, which would generate a deepening of the MSR zone in the sediments that become more

oxic at the K-Pg. This decrease in the benthic-planktic difference could also be related to the negative excursion observed at Seymour Island, though it seems to occur earlier at Shatsky rise. However, a signal of diagenetic origin is harder to interpret in terms of absolute age as it is, by definition, asynchronous.

We reveal, for the first time, a heterogeneous signal from the same sample that allow us to record both global (seawater) and local (diagenesis/redox conditions in the pore fluid) signals across the K-Pg boundary and document a connection between the sulfur and carbon cycle never explored before.

This exciting result requires confirmation and further work, that will guide my research project for the next ten years. Or more.

Annex I: Calcium isotopes: new calibrations, and additional paleoenvironmental information.

Annex II. Research project: the sulfur cycle reconstructed, from rivers to the depths of the ocean.

I. Interactions between biogeochemical cycles control the composition of the ocean-atmosphere system.

II. Methodology, approach, and tasks

My project aims at providing an unprecedented view of the modern and past sulfur cycle measuring $\delta^{34}S$ and SIF for the main sulfur fluxes to the ocean and for the ocean itself to calculate f_{pyr} and pyrite oxidation on land. To obtain the necessary nature and diversity of $\delta^{34}S_{sw}$ records, single-species foraminifera samples are therefore of high interest (Rennie et al., 2018). However, $\Delta^{33}S$ precision of the Neptune method is barely sufficient for most SIF investigations, because the ^{32}SH interference pushes the instrument to its limits in terms of mass resolution and plasma stability and makes it very sensitive to air injection. Furthermore, the argon plasma contains ^{36}Ar that interferes with ^{36}S and thus $\Delta^{36}S$ cannot be measured at all. We need a method to measure SIF at high precision in small samples (river waters, foraminifera) to move forward in biogeochemical cycle and Earth system investigations. I will combine MC-ICP-MS and SIF thanks to a new generation of MC-ICP-MS equipped with a reaction-collision cell. The project can be divided into three tasks that focus on different parts of the investigation of f_{pyr}.

1. **Task 1 - Development of multiple sulfur isotope measurements with a collision cell and constraining the modern sulfur cycle**

Collaborators: Aimeryc Schumacher, Erica Erlanger, Thomas Rigaudier (CRPG), Julien Bouchez (IPGP), Sophie Opfergelt (Université de Louvain). I intend to include at least a postdoc and a grad student in this task.

Background: Three fluxes need to be known to fully describe the oceanic sulfur cycle: i) inputs, ii) output as evaporite and iii) output as sedimentary pyrites. The evaporite output flux is assumed to bear the same isotopic composition as seawater. Estimates exist for the isotopic composition of pyrite (Johnston et al., 2008). Rivers supply approximately 75 % to 95 % of sulfate sources to the ocean (4.7 Tmol/yr today, including 1.3 Tmol/yr from anthropogenic sources), riverine input isotopic compositions therefore allow us to approximate those of F_{in}. Sulfur pollution (Brenot et al., 2007) is a major health issue (van Zelm et al., 2008) and a threat to freshwater wetlands (Lamers et al., 2002; Pester et al., 2012), key actors of the carbon cycle. To estimate the $\delta^{34}S$ and SIF of F_{in}, we will average the values we will measure for

dissolved sulfate in existing collection of samples from the world main rivers (e.g. Gaillardet et al., 1999), collect new samples, and correct for anthropogenic inputs. $\delta^{34}S_{in}$ has been estimated (Burke et al., 2018b), $\Delta^{33}S$ (with the exception of some rivers draining Archean terranes; e.g. Torres et al., 2018) and $\Delta^{36}S$ values of rivers remain to be measured. For example, Tostevin et al. (2014) center the $\delta^{34}S$ values of rivers on an "accepted" value of 8‰, which is more positive than the data-based 4.8 ‰ average (Burke et al., 2018) and no constraints exist. In return, SIF provide decisive information on pyrite oxidation on land. Such estimation is critical for two reasons. First, pyrite oxidation is a sink for atmospheric oxygen. Second, it produces a source sulfuric acid that dissolves rocks and thus reduces CO_2 consumption by competing with carbonic acid during weathering (e.g. Calmels et al., 2007). We will investigate whether sulfate is conservative on land because it could be partially consumed during MSR (Turchyn et al., 2013), jeopardizing the conservation assumption and biasing pyrite oxidation estimates. However, estimating the amount of MSR on land can also further constrain the interactions of MSR and methanogenesis, for instance in wetlands. Finally, we will verify whether modern rivers are biased by the dissolution of young evaporites (Halevy et al., 2012). By improving the estimation of rivers $\delta^{34}S$ and SIF values, we will improve our understanding of the global pyrite weathering flux and improve our estimates of f_{pyr}.

Instruments, protocols, samples: The existing Neptune method does not allow $\Delta^{33}S$ measurements with a precision better than 0.20 ‰, of the same order as the SIF investigated. The required precision (2σ) would be ideally 0.03 ‰ for $\Delta^{33}S$ and 0.30 ‰ for $\Delta^{36}S$. Because ^{33}S is measured on the extremely narrow part of the ^{33}S peak shoulder that is free of the ^{32}SH interference, the data is extremely sensitive to any instability, such as air injection in the plasma during the transition between samples. The precision can be improved using the collision cell to remove ^{32}SH and using continuous flow injection to prevent air injection in the plasma. Furthermore, the argon plasma (and the presence of ^{36}Ar) prohibits $\Delta^{36}S$ measurements. Thanks to its collision cell, CC-MC-ICP-MS completely remove argon after the ionization is complete, thereby allowing measurement of ^{36}S (Fig. 83). The CC-MC-ICP-MS at the CRPG will be equipped with two 10^{12} ohm resistor amplifiers to improve the precision on ^{33}S and ^{36}S. 10^{12} is preferable to 10^{13} as it allows having the same resistor on ^{33}S and ^{36}S and prevents calibration issues. Better room temperature control than at the Nu Instrument factory will improve precision compared to the first test (0.8‰ 2σ). Samples need to be purified following an established protocol using acid solutions (Paris et al., 2014a).

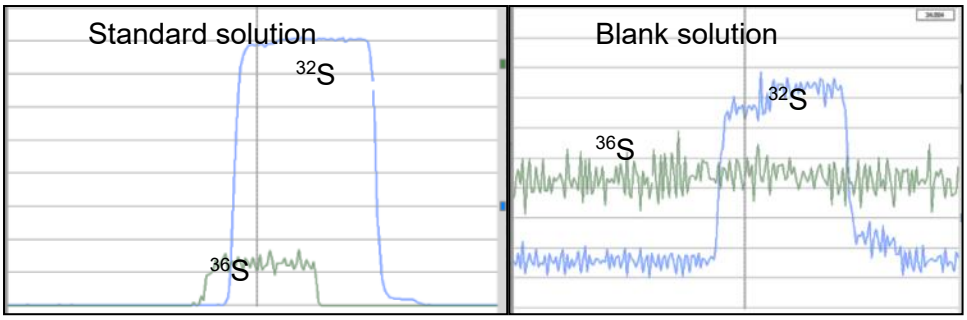

Figure 87. Preliminary results on the CC-MC-ICP-MS SAPPHIRE obtained at the Nu Instrument factory: the collision cell removes entirely ^{36}Ar from ^{36}S measured in standard solution and acid blank solution.

Objectives and means: I have access to major river sample collections through collaborations with two world specialists on river chemistry (Christian France-Lanord, CRPG, and Julien Bouchez, IPGP). These samples are already analyzed for major and trace element concentrations and various isotopic systems. Their composition can be corrected for atmospheric and anthropogenic inputs (e.g. Gaillardet et al., 1999; Lemarchand et al., 2002). Samples have been filtered upon collection and stored in refrigerated rooms. They come from Himalayan, Amazonian and other world rivers that represent over 50% of the world's river discharge. In addition, new pyrite data from existing oceanic sediments will be acquired to better constrain $\delta^{34}S$ and the SIF of F_{pyr}.

1.1-What are the world average $\delta^{34}S$ and SIF of rivers? For the world average to be geologically relevant, anthropogenic inputs such as fertilizers or acid rains must be assessed and corrected (Brenot et al., 2007). We will compare main river stems and their tributaries, analyzing rain samples, river samples up and downstream from a major urban or agriculture area, using time series and by direct analyses of possible pollutants. Case studies will add constrains on the anthropogenic bias, such as the Seine, Danube, and Rhine rivers or the Ganges-Brahmaputra and Amazon systems, where many samples are already available. Consequently, we will provide an unbiased estimate of f_{pyr}.

1.2- What is the relative proportion of sulfate that comes from pyrite oxidation? Each source of sulfur has a different $\delta^{34}S$-$\Delta^{33}S$-$\Delta^{36}S$ composition and the effect of mixing on SIF is not linear (Fig. 82). Once corrected from human pollution, the relative contribution of each source can be disentangled using mixing diagrams or mass-balance calculations if the geological context is sufficiently characterized and SIF add dimensions to those diagrams. Mixing different reservoirs, with or without MSR will have distinct effects of $\Delta^{33}S$ and $\Delta^{36}S$. When possible, we will analyze $\delta^{18}O$ of oxygen from dissolved sulfate (Calmels et al., 2007), or additional isotopic systems (e.g. B, Li or Sr; (Guinoiseau et al., 2018; Louvat et al., 2011) to add further dimensions to the diagrams. We will apply the approach at least to the Ganges-Brahmaputra, the Amazon, and European basins, some of the main sources of sulfate to the ocean. When

possible we will collect (or rely on existing samples and data) and analyze sulfur sources: evaporites, pyrites, hydrothermal sulfur if relevant and rain samples, to develop mixing models (Gunnarsson-Robin et al., 2017; McDermott et al., 2015; Ono et al., 2012, 2007).

1.3- A focus on wetlands and permafrost areas will also help understand sulfur cycle in these regions that are critical with respect to the ongoing climate crisis as MSR likely mitigates methane emission from wetlands (Pester et al., 2012). SIF will help understand the extent of the cryptic sulfur cycle in both established wetlands and in thawing permafrost areas. Sulfur data will be combined with ongoing work on iron and nitrogen and collaborations with ecologists will be developed to analyze microorganism population dynamics.

1.4- Is the geologically-recent sulfur riverine input biased by young evaporite recycling (Halevy et al., 2012)? Water samples from rivers draining areas older than 20 Ma cannot be affected by such bias. The Tibetan Sedimentary Series and the High Himalayan Crystalline Core are necessary targets. Ideally, a field trip to the Yarlung Tsangpo river and its sulfate sources will provide samples necessary to document a part of the system with no influence of young sediments. If the $\delta^{34}S$ of dissolved sulfate is lower than averaged world rivers, it would support the control the $\delta^{34}S$ of modern rivers by young oceanic evaporites.

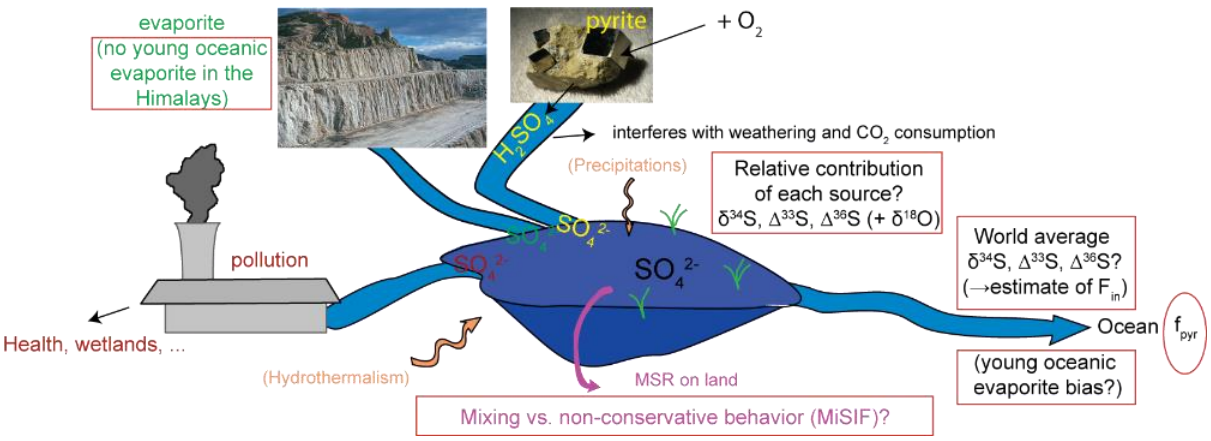

Figure 88. The main objectives of task 1: using $\delta^{34}S$ and SIF of dissolved sulfate in rivers and their source material to calculate (1) the world average of $\delta^{34}S$ and SIF of sulfate delivered to the ocean (F_{in}) and a possible bias due to young oceanic evaporites (2) sulfur conservation on land, (3) pyrite oxidation.

2. Task 2 - The role of sulfur in biomineralization and transfer function of sulfur isotopes into the sedimentary record: vital effects and diagenesis.

Collaborators: Claire Rollion-Bard (IPGP), David Evans and Anthea Arns (Max Planck Institute) Anne Gothmann (St Olaf), Jennifer Fehrenbacher (OSU), Catherine Zimmerman (CRPG), one postdoc.

Background: Foraminifera constitute a critical archive for sulfur isotope reconstructions. Unlike barites, they can be measured in different environments (e.g. benthic vs. planktic), and they

allow better age control through biostratigraphy and direct correlations with other carbonate-based paleoenvironmental proxies (e.g. $\delta^{13}C$, $\delta^{18}O$, Mg/Ca). Task 2 focuses on sulfate incorporation mechanisms and on how $\delta^{34}S$, $\Delta^{33}S$ and $\Delta^{36}S$ are transferred to foraminiferal calcite and preserved in sediments. Overall, the paths for sulfur incorporation are unknown. The question of sulfur/sulfate incorporation in biogenic carbonates must be addressed for two reasons. First, the sulfate concentration of a solution affects the crystallography of the calcium carbonate that precipitates. At high sulfate concentrations, calcite precipitates less easily than aragonite (Bots et al., 2011). Given that sulfate is very concentrated in today's ocean and that calcite is a naturally occurring biogenic carbonate, for instance in foraminifera, mechanisms must exist to control sulfate in the precipitating fluid of biomineralizing organisms. Sulfate therefore affects mineralogy. Second, sulfate plays also a key role in organic molecules that lead the biomineralization and it is actively debated whether sulfate groups substitute to carbonate ions, are linked to organic molecules, or both (e.g. Cuif et al., 2003; Paris et al., 2014b; Richardson et al., 2019; Rose et al., 2019; van Dijk et al., 2017). Sulfur overall plays many roles in biomineralization, as detailed in Chapter IV. The second major goal is to understand the mechanisms and role of sulfur incorporation in biomineralization.

Instruments, protocols, samples: Task 2 requires the use of the CC-MC-ICP-MS soon available at the CRPG, the nano-SIMS (nano-Secondary Ion Mass Spectrometry) available at the MNHN as a National facility, synchrotron radiations available in world facilities (e.g. SLAC - USA; SOLEIL and ESRF - France). Protocols for growing foraminifera on Catalina Island (USA) will be used and a new set-up for precipitating carbonates will be developed at the CRPG with ideally the help from a postdoc.

2.1- Are ^{33}S and ^{36}S solely affected by inorganic kinetic or equilibrium isotope fractionation or by vital effects as well? Minor isotopes fractionations have not been determined in inorganic or biogenic carbonates. A postdoc will set-up experiments following a protocol that we have already used to determine equilibrium and kinetic $\delta^{34}S$ effects in precipitating inorganic calcite and aragonite (Barkan et al., 2020). They will also decouple calcium, sulfate, and carbonate ion activities in the solutions to understand the link between solution chemistry and CAS incorporation. I will pursue foraminifera culture experiments on Catalina Island (USA) using existing protocols (e.g. Paris et al., 2014b). We will explore the effect of $\delta^{34}S_{sw}$, seawater composition (e.g. sulfate concentration) or temperature. The results will inform whether biomineralization affects SIF signatures and provide more information of the possibility to use CAS to reconstruct past seawater sulfate or carbonate ion concentrations.

2.2- How is sulfur incorporated in foraminiferal calcite? Is it passively (endocytosis of seawater, e.g. Bentov et al., 2009) or actively (pumping of sulfate, Paris et al., in prep) brought to the calcification site? Synchrotron X-ray Absorption Near Edge Spectroscopy (XANES) and micro–

X-ray Diffraction (μXRD) lines will help decipher sulfur speciation and its link to foraminiferal crystallography. As the activity of sulfate in the solution plays a role on carbonate mineralogy, it is a question that must be solved. In order to understand whether all sulfur in foraminiferal calcite is derived from seawater or if some comes from the food consumed by the foraminifer, we will lead experiments using spiked sulfur. First, the seawater where the foraminifera grow will be spiked with ^{33}S. In a second experiment, the food source will be grown in spiked seawater. In both cases, a couple of tests will be mapped, with cytoplasm content, if possible, on the nano-SIMS to understand more precisely where the spiked sulfur is located. We will dissolve the remainder of the cultivated tests and analyze them by CC-MC- ICP-MS to establish a global sulfur budget of the test.

2.3- In order to understand the role played by ACC (Amorphous Calcium Carbonate) in biomineralization, and its part in controlling CAS content and sulfur isotopic compositions, I will work in collaboration with David Evans and Anthea Arns who precipitated ACC in solutions with different concentration of sulfate or magnesium. I will also measure calcium isotopes in those samples, after having developed calcium isotope measurements on the CC-MC-ICP-MS. I will also extend my work on biomineralization by collaborating with Anne Gothmann who grows corals in controlled conditions to understand which aspect(s) of seawater chemistry controls the elements and isotopic compositions of their skeletons. As they are grown in controlled, varying, and decoupled DIC, pH, and CO_3^{2-} concentration, they are a perfect target to understand if the CAS content reflects the carbonate ion concentration of seawater.

2.4- Can we better constrain diagenetic processes affecting foraminifera and understand if benthic and planktic foraminifera react differently and can we use SIF to recognize carbonates that underwent diagenesis? Core-tops and water column foraminifera will be used to study early diagenesis using samples obtained in collaboration with Will Berelson (USC) and collecting additional samples. A systematic comparison of planktic and benthic foraminifera from shallow and deep environments with different sedimentation rates will be explored. In addition, experiments using seawater with spiked sulfate ($^{33}SO_4$) will help understand re-equilibration processes between pore waters and foraminifera. Samples will be run on the CC-MC-ICP-MS and the nano-SIMS. Because diagenesis may lead to the incorporation of isotopically evolved sulfate, working on modern carbonates known to have been diagenetically modified might help develop SIF as a tool to investigate diagenesis and help recognize seawater from pore water signatures in ancient carbonates. In addition, applying the planktic-benthic comparison to modern depth of MSR zones will help develop this potential new tool.

3. Task 3 - A continuous 100 Myr record of the sulfur cycle through seawater and diagenetic processes.

Collaborators: Annachiara Bartolini (MNHN), A. Schumacher (CRPG), C. Zimmerman (CRPG), one postdoc and one PhD student.

Background: This task will result in a multiple sulfur isotopic record of sulfate from the world ocean over the last 100 Myr based on sulfate from both planktic and benthic foraminifera extracted from IODP cores (International Ocean Discovery Program). In order to understand whether long-term changes in $\delta^{34}S$ are linked or not to f_{pyr}, the planktic-benthic comparison might be decisive. I intend to deliver a composite low-resolution single-species record from 100 to 0 Ma (~1 point/400 kyr total ~250 points) using single-species planktic and benthic foraminifera samples from different cores and basins (Atlantic, Pacific, Indian). Geochemical proxies and micropaleontological observations will provide the background for checking paleoenvironmental conditions and diagenesis. To understand whether (and why) seawater sulfur isotope compositions can quickly evolve over timescales shorter than 1 Myr, we will produce 2 Myr multiple sulfur isotopic records (~1 point/20 kyr, 3 times 50 points) around the PETM and OAE 2 as well as additional K-Pg records. Finally, we will ensure whether the current residence time of sulfur in seawater is longer than 10 Myr or not, an assumption upon which most interpretations of the modern sulfur cycle rely.

Instruments, protocols, samples: Picking, cleaning and analysis of foraminifera will be performed at CRPG with help from A. Bartolini, the micropaleontologist in charge of the foraminifera collection of the MNHN in Paris. SEM observations will be performed at CRPG or MNHN. Records will be based on single-species foraminifera samples. Because no species cover such time span, we will need to use a succession of different species. Each species is characterized by a different vital effect. Since ancient species are extinct, we will cross-calibrate the vital effects (Fig. 85): when two species overlap in a sample or more, we can calculate the offset between them and apply this offset to correct the $\delta^{34}S_{CAS}$ measured. This method is already used for reconstructing seawater $\delta^{18}O$ using foraminifera (Fig. 1).

Objectives and means: The main objectives of this work can be summarized as follows.

3.2- Are the existing carbonate $\delta^{34}S_{sw}$ records reliable? Because the single-species method allows us to provide records as reliable as barite on the long term, the method will be applied to the OAE2, K-Pg boundary and PETM events. CAS records will be based on sediments from various relevant IODP sites for which we already have samples available in the Atlantic, Pacific, and Indian oceans. We will compare benthic and planktonic foraminifera when possible and for periods where anoxia or dysoxia has been described (AOE 2, PETM), we will try to explore the $\delta^{34}S_{sw}$ value at different depths along the Oxygen Minimum Zone to understand if a heterogeneity of $\delta^{34}S_{sw}$ with depth occurred, as barite does not allow to do so. We will request

additional samples from relevant IODP legs. A grad student will contribute to data acquisition. $\Delta^{33}S$ and $\Delta^{36}S$ will be measured along with $\delta^{34}S$ to better establish the evolution of f_{pyr}. We will extend an existing ^{34}S-^{32}S box-model (Rennie et al., 2018) to ^{33}S-^{36}S to reconstruct f_{pyr} over the last 100 Myr of Earth's history using also our new constraints on F_{in}.

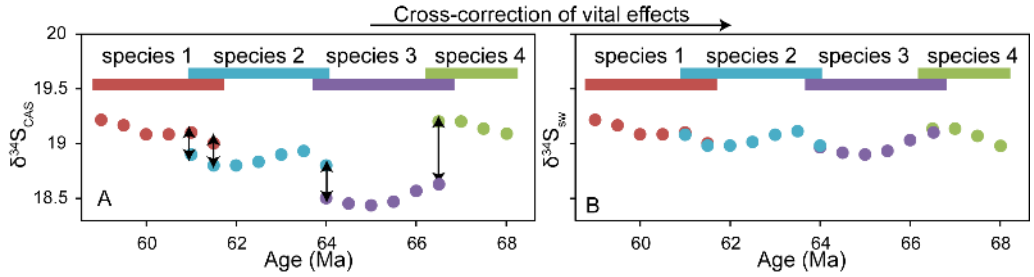

Figure 89. Cross-calibration: When two different species overlap, respective vital effects can be corrected (the theoretical example of the K-Pg boundary).

3.2 – Can we reconstruct the evolution of diagenetic processes? The comparison between planktic and benthic foraminifera might provide additional information in the cases where the two populations would yield different values. Data must also be acquired on Quaternary cores to understand the processes that generate the $\delta^{34}S_{CAS}$ "gradient" and how it could be interpreted in terms of local MSR or migration of the MSR zone and its link to the AOM zone. When possible, the evaluation of diagenetic processes evolution will be compared to pyrite data. Indeed, microanalyses of pyrites also reveal the complex history of diagenetic processes (e.g. Liu et al., 2019; Pasquier et al., 2021, 2017). By doing so, we will bring new and original constraints on fluxes associated to the anaerobic part of the carbon cycle, with major implications for our understanding of the Earth system. In the longer term, discussion with modelers such as Guillaume Le Hir and Yannick Donnadieu will be necessary.

3.3- Is the residence time of sulfur properly known? Working with samples from different basins will allow us to assess whether changes are identical between the main oceanic basins, a question hitherto unaddressed. We will develop low resolution records (~1 point/400 kyr) from different locations and compare, when possible, the signals recorded by planktic and benthic foraminifera. Over the last 15 Myr, we will use the Mediterranean, Black and Red Seas as natural laboratories to understand the effect of evaporite deposition, rifting or anoxia. As smaller basins that have been more or less isolated in the recent geological past, they might show more drastic isotopic changes than the open ocean. A postdoc will contribute to data acquisition and interpretation.

In case of poor preservation of foraminifera in the targeted cores, if successions are not continuous or cross-calibration of vital effects is not possible, we will request more IODP samples or develop field trips to collect samples on outcrops. If the SIF method cannot be as

precise as required, other isotopic systems (e.g. $\delta^{44/40}Ca$ – see Annex II) will be used to nonetheless constrain carbon and/or sulfur fluxes such as carbonate precipitation or oceanic hydrothermalism.

4. Summary of the project

Many fundamental questions remain unanswered about past and modern sulfur cycles that can be solved through the analyses of multiple sulfur isotopes in rivers and foraminiferal calcite, yet no method exists for measuring SIF in single-species foraminifera samples (Fig. 86). Similarly, many river water samples in existing collections are too small for precise SIF measurements. I intend to lead the development of an analytical method that will allow us to measure SIF in such samples.

The analytical development necessary to measure sulfur isotopes will take place on a MC-ICP-MS equipped with a collision cell (CC-MC-ICP-MS). The cell can remove the interferences due to ^{36}Ar and ^{32}SH and all four sulfur isotopes can be measured. One of the challenges is improving the reproducibility of the measurements to reach the precision that allows SIF investigation. In addition to the current project, such method will be useful to the ice core community, those investigating microbial metabolisms and even to biomedical research. Our understanding of the sulfur cycle will improve because we will be able to evaluate (1) today's f_{pyr} and the contribution of pyrite oxidation to the modern riverine budget and (2) a new reconstruction of f_{pyr} over the last 100 Myr of Earth's history.

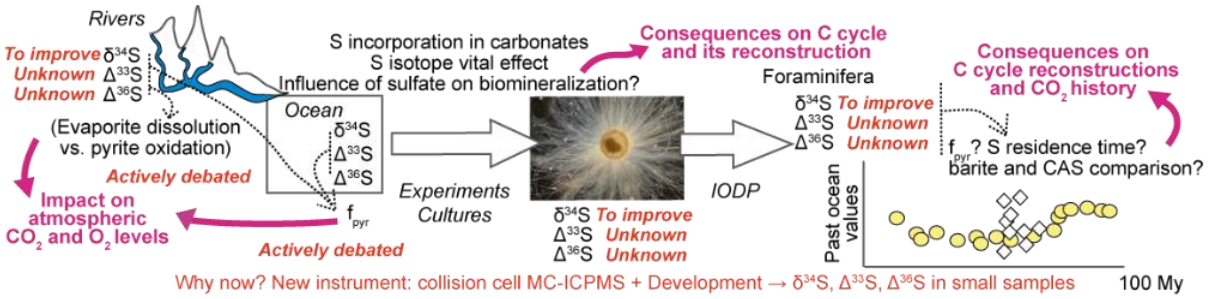

Figure 90. Summary of the expected results.

1. We must document the world average values of SIF for riverine sulfate because the comparison between riverine inputs and seawater is necessary for estimating f_{pyr}. Major sulfur isotope fractionation $^{34}\alpha_{pyr\text{-}sw}$ and the difference between λ_{ref} and λ_{MSR} lead to distinct $\delta^{34}S$, $\Delta^{33}S$ and $\Delta^{36}S$ values for the ocean, oceanic inputs, and outputs. More importantly, the degree to which they are different depends on the value of f_{pyr}. In an evaporite-dominated ocean (low f_{pyr}), $\delta^{34}S$, $\Delta^{33}S$ and $\Delta^{36}S$ of seawater are closer to the signatures of the input compared to high f_{pyr} conditions. Hence, it is necessary to assess these unknowns of the modern sulfur cycle by measuring the isotopic composition of dissolved sulfate in world rivers to determine (instead

of assuming) the values of $\Delta^{33}S$ and $\Delta^{36}S$. Each three isotopic compositions of F_{in} compared to those of seawater will provide three separate f_{pyr} equations (e.g. eq. 1 and 2) In addition, $\Delta^{33}S$ and $\Delta^{36}S$ evolve differently in the case of mixing between two endmembers and occurrence of MSR (Johnston et al., 2011). Therefore, these signatures will also provide further independent ways to determine if sulfur is conservative or not on land and evaluate the relative contribution of oxidized pyrite and dissolved evaporite to the world budget of riverine sulfate. We will also measure $\delta^{18}O$ values of sulfate oxygen, when samples allow it, as a supplementary constraint to pyrite oxidation on land (Calmels et al., 2007).

2. We need to understand how the signature of dissolved seawater sulfate is transferred to (biogenic) carbonates and preserved in sediments has been an interrogation since the first measurements of sulfur isotopes in foraminifera (Burdett et al., 1989). Following the development of sulfur isotope measurement by MC-ICP-MS, we were finally able to calibrate for the first time sulfur isotope vital effects (Paris et al., 2014b). We also provided reliable framework in which to understand sulfur isotope fractionations through inorganic carbonate precipitation experiments (Barkan et al., 2020). We led new investigations on diagenesis (Present et al., 2019, 2015). A lot remains to understand about sulfate content and $\delta^{34}S$ in both inorganic (including ACC) and biogenic carbonates; nothing is known about the minor isotope composition of carbonates. Thus, inorganic precipitation and culture experiments will provide the necessary constraints on sulfur incorporation in carbonate and improve our understanding of how sulfate controls calcium carbonate poly(a)morphism and stability.

3. Reconstructing f_{pyr} through the last 100 Myr of Earth's history using multiple sulfur isotope composition in single-species foraminifera samples will allow us to quantify a critical flux of the past sulfur cycle. This project will result in a new $\delta^{34}S$, $\Delta^{33}S$ and $\Delta^{36}S$ record covering the global cooling recorded over the last 100 Myr and document the role played by pyrite. Detailed records will focus on the main carbon cycle disruptions of the last 100 My, namely the PETM, the K-Pg boundary and OAE2. Using single-species foraminifera samples and comparing benthic and planktic populations, we will be able to explain why different archives provide different information of the sulfur cycle and to provide crucial insights into the sulfur and carbon cycles. Our new records will be as reliable as the barite record and they will demonstrate the reality, or not, of rapid $\delta^{34}S$ changes and document seawater SIF history. Box-modelling will rely on those results to calculate pyrite burial fluxes, necessary to fully describe the past and modern sulfur, as well as carbon and oxygen, cycles.

5. Timetable

year:	2	4	6	8	10
Task 1					

	Analytical development Collecting river samples and source materials Sample analyses (CC-MC- ICP-MS, IRMS) Delivery (PhD defense, papers, conferences)	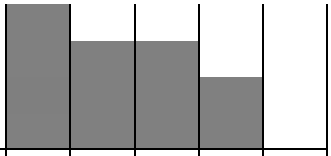
Task 2	Inorganic carbonate experiments Foraminifera cultures Sample analyses (Nano-SIMS, synchrotron, CC-MC- ICP-MS) Delivery (papers, conferences)	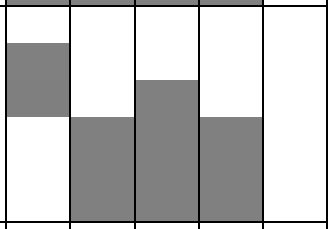
Task 3	Gathering IODP samples Preparing foraminifera (picking, cleaning, MEB) Sample analyses (CC-MC- ICP-MS), modelling Delivery (PhD defense, papers, conferences)	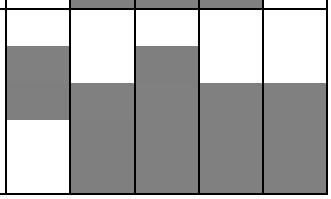

Annex III: Resume, research management, teaching, outreach, supervision

I. Resume

Guillaume Paris – Chargé de recherche – Isotopic geochemistry - curriculum vitae

CRPG - UMR 7358 - CNRS-UL

15 rue Notre Dame des Pauvres 54500 Vandœuvre les Nancy – France

email: guillaume.paris@univ-lorraine.fr phone: +33 67012519

Research interests:

- Sulfur cycle and its influence on carbon and oxygen cycles
- Archean sulfur cycle and atmospheric oxygen content in early Earth's atmosphere,
- Biomineralization and vital effects
- Oceanic chemistry (alkalinity, pH, dissolved inorganic carbon),
- Reconstruction of seawater pH using boron isotopes,
- Microbial sulfate reduction in oceanic sediments and continental environments,
- Proxy calibration for reconstructing sulfur cycle throughout Earth's history. and

Professional activities:

- **Since 2016:** « Chargé de recherche » (Researcher) at Centre National de la Recherche Scientifique, Centre de Recherches Pétrographiques et Géochimiques (Nancy, France)
- **09/2013-07/2016:** Assistant Research Scientist - California Institute of Technology (Pasadena, CA, USA), with Prof. Jess F. Adkins
- **09/2010-08/2013:** Postdoctoral position, Geological and Planetary Science division (Camille and Henry Dreyfus Environmental Chemistry Fellow, 2010 to 2012), California Institute of Technology, (Pasadena, CA, USA) with Prof. Jess F Adkins and Prof. Alex L Sessions.
- **12/2009-07/2010:** Postdoctoral "ATER" position (Research and Teaching) at the IPGP (Paris Earth Physics Institute; Paris, France).
- **2006-2009**: PhD student IPGP, French Institute of Petroleum (IFP), National Museum of Natural History (MNHN) and the Environment and Climate Sciences Laboratory (LSCE) under the supervision of Prof. Jérôme Gaillardet, co-advised by Prof. Annachiara Bartolini, Prof. Yannick Donnadieu and Dr. Valerie Beaumont.
- **2006**: Training research engineer at Veolia Water Research Center (Paris, France).
- **2004**: Training engineer at the Environment Department of the City of Toulouse (Toulouse, France).

Education:

- **2023**: HDR – Université de Lorraine
- **2009**: PhD obtained with Honors - IPGP (Paris, France).
- **2006**: Master of Science - "Geology, Risk, Environment" - Louis Pasteur University and Engineer diploma, EOST - Earth Science School and Observatory (Strasbourg, France)
- **2005**: Engineer diploma, ENSG – National School of Geology (Nancy, France).

Supervision:

PhD defense jury
Christian Ercolani (examinateur, 2020)
Sara Milner Garcia (examinateur, 2018)
PhD « Comité de suivi individualisé »
Mathieu Buisson (IPGP, 2018-2022)
Ana Calves (CR2P, 2020-2024)
Thomas Obin (GeoRessources, 2020-2024)
Blandine Godet (CRPG, 2022-)
Mahaud Chavanieu (CRPG, 2023-)

Skills:

- Mass spectrometry (HR-MC-ICPMS, Quadrupole ICP-MS; occasional user of TIMS and (Nano)SIMS), Ion Chromatography, Trace metal clean laboratory
- Occasional synchrotron beamline user (XANES, XRF, XRD)
- Rock-Eval (Determination of organic and mineral carbon content of a sample and type of organic matter)
- Microscopy: Optical Microscopy, Secondary Electron Microscopy (SEM) user
- Computing skills: Matlab, use of geochemical carbon cycle box-model GEOCLIM

Field experience:

- **2016**: field trip to the Guadalup Mountains
- **2014**: Archean sample collection in South Africa (1 week)
- **2013**: cruise on the R/V New Horizon in the Santa Barbara basin (10 days, PI: Tomoko Komada, SFSU)
- **2011, 2014**: Growing foraminifera on Catalina Island (1 week)
- **2008**: Triassic-Jurassic boundary sample collection in the UK and in Austria (1 week each)
- **2004**: Geological mapping in the French Pyrenees (3 weeks)

Awards and contribution to the community:

- Reviewer for ANR (France), ISF (Israel), INSU calls (CNRS), University local calls, NSF (USA), NWO (Netherland), Royal Society (UK)
- **2021-2025**: Elected member of the CoNRS section 18 (evaluation and recruitment of CNRS researchers, 3 months/year)
- **2017-2024**: scientific manager of the IRISS platform (5 days/months: daily life of the platform, acquisition of new instruments, renewal, “tariffication”, sitting in various meetings such as RéGEF or Anatelo)
- **2017-2024**: Animator of the CYCLA group at CRPG (scientific animation, sitting in the CRPG direction committee, attracting young scientists to CRPG – 6h/months) .
- **2018-2024:** Elected member of the CRPG council
- **2019:** co-organizer of the “journées prospectives transverses de l’INSU” on geological crises
- **2017-present**: creation and animation of the PALEOS newsletter (~5/year)
- **2017, 2019**: Session co-chair (Goldschmidt 2017, 2019, a session proposed in 2023 and merged)
- **2011**: Goldschmidt Conference 2011 - Best student presentation award

- **2010-present**: Reviewer for Geology, Economical Geology, Applied Geochemistry, Palaeo3, Chemical Geology, Analytical and Bioanalytical Chemistry, JAAS, Nature Communications, Science Advances, GCA, EPSL, GGR (now, 5 to 10 reviews a year).
- **2007-2009**: Member of the IPGP Scientific Council.
- **2003**: Member of the association for welcoming and assisting foreign students at the Lorraine National Polytechnic Institute.

Teaching and training:

- **2023-present:** Seminars for public servants on climate change (10h/year,)
- **2023- present:** Climate lectures at the Mines school of Nancy (10h/year)
- **2022, 2024:** Organization of the PALEOS summer school (50 people)
- **2019-2022**: Training for middle and high school teachers - Maison pour la science and Union des Professeurs de Physique Chimie : (carbon cycle and climate crisis).
- **2018-present** Organization of the paleoclimate and climate change optional week at ENSG (15h/year) and contribution to the geochemistry module at ENSG (20h/year)
- **2010-2016:** Training and supervision of MC-ICPMS Neptune users at Caltech
- **2011, 2012:** Participation in seminar classes at USC and Caltech, creation of lecture material
- **2010:** Teaching Assistant, IPGP-University Paris VII: Biosphere-geosphere interactions (seminar class for undergraduate, improving teaching material) and Bibliographical reports on biogeochemical cycles
- **2008:** Field trip - initiation to geology (Classe préparatoire aux grandes écoles, lycée Henry IV)

Science communication and dissemination:

2023
- Tribute to Lorius
- Pint of science
- 1 article on sulfur cycle for the Planète Terre website (ENS Lyon)
- 1 article for The Conversation

2022
- Intervention on climate change at the Maxéville Prison
- Journée résilience et changement climatique - Université de Lorraine
- 1 article for The Conversation (history of the ozone layer)

2021
- France 3 Lorraine evening news on snow in the Vosges
- Université d'été foyer rural 54
- Jardins éphémères (L'eau sur Terre, avec Laurette Piani)
- Vigie de l'eau (Vittel)
- Portes ouvertes Crédit Mutuel : causes et conséquences du réchauffement climatique
- Intervention DR06
- 3 articles pour The Conversation (Why is the Earth blue ?).

2020
- France Inter : interview with Laurette Piani on the origin of water and oceans on Earth (La Terre au carré)
- France 3 Lorraine dimanche en politique : interview on climate change and snow in the Vosges mountains
- Jardins éphémères (Déserts glacés, with Pierre-Henri Blard)
- 5 articles for The Conversation France (water origins, with Laurette Piani)

2019 :

- NCYMUN -Nancy Model united nations. Conférence grand public pour des lycéens.
- Jardins éphémères de Nancy : Empreinte des humains sur le cycle du carbone et le climat, with Pierre-Henri Blard
- 5 articles for The Conversation France (dinosaur extinction, carbon cycle and climate crisis)

2018 :
- conférence dans le cadre de la cérémonie de remise des prix des 12e Olympiades des Géosciences organisées par le rectorat à l'ENSG.

Invited seminar speaker and conferences:

- University of Misasa, Japan (2010)
- CRPG, Nancy, France (2010)
- University of Southern California, USA (2012)
- Institut de Physique du Globe, France (2012)
- University of California, Riverside, USA (2013)
- University of Colorado, Boulder, USA (2015)
- Cambridge, UK (2016)
- University of Oxford (2016)
- Institut de Physique du Globe de Paris (2017)
- Institut des Sciences de la Terre d'Orléans (2017)
- Invited talk at Goldschmidt (2017)
- GDR Vie, Climat, Environnement (2019)
- ETH, Zurich, Suisse (2019)
- Invited talk at Goldschmidt (2019)
- GDR Vie, Climat, Environnement (2021)
- LGL-TPE (Lyon, 2023)
- GDR Clim2Past (2023)
- Biogeosciences (Dijon, 2024)

Publications (student and postdocs I (co)advised:*

1. Paris G. *Determination of Unbiased $\delta^{34}S$ and $\Delta^{33}S$ Values by MC-ICP-MS Using Down to 30 nmol of Sulfur* (2023) Geostandards and Geoanalytical Research 48: 29-42. https://doi.org/10.1111/ggr.12535
2. Jouini A.*., G. Paris, G. Caro, A. *Bartolini, S. Gardin Constraining oceanic carbonate chemistry evolution during the Cretaceous-Paleogene transition: Combined benthic and planktonic calcium isotope records from the equatorial Pacific ocean* Earth and Planetary Science Letters 619, 118305 https://doi.org/10.1016/j.epsl.2023.118305
3. Thaler C.*, G. Paris, M. Dellinger, D. Dissard, S. Berland, A. Marie, A. Labat, A. Bartolini (2023) *Impact of seawater sulfate concentration on sulfur concentration and isotopic composition in calcite of two cultured benthic foraminifera* Biogeosciences, 20, 5177–5198, https://doi.org/10.5194/egusphere-2023-631
4. Laurent D., Barré G., Durlet C., Cartigny P., Carpentier C., Paris G., Collon P., Pironon J., Gaucher E.C. (2023) *Unravelling biotic versus abiotic processes in the development of large sulfuric-acid karsts* Geology 51 (3): 262–267. https://doi.org/10.1130/G50658.1
5. Dasari S*, Paris G., Charreau J., Savarino J. (2022) *Sulfur-isotope anomalies recorded in Antarctic ice cores as a potential proxy for tracing past ozone layer depletion events* PNAS Nexus 1 (4), pgac170
6. Dasari S.*, Paris G, Saar B, Pei Q. Cong Z. Widory D. (2022) *Sulfur Isotope Anomalies ($\Delta^{33}S$) in Urban Air Pollution Linked to Mineral-Dust-Associated Sulfate*, Environ. Sci. Technol. Lett., 9, 7, 604–610 https://doi.org/10.1021/acs.estlett.2c00312
7. Laurent D., Durlet C., Barré, G., Sorriaux, P., Audra P., Cartigny, P., Carpentier C., Paris G., Collon P., Rigaudier T., Pironon J., Gaucher E. (2021) ***Epigenic vs. hypogenic speleogenesis governed by H_2S/CO_2 hydrothermal input and Quaternary icefield dynamics (NE French Pyrenees)*** Geomorphology, 387, 107769. 10.1016/j.geomorph.2021.107769
8. Paris G., Fischer W.W., Johnson, J., Webb S., Present T.M., Sessions A. L., Adkins J. F., (2020) *Deposition of sulfate aerosols with positive $\Delta^{33}S$ in the Neoarchean,* Geochimica et Cosmochimica Acta, 285, 1-20, 10.1016/j.gca.2020.06.028

9. Barkan Y*., Paris G., Webb S.M., Adkins J. F., Halevy I. (2020) *Sulfur isotope fractionation between aqueous and carbonate-associated sulfate in abiotic calcite and aragonite*, *Geochimica et Cosmochimica Acta,* 280, 317-330, https://doi.org/10.1016/j.gca.2020.03.022
10. Bekaert D. V., Broadley M. W., Delarue F., Druzhinina Z., Paris G., Robert F., Sugitani K., Marty B. (2020) *Xenon isotopes in Archean and Proterozoic insoluble organic matter: A robust indicator of syngenecity?,* Precambrian Research 336, 105505.
11. Present, T.M.P*, M. Gutierrez, G. Paris, C. Kerans, J.P. Grotzinger, J.F. Adkins (2019) *Diagenetic controls on the isotopic composition of carbonate-associated sulphate in the Permian Capitan Reef Complex, West Texas,* Sedimentology https://doi.org/10.1111/sed.12615
12. Burke, A., Present, T. M., Paris, G., Rae, E. C. M., Sandilands, B. H., et al. (2018). Sulfur isotopes in rivers: Insights into global weathering budgets, pyrite oxidation, and the modern sulfur cycle. *Earth and Planetary Science Letters*, *496*, 168–177. https://doi.org/10.1016/j.epsl.2018.05.022
13. Dellinger, M., West, A. J., Paris, G., Adkins, J. F., Pogge von Strandmann, P. A. E., Ullmann, C. V., et al. (2018). The Li isotope composition of marine biogenic carbonates: Patterns and mechanisms. *Geochimica et Cosmochimica Acta*, *236*, 315–335. https://doi.org/10.1016/j.gca.2018.03.014
14. Guinoiseau, D., Paris, G., Chen, J., Chetelat, B., Rocher, V., Guérin, S., Gaillardet, J., (2018) Are boron isotopes a reliable tracer of anthropogenic inputs to rivers over time? Science of the Total Environment *626*, 1057-1068 https://doi.org/10.1016/j.scitotenv.2018.01.159
15. Rennie, V. C. F.*, Paris, G., Sessions, A. L., Abramovich, S., Turchyn, A. V., & Adkins, J. F. (2018). Cenozoic record of δ 34 S in foraminiferal calcite implies an early Eocene shift to deep-ocean sulfide burial. *Nature Geoscience*, *11*(10), 761–765 https://doi.org/10.1038/s41561-018-0200-y
16. Torres, M. A*., Paris, G., Adkins, J. F., & Fischer, W. W. (2018). Riverine evidence for isotopic mass balance in the Earth's early sulfur cycle. *Nature Geoscience*, *11*(9). https://doi.org/10.1038/s41561-018-0184-7
17. McConnell, J.R., A. Burke, N.W. Dunbar, P. Köhler, J.L. Thomas, M.M. Arienzo, N.J. Chellman, O.J.,Maselli; M. Sigl, J.F. Adkins, D. Baggenstos, J.F. Burkhart, E.J. Brook, C. Buizert, J. Cole-Dai, T.J. Fudge, G. Knorr, H.-F. Graf, M.M. Grieman, N. Iverson, K. C. McGwire, R. Mulvaney, G. Paris, R.H. Rohdes, R.S. Saltzman, J.P. Severinghaus, J.P. Steffensen, K.C. Taylor, G. Winckler. (2017) *Synchronous volcanic eruptions and abrupt climate change ~17.7 ka plausibly linked by stratospheric ozone depletion* , PNAS 114 (38) 10035-10040 www.pnas.org/cgi/doi/10.1073/pnas.1705595114
18. Sim M.-S., V. Orphan, J.F. Adkins, G. Paris, A.L. Sessions (2017) *Quantification and isotopic analysis of intracellular sulfur metabolites in the dissimilatory sulfate reduction pathway* Geochimica et Cosmochimica Acta 206 57-72 http://dx.doi.org/10.1016/j.gca.2017.02.024
19. Blättler C.L., L.R. Kump, W.W. Fischer, G. Paris, J.J. Kasbohm and J.A. Higgins, (2017) *Constraints on ocean carbonate chemistry and pCO_2 in the Archaean and Palaeoproterozoic.* Nature Geoscience 10 41-45 https://doi.org/10.1038/NGEO2844
20. Torres M.A., A.J. West, K. Clark, G. Paris, J. Bouchez, C. Ponton, S. Feakins, V. Galy, J.F. Adkins, (2016) *The acid and alkalinity budgets of weathering in the Andes-Amazon system: Insights into the erosional control of global biogeochemical cycles?* EPSL 450 381-391 http://dx.doi.org/10.1016/j.epsl.2016.06.012
21. Nédélec A., J.-L. Paquette, P. Antonio, G. Paris, *A-type stratoid granites of Madagascar revisited: age, source and links with the break-up of Rodinia.* (2016) Precambrian Research 280 231-248
22. Paris G., Donnadieu Y, Beaumont V, Fluteau F, Goddéris Y, (2016) *Geochemical consequences of intense pulse-like degassing during the onset of the Central Atlantic Magmatic Province.* Palaeo3 441 74-82 https://doi.org/10.1016/j.palaeo.2015.04.011
23. Present, TM*, G. Paris, Burke A, Fischer WW, Adkins JF, (2015) *Large Carbonate Associated Sulfate isotopic variability between brachiopods, micrite, and other sedimentary components in Late Ordovician strata.* EPSL 432 187-198 http://dx.doi.org/10.1016/j.epsl.2015.10.005
24. Paris G., Adkins JF, Sessions AL, Webb SM, Fischer WW, (2014) *Neoarchean carbonate-associated sulfate records positive $\Delta^{33}S$ anomalies.* Science, 346 (6210) 739-741. https://doi.10.1126/science.1258211
25. Crowe S.A. and Paris G., Katsev S, Jones C, Kim S-T, Zerkle A, Nomosatryo S, Fowle DA, Adkins JF, Sessions AL, Farquhar J, and Canfield DE, *Sulfate was a trace constituent of Archean seawater.* (2014) Science, 346 (6210) 735-739 https://doi:10.1126/science.1258966 (co first-author)
26. Louvat P, Moureau J, G. Paris, Noireaux J, Bouchez J, Gaillardet J; (2014) *A fully automated direct injection nebulizer (d-DIHEN) for MC-ICP-MS isotope analysis: application to boron isotope ratio measurements.* JAAS **29**, 1698-1707. https://10.1039/C4JA00098F
27. Paris G., J.S. Fehrenbacher, A.L. Sessions, H.J. Spero, J.F. Adkins (2014) *Experimental determination of carbonate-associated sulfate $\delta^{34}S$ in planktonic foraminifera shells.* G-cubed, 15, 1452-1461
28. Paris G., Sessions A.L, Subhas A.V, Adkins J.F (2013) *MC-ICPMS measurement of $\delta^{34}S$ and $\Delta^{33}S$ in small amounts of dissolved sulfate.* Chem Geol, 345, 50-61. http://dx.doi.org/10.1016/j.chemgeo.2013.02.022
29. Foster G.L., B. Hönisch, G. Paris, G.S. Dwyer, J.W.B. Rae, T. Elliott, J. Gaillardet, N.G. Hemming, P. Louvat, A. Vengosh (2013) *Interlaboratory comparison of boron isotope analyses of boric acid, seawater and marine $CaCO_3$ by MC-ICPMS and NTIMS* Chem Geol; 358, 1-14. http://dx.doi.org/10.1016/j.chemgeo.2013.08.027
30. Louvat P., J. Bouchez, G. Paris (2011) *Boron isotopes measurements by MC-ICP-MS using direct injection nebulization: optimization and application to carbonate and seawater samples.* Geoanalytical and Geostandard Research 35 (1), 75-88. https://doi.org/10.1111/j.1751-908X.2010.00057.x
31. Louvat P., J. Gaillardet, G. Paris, C. Dessert (2011) *Boron isotope ratios of surface waters in Guadeloupe, Lesser Antilles.* Applied Geochemistry S76-S79. https://doi:10.1016/j.apgeochem.2011.03.035

32. Paris G., A. Bartolini, Y. Donnadieu, V. Beaumont, J. Gaillardet (2010) *Investigating boron isotopes in a middle Jurassic micritic sequence: Primary vs. diagenetic signal.* Chem Geol 275, 117-126. https://doi:10.1016/j.chemgeo.2010.03.013
33. Clémence M.-E., A. Bartolini, S. Gardin, G. Paris, V. Beaumont, K. Page, (2010) *Early-Hettangian Benthic-planktonic coupling at Doniford (SW England): Implications for the renewal of the carbonate pelagic production in the aftermath of the end-Triassic crisis.* Palaeo3 295 (1-2): 102-115.
34. Paris G., J. Gaillardet, P. Louvat (2010) *Geological evolution of seawater boron isotopic composition recorded in evaporites.* Geology 38(11). https://doi:10.1130/G31321.1
35. Paris G., V. Beaumont, A. Bartolini, S. Gardin, M.-E. Clémence, K. Page, (2010) *Nitrogen isotope record of a perturbed paleoecosystem in the aftermath of the end-Triassic crisis, Doniford section, SW England.* G-cubed 11, Q08021. https://doi:10.1029/2010GC003161
36. Clémence M.-E., A. Bartolini, S. Gardin, G. Paris, V. Beaumont, J. Guex, (2010) *Bentho-planktonic evidence from the Austrian Alps for a decline in sea-surface carbonate production at the end of the Triassic.* Swiss Journal of Geoscience 103:293–315.

.

II. Supervised students and postdoctoral collaborators.

1. Co-supervision of Master and other students.

2020: Lucie Schaaf, M1 (with Julien Charreau), 2023: Lenny Riguet, M2 (with Célia Dalou)

Second year of the geology engineering school of Nancy (ENSG)/L3 : 1 to 4 students per year.

Voluntary internships: Erwann Le Gourrierec 2020 (L1); Philip Bourgeois 2020 (2A ENSG, with Guillaume Caro), Sophie Coural 2018 (2A ENSG)

2. Co-supervision of grad students.

1. Theodore M Present (2011-2018, director: Jess Adkins – Caltech), 2 co-published articles (Present et al., 2019, 2015). Ted is currently a Research Scientist at Caltech;

2. Victoria CF Rennie (2012-2016, director: Sasha Turchyn – Cambridge), 1 co-published article (Rennie et al., 208). Vicky is currently retraining after the birth of her second child.

3. Arbia Jouini (2018-2023, HDR director: Raphael Pik, CRPG), 1 co-published article (Arbia et al., 2023), 1 more to write. Arbia has just defended her thesis.

3. Assistance in the supervision of grad students (laboratory training and/or part scientific co-supervision).

Morgan Raven (2010-2015, director; Jess Adkins, Alex Session – Caltech). Morgan is currently on tenure track at University of California, Santa Barbara (USA)

Mark Torres (2010-2015, director; Josh West – University of Southern California). Marc is currently on tenure track at Rice University (USA) 1 co-published article during his PhD thesis, 1 during his postdoc (Torres et al., 2018, 2016).

Sophie Hines (2011-2017, director: Jess Adkins – Caltech). Sophie is currently on tenure track at WHOI (USA)

Yigal Barkan (2015-2020, director Itay Halevi, Weizmann Institute) 1 co-published paper, 1 in progress (Barkan et al., 2020, in prep). Yigal is retraining after the birth of his second child.

4. Collaborations with postdoctoral fellows.

I co-supervised Caroline Thaler during her postdoctoral fellowship on the importance of sulfur in the biomineralization and biology of benthic foraminifera (Thaler et al., preprint).

I am co-supervisor of the Marie Curie postdoctoral fellowship of Sanjeev Dasari on the study of sulfur isotopes in ice cores to highlight the existence of a UV window during the magnetic excursion of Laschamps and in urban pollution (Dasari et al., 2023, 2022a, 2022b).

Though not a direct supervisor, I closely collaborated with Andrea Burke, Min-Sub Sim and Mark Torres during their postdoctoral years at Caltech, training them on the sulfur method and MC-ICP-MS approach and I worked with Dimitri Laurent at Georessources.

III. Societal and environmental impact.

1. Diversity and inclusion.

Most of my projects combine the richness and diversity of different profiles of researchers. I am convinced that, due to how gender influences the way people are perceived and evaluated, both in and out of the lab, it is part of my role as a researcher to be proactive about addressing differences and inequalities. Not only to contribute to turning the lab into a place where all are welcome, but also to contribute to an active, creative and blossoming research that can help us address the challenges ahead of us.

France does not allow collection of statistics on parameters other than gender or handicap. The result is that social and racial profiles lack detail, with very little leverage and tools to work on addressing diversity and inclusion. Similar assertions can be made regarding members of the LGBTQQIA+ communities.

I am firmly convinced that working to hire people with different perceptions on how research should be conducted (for example, both “agency” and “communion” – oriented individuals) can only lead to increased diversity in the long run. CNRS is actively encouraging hiring committees to consider the diversity of individual paths given that a sense of advantage tends to orient a person toward greater agency as opposed to communion while a sense of disadvantage orients a person toward greater communion as opposed to agency (Rucker et al., 2018). Both of these orientations should be valued. Moreover, it is important to recognize that the idea of “excellence” can become an excuse for social reproduction, which can sustain social inequalities. The culture of valuing researchers with high publication and citation rates favors those who are agency-oriented and disfavors those who are communion-oriented, which is problematic given that, for instance, women are often more communion-oriented than men. (Ross et al., 2022; Fig. 87). Geographical and languages biases and barriers exist as well, as non-English speaking people are necessarily disadvantaged in modern science (e.g. Igoumenou et al., 2014; Van Leeuwen et al., 2001). Thus, new for valuing a person’s contributions to research must be defined.

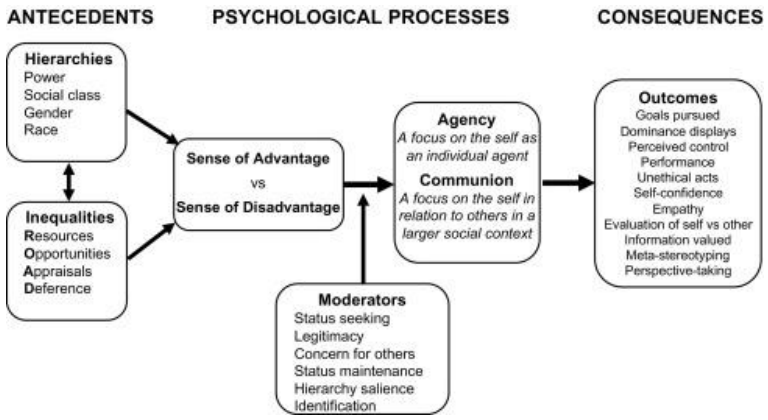

Figure 91. The agency and communion dimensions and how they contribute to strengthening biases if they are not properly considered (Ross et al., 2022)

I am also convinced that more needs to be done at the educational level. As a CNRS researcher, I don't have a teaching load. However, through students I interact with, outreach activities, in all the hiring committees I sit on, and through my political orientations, I do my best to improve diversity and inclusion.

2. Environmental footprint.

It goes without saying that we live in a major environmental, climate and biodiversity crisis. As a researcher in Earth science and a human being, I know that we must all work on and act upon it, as a moral and ethical obligation. As a result, I do try to connect more and more of my research to questions around health and pollution, even though they are not described in this project.

In order to improve the sustainably of my research and that of CNRS, I contribute to the "Ecoresponsabilité" group of the CRPG and the OTELo consortium (Observatoire Terre Environnement Lorraine) and contributed to calculate the carbon footprint of our research unit. Average CO_2 emissions of CRPG members are ~8 tCO_2/yr/people. Roughly, 1 tCO_2 comes from home-work travels, 1 tCO_2 comes from field trips, 2 tCO_2 are linked to the building energy consumption), as determined by Manon Schmitt during her M2 internship. and the remaining 4 tCO_2 are due to all the purchases necessary around the laboratories of CRPG. In my own case, I have started with the obvious. I do not own and use a car to go to work and I've actively reduced long-distance travels. I cannot suppress them entirely, not only because field trips and conferences are part of my work, but also because human exchange is necessary. Overall, the main environmental impact of my research comes from purchase of consumable materials and acquisition of new instruments.

There is consequently a need for a major change of behavior of companies and funding agencies. On the one hand, instruments that can be fully repaired and renewed would be a huge step forward. On the other hand, the possibility of finding funds not to buy a new machine

but to repair or upgrade the ones we have would also be a game changer. As long as the notion of planetary limit is not considered by the people who manage research and define grants, my ability to reduce my carbon and environmental footprint is limited. As of today, the only way to further decrease the environmental impact of my work would be to share, reuse and recycle further amounts of material and chemical reagents as well as reduce my research activities.

IV. Fundings.

1. Funded projects.

i. Research project as PI.

- 2017: OTELo (OSU Nancy) young researcher (€14.3k)

- 2017: INSU-Tellus INTERRVIE (Fractionation of sulfur and calcium isotopes in inorganic carbonates, collaboration with the Weizman Institute, 7.5 k€)

- 2019: INSU-Tellus SYSTER (Disruptions of the sulfur cycle along the K-Pg boundary, 6 k€)

- 2020: IODP-France (Reconstructing the calcium cycle along the K-Pg boundary, 5 k€)

- 2020: INSU-LEFE (REVA) on the analysis of sulfur in ice cores to understand the reality of a UV window during the excursion of the magnetic field of Mono-Laschamps – based on an idea by Julien Charreau (3 k€)

- 2023: INSU-LEFE (CaBo) Vital effects and fractionation of Calcium and Boron isotopes in biogenic carbonates (17k€ over two years)

ii. Research project as a co-PI.

- 2022: interdisciplinary OTELo project NEO (The neodymium isotope ratio $^{143}Nd/^{144}Nd$ as a biogeochemical tracer in forest ecosystems of eastern France?) with Anne Poszwa as a co-PI (13k€ over 2 years)

- INSU-INTERVIE project led by Annachiara Bartolini on sulfur in benthic foraminifera (2019).

- INSU-LEFE CULTFORAM as a co-PI on this project led by Claire Rollion-Bard on possible biases when evaluating vital effects on isotopic fractionations of boron and lithium in benthic foraminifera (2021, 30k€ over 3 years) and CULTFORAM 2 (2023, 20 k€ over 3 years)

- Marie-Skłodowska Curie postdoctoral grant attributed to Sanjeev Dasari under the supervision of Joël Savarino and Guillaume Paris (2020-2022).

I am co-leader of the ANR HUNIWERS (ANR-18-CE22-0009-06) for the CRPG (PI: Edwige Pons-Branchu, LSCE). In this project, I am responsible for part of the geochemical component

on urban speleothems analyzed as part of a diachronic study of the pollution of the Parisian conurbation during its recent history.

iii. Research project as a participant.

- INSU-LEFE ETOB project, led by Annachiara Bartolini, funded over one year (2021). This project proposes to evaluate the environmemntal consequences of sulfur emissions from the Toba super-eruption (7k€).

- OTELo project led by Laure Giamberini (LIEC) to measure S, Cu and Zn isotopes from fish livers from Central Europe

- INSU-PNP project, led by Guillaume Caro, on the recycling of sulfur in Eoarchean rocks.

iv. Non-funded projects.

I submitted an ANR project 4 times, an ERC project and two INSU projects who did not get funded. I intend to submit an ERC grant again this year.

2. Projects other than research.

- 2020: FEDER STEHLo project for the construction of the OTELo clean room platform at CRPG – 900 k€.

-2020: 300 k€ obtained from Université de Lorraine for the purchase of the CC-MC-ICP-MS

- 2021: first PALEOS summer school (CNRS: 10 k€, IODP-France 5 k€, OSU OTELo : 1 k€)

- 2023: second PALEOS summer school (IODP-France 5 k€, OSU OTELo: 1 k€)

V. Teaching and outreach.

1. Teaching.

As a chargé de recherche at CNRS, teaching is not a requirement. I nonetheless consider it a part of my work and actively seek to teach. I contribute to the Master 2 “CYCLA” Module of the CRPG. In this module, I present a 3-hour course on the sulfur cycle throughout Earth's history. As part of the teaching at ENSG (National School of Geology) in Nancy, I contribute to David Bekaert’s General Geochemistry module. Within this module, I give a lecture on paleoclimates throughout the history of the Earth (2 hours) as well as a part of associated tutorials (9 to 15 hours depending on the year). I also give the class on biogeochemical cycles (2 hours) and associated tutorials (9 to 15 hours depending on the year from 2020). I am also responsible for the optional module "Paleoclimates" which is part of the optional course "History of the Earth" (24 hours). The aim of this module is to train students in the history of the carbon cycle and climate on Earth, to understand the parameters regulating the climate and their evolution.

This course also presents the main climate “proxies”. I give 8 hours of lessons there. This module is popular with students given the positive feedback provided. Since 2020 I have participated in the “Climate and weather” training for secondary school teachers organized by the Maison pour la Science of the University of Lorraine (3 hours). Since 2021, I have also contributed to running the “Fresque du climat” workshop, which I helped run at the Nancy School of Mines and at ENSG. (2*3h).

2. Outreach.

I believe that outreach is also a part of my work as a scientist. It serves many purposes. First, sharing scientific knowledge and being transparent about what is known and what can be improved is a way to reinforce the general support to actions required to reduce climate change and our footprint on biodiversity and the environment. Second, bringing science to places where it is not always put forward is a way to contribute to attracting new people and new profiles to the academic field. For this reason, I became a member of the CRPG communication cell and intend to keep on participating and giving time to outreach events.

I wrote or co-wrote 13 articles for The Conversation, with a total of nearly 500000 readers. Many of those articles are collaborative and I have written articles on climate change, the history of oceans and water on Earth, the ozone layer or dinosaur extinction. I bring science to places like “Les Jardins Ephémères” on the Place Stanislas in Nancy, the Summer University of the Meurthe et Moselle “Foyer rural” association, the penitentiary center of Maxéville, or even to a general assembly of the Crédit Mutuel de Lorraine. I also contribute to the training of high and middle school teachers on (paleo)climate science. I responded to the request of the French government to contribute to a new series of seminars for public servants and intend to take a role in the new “GREC”: the Groupement régional d’experts sur le climat, a local version of the IPCC (or GIEC in French).

VI. Research management.

1. At CRPG.

i. Team animation.

The CRPG is not divided into teams but into themes, including the CYCLA theme (Cycles, Atmosphere, Climate – 9 researchers). I have been running it since 2017 with the support of Christophe Cloquet and now with David Bekaert. I was very involved in writing the HCERES report and the project in 2021 and the new website creation (logo designed by Thomas Rigaudier). Together with Pierre-Henri Blard, I actively contributed to define hiring profiles and to attract candidates to CRPG. Despite the retirement of two CYCLA members, we also

attracted two young scientists, David Bekaert and Charlotte Prud'homme, as well as a senior researcher, Sune Nielsen.

C R P G | Centre de Recherches Pétrographiques et Géochimiques

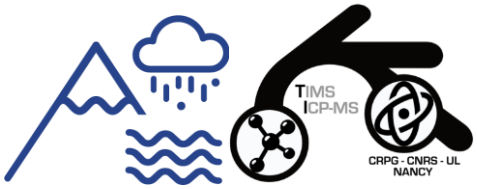

ii. MC ICP-MS-TIMS platform.

The platform houses an MC- ICP-MS Neptune Plus, an ICP-MS X-series, a TIMS Triton plus and various other equipment. It brings together four PAR (Personnel d'Appui à la Recherche, 2 Ingénieurs d'étude and 2 Assistants ingénieurs) and there are 6 of us researchers who use it frequently. It is also used locally within the OSU and nationally through the SARMi. Since September 2018 I have been the scientific manager of the MC- ICP-MS/TIMS platform and CRPG clean rooms. I am in charge of supervising the instrument schedule, organizing bimonthly meetings with the users, discussing and assisting the lab engineers in their work. Part of my role also consists in attracting new researchers, writing grants to obtain fundings for new instruments (degassing bench for the TIMS, Ion Chromatography System, clean labs, CC-MC-ICP-MS) and sitting in different committees (RéGEF, Comité de direction).

Finally, one of the main administrative tasks at the moment is defining the way analyzes need to be paid, and to obtain the INFRA+ quality label within the Université de Lorraine as part of the ANATELo network and at CNRS, through the RéGEF network (Réseau Géochimique Français). I was also a member of the technical steering committee for monitoring the implementation of a new clean room platform at the CRPG, a project for which I obtained 900k€ via a project submitted to the FEDER Grand Est. I contributed to the definition of scientific and technical needs, at the preliminary project stage, consultation of companies and site monitoring. At the moment, I am actively involved in the funding and purchase of the CC-MC-ICP-MS.

iii. Others.

I am an elected member of the laboratory council and member of the CRPG "Comité de direction" and I contribute to the newly founded "Com" group.

2. **In Nancy.**

I am a member of the OSU OTELo eco-responsibility group (implementation of carbon footprint, collective reflection, and scientific animation). I contributed to the development of the EPHemeris project co-supported by the OTELo OSU in collaboration with various laboratories of the University of Lorraine (Sociology, Geography, Neurosciences, Biology, among others) as part of a Call for Expressions of Interest of the LUE i-Site on structuring calls within the University of Lorraine.

I sat for 5 years on the CRHSCT of DR06 and was a member of the monitoring group for the reorganization of INIST (2017-2021). The latter involved sensitive human resources issues as 53 people had to leave their ongoing functions and find new ones, either at INIST, or elsewhere. Over 17 people had to be assisted over two years to find a new place.

3. **Collective responsibilities within the CNRS and the French community.**

I have been an elected member in section 18 since 2021. As such, I participate in the evaluation of the careers and promotion requests of other research scientists at CNRS, and I am a member of the hiring committee (workload of ~two months per year, for 5 years). I am the parity referent of the section, and a member of the CPE (Comité Parité Egalité), a committee in charge of making proposals to, and monitoring the actions of, the Mission for the Place of Women (Mission pour la Place Des Femmes, MDPF, 3-hour meetings every other month). I participated in the first wave of reflection of the INSU “Prospectives” via the OSUs for the theme "Major crises" within the grouping of Eastern OSUs (THETA, ObAS, EOST, OTELo). I then co-organized the joint workshop between challenges 3 and 4 in Dijon as responsible for challenge 3 and participated in the various associated meetings.

Finally, I am an active member of the paleo community in France. For the past four years, I have hosted a newsletter sent to more than 350 people, every two months on average, and I have organized a summer school in 2022 (45 people), with a second one that will take place in 2024. These structuring actions are very appreciated and will continue in the future.

General conclusion.

Over the last decade, I contributed to improving our understanding of the past and modern sulfur cycles, with many implications for the description and quantification of the carbon and oxygen cycles. Therefore, I aided in strengthening our understanding of the mechanisms that control the composition of the ocean-atmosphere system.

To do so, I've been developing a new method to measure sulfur isotope ratios in small samples, because sulfur isotope ratios are a prime tool for studying the current and ancient sulfur cycle. I've also been developing many collaborations and supervising undergraduate students and graduate students.

Through work on modern rivers with Mark Torres, Chenyang Lin, Andrea Burke and Erica Erlanger, we contributed to reappraising the role of pyrite oxidation in the modern carbon and oxygen budgets through careful estimates of sulfuric acid-driven weathering. I also contributed to reexploring sulfur isotope fractionation during Min-Sum Sim's postdoc and through collaborations with Sean Crowe.

Regarding the reconstructions of the past sulfur cycle, our work has focused on improving our understanding of the carbonate archive as a recorder of the sulfur cycle, and the parameters that control the isotopic composition of rivers and of the ocean. Together with many people including Caroline Thaler (during their postdoc) and Yigal Barkan (during their PhD), I showed that carbonates record the sulfur isotopic composition of seawater, albeit with offsets that depend on the species studied. Through Ted Present's PhD work and other collaborations, we demonstrated that seawater sulfur isotope ratios are preserved in carbonates throughout the rock's history and that biogenic carbonates must be preferentially targeted. However, Ted demonstrated the heterogeneity of the effects of diagenesis, even within a hand sample. Finally, thanks to Vicky Rennie and Arbia Jouini's PhDs, we have demonstrated that CAS can provide extremely useful information about paleoenvironments, as shown by the reconstruction of the Cenozoic and the K-Pg boundary sulfur isotope ratio. They produced the first monospecific foraminifera records and showed that not only can CAS be used to produce high fidelity records of past seawater $\delta^{34}S$ values, but also that careful picking of benthic and planktic foraminifera can help reconstruct the history of diagenetic processes.

This very important result is going to structure part of my research for the next years as I intend to develop new records combining planktic and benthic foraminifera at different timescales through the last 100 Myr. I will also keep on exploring the sulfur isotope ratios of modern rivers to fully constrain the isotope signature of the riverine input to the ocean using not only $\delta^{34}S$ but also $\Delta^{33}S$ and $\Delta^{36}S$, after new analytical developments using a CC-MC-ICP-MS.

Finally, I also intend to pursue my investment in research management, teaching and outreach, so that the time spent in the laboratory becomes more meaningful. Multiple challenges are indeed upon us and we must face them: the global climate and biodiversity crises, social inequalities and multiple biases within society. By helping structuring part of the Earth science community, participating in outreach activities whenever possible, bring science to general audiences, policy makers, public workers and private deciders, and finally by ensuring unbiased selection of future researchers, I hope to contribute to attenuate the consequences of the current paths we collectively follow.

List of bibliographical references

Abramovich, S., Keller, G., 2003. Planktonic foraminiferal response to the latest Maastrichtian abrupt warm event: a case study from South Atlantic DSDP Site 525A. Marine Micropaleontology 48, 225–249. https://doi.org/10.1016/S0377-8398(03)00021-5

Adams, A., Daval, D., Baumgartner, L.P., Bernard, S., Vennemann, T., Cisneros-Lazaro, D., Stolarski, J., Baronnet, A., Grauby, O., Guo, J., Meibom, A., 2023. Rapid grain boundary diffusion in foraminifera tests biases paleotemperature records. Communications Earth & Environment 4, 144. https://doi.org/10.1038/s43247-023-00798-2Al

Adams, D.D., Hurtgen, M.T., Sageman, B.B., 2010. Volcanic triggering of a biogeochemical cascade during Oceanic Anoxic Event 2. Nature Geosci 3, 201–204. http://www.nature.com/ngeo/journal/v3/n3/suppinfo/ngeo743_S1.html

Addadi, L., Moradian, J., Shay, E., Maroudas, N.G., Weiner, S., 1987. A chemical model for the cooperation of sulfates and carboxylates in calcite crystal nucleation: Relevance to biomineralization. Proceedings of the National Academy of Sciences 84, 2732–2736.

Addadi, L., Raz, S., Weiner, S., 2003. Taking Advantage of Disorder: Amorphous Calcium Carbonate and Its Roles in Biomineralization. Advanced Materials 15, 959–970. https://doi.org/10.1002/adma.200300381

Adkins, J.F., Boyle, E.A., Curry, W.B., Lutringer, A., 2003. Stable isotopes in deep-sea corals and a new mechanism for "vital effects." Geochimica et cosmochimica acta 67, 1129–1143. https://doi.org/10.1016/S0016-7037(02)01203-6

Ahm, A.-S.C., Bjerrum, C.J., Blättler, C.L., Swart, P.K., Higgins, J.A., 2018. Quantifying early marine diagenesis in shallow-water carbonate sediments. Geochimica et Cosmochimica Acta 236, 140–159. https://doi.org/10.1016/j.gca.2018.02.042

Aizenberg, J., Addadi, L., Weiner, S., Lambert, G., 1996. Stabilization of amorphous calcium carbonate by specialized macromolecules in biological and synthetic precipitates. Advanced Materials 8, 222–226. https://doi.org/10.1002/adma.19960080307

Aizenberg, J., Lambert, G., Weiner, S., Addadi, L., 2002. Factors Involved in the Formation of Amorphous and Crystalline Calcium Carbonate: A Study of an Ascidian Skeleton. J. Am. Chem. Soc. 124, 32–39. https://doi.org/10.1021/ja016990l

Aizenberg, J., Weiner, S., Addadi, L., 2003. Coexistence of Amorphous and Crystalline Calcium Carbonate in Skeletal Tissues. Connective Tissue Research 44, 20–25. https://doi.org/10.1080/03008200390152034

Akiva-Tal, A., Kababya, S., Balazs, Y.S., Glazer, L., Berman, A., Sagi, A., Schmidt, A., 2011. In situ molecular NMR picture of bioavailable calcium stabilized as amorphous $CaCO_3$ biomineral in crayfish gastroliths. Proceedings of the National Academy of Sciences 108, 14763–14768. https://doi.org/10.1073/pnas.1102608108

Albalat, E., Telouk, P., Balter, V., Fujii, T., Bondanese, V.P., Plissonnier, M.-L., Vlaeminck-Guillem, V., Baccheta, J., Thiam, N., Miossec, P., Zoulim, F., Puisieux, A., Albarède, F., 2016. Sulfur isotope analysis by MC-ICP-MS and application to small medical samples. J. Anal. At. Spectrom. 31, 1002–1011. https://doi.org/10.1039/C5JA00489F

Alegret, L., Arreguín-Rodríguez, G.J., Trasviña-Moreno, C.A., Thomas, E., 2021. Turnover and stability in the deep sea: Benthic foraminifera as tracers of Paleogene global change. Global and Planetary Change 196, 103372. https://doi.org/10.1016/j.gloplacha.2020.103372

Alegret, L., Thomas, E., 2009. Food supply to the seafloor in the Pacific Ocean after the Cretaceous/Paleogene boundary event. Marine Micropaleontology 73, 105–116. https://doi.org/10.1016/j.marmicro.2009.07.005

Alegret, L., Thomas, E., 2004. Benthic foraminifera and environmental turnover across the Cretaceous/Paleogene boundary at Blake Nose (ODP Hole 1049C, Northwestern Atlantic). Palaeogeography, Palaeoclimatology, Palaeoecology 208, 59–83. https://doi.org/10.1016/j.palaeo.2004.02.028

Alegret, L., Thomas, E., Lohmann, K.C., 2012. End-Cretaceous marine mass extinction not caused by productivity collapse. Proceedings of the National Academy of Sciences 109, 728–732. https://doi.org/10.1073/pnas.1110601109

Algeo, T.J., Luo, G.M., Song, H.Y., Lyons, T.W., Canfield, D.E., 2015. Reconstruction of secular variation in seawater sulfate concentrations. Biogeosciences 12, 2131–2151. https://doi.org/10.5194/bg-12-2131-2015

AlKhatib, M., Eisenhauer, A., 2017a. Calcium and strontium isotope fractionation during precipitation from aqueous solutions as a function of temperature and reaction rate; II. Aragonite. Geochimica et Cosmochimica Acta 209, 320–342. https://doi.org/10.1016/j.gca.2017.04.012

AlKhatib, M., Eisenhauer, A., 2017b. Calcium and strontium isotope fractionation in aqueous solutions as a function of temperature and reaction rate; I. Calcite. Geochimica et Cosmochimica Acta 209, 296–319. https://doi.org/10.1016/j.gca.2016.09.035

Aloisi, G., Guibourdenche, L., Natalicchio, M., Caruso, A., Haffert, L., El Kilany, A., Dela Pierre, F., 2022. The geochemical riddle of "low-salinity gypsum" deposits. Geochimica et Cosmochimica Acta 327, 247–275. https://doi.org/10.1016/j.gca.2022.03.033

Alvarez, L.W., Alvarez, W., Asaro, F., Michel, H.V., 1980. Extraterrestrial Cause for the Cretaceous-Tertiary Extinction. Science 208, 1095–1108.

Amrani, A., Sessions, A.L., Adkins, J.F., 2009. Compound-Specific δ34S Analysis of Volatile Organics by Coupled GC/Multicollector-ICPMS. Anal. Chem. 81, 9027–9034. https://doi.org/10.1021/ac9016538

Anagnostou, E., John, E.H., Edgar, K.M., Foster, G.L., Ridgwell, A., Inglis, G.N., Pancost, R.D., Lunt, D.J., Pearson, P.N., 2016. Changing atmospheric CO2 concentration was the primary driver of early Cenozoic climate. Nature 533, 380–384. https://doi.org/10.1038/nature17423

Angell, R.W., 1967. The Test Structure and Composition of the Foraminifer Rosalina floridana*. The Journal of Protozoology 14, 299–307. https://doi.org/10.1111/j.1550-7408.1967.tb02001.x

Antler, G., Turchyn, A.V., Ono, S., Sivan, O., Bosak, T., 2017. Combined 34S, 33S and 18O isotope fractionations record different intracellular steps of microbial sulfate reduction. Geochimica et Cosmochimica Acta 203, 364–380. https://doi.org/10.1016/j.gca.2017.01.015

Archibald, J.D., Clemens, W.A., Padian, K., Rowe, T., Macleod, N., Barrett, P.M., Gale, A., Holroyd, P., Sues, H.-D., Arens, N.C., Horner, J.R., Wilson, G.P., Goodwin, M.B., Brochu, C.A., Lofgren, D.L., Hurlbert, S.H., Hartman, J.H., Eberth, D.A., Wignall, P.B., Currie, P.J., Weil, A., Prasad, G.V.R., Dingus, L., Courtillot, V., Milner, Angela, Milner, Andrew, Bajpai, S., Ward, D.J., Sahni, A., 2010. Cretaceous Extinctions: Multiple Causes. Science 328, 973. https://doi.org/10.1126/science.328.5981.973-a

Arenillas, I., Arz, J.A., Grajales-Nishimura, J.M., Meléndez, A., Rojas-Consuegra, R., 2016. The Chicxulub impact is synchronous with the planktonic foraminifera mass extinction at the Cretaceous/Paleogene boundary: new evidence from the Moncada section, Cuba. Geologica Acta 17.

Arenillas, I., Arz, J.A., Grajales-Nishimura, J.M., Murillo-Muñetón, G., Alvarez, W., Camargo-Zanoguera, A., Molina, E., Rosales-Domínguez, C., 2006. Chicxulub impact event is Cretaceous/Paleogene boundary in age: New micropaleontological evidence. Earth and Planetary Science Letters 249, 241–257. https://doi.org/10.1016/j.epsl.2006.07.020

Artemieva, N., Morgan, J., Expedition 364 party, 2017. Quantifying the Release of Climate-Active Gases by Large Meteorite Impacts With a Case Study of Chicxulub. Geophysical Research Letters 44, 10,180-10,188. https://doi.org/10.1002/2017GL074879

Arvidson, R.S., Mackenzie, F.T., 1999. The dolomite problem; control of precipitation kinetics by temperature and saturation state. Am J Sci 299, 257. https://doi.org/10.2475/ajs.299.4.257

Ault, W.U., Kulp, J.L., 1959. Isotopic geochemistry of sulphur. Geochimica et Cosmochimica Acta 16, 201–235. https://doi.org/10.1016/0016-7037(59)90112-7

Baldermann, A., Deditius, A.P., Dietzel, M., Fichtner, V., Fischer, C., Hippler, D., Leis, A., Baldermann, C., Mavromatis, V., Stickler, C.P., Strauss, H., 2015. The role of bacterial sulfate reduction during dolomite precipitation: Implications from Upper Jurassic platform carbonates. Chemical Geology 412, 1–14. https://doi.org/10.1016/j.chemgeo.2015.07.020

Banner, J.L., Hanson, G.N., 1990. Calculation of simultaneous isotopic and trace element variations during water-rock interaction with applications to carbonate diagenesis. Geochimica et Cosmochimica Acta 54, 3123–3137.

Bao, H., Thiemens, M.H., Farquhar, J., Campbell, D.A., Lee, C.C.-W., Heine, K., Loope, D.B., 2000. Anomalous 17O compositions in massive sulphate deposits on the Earth. Nature 406, 176–178. https://doi.org/10.1038/35018052

Barkan, Y., Paris, G., Webb, S.M., Adkins, J.F., Halevy, I., 2020. Sulfur isotope fractionation between aqueous and carbonate-associated sulfate in abiotic calcite and aragonite. Geochimica et Cosmochimica Acta 280, 317–339. https://doi.org/10.1016/j.gca.2020.03.022

Barkan, Y., Pramanik, C., Yam, R., Shemesh, A., Petersen, S., Jouini, A., Paris, G., Caro, G., Halevy, I., in prep. Oxygen, sulfur, calcium and carbonate clumped isotopes in sulfate-bearing calcite and aragonite. Geochimica et Cosmochimica Acta.

Barnet, J., 2018. Investigating Climate Change and Carbon Cycling during the Latest Cretaceous to Paleogene (~67–52 million years ago); new geochemical records from the South Atlantic and Indian oceans.

Baronnet, A., Cuif, J.-P., Dauphin, Y., Farre, B., Nouet, J., 2008. Crystallization of biogenic Ca-carbonate within organo-mineral micro-domains. Structure of the calcite prisms of the Pelecypod Pinctada margaritifera (Mollusca) at the submicron to nanometre ranges. Mineralogical Magazine 72, 617–626.

Barrera, E., Keller, G., 1994. Productivity across the Cretaceous/Tertiary boundary in high latitudes. Geological Society of America Bulletin 106, 1254–1266. https://doi.org/10.1130/0016-7606(1994)106<1254:PATCTB>2.3.CO;2

Baumgarten, S., Laudien, J., Jantzen, C., Häussermann, V., Försterra, G., 2014. Population structure, growth and production of a recent brachiopod from the Chilean fjord region. Marine Ecology 35, 401–413. https://doi.org/10.1111/maec.12097

Baumgartner, L.K., Reid, R.P., Dupraz, C., Decho, A.W., Buckley, D., Spear, J., Przekop, K.M., Visscher, P.T., 2006. Sulfate reducing bacteria in microbial mats: changing paradigms, new discoveries. Sedimentary Geology 185, 131–145.

Bé, A.W.H., Hemleben, C., Anderson, O.R., Spindler, M., 1979. Chamber Formation in Planktonic Foraminifera. Micropaleontology 25, 294–307. https://doi.org/10.2307/1485304

Beaudoin, G., Taylor, B.E., Rumble Iii, D., Thiemens, M., 1994. Variations in the sulfur isotope composition of troilite from the Cañon Diablo iron meteorite. Geochimica et cosmochimica acta 58, 4253–4255. https://doi.org/10.1016/0016-7037(94)90277-1

Beaulieu, E., Goddéris, Y., Donnadieu, Y., Labat, D., Roelandt, C., 2012. High sensitivity of the continental-weathering carbon dioxide sink to future climate change. Nature Climate Change 2, 346–349. https://doi.org/10.1038/nclimate1419

Beaulieu, E., Goddéris, Y., Labat, D., Roelandt, C., Calmels, D., Gaillardet, J., 2011. Modeling of water-rock interaction in the Mackenzie basin: Competition between sulfuric and carbonic acids. Chemical Geology 289, 114–123. https://doi.org/10.1016/j.chemgeo.2011.07.020

Beerling, D.J., Lomax, B.H., Royer, D.L., Upchurch, G.R., Kump, L.R., 2002. An atmospheric pCO_2 reconstruction across the Cretaceous-Tertiary boundary from leaf megafossils. Proceedings of the National Academy of Sciences 99, 7836–7840. https://doi.org/10.1073/pnas.122573099

Beniash, E., Addadi, L., Weiner, S., 1999. Cellular control over spicule formation in sea urchin embryos: A structural approach. Journal of structural biology 125, 50–62.

Beniash, E., Aizenberg, J., Addadi, L., Weiner, S., 1997. Amorphous calcium carbonate transforms into calcite during sea urchin larval spicule growth. Proceedings of the Royal Society of London. Series B: Biological Sciences 264, 461–465.

Bentov, S., Brownlee, C., Erez, J., 2009. The role of seawater endocytosis in the biomineralization process in calcareous foraminifera. Proceedings of the National Academy of Sciences 106, 21500–21504. https://doi.org/10.1073/pnas.0906636106

Bentov, S., Erez, J., 2006. Impact of biomineralization processes on the Mg content of foraminiferal shells: A biological perspective. Geochemistry, Geophysics, Geosystems 7, Q01P08. https://doi.org/10.1029/2005gc001015

Bernasconi, S.M., Meier, I., Wohlwend, S., Brack, P., Hochuli, P.A., Bläsi, H., Wortmann, U.G., Ramseyer, K., 2017. An evaporite-based high-resolution sulfur isotope record of Late Permian and Triassic seawater sulfate. Geochimica et Cosmochimica Acta 204, 331–349. https://doi.org/10.1016/j.gca.2017.01.047

Berner, R.A., 2006. GEOCARBSULF: A combined model for Phanerozoic atmospheric O_2 and CO_2. Geochimica et Cosmochimica Acta 70, 5653–5664.

Berner, R.A., 1994. GEOCARB II a revised model of atmospheric CO_2 over Phanerozoic time. American Journal of Science 294, 56–31.

Berner, R.A., 1993. Weathering and its effect on atmospheric CO_2 over Phanerozoic time. Chemical Geology 107, 373–374.

Berner, R.A., 1991. A model for atmospheric CO_2 over Phanerozoic time. American Journal of Science 291, 339.

Berner, R.A., 1984. Sedimentary pyrite formation: An update. Geochimica et Cosmochimica Acta 48, 605–615. https://doi.org/10.1016/0016-7037(84)90089-9

Berner, R.A., 1975. The role of magnesium in the crystal growth of calcite and aragonite from sea water. Geochimica et Cosmochimica Acta 39, 489–504. https://doi.org/10.1016/0016-7037(75)90102-7

Berner, R.A., 1966. Chemical diagenesis of some modern carbonate sediments. Am J Sci 264, 1. https://doi.org/10.2475/ajs.264.1.1

Berner, Robert A, Raiswell, R., 1983. Burial of organic carbon and pyrite sulfur in sediments over phanerozoic time: a new theory. Geochimica et Cosmochimica Acta 47, 855–862. https://doi.org/10.1016/0016-7037(83)90151-5

Berner, R.A., Lasaga, A.C., Garrels, R.M., 1983. The carbonate-silicate geochemical cycle and its effect on atmospheric carbon dioxide over the past 100 million years. American Journal of Science 283, 641.

Berner, R.A., Scott, M.R., Thomlinson, C., 1970. CARBONATE ALKALINITY IN THE PORE WATERS OF ANOXIC MARINE SEDIMENTS1. Limnology and Oceanography 15, 544–549. https://doi.org/10.4319/lo.1970.15.4.0544

Bernhard, J.M., Blanks, J.K., Hintz, C.J., Chandler, G.T., 2004. Use of the fluorescent calcite marker calcein to label foraminiferal tests. Journal of Foraminiferal Research 34, 96–101. https://doi.org/10.2113/0340096

Birch, H.S., Coxall, H.K., Pearson, P.N., Kroon, D., Schmidt, D.N., 2016. Partial collapse of the marine carbon pump after the Cretaceous-Paleogene boundary. Geology 44, 287–290. https://doi.org/10.1130/G37581.1

Bischoff, J.L., 1968. Kinetics of calcite nucleation: Magnesium ion inhibition and ionic strength catalysis. Journal of Geophysical Research (1896-1977) 73, 3315–3322. https://doi.org/10.1029/JB073i010p03315

Blättler, C.L., Henderson, G.M., Jenkyns, H.C., 2012. Explaining the Phanerozoic Ca isotope history of seawater. Geology 40, 843–846. https://doi.org/10.1130/G33191.1

Blättler, C.L., Miller, N.R., Higgins, J.A., 2015. Mg and Ca isotope signatures of authigenic dolomite in siliceous deep-sea sediments. Earth and Planetary Science Letters 419, 32–42. https://doi.org/10.1016/j.epsl.2015.03.006

Blue, C.R., Dove, P.M., 2015. Chemical controls on the magnesium content of amorphous calcium carbonate. Geochimica et Cosmochimica Acta 148, 23–33. https://doi.org/10.1016/j.gca.2014.08.003

Blue, C.R., Giuffre, A., Mergelsberg, S., Han, N., De Yoreo, J.J., Dove, P.M., 2017. Chemical and physical controls on the transformation of amorphous calcium carbonate into crystalline CaCO3 polymorphs. Geochimica et Cosmochimica Acta 196, 179–196. https://doi.org/10.1016/j.gca.2016.09.004

Boetius, A., Ravenschlag, K., Schubert, C.J., Rickert, D., Widdel, F., Gieseke, A., Amann, R., Jørgensen, B.B., Witte, U., Pfannkuche, O., 2000. A marine microbial consortium apparently mediating anaerobic oxidation of methane. Nature 407, 623–626. https://doi.org/10.1038/35036572

Böhm, F., Gussone, N., Eisenhauer, A., Dullo, W.-C., Reynaud, S., Paytan, A., 2006. Calcium isotope fractionation in modern scleractinian corals. Geochimica et Cosmochimica Acta 70, 4452–4462. https://doi.org/10.1016/j.gca.2006.06.1546

Bots, P., Benning, L.G., Rickaby, R.E.M., Shaw, S., 2011. The role of SO4 in the switch from calcite to aragonite seas. Geology 39, 331–334. https://doi.org/10.1130/G31619.1

Bots, P., Benning, L.G., Rodriguez-Blanco, J.-D., Roncal-Herrero, T., Shaw, S., 2012. Mechanistic Insights into the Crystallization of Amorphous Calcium Carbonate (ACC). Crystal Growth & Design 12, 3806–3814. https://doi.org/10.1021/cg300676b

Bottrell, S.H., Newton, R.J., 2006. Reconstruction of changes in global sulfur cycling from marine sulfate isotopes. Earth-Science Reviews 75, 59–83. https://doi.org/10.1016/j.earscirev.2005.10.004

Bouchez, J., Beyssac, O., Galy, V., Gaillardet, J., France-Lanord, C., Maurice, L., Moreira-Turcq, P., 2010. Oxidation of petrogenic organic carbon in the Amazon floodplain as a source of atmospheric CO2. Geology 38, 255–258. https://doi.org/10.1130/G30608.1

Bouilhol, P., Jagoutz, O., Hanchar, J.M., Dudas, F.O., 2013. Dating the India–Eurasia collision through arc magmatic records. Earth and Planetary Science Letters 366, 163–175. https://doi.org/10.1016/j.epsl.2013.01.023

Boyle, E., Berry, J., Erez, J., Tishler, C., 2002. Sulfur in foraminifera shells, a new paleoceanographic proxy for carbonate ion in seawater. Presented at the AGU Fall Meeting Abstracts, pp. PP52B-13.

Bradley, A.S., Leavitt, W.D., Johnston, D.T., 2011. Revisiting the dissimilatory sulfate reduction pathway. Geobiology 9, 446–457. https://doi.org/10.1111/j.1472-4669.2011.00292.x

Bradley, A.S., Leavitt, W.D., Schmidt, M., Knoll, A.H., Girguis, P.R., Johnston, D.T., 2016. Patterns of sulfur isotope fractionation during microbial sulfate reduction. Geobiology 14, 91–101. https://doi.org/10.1111/gbi.12149

Bralower, T.J., Premoli-Silva, I., Malone, M.J., Shipboard Scientific Party, 2002. Site 1209 (Initial Reports No. 198), Proceedings of the Ocean Drilling Program.

Brand, U., Veizer, J., 1981. Chemical diagenesis of a multicomponent system—II, Stable isotopes. Journal of Sedimentary Petrology 51, 987–998.

Brand, U., Veizer, J., 1980. Chemical diagenesis of a multicomponent carbonate system; 1, Trace elements. Journal of Sedimentary Research 50, 1219–1236.

Brenot, A., Carignan, J., France-Lanord, C., Benoît, M., 2007. Geological and land use control on $\delta^{34}S$ and $\delta^{18}O$ of river dissolved sulfate: The Moselle river basin, France. Chemical Geology 244, 25–41. https://doi.org/10.1016/j.chemgeo.2007.06.003

Broecker, W.S., 1970. A boundary condition on the evolution of atmospheric oxygen. Journal of Geophysical Research (1896-1977) 75, 3553–3557. https://doi.org/10.1029/JC075i018p03553

Brunner, B., Bernasconi, S.M., 2005. A revised isotope fractionation model for dissimilatory sulfate reduction in sulfate reducing bacteria. Geochimica et Cosmochimica Acta 69, 4759–4771. https://doi.org/10.1016/j.gca.2005.04.015

Brunner, B., Bernasconi, S.M., Kleikemper, J., Schroth, M.H., 2005. A model for oxygen and sulfur isotope fractionation in sulfate during bacterial sulfate reduction processes. Geochimica et Cosmochimica Acta 69, 4773–4785. https://doi.org/10.1016/j.gca.2005.04.017

Bryant, R.N., Present, T.M., Ahm, A.-S.C., McClelland, H.-L.O., Razionale, D., Blättler, C.L., 2022. Early diagenetic constraints on Permian seawater chemistry from the Capitan Reef. Geochimica et Cosmochimica Acta 328, 1–18.

Bryant, R.N., Richardson, J.A., Kalia, T.C., Gros, O., Lopez-Garriga, J., Blättler, C.L., 2023. Inorganic sulfate− based signatures of chemosymbiosis in modern infaunal lucinids. Geology.

Burdett, J.W., Arthur, M.A., Richardson, M., 1989. A Neogene seawater sulfur isotope age curve from calcareous pelagic microfossils. Earth and Planetary Science Letters 94, 189–198. https://doi.org/10.1016/0012-821X(89)90138-6

Burdige, D.J., 2007. Preservation of Organic Matter in Marine Sediments: Controls, Mechanisms, and an Imbalance in Sediment Organic Carbon Budgets? Chem. Rev. 107, 467–485. https://doi.org/10.1021/cr050347q

Burke, A., Present, T.M., Paris, G., Rae, E.C.M., Sandilands, B.H., Gaillardet, J., Peucker-Ehrenbrink, B., Fischer, W.W., McClelland, J.W., Spencer, R.G.M., Voss, B.M., Adkins, J.F., 2018a. Sulfur isotopes in rivers: Insights into global weathering budgets, pyrite oxidation, and the modern sulfur cycle. Earth and Planetary Science Letters 496, 168–177. https://doi.org/10.1016/j.epsl.2018.05.022

Burke, A., Present, T.M., Paris, G., Rae, E.C.M., Sandilands, B.H., Gaillardet, J., Peucker-Ehrenbrink, B., Fischer, W.W., McClelland, J.W., Spencer, R.G.M., Voss, B.M., Adkins, J.F., 2018b. Sulfur isotopes in rivers: Insights into global weathering budgets, pyrite oxidation, and the modern sulfur cycle. Earth and Planetary Science Letters 496, 168–177. https://doi.org/10.1016/j.epsl.2018.05.022

Buschendorf, Fr., Nielsen, H., Puchelt, H., Ricke, W., 1963. Schwefel-Isotopen-Untersuchungen am Pyrit-Sphalerit-Baryt-Lager Meggen/Lenne (Deutschland) und an verschiedenen Devon-Evaporiten. Geochimica et Cosmochimica Acta 27, 501–523. https://doi.org/10.1016/0016-7037(63)90085-1

Busenberg, E., Plummer, L.N., 1985. Kinetic and thermodynamic factors controlling the distribution of SO_3^{2-} and Na^+ in calcites and selected aragonites. Geochimica et Cosmochimica Acta 49, 713–725. https://doi.org/10.1016/0016-7037(85)90166-8

Callbeck, C.M., Lavik, G., Ferdelman, T.G., Fuchs, B., Gruber-Vodicka, H.R., Hach, P.F., Littmann, S., Schoffelen, N.J., Kalvelage, T., Thomsen, S., Schunck, H., Löscher, C.R., Schmitz, R.A., Kuypers, M.M.M., 2018. Oxygen minimum zone cryptic sulfur cycling sustained by offshore transport of key sulfur oxidizing bacteria. Nature Communications 9, 1729. https://doi.org/10.1038/s41467-018-04041-x

Calmels, D., Gaillardet, J., Brenot, A., France-Lanord, C., 2007. Sustained sulfide oxidation by physical erosion processes in the Mackenzie River basin: Climatic perspectives. Geology 35, 1003–1006. https://doi.org/10.1130/G24132A.1

Canfield, D.E., 2013. Sulfur isotopes in coal constrain the evolution of the Phanerozoic sulfur cycle. Proceedings of the National Academy of Sciences 110, 8443–8446. https://doi.org/10.1073/pnas.1306450110

Canfield, D. E., 2004. The evolution of the Earth surface sulfur reservoir. American Journal of Science 304, 839–861. https://doi.org/10.2475/ajs.304.10.839

Canfield, Donald E, 2004. The evolution of the Earth surface sulfur reservoir. Am J Sci 304, 839. https://doi.org/10.2475/ajs.304.10.839

Canfield, Donald E., Farquhar, J., Zerkle, A.L., 2010. High isotope fractionations during sulfate reduction in a low-sulfate euxinic ocean analog. Geology 38, 415–418. https://doi.org/10.1130/g30723.1

Canfield, D.E., Olesen, C.A., Cox, R.P., 2006. Temperature and its control of isotope fractionation by a sulfate-reducing bacterium. Geochimica et Cosmochimica Acta 70, 548–561. https://doi.org/10.1016/j.gca.2005.10.028

Canfield, D.E., Raiswell, R., 1999. The evolution of the sulfur cycle. American Journal of Science 299, 697–723. https://doi.org/10.2475/ajs.299.7-9.697

Canfield, Donald E, Stewart, F.J., Thamdrup, B., De Brabandere, L., Dalsgaard, T., Delong, E.F., Revsbech, N.P., Ulloa, O., 2010. A Cryptic Sulfur Cycle in Oxygen-Minimum–Zone Waters off the Chilean Coast. Science 330, 1375–1378. https://doi.org/10.1126/science.1196889

Canfield, D.E., Teske, A., 1996. Late Proterozoic rise in atmospheric oxygen concentration inferred from phylogenetic and sulphur-isotope studies. Nature 382, 127–132. https://doi.org/10.1038/382127a0

Cartwright, J.H.E., Checa, A.G., Gale, J.D., Gebauer, D., Sainz-Díaz, C.I., 2012. Calcium Carbonate Polyamorphism and Its Role in Biomineralization: How Many Amorphous Calcium Carbonates Are There? Angewandte Chemie International Edition 51, 11960–11970. https://doi.org/10.1002/anie.201203125

Castro-Claros, J.D., Checa, A., Lucena, C., Pearson, J.R., Salas, C., 2021. Shell-adductor muscle attachment and Ca^{2+} transport in the bivalves Ostrea stentina and Anomia ephippium. Acta Biomaterialia 120, 249–262. https://doi.org/10.1016/j.actbio.2020.09.053

Chambers, L.A., Trudinger, P.A., Smith, J.W., Burns, M.S., 1975. Fractionation of sulfur isotopes by continuous cultures of Desulfovibrio desulfuricans. Can. J. Microbiol. 21, 1602–1607. https://doi.org/10.1139/m75-234

Chen, S., Gagnon, A.C., Adkins, J.F., 2018. Carbonic anhydrase, coral calcification and a new model of stable isotope vital effects. Geochimica et Cosmochimica Acta 236, 179–197. https://doi.org/10.1016/j.gca.2018.02.032

Chenet, A.-L., Courtillot, V., Fluteau, F., Gérard, M., Quidelleur, X., Khadri, S.F.R., Subbarao, K.V., Thordarson, T., 2009. Determination of rapid Deccan eruptions across the Cretaceous-Tertiary boundary using paleomagnetic secular variation: 2.

Constraints from analysis of eight new sections and synthesis for a 3500-m-thick composite section. J. Geophys. Res. 114, B06103. https://doi.org/10.1029/2008jb005644

Christensen, L.E., Brunner, B., Truong, K.N., Mielke, R.E., Webster, C.R., Coleman, M., 2007. Measurement of Sulfur Isotope Compositions by Tunable Laser Spectroscopy of SO2. Anal. Chem. 79, 9261–9268. https://doi.org/10.1021/ac071040p

Cisneros-Lazaro, D., Adams, A., Guo, J., Bernard, S., Baumgartner, L.P., Daval, D., Baronnet, A., Grauby, O., Vennemann, T., Stolarski, J., Escrig, S., Meibom, A., 2022. Fast and pervasive diagenetic isotope exchange in foraminifera tests is species-dependent. Nature Communications 13, 113. https://doi.org/10.1038/s41467-021-27782-8

Clarkson, J.R., Price, T.J., Adams, C.J., 1992. Role of metastable phases in the spontaneous precipitation of calcium carbonate. J. Chem. Soc., Faraday Trans. 88, 243–249. https://doi.org/10.1039/FT9928800243

Claypool, G.E., Holser, W.T., Kaplan, I.R., Sakai, H., Zak, I., 1980. The age curves of sulfur and oxygen isotopes in marine sulfate and their mutual interpretation. Chemical Geology 28, 199–260. https://doi.org/10.1016/0009-2541(80)90047-9

Coplen, T.B., Krouse, H.R., 1998. Sulphur isotope data consistency improved. Nature 392, 32–32. https://doi.org/10.1038/32080

Courtillot, V., Fluteau, F., 2014. A review of the embedded time scales of flood basalt volcanism with special emphasis on dramatically short magmatic pulses, in: Keller, G., Kerr, A.C. (Eds.), Volcanism, Impacts, and Mass Extinctions: Causes and Effects. Geological Society of America.

Craddock, P.R., Rouxel, O.J., Ball, L.A., Bach, W., 2008. Sulfur isotope measurement of sulfate and sulfide by high-resolution MC-ICP-MS. Chemical Geology 253, 102–113. https://doi.org/10.1016/j.chemgeo.2008.04.017

Craig, H., 1953. The geochemistry of the stable carbon isotopes. Geochimica et Cosmochimica Acta 3, 53–92. https://doi.org/10.1016/0016-7037(53)90001-5

Cramer, B.S., Toggweiler, J.R., Wright, J.D., Katz, M.E., Miller, K.G., 2009. Ocean overturning since the Late Cretaceous: Inferences from a new benthic foraminiferal isotope compilation. Paleoceanography 24. https://doi.org/10.1029/2008PA001683

Crémière, A., Pellerin, A., Wing, B.A., Lepland, A., 2020. Multiple sulfur isotopes in methane seep carbonates track unsteady sulfur cycling during anaerobic methane oxidation. Earth and Planetary Science Letters 532, 115994. https://doi.org/10.1016/j.epsl.2019.115994

Crockford, P.W., Kunzmann, M., Bekker, A., Hayles, J., Bao, H., Halverson, G.P., Peng, Y., Bui, T.H., Cox, G.M., Gibson, T.M., Wörndle, S., Rainbird, R., Lepland, A., Swanson-Hysell, N.L., Master, S., Sreenivas, B., Kuznetsov, A., Krupenik, V., Wing, B.A., 2019. Claypool continued: Extending the isotopic record of sedimentary sulfate. Chemical Geology 513, 200–225. https://doi.org/10.1016/j.chemgeo.2019.02.030

Crowe, S.A., Paris, G., Katsev, S., Jones, C., Kim, S.-T., Zerkle, A.L., Nomosatryo, S., Fowle, D.A., Adkins, J.F., Sessions, A.L., Farquhar, J., Canfield, D.E., 2014. Sulfate was a trace constituent of Archean seawater. Science 346, 735–739. https://doi.org/10.1126/science.1258966

Cuif, J.-P., Dauphin, Y., Doucet, J., Salome, M., Susini, J., 2003. XANES mapping of organic sulfate in three scleractinian coral skeletons. Geochimica et Cosmochimica Acta 67, 75–83. https://doi.org/10.1016/S0016-7037(02)01041-4

Cuif, J.P., Dauphin, Y., Farre, B., Nehrke, G., Nouet, J., Salomé, M., 2008. Distribution of sulphated polysaccharides within calcareous biominerals suggests a widely shared two-step crystallization process for the microstructural growth units. Mineralogical Magazine 72, 233–237. https://doi.org/10.1180/minmag.2008.072.1.233

Cusack, M., Dauphin, Y., Cuif, J.-P., Salomé, M., Freer, A., Yin, H., 2008. Micro-XANES mapping of sulphur and its association with magnesium and phosphorus in the shell of the brachiopod, Terebratulina retusa. Chemical Geology 253, 172–179. https://doi.org/10.1016/j.chemgeo.2008.05.007

Cusack, M., Freer, A., 2008. Biomineralization: Elemental and Organic Influence in Carbonate Systems. Chem. Rev. 108, 4433–4454. https://doi.org/10.1021/cr078270o

Dameron, S.N., Leckie, R.M., Clark, K., MacLeod, K.G., Thomas, D.J., Lees, J.A., 2017. Extinction, dissolution, and possible ocean acidification prior to the Cretaceous/Paleogene (K/Pg) boundary in the tropical Pacific. Palaeogeography, Palaeoclimatology, Palaeoecology 485, 433–454. https://doi.org/10.1016/j.palaeo.2017.06.032

Das, A., Chung, C.-H., You, C.-F., Shen, M.-L., 2012. Application of an improved ion exchange technique for the measurement of $\delta^{34}S$ values from microgram quantities of sulfur by MC-ICPMS. Journal of Analytical Atomic Spectrometry 27, 2088–2093.

Dasari, S., Paris, G., Charreau, J., Savarino, J., 2022a. Sulfur-isotope anomalies recorded in Antarctic ice cores as a potential proxy for tracing past ozone layer depletion events. PNAS Nexus 1, pgac170. https://doi.org/10.1093/pnasnexus/pgac170

Dasari, S., Paris, G., Pei, Q., Cong, Z., Widory, D., 2023. Tracing the origin of elevated springtime atmospheric sulfate on the southern Himalayan-Tibetan plateau. Environ. Sci.: Adv. 2, 1110–1118. https://doi.org/10.1039/D3VA00085K

Dasari, S., Paris, G., Saar, B., Pei, Q., Cong, Z., Widory, D., 2022b. Sulfur Isotope Anomalies ($\Delta^{33}S$) in Urban Air Pollution Linked to Mineral-Dust-Associated Sulfate. Environ. Sci. Technol. Lett. 9, 604–610. https://doi.org/10.1021/acs.estlett.2c00312

Dauphin, Y., 2006. Mineralizing matrices in the skeletal axes of two Corallium species (Alcyonacea). Comparative Biochemistry and Physiology Part A: Molecular & Integrative Physiology 145, 54–64. https://doi.org/10.1016/j.cbpa.2006.04.029

Dauphin, Y., Ball, A.D., Castillo-Michel, H., Chevallard, C., Cuif, J.-P., Farre, B., Pouvreau, S., Salomé, M., 2013. In situ distribution and characterization of the organic content of the oyster shell Crassostrea gigas (Mollusca, Bivalvia). Micron 44, 373–383. https://doi.org/10.1016/j.micron.2012.09.002

Dauphin, Y., Cuif, J., Doucet, J., Salomé, M., Susini, J., Williams, C., 2003a. In situ mapping of growth lines in the calcitic prismatic layers of mollusc shells using X-ray absorption near-edge structure (XANES) spectroscopy at the sulphur K-edge. Marine Biology 142, 299–304. https://doi.org/10.1007/s00227-002-0950-2

Dauphin, Y., Cuif, J.-P., Doucet, J., Salomé, M., Susini, J., Terry Willams, C., 2003b. In situ chemical speciation of sulfur in calcitic biominerals and the simple prism concept. Journal of Structural Biology 142, 272–280. https://doi.org/10.1016/S1047-8477(03)00054-6

Dauphin, Y., Cuif, J.-P., Salomé, M., Susini, J., 2005. Speciation and distribution of sulfur in a mollusk shell as revealed by in situ maps using X-ray absorption near-edge structure (XANES) spectroscopy at the S K-edge. American Mineralogist 90, 1748–1758. https://doi.org/10.2138/am.2005.1640

Dauphin, Y., Cuif, J.-P., Williams, C.T., 2008. Soluble organic matrices of aragonitic skeletons of Merulinidae (Cnidaria, Anthozoa). Comparative Biochemistry and Physiology Part B: Biochemistry and Molecular Biology 150, 10–22. https://doi.org/10.1016/j.cbpb.2008.01.002

Dauphin, Y., Luquet, G., Salomé, M., Bellot-Gurlet, L., Cuif, J.-P., 2018. Structure and composition of Unio pictorum shell: arguments for the diversity of the nacroprismatic arrangement in molluscs. Journal of Microscopy 270, 156–169. https://doi.org/10.1111/jmi.12669

Davidson, M.M., Bisher, M.E., Pratt, L.M., Fong, J., Southam, G., Pfiffner Susan M., Reches Z., Onstott Tullis C., 2009. Sulfur Isotope Enrichment during Maintenance Metabolism in the Thermophilic Sulfate-Reducing Bacteriu*m Desulfotomaculum putei*. Applied and Environmental Microbiology 75, 5621–5630. https://doi.org/10.1128/AEM.02948-08

De Goeyse, S., Webb, A.E., Reichart, G.-J., De Nooijer, L.J., 2021. Carbonic anhydrase is involved in calcification by the benthic foraminifer Amphistegina lessonii. Biogeosciences 18, 393–401.

De La Rocha, C.L., DePaolo, D.J., 2000. Isotopic Evidence for Variations in the Marine Calcium Cycle Over the Cenozoic. Science 289, 1176. https://doi.org/10.1126/science.289.5482.1176

de Nooijer, L.J., Langer, G., Nehrke, G., Bijma, J., 2009a. Physiological controls on seawater uptake and calcification in the benthic foraminifer Ammonia tepida. Biogeosciences 6, 2669–2675.

de Nooijer, L.J., Spero, H.J., Erez, J., Bijma, J., Reichart, G.J., 2014. Biomineralization in perforate foraminifera. Earth-Science Reviews 135, 48–58. https://doi.org/10.1016/j.earscirev.2014.03.013

de Nooijer, L.J., Toyofuku, T., Kitazato, H., 2009b. Foraminifera promote calcification by elevating their intracellular pH. Proc Natl Acad Sci USA 106, 15374. https://doi.org/10.1073/pnas.0904306106

de Souza, G.F., Vance, D., Sieber, M., Conway, T.M., Little, S.H., 2022. Re-assessing the influence of particle-hosted sulphide precipitation on the marine cadmium cycle. Geochimica et Cosmochimica Acta 322, 274–296. https://doi.org/10.1016/j.gca.2022.02.009

De Yoreo, J.J., Gilbert, P.U.P.A., Sommerdijk, N.A.J.M., Penn, R.L., Whitelam, S., Joester, D., Zhang, H., Rimer, J.D., Navrotsky, A., Banfield, J.F., Wallace, A.F., Michel, F.M., Meldrum, F.C., Cölfen, H., Dove, P.M., 2015. Crystallization by particle attachment in synthetic, biogenic, and geologic environments. Science 349, aaa6760. https://doi.org/10.1126/science.aaa6760

Dehairs, F., Chesselet, R., Jedwab, J., 1980. Discrete suspended particles of barite and the barium cycle in the open ocean. Earth and Planetary Science Letters 49, 528–550. https://doi.org/10.1016/0012-821X(80)90094-1

Dellinger, M., West, A.J., Paris, G., Adkins, J.F., Pogge von Strandmann, P.A.E., Ullmann, C.V., Eagle, R.A., Freitas, P., Bagard, M.-L., Ries, J.B., Corsetti, F.A., Perez-Huerta, A., Kampf, A.R., 2018. The Li isotope composition of marine biogenic carbonates: Patterns and mechanisms. Geochimica et Cosmochimica Acta 236, 315–335. https://doi.org/10.1016/j.gca.2018.03.014

Deloule, E., Allegre, C.J., Doe, B.R., 1986. Lead and sulfur isotope microstratigraphy in galena crystals from mississippi valley-type deposits. Econ Geol 81, 1307–1321. https://doi.org/10.2113/gsecongeo.81.6.1307

Deng, K., Yang, S., Guo, Y., 2022. A global temperature control of silicate weathering intensity. Nature Communications 13, 1781. https://doi.org/10.1038/s41467-022-29415-0

DePaolo, D.J., 2011. Surface kinetic model for isotopic and trace element fractionation during precipitation of calcite from aqueous solutions. Geochimica et Cosmochimica Acta 75, 1039–1056. https://doi.org/10.1016/j.gca.2010.11.020

D'Hondt, S., 2005. CONSEQUENCES OF THE CRETACEOUS/PALEOGENE MASS EXTINCTION FOR MARINE ECOSYSTEMS 25.

D'Hondt, S., Donaghay, P., Zachos, J.C., Luttenberg, D., Lindinger, M., 1998. Organic Carbon Fluxes and Ecological Recovery from the Cretaceous-Tertiary Mass Extinction. Science 282, 276–279. https://doi.org/10.1126/science.282.5387.276

D'Hondt, S., Keller, G., 1991. Some patterns of planktic foraminiferal assemblage turnover at the Cretaceous-Tertiary boundary. Marine Micropaleontology 17, 77–118. https://doi.org/10.1016/0377-8398(91)90024-Z

Di, P., Li, N., Gong, S., Peckmann, J., Wang, S., Chen, D., Yan, W., 2023. Carbonate-associated sulfate as an archive of sulfur and oxygen stable isotope composition of seawater sulfate: Evidence from reef carbonate rocks of the southern South China Sea. Chemical Geology 121699. https://doi.org/10.1016/j.chemgeo.2023.121699

Dickson, A.G., 1992. The development of the alkalinity concept in marine chemistry. Marine Chemistry 40, 49–63. https://doi.org/10.1016/0304-4203(92)90047-E

Dickson, A.G., 1981. An exact definition of total alkalinity and a procedure for the estimation of alkalinity and total inorganic carbon from titration data. Deep Sea Research Part A. Oceanographic Research Papers 28, 609–623. https://doi.org/10.1016/0198-0149(81)90121-7

Dickson, J.A.D., Coleman, M.L., 1990. Changes in Carbon and Oxygen Isotope Composition during Limestone Diagenesis, in: Carbonate Diagenesis. pp. 259–270. https://doi.org/10.1002/9781444304510.ch21

Dilling, W., Cypionka, H., 1990. Aerobic respiration in sulfate-reducing bacteria*. FEMS Microbiology Letters 71, 123–127. https://doi.org/10.1111/j.1574-6968.1990.tb03809.x

Ding, T., Valkiers, S., Kipphardt, H., De Bièvre, P., Taylor, P.D.P., Gonfiantini, R., Krouse, R., 2001. Calibrated sulfur isotope abundance ratios of three IAEA sulfur isotope reference materials and V-CDT with a reassessment of the atomic weight of sulfur. Geochimica et Cosmochimica Acta 65, 2433–2437. https://doi.org/10.1016/s0016-7037(01)00611-1

Dissard, D., Nehrke, G., Reichart, G.-J., Bijma, J., 2010. Impact of seawater pCO_2 on calcification and Mg/Ca and Sr/Ca ratios in benthic foraminifera calcite: results from culturing experiments with Ammonia tepida. Biogeosciences 7, 81–93.

Drake, J.L., Mass, T., Stolarski, J., Von Euw, S., van de Schootbrugge, B., Falkowski, P.G., 2020. How corals made rocks through the ages. Global Change Biology 26, 31–53. https://doi.org/10.1111/gcb.14912

Dunham, R.J., 1962. Classification of carbonate rocks according to depositional textures.

Dupré, B., Dessert, C., Oliva, P., Goddéris, Y., Viers, J., François, L., Millot, R., Gaillardet, J., 2003. Rivers, chemical weathering and Earth's climate. Comptes rendus-Géoscience 335, 1141–1160.

Dutton, A., Lohmann, K.C., Leckie, R.M., 2005. Insights from the Paleogene tropical Pacific: Foraminiferal stable isotope and elemental results from Site 1209, Shatsky Rise. Paleoceanography 20. https://doi.org/10.1029/2004PA001098

Ebelmen, J.-J., 1855. Recueil des travaux scientifiques. Mallet-Bachelier.

Edwards, C.T., Fike, D.A., Saltzman, M.R., 2019. Testing carbonate-associated sulfate (CAS) extraction methods for sulfur isotope stratigraphy: A case study of a Lower–Middle Ordovician carbonate succession, Shingle Pass, Nevada, USA. Chemical Geology 529, 119297. https://doi.org/10.1016/j.chemgeo.2019.119297

Elliot, D.H., Askin, R.A., Kyte, F.T., Zinsmeister, W.J., 1994. Iridium and dinocysts at the Cretaceous-Tertiary boundary on Seymour Island, Antarctica: implications for the KT event. Geology 22, 675–678.

Emiliani, C., Edwards, G., 1953. Tertiary Ocean Bottom Temperatures. Nature 171, 887–888. https://doi.org/10.1038/171887c0

England, J., Cusack, M., Lee, M.R., 2007. Magnesium and sulphur in the calcite shells of two brachiopods, Terebratulina retusa and Novocrania anomala. Lethaia 40, 2–10. https://doi.org/10.1111/j.1502-3931.2006.00001.x

Erez, J., 2003. The Source of Ions for Biomineralization in Foraminifera and Their Implications for Paleoceanographic Proxies. Reviews in Mineralogy and Geochemistry 54, 115–149. https://doi.org/10.2113/0540115

Erlanger, E., Bufe, A., Paris, G., D'Angeli, I., Pisani, L., Kemeny, P.C., Stammeier, J., Haghipour, N., Hovius, N., in review. Uncorking the Orogenic Prosecco Bottle. Nature Geoscience.

Evans, D., Erez, J., Oron, S., Müller, W., 2015. Mg/Ca-temperature and seawater-test chemistry relationships in the shallow-dwelling large benthic foraminifera Operculina ammonoides. Geochimica et Cosmochimica Acta 148, 325–342. https://doi.org/10.1016/j.gca.2014.09.039

Evans, D., Gray, W.R., Rae, J.W.B., Greenop, R., Webb, P.B., Penkman, K., Kröger, R., Allison, N., 2020. Trace and major element incorporation into amorphous calcium carbonate (ACC) precipitated from seawater. Geochimica et Cosmochimica Acta 290, 293–311. https://doi.org/10.1016/j.gca.2020.08.034

Evans, D., Müller, W., Erez, J., 2018. Assessing foraminifera biomineralisation models through trace element data of cultures under variable seawater chemistry. Geochimica et Cosmochimica Acta 236, 198–217. https://doi.org/10.1016/j.gca.2018.02.048

Evans, D., Wade, B.S., Henehan, M., Erez, J., Müller, W., 2016. Revisiting carbonate chemistry controls on planktic foraminifera Mg/Ca: Implications for sea surface temperature and hydrology shifts over the Paleocene–Eocene Thermal Maximum and Eocene–Oligocene transition. Climate of the Past 12, 819–835.

Falini, G., Albeck, S., Weiner, S., Addadi, L., 1996. Control of Aragonite or Calcite Polymorphism by Mollusk Shell Macromolecules. Science 271, 67–69. https://doi.org/10.1126/science.271.5245.67

Falini, G., Fermani, S., Goffredo, S., 2015. Coral biomineralization: A focus on intra-skeletal organic matrix and calcification. Seminars in Cell & Developmental Biology 46, 17–26. https://doi.org/10.1016/j.semcdb.2015.09.005

Fantle, M.S., 2015. Calcium isotopic evidence for rapid recrystallization of bulk marine carbonates and implications for geochemical proxies. Geochimica et Cosmochimica Acta 148, 378–401. https://doi.org/10.1016/j.gca.2014.10.005

Fantle, M.S., Barnes, B.D., Lau, K.V., 2020. The Role of Diagenesis in Shaping the Geochemistry of the Marine Carbonate Record. Annu. Rev. Earth Planet. Sci. 48, 549–583. https://doi.org/10.1146/annurev-earth-073019-060021

Fantle, M.S., DePaolo, D.J., 2007. Ca isotopes in carbonate sediment and pore fluid from ODP Site 807A: The Ca2+(aq)–calcite equilibrium fractionation factor and calcite recrystallization rates in Pleistocene sediments. Geochimica et Cosmochimica Acta 71, 2524–2546. https://doi.org/10.1016/j.gca.2007.03.006

Fantle, M.S., Higgins, J., 2014. The effects of diagenesis and dolomitization on Ca and Mg isotopes in marine platform carbonates: Implications for the geochemical cycles of Ca and Mg. Geochimica et Cosmochimica Acta 142, 458–481. https://doi.org/10.1016/j.gca.2014.07.025

Fantle, M.S., Ridgwell, A., 2020. Towards an understanding of the Ca isotopic signal related to ocean acidification and alkalinity overshoots in the rock record. Chemical Geology 547, 119672. https://doi.org/10.1016/j.chemgeo.2020.119672

Farquhar, J., Jackson, T.L., Thiemens, M.H., 2000a. A ^{33}S enrichment in ureilite meteorites: evidence for a nebular sulfur component. Geochimica et Cosmochimica Acta 64, 1819–1825. https://doi.org/10.1016/s0016-7037(00)00356-2

Farquhar, J., Johnston, D.T., Wing, B.A., Habicht, K.S., Canfield, D.E., Airieau, S., Thiemens, M.H., 2003. Multiple sulphur isotopic interpretations of biosynthetic pathways: implications for biological signatures in the sulphur isotope record. Geobiology 1, 27–36. https://doi.org/10.1046/j.1472-4669.2003.00007.x

Farquhar, J., Savarino, J., Jackson, T.L., Thiemens, M.H., 2000b. Evidence of atmospheric sulphur in the martian regolith from sulphur isotopes in meteorites. Nature 404, 50–52. https://doi.org/10.1038/35003517

Fehrenbacher, J.S., Russell, A.D., Davis, C.V., Gagnon, A.C., Spero, H.J., Cliff, J.B., Zhu, Z., Martin, P., 2017. Link between light-triggered Mg-banding and chamber formation in the planktic foraminifera Neogloboquadrina dutertrei. Nature Communications 8, 15441. https://doi.org/10.1038/ncomms15441

Fernández-Díaz, L., Fernández-González, Á., Prieto, M., 2010. The role of sulfate groups in controlling CaCO3 polymorphism. Geochimica et Cosmochimica Acta 74, 6064–6076. https://doi.org/10.1016/j.gca.2010.08.010

Fichtner, V., Strauss, H., Immenhauser, A., Buhl, D., Neuser, R.D., Niedermayr, A., 2017. Diagenesis of carbonate associated sulfate. Chemical Geology 463, 61–75. https://doi.org/10.1016/j.chemgeo.2017.05.008

Fichtner, V., Strauss, H., Mavromatis, V., Dietzel, M., Huthwelker, T., Borca, C.N., Guagliardo, P., Kilburn, M.R., Göttlicher, J., Pederson, C.L., Griesshaber, E., Schmahl, W.W., Immenhauser, A., 2018. Incorporation and subsequent diagenetic alteration of sulfur in Arctica islandica. Chemical Geology 482, 72–90. https://doi.org/10.1016/j.chemgeo.2018.01.035

Fike, D.A., Bradley, A.S., Leavitt, W.D., 2016. Geomicrobiology of sulfur. Ehrlich's geomicrobiology 3–8.

Fike, D.A., Bradley, A.S., Rose, C.V., 2015. Rethinking the Ancient Sulfur Cycle. Annu. Rev. Earth Planet. Sci. 43, 593–622. https://doi.org/10.1146/annurev-earth-060313-054802

Fike, D.A., Grotzinger, J.P., 2008. A paired sulfate–pyrite $\delta^{34}S$ approach to understanding the evolution of the Ediacaran–Cambrian sulfur cycle. Geochimica et Cosmochimica Acta 72, 2636–2648. https://doi.org/10.1016/j.gca.2008.03.021

Fitz, R.M., Cypionka, H., 1990. Formation of thiosulfate and trithionate during sulfite reduction by washed cells of Desulfovibrio desulfuricans. Archives of Microbiology 154, 400–406.

Fleet, M.E., 2005. XANES spectroscopy of sulfur in Earth materials. The Canadian Mineralogist 43, 1811–1838. https://doi.org/10.2113/gscanmin.43.6.1811

Folk, R.L., 1959. Practical petrographic classification of limestones. AAPG bulletin 43, 1–38.

Font, E., Adatte, T., Sial, A.N., Drude de Lacerda, L., Keller, G., Punekar, J., 2016. Mercury anomaly, Deccan volcanism, and the end-Cretaceous mass extinction. Geology 44, 171–174. https://doi.org/10.1130/G37451.1

Fox, E., Meyer, E., Panasiak, N., Taylor, A.R., 2018. Calcein Staining as a Tool to Investigate Coccolithophore Calcification. Frontiers in Marine Science 5.

François, L.M., Walker, J.C.G., 1992. Modelling the Phanerozoic carbon cycle and climate; constraints from the 87 Sr/86 Sr isotopic ratio of seawater. American Journal of Science 292, 81.

Friedrich, O., Norris, R.D., Erbacher, J., 2012. Evolution of middle to Late Cretaceous oceans—A 55 m.y. record of Earth's temperature and carbon cycle. Geology 40, 107–110. https://doi.org/10.1130/G32701.1

Froelich, P.N., Klinkhammer, G.P., Bender, M.L., Luedtke, N.A., Heath, G.R., Cullen, D., Dauphin, P., Hammond, D., Hartman, B., Maynard, V., 1979. Early oxidation of organic matter in pelagic sediments of the eastern equatorial Atlantic: suboxic diagenesis. Geochimica et Cosmochimica Acta 43, 1075–1090. https://doi.org/10.1016/0016-7037(79)90095-4

Gagnon, A.C., Adkins, J.F., Erez, J., 2012. Seawater transport during coral biomineralization. Earth and Planetary Science Letters 329–330, 150–161. https://doi.org/10.1016/j.epsl.2012.03.005

Gagnon, A.C., Adkins, J.F., Fernandez, D.P., Robinson, L.F., 2007. Sr/Ca and Mg/Ca vital effects correlated with skeletal architecture in a scleractinian deep-sea coral and the role of Rayleigh fractionation. Earth and Planetary Science Letters 261, 280–295. https://doi.org/10.1016/j.epsl.2007.07.013

Gaillardet, J., Calmels, D., Romero-Mujalli, G., Zakharova, E., Hartmann, J., 2019. Global climate control on carbonate weathering intensity. Chemical Geology 527, 118762. https://doi.org/10.1016/j.chemgeo.2018.05.009

Gaillardet, J., Dupré, B., Louvat, P., Allègre, C.J., 1999. Global silicate weathering and CO2 consumption rates deduced from the chemistry of large rivers. Chemical Geology 159, 3–30. https://doi.org/10.1016/S0009-2541(99)00031-5

Gaillardet, J., Galy, A., 2008. Himalaya--Carbon Sink or Source? Science 320, 1727.

Gallagher, K.L., Kading, T.J., Braissant, O., Dupraz, C., Visscher, P.T., 2012. Inside the alkalinity engine: the role of electron donors in the organomineralization potential of sulfate-reducing bacteria. Geobiology 10, 518–530.

Galy, A., France-Lanord, C., 1999. Weathering processes in the Ganges–Brahmaputra basin and the riverine alkalinity budget. Chemical Geology 159, 31–60. https://doi.org/10.1016/S0009-2541(99)00033-9

Galy, V., France-Lanord, C., Beyssac, O., Faure, P., Kudrass, H., Palhol, F., 2007. Efficient organic carbon burial in the Bengal fan sustained by the Himalayan erosional system. Nature 450, 407–410.

Gauci, V., Matthews, E., Dise, N., Walter, B., Koch, D., Granberg, G., Vile, M., 2004. Sulfur pollution suppression of the wetland methane source in the 20th and 21st centuries. Proceedings of the National Academy of Sciences 101, 12583–12587. https://doi.org/10.1073/pnas.0404412101

Geng, L., Savarino, J., Caillon, N., Gautier, E., Farquhar, J., Dottin III, J.W., Magalhães, N., Hattori, S., Ishino, S., Yoshida, N., Albarède, F., Albalat, E., Cartigny, P., Ono, S., Thiemens, M.H., 2019. Intercomparison measurements of two 33S-enriched sulfur isotope standards. J. Anal. At. Spectrom. 34, 1263–1271. https://doi.org/10.1039/C8JA00451J

Gilbert, P.U.P.A., Bergmann, K.D., Boekelheide, N., Tambutté, S., Mass, T., Marin, F., Adkins, J.F., Erez, J., Gilbert, B., Knutson, V., Cantine, M., Hernández, J.O., Knoll, A.H., 2022. Biomineralization: Integrating mechanism and evolutionary history. Science Advances 8, eabl9653. https://doi.org/10.1126/sciadv.abl9653

Giri, S.J., Swart, P.K., 2019. The influence of seawater chemistry on carbonate-associated sulfate derived from coral skeletons. Palaeogeography, Palaeoclimatology, Palaeoecology 521, 72–81. https://doi.org/10.1016/j.palaeo.2019.02.011

Gislason, S.R., Arnorsson, S., Armannsson, H., 1996. Chemical weathering of basalt in Southwest Iceland; effects of runoff, age of rocks and vegetative/glacial cover. American Journal of Science 296, 837.

Giuffre, A.J., Gagnon, A.C., De Yoreo, J.J., Dove, P.M., 2015. Isotopic tracer evidence for the amorphous calcium carbonate to calcite transformation by dissolution–reprecipitation. Geochimica et Cosmochimica Acta 165, 407–417. https://doi.org/10.1016/j.gca.2015.06.002

Goddéris, Y., Donnadieu, Y., Tombozafy, M., Dessert, C., 2008. Shield effect on continental weathering: Implication for climatic evolution of the Earth at the geological timescale. Geoderma 145, 439–448.

Goetschl, K.E., Purgstaller, B., Dietzel, M., Mavromatis, V., 2019. Effect of sulfate on magnesium incorporation in low-magnesium calcite. Geochimica et Cosmochimica Acta 265, 505–519. https://doi.org/10.1016/j.gca.2019.07.024

Goldberg, E.D., Somayajulu, B.L.K., Galloway, J., Kaplan, I.R., Faure, G., 1969. Differences between barites of marine and continental origins. Geochimica et Cosmochimica Acta 33, 287–289. https://doi.org/10.1016/0016-7037(69)90145-8

Gomes, M.L., Hurtgen, M.T., 2015. Sulfur isotope fractionation in modern euxinic systems: Implications for paleoenvironmental reconstructions of paired sulfate–sulfide isotope records. Geochimica et Cosmochimica Acta 157, 39–55. https://doi.org/10.1016/j.gca.2015.02.031

Gomes, M.L., Hurtgen, M.T., Sageman, B.B., 2016. Biogeochemical sulfur cycling during Cretaceous oceanic anoxic events: A comparison of OAE1a and OAE2. Paleoceanography 31, 233–251. https://doi.org/10.1002/2015PA002869

Gonfiantini, R., Stichler, W., Rozanski, K., 1995. Standards and intercomparison materials distributed by the International Atomic Energy Agency for stable isotope measurements (No. 1011–4289). International Atomic Energy Agency (IAEA).

Gothmann, A.M., Gagnon, A.C., 2021. The primary controls on U/Ca and minor element proxies in a cold-water coral cultured under decoupled carbonate chemistry conditions. Geochimica et Cosmochimica Acta 315, 38–60. https://doi.org/10.1016/j.gca.2021.09.020

Gout, E., Rébeillé, F., Douce, R., Bligny, R., 2014. Interplay of Mg2+, ADP, and ATP in the cytosol and mitochondria: Unravelling the role of Mg2+ in cell respiration. Proceedings of the National Academy of Sciences 111, E4560–E4567. https://doi.org/10.1073/pnas.1406251111

Gregg, J.M., Bish, D.L., Kaczmarek, S.E., Machel, H.G., 2015. Mineralogy, nucleation and growth of dolomite in the laboratory and sedimentary environment: a review. Sedimentology 62, 1749–1769.

Griffith, E.M., Fantle, M.S., Eisenhauer, A., Paytan, A., Bullen, T.D., 2015. Effects of ocean acidification on the marine calcium isotope record at the Paleocene–Eocene Thermal Maximum. Earth and Planetary Science Letters 419, 81–92. https://doi.org/10.1016/j.epsl.2015.03.010

Griffith, E.M., Paytan, A., 2012. Barite in the ocean – occurrence, geochemistry and palaeoceanographic applications. Sedimentology 59, 1817–1835. https://doi.org/10.1111/j.1365-3091.2012.01327.x

Griffith, E.M., Paytan, A., Kozdon, R., Eisenhauer, A., Ravelo, A.C., 2008. Influences on the fractionation of calcium isotopes in planktonic foraminifera. Earth and Planetary Science Letters 268, 124–136. https://doi.org/10.1016/j.epsl.2008.01.006

Gross, M.G., 1964. Variations in the O18/O16 and C13/C12 Ratios of Diagenetically Altered Limestones in the Bermuda Islands. The Journal of Geology 72, 170–194. https://doi.org/10.1086/626975

Guibourdenche, L., Cartigny, P., Dela Pierre, F., Natalicchio, M., Aloisi, G., 2022. Cryptic sulfur cycling during the formation of giant gypsum deposits. Earth and Planetary Science Letters 593, 117676. https://doi.org/10.1016/j.epsl.2022.117676

Guinoiseau, D., Louvat, P., Paris, G., Chen, J.-B., Chetelat, B., Rocher, V., Guérin, S., Gaillardet, J., 2018. Are boron isotopes a reliable tracer of anthropogenic inputs to rivers over time? Science of The Total Environment 626, 1057–1068. https://doi.org/10.1016/j.scitotenv.2018.01.159

Gunnarsson-Robin, J., Stefánsson, A., Ono, S., Torssander, P., 2017. Sulfur isotopes in Icelandic thermal fluids. Journal of Volcanology and Geothermal Research. https://doi.org/10.1016/j.jvolgeores.2017.01.021

Gunter, T.E., Yule, D.I., Gunter, K.K., Eliseev, R.A., Salter, J.D., 2004. Calcium and mitochondria. FEBS Letters 567, 96–102. https://doi.org/10.1016/j.febslet.2004.03.071

Guo, W., Cecchetti, A.R., Wen, Y., Zhou, Q., Sedlak, D.L., 2020. Sulfur cycle in a wetland microcosm: extended 34S-stable isotope analysis and mass balance. Environmental science & technology 54, 5498–5508.

Guo, Y., Deng, W., Liu, X., Kong, K., Yan, W., Wei, G., 2021. Clumped isotope geochemistry of island carbonates in the South China Sea: Implications for early diagenesis and dolomitization. Marine Geology 437, 106513. https://doi.org/10.1016/j.margeo.2021.106513

Gussone, N., Böhm, F., Eisenhauer, A., Dietzel, M., Heuser, A., Teichert, B.M.A., Reitner, J., Wörheide, G., Dullo, W.-C., 2005. Calcium isotope fractionation in calcite and aragonite. Geochimica et Cosmochimica Acta 69, 4485–4494. https://doi.org/10.1016/j.gca.2005.06.003

Gussone, N., Eisenhauer, A., Heuser, A., Dietzel, M., Bock, B., Böhm, F., Spero, H.J., Lea, D.W., Bijma, J., Nägler, T.F., 2003. Model for kinetic effects on calcium isotope fractionation (δ44Ca) in inorganic aragonite and cultured planktonic foraminifera. Geochimica et Cosmochimica Acta 67, 1375–1382. https://doi.org/10.1016/S0016-7037(02)01296-6

Gussone, N., Hönisch, B., Heuser, A., Eisenhauer, A., Spindler, M., Hemleben, C., 2009. A critical evaluation of calcium isotope ratios in tests of planktonic foraminifers. Geochimica et Cosmochimica Acta 73, 7241–7255. https://doi.org/10.1016/j.gca.2009.08.035

Gussone, N., Langer, G., Thoms, S., Nehrke, G., Eisenhauer, A., Riebesell, U., Wefer, G., 2006a. Cellular calcium pathways and isotope fractionation in Emiliania huxleyi. Geology 34, 625–628. https://doi.org/10.1130/G22733.1

Gussone, N., Langer, G., Thoms, S., Nehrke, G., Eisenhauer, A., Riebesell, U., Wefer, G., 2006b. Cellular calcium pathways and isotope fractionation in Emiliania huxleyi. Geology 34, 625–628. https://doi.org/10.1130/G22733.1

Gutowska, M.S., Mitchell, C.A., 1945. Carbonic Anhydrase in the Calcification of the Egg Shell*. Poultry Science 24, 159–167. https://doi.org/10.3382/ps.0240159

Habicht, K.S., Gade, M., Thamdrup, B., Berg, P., Canfield, D.E., 2002. Calibration of Sulfate Levels in the Archean Ocean. Science 298, 2372–2374. https://doi.org/10.1126/science.1078265

Halevy, I., Peters, S.E., Fischer, W.W., 2012. Sulfate Burial Constraints on the Phanerozoic Sulfur Cycle. Science 337, 331–334. https://doi.org/10.1126/science.1220224

Han, N., Blue, C.R., De Yoreo, J.J., Dove, P.M., 2013. The Effect of Carboxylates on the Mg Content of Calcites that Transform from ACC. Procedia Earth and Planetary Science 7, 223–227. https://doi.org/10.1016/j.proeps.2013.03.224

Hardie, Lawrence A., 1984. Evaporites; marine or non-marine? Am J Sci 284, 193. https://doi.org/10.2475/ajs.284.3.193

Harrison, A., Thode, H., 1958. Mechanism of the bacterial reduction of sulphate from isotope fractionation studies. Transactions of the Faraday Society 54, 84–92.

Hebting, Y., Schaeffer, P., Behrens, A., Adam, P., Schmitt, G., Schneckenburger, P., Bernasconi, S.M., Albrecht, P., 2006. Biomarker Evidence for a Major Preservation Pathway of Sedimentary Organic Carbon. Science 312, 1627–1631. https://doi.org/10.1126/science.1126372

Helman, Y., Natale, F., Sherrell, R.M., LaVigne, M., Starovoytov, V., Gorbunov, M.Y., Falkowski, P.G., 2008. Extracellular matrix production and calcium carbonate precipitation by coral cells in vitro. Proceedings of the National Academy of Sciences 105, 54–58. https://doi.org/10.1073/pnas.0710604105

Hemleben, C., Erson, O., Berthold, W., Spindler, M., 1986. Calcification and chamber formation in Foraminifera-a brief overview. Biomineralization in lower plants and animals (BSC Leadbeater, R Riding, eds) Clarendon Press, Oxford 237–249.

Henehan, M.J., Ridgwell, A., Thomas, E., Zhang, S., Alegret, L., Schmidt, D.N., Rae, J.W.B., Witts, J.D., Landman, N.H., Greene, S.E., Huber, B.T., Super, J.R., Planavsky, N.J., Hull, P.M., 2019. Rapid ocean acidification and protracted Earth system recovery followed the end-Cretaceous Chicxulub impact. Proc Natl Acad Sci USA 116, 22500. https://doi.org/10.1073/pnas.1905989116

Higgins, J.A., Blättler, C.L., Lundstrom, E.A., Santiago-Ramos, D.P., Akhtar, A.A., Crüger Ahm, A.-S., Bialik, O., Holmden, C., Bradbury, H., Murray, S.T., Swart, P.K., 2018. Mineralogy, early marine diagenesis, and the chemistry of shallow-water carbonate sediments. Geochimica et Cosmochimica Acta 220, 512–534. https://doi.org/10.1016/j.gca.2017.09.046

Higgins, J.A., Schrag, D.P., 2012. Records of Neogene seawater chemistry and diagenesis in deep-sea carbonate sediments and pore fluids. Earth and Planetary Science Letters 357–358, 386–396. https://doi.org/10.1016/j.epsl.2012.08.030

Hildebrand, A.R., Penfield, G.T., Kring, D.A., Pilkington, M., Camargo Z., A., Jacobsen, S.B., Boynton, W.V., 1991. Chicxulub Crater: A possible Cretaceous/Tertiary boundary impact crater on the Yucatán Peninsula, Mexico. Geology 19, 867–871. https://doi.org/10.1130/0091-7613(1991)019<0867:CCAPCT>2.3.CO;2

Hill, C.A., 1990. Sulfuric acid speleogenesis of Carlsbad Cavern and its relationship to hydrocarbons, Delaware Basin, New Mexico and Texas. AAPG bulletin 74, 1685–1694.

Hippler, D., Eisenhauer, A., Nägler, T.F., 2006. Tropical Atlantic SST history inferred from Ca isotope thermometry over the last 140ka. Geochimica et Cosmochimica Acta 70, 90–100. https://doi.org/10.1016/j.gca.2005.07.022

Hippler, D., Kozdon, R., Darling, K.F., Eisenhauer, A., Nägler, T.F., 2009. Calcium isotopic composition of high-latitude proxy carrier Neogloboquadrina pachyderma (sin.). Biogeosciences 6, 1–14. https://doi.org/10.5194/bg-6-1-2009

Hippler, D., Schmitt, A.-D., Gussone, N., Heuser, A., Stille, P., Eisenhauer, A., Nägler, T.F., 2003. Calcium Isotopic Composition of Various Reference Materials and Seawater. Geostandards Newsletter 27, 13–19. https://doi.org/10.1111/j.1751-908X.2003.tb00709.x

Hoffmeister, J., Multer, H., 1968. Geology and origin of the Florida Keys. Geological Society of America Bulletin 79, 1487–1502.

Holland, H.D., Zimmermann, H., 2000. The dolomite problem Revisited1. International Geology Review 42, 481–490.

Holser, W.T., 1977. Catastrophic chemical events in the history of the ocean. Nature 267, 403–408.

Holser, W.T., Kaplan, I.R., 1966. Isotope geochemistry of sedimentary sulfates. Chemical Geology 1, 93–135. https://doi.org/10.1016/0009-2541(66)90011-8

Hongfu, Y., Kexin, Z., Jinnan, T., Zunyi, Y., Shunbao, W., 2001. The Global Stratotype Section and Point (GSSP) of the Permian-Triassic Boundary. International Union of Geological Sciences 24, 102–114. https://doi.org/10.18814/epiiugs/2001/v24i2/004

Horita, J., Zimmermann, H., Holland, H.D., 2002. Chemical evolution of seawater during the Phanerozoic: Implications from the record of marine evaporites. Geochimica et Cosmochimica Acta 66, 3733–3756.

Howarth, R.W., Teal, J.M., 1979. Sulfate reduction in a New England salt marsh 1. Limnology and Oceanography 24, 999–1013.

Hudson, J., 1977. Stable isotopes and limestone lithification. Journal of the Geological Society 133, 637–660.

Hull, P.M., Bornemann, A., Penman, D.E., Henehan, M.J., Norris, R.D., Wilson, P.A., Blum, P., Alegret, L., Batenburg, S.J., Bown, P.R., Bralower, T.J., Cournede, C., Deutsch, A., Donner, B., Friedrich, O., Jehle, S., Kim, H., Kroon, D., Lippert, P.C., Loroch, D., Moebius, I., Moriya, K., Peppe, D.J., Ravizza, G.E., Röhl, U., Schueth, J.D., Sepúlveda, J., Sexton, P.F., Sibert, E.C., Śliwińska, K.K., Summons, R.E., Thomas, E., Westerhold, T., Whiteside, J.H., Yamaguchi, T., Zachos, J.C., 2020. On impact and volcanism across the Cretaceous-Paleogene boundary. Science 367, 266. https://doi.org/10.1126/science.aay5055

Hull, P.M., Norris, R.D., 2011. Diverse patterns of ocean export productivity change across the Cretaceous-Paleogene boundary: New insights from biogenic barium: CRETACEOUS-PALEOGENE EXPORT PRODUCTIVITY. Paleoceanography 26, n/a-n/a. https://doi.org/10.1029/2010PA002082

Hulston, J.R., Thode, H.G., 1965. Variations in the S33, S34, and S36 Contents of Meteorites and Their Relation to Chemical and Nuclear Effects. Journal of Geophysical Research 70, 3475–3484. https://doi.org/10.1029/JZ070i014p03475

IAEA, 2020. Reference sheet - reference materials for [delta]34S-isotope values IAEA-S-1 (NIST-RM8554), IAEA-S-2 (NIST-RM8555), IAEA-S-3 (NIST-RM8529).

Igoumenou, A., Ebmeier, K., Roberts, N., Fazel, S., 2014. Geographic trends of scientific output and citation practices in psychiatry. BMC Psychiatry 14, 332. https://doi.org/10.1186/s12888-014-0332-6

Jacob, D.E., Soldati, A.L., Wirth, R., Huth, J., Wehrmeister, U., Hofmeister, W., 2008. Nanostructure, composition and mechanisms of bivalve shell growth. Geochimica et Cosmochimica Acta 72, 5401–5415. https://doi.org/10.1016/j.gca.2008.08.019

Jacob, D.E., Wirth, R., Agbaje, O.B.A., Branson, O., Eggins, S.M., 2017. Planktic foraminifera form their shells via metastable carbonate phases. Nature Communications 8, 1265. https://doi.org/10.1038/s41467-017-00955-0

Jagoutz, O., Royden, L., Holt, A.F., Becker, T.W., 2015. Anomalously fast convergence of India and Eurasia caused by double subduction. Nature Geoscience 8, 475–478. https://doi.org/10.1038/ngeo2418

John, S.G., Adkins, J.F., 2010. Analysis of dissolved iron isotopes in seawater. Marine Chemistry 119, 65–76. https://doi.org/10.1016/j.marchem.2010.01.001

Johnson, D.L., Grossman, E.L., Webb, S.M., Adkins, J.F., 2020. Brachiopod δ34SCAS microanalyses indicate a dynamic, climate-influenced Permo-Carboniferous sulfur cycle. Earth and Planetary Science Letters 546, 116428. https://doi.org/10.1016/j.epsl.2020.116428

Johnson, D.L., Present, T.M., Li, M., Shen, Y., Adkins, J.F., 2021. Carbonate associated sulfate (CAS) δ34S heterogeneity across the End-Permian Mass Extinction in South China. Earth and Planetary Science Letters 574, 117172. https://doi.org/10.1016/j.epsl.2021.117172

Johnston, D., Farquhar, J., Habicht, K.S., Canfield, D.E., 2008. Sulphur isotopes and the search for life: strategies for identifying sulphur metabolisms in the rock record and beyond. Geobiology 6, 425–435. https://doi.org/doi.org/10.1111/j.1472-4669.2008.00171.x

Johnston, D.T., 2011. Multiple sulfur isotopes and the evolution of Earth's surface sulfur cycle. Earth-Science Reviews 106, 161–183. https://doi.org/10.1016/j.earscirev.2011.02.003

Johnston, D.T., Farquhar, J., Canfield, D.E., 2007. Sulfur isotope insights into microbial sulfate reduction: When microbes meet models. Geochimica et cosmochimica acta 71, 3929–3947. https://doi.org/10.1016/j.gca.2007.05.008

Johnston, D.T., Farquhar, J., Wing, B.A., Kaufman, A.J., Canfield, D.E., Habicht, K.S., 2005. Multiple sulfur isotope fractionations in biological systems: A case study with sulfate reducers and sulfur disproportionators. American Journal of Science 305, 645–660. https://doi.org/10.2475/ajs.305.6-8.645

Johnston, D.T., Gill, B.C., Masterson, A., Beirne, E., Casciotti, K.L., Knapp, A.N., Berelson, W., 2014. Placing an upper limit on cryptic marine sulphur cycling. Nature 513, 530–533. https://doi.org/10.1038/nature13698

Jones, D.S., Fike, D.A., 2013. Dynamic sulfur and carbon cycling through the end-Ordovician extinction revealed by paired sulfate–pyrite $\delta^{34}S$. Earth and Planetary Science Letters 363, 144–155. https://doi.org/10.1016/j.epsl.2012.12.015

Jørgensen, B.B., 1979. A theoretical model of the stable sulfur isotope distribution in marine sediments. Geochimica et Cosmochimica Acta 43, 363–374. https://doi.org/10.1016/0016-7037(79)90201-1

Jørgensen, B.B., 1977. Bacterial sulfate reduction within reduced microniches of oxidized marine sediments. Marine Biology 41, 7–17. https://doi.org/10.1007/BF00390576

Jørgensen, B.B., Kasten, S., 2006. Sulfur Cycling and Methane Oxidation, in: Schulz, H.D., Zabel, M. (Eds.), Marine Geochemistry. Springer Berlin Heidelberg, Berlin, Heidelberg, pp. 271–309. https://doi.org/10.1007/3-540-32144-6_8

Jouini, A., 2023. S et Ca à la limite K-Pg. Université de Lorraine.

Jouini, A., Paris, G., Caro, G., Bartolini, A., Gardin, S., 2023. Constraining oceanic carbonate chemistry evolution during the Cretaceous-Paleogene transition: Combined benthic and planktonic calcium isotope records from the equatorial Pacific Ocean. Earth and Planetary Science Letters 619, 118305. https://doi.org/10.1016/j.epsl.2023.118305

Jurikova, H., Liebetrau, V., Gutjahr, M., Rollion-Bard, C., Hu, M.Y., Krause, S., Henkel, D., Hiebenthal, C., Schmidt, M., Laudien, J., Eisenhauer, A., 2019. Boron isotope systematics of cultured brachiopods: Response to acidification, vital effects and implications for palaeo-pH reconstruction. Geochimica et Cosmochimica Acta 248, 370–386. https://doi.org/10.1016/j.gca.2019.01.015

Kah, L.C., Lyons, T.W., Frank, T.D., 2004. Low marine sulphate and protracted oxygenation of the Proterozoic biosphere. Nature 431, 834–838. http://www.nature.com/nature/journal/v431/n7010/suppinfo/nature02974_S1.html

Kaiho, K., Kajiwara, Y., Chen, Z.-Q., Gorjan, P., 2006. A sulfur isotope event at the end of the Permian. Chemical Geology 235, 33–47. https://doi.org/10.1016/j.chemgeo.2006.06.001

Kaiho, K., Kajiwara, Y., Nakano, T., Miura, Y., Kawahata, H., Tazaki, K., Ueshima, M., Chen, Z., Shi, G.R., 2001. End-Permian catastrophe by a bolide impact: evidence of a gigantic release of sulfur from the mantle. Geology 29, 815–818.

Kaiho, K., Kajiwara, Y., Ueshima, M., Takeda, N., Kawahata, H., Arinobu, T., Ishiwatari, R., Hirai, A., Lamolda, M., 1999. Oceanic primary productivity and dissolved oxygen levels at the Cretaceous/Tertiary Boundary: Their decrease, subsequent warming, and recovery. Paleoceanography 14, 511–524. https://doi.org/10.1029/1999PA900022

Kajiwara, Y., Yamakita, S., Ishida, K., Ishiga, H., Imai, A., 1994. Development of a largely anoxic stratified ocean and its temporary massive mixing at the Permian/Triassic boundary supported by the sulfur isotopic record. Palaeogeography, Palaeoclimatology, Palaeoecology 111, 367–379. https://doi.org/10.1016/0031-0182(94)90072-8

Kampschulte, A., Bruckschen, P., Strauss, H., 2001. The sulphur isotopic composition of trace sulphates in Carboniferous brachiopods: implications for coeval seawater, correlation with other geochemical cycles and isotope stratigraphy. Chemical Geology 175, 149–173. https://doi.org/10.1016/S0009-2541(00)00367-3

Kampschulte, A., Strauss, H., 2004. The sulfur isotopic evolution of Phanerozoic seawater based on the analysis of structurally substituted sulfate in carbonates. Chemical Geology 204, 255–286. https://doi.org/10.1016/j.chemgeo.2003.11.013

Kaneoka, I., 1980. 40Ar/39Ar dating on volcanic rocks of the Deccan Traps, India. Earth and Planetary Science Letters 46, 233–243. https://doi.org/10.1016/0012-821X(80)90009-6

Kaplan, I.R., Emery, K.O., Rittenbebg, S.C., 1963. The distribution and isotopic abundance of sulphur in recent marine sediments off southern California. Geochimica et Cosmochimica Acta 27, 297–331. https://doi.org/10.1016/0016-7037(63)90074-7

Kaplan, I.R., Rittenberg, S.C., 1964. Microbiological Fractionation of Sulphur Isotopes. Journal of General Microbiology 34, 195–212. https://doi.org/10.1099/00221287-34-2-195

Keller, G., Adatte, T., Bhowmick, P.K., Upadhyay, H., Dave, A., Reddy, A.N., Jaiprakash, B.C., 2012. Nature and timing of extinctions in Cretaceous-Tertiary planktic foraminifera preserved in Deccan intertrappean sediments of the Krishna–Godavari Basin, India. Earth and Planetary Science Letters 341–344, 211–221. https://doi.org/10.1016/j.epsl.2012.06.021

Keller, G., Adatte, T., Pardo, A., Bajpai, S., Khosla, A., Samant, B., 2010. Cretaceous Extinctions: Evidence Overlooked. Science 328, 974. https://doi.org/10.1126/science.328.5981.974-a

Keller, G., Barrera, E., Schmitz, B., Mattson, E., 1993. Gradual mass extinction, species survivorship, and long-term environmental changes across the Cretaceous-Tertiary boundary in high latitudes. Geological Society of America Bulletin 105, 979–997. https://doi.org/10.1130/0016-7606(1993)105<0979:GMESSA>2.3.CO;2

Keller, G., Mateo, P., Monkenbusch, J., Thibault, N., Punekar, J., Spangenberg, J.E., Abramovich, S., Ashckenazi-Polivoda, S., Schoene, B., Eddy, M.P., Samperton, K.M., Khadri, S.F.R., Adatte, T., 2020. Mercury linked to Deccan Traps volcanism, climate change and the end-Cretaceous mass extinction. Global and Planetary Change 194, 103312. https://doi.org/10.1016/j.gloplacha.2020.103312

Keller, G., Mateo, P., Punekar, J., Khozyem, H., Gertsch, B., Spangenberg, J., Bitchong, A.M., Adatte, T., 2018. Environmental changes during the Cretaceous-Paleogene mass extinction and Paleocene-Eocene Thermal Maximum: Implications for the Anthropocene. Gondwana Research 56, 69–89. https://doi.org/10.1016/j.gr.2017.12.002

Kemeny, P.C., Lopez, G.I., Dalleska, N.F., Torres, M., Burke, A., Bhatt, M.P., West, A.J., Hartmann, J., Adkins, J.F., 2021. Sulfate sulfur isotopes and major ion chemistry reveal that pyrite oxidation counteracts CO2 drawdown from silicate weathering in the Langtang-Trisuli-Narayani River system, Nepal Himalaya. Geochimica et Cosmochimica Acta 294, 43–69. https://doi.org/10.1016/j.gca.2020.11.009

Kemeny, P.C., Torres, M.A., 2021. Presentation and applications of mixing elements and dissolved isotopes in rivers (MEANDIR), a customizable MATLAB model for Monte Carlo inversion of dissolved river chemistry. Am J Sci 321, 579. https://doi.org/10.2475/05.2021.03

Kemeny, Preston C., Torres, M.A., Lamb, M.P., Webb, S.M., Dalleska, N., Cole, T., Hou, Y., Marske, J., Adkins, J.F., Fischer, W.W., 2021. Organic sulfur fluxes and geomorphic control of sulfur isotope ratios in rivers. Earth and Planetary Science Letters 562, 116838. https://doi.org/10.1016/j.epsl.2021.116838

Khalifa, G.M., Kirchenbuechler, D., Koifman, N., Kleinerman, O., Talmon, Y., Elbaum, M., Addadi, L., Weiner, S., Erez, J., 2016. Biomineralization pathways in a foraminifer revealed using a novel correlative cryo-fluorescence–SEM–EDS technique. Journal of Structural Biology 196, 155–163. https://doi.org/10.1016/j.jsb.2016.01.015

Killingsworth, B.A., Bao, H., Kohl, I.E., 2018. Assessing pyrite-derived sulfate in the Mississippi River with four years of sulfur and triple-oxygen isotope data. Environmental science & technology 52, 6126–6136.

Killingsworth, B.A., Cartigny, P., Hayles, J.A., Thomazo, C., Sansjofre, P., Pasquier, V., Lalonde, S.V., Philippot, P., 2022. Towards a holistic sulfate-water-O2 triple oxygen isotope systematics. Chemical Geology 588, 120678.

Kitano, Y., Okumura, M., Idogaki, M., 1975. Incorporation of sodium, chloride and sulfate with calcium carbonate. Geochem. J 9, 75–84.

Kısakürek, B., Eisenhauer, A., Böhm, F., Hathorne, E.C., Erez, J., 2011. Controls on calcium isotope fractionation in cultured planktic foraminifera, Globigerinoides ruber and Globigerinella siphonifera. Geochimica et Cosmochimica Acta 75, 427–443. https://doi.org/10.1016/j.gca.2010.10.015

Klaas, C., Archer, D.E., 2002. Association of sinking organic matter with various types of mineral ballast in the deep sea: Implications for the rain ratio. Global Biogeochem. Cycles 16, 1116.

Knittel, K., Boetius, A., 2009. Anaerobic Oxidation of Methane: Progress with an Unknown Process. Annu. Rev. Microbiol. 63, 311–334. https://doi.org/10.1146/annurev.micro.61.080706.093130

Kontrec, J., Kralj, D., Brečević, L., Falini, G., Fermani, S., Noethig-Laslo, V., Mirosavljević, K., 2004. Incorporation of Inorganic Anions in Calcite. Eur. J. Inorg. Chem. 2004, 4579–4585. https://doi.org/10.1002/ejic.200400268

Kozdon, R., Kelly, D.C., Kitajima, K., Strickland, A., Fournelle, J.H., Valley, J.W., 2013. In situ $\delta^{18}O$ and Mg/Ca analyses of diagenetic and planktic foraminiferal calcite preserved in a deep-sea record of the Paleocene-Eocene thermal maximum. Paleoceanography 28, 517–528. https://doi.org/10.1002/palo.20048

Krouse, H., Coplen, T., 1997. Reporting of relative sulfur isotope-ratio data. Pure and Applied Chemistry 69, 293–295.

Kump, L.R., 1991. Interpreting carbon-isotope excursions; Strangelove oceans. Geology 19, 299–302.

Kump, L.R., Brantley, S.L., Arthur, M.A., 2000. Chemical weathering, atmospheric CO2, and climate. Annual Review of Earth and Planetary Sciences 28, 611–667.

Kurtz, A.C., Kump, L.R., Arthur, M.A., Zachos, J.C., Paytan, A., 2003. Early Cenozoic decoupling of the global carbon and sulfur cycles. Paleoceanography 18, 1090. https://doi.org/10.1029/2003pa000908

Lamers, L.P.M., Falla, S.-J., Samborska, E.M., Dulken, I.A.R. van, Hengstum, G. van, Roelofs, J.G.M., 2002. Factors controlling the extent of eutrophication and toxicity in sulfate-polluted freshwater wetlands. Limnology and Oceanography 47, 585–593. https://doi.org/10.4319/lo.2002.47.2.0585

Land, L.S., 1967. Diagenesis of skeletal carbonates. Journal of Sedimentary Research 37, 914–930.

Landergren, S., 1954. On the relative abundance of the stable carbon isotopes in marine sediments. Deep Sea Research (1953) 1, 98–120. https://doi.org/10.1016/0146-6313(54)90021-0

Langer, G., Gussone, N., Nehrke, G., Riebesell, U., Eisenhauer, A., Kuhnert, H., Rost, B., Trimborn, S., Thoms, S., 2006. Coccolith strontium to calcium ratios in Emiliania huxleyi: The dependence on seawater strontium and calcium concentrations. Limnology and Oceanography 51, 310–320. https://doi.org/10.4319/lo.2006.51.1.0310

Langer, G., Nehrke, G., Thoms, S., Stoll, H., 2009. Barium partitioning in coccoliths of Emiliania huxleyi. Geochimica et Cosmochimica Acta 73, 2899–2906. https://doi.org/10.1016/j.gca.2009.02.025

Langer, M.R., 1992. Biosynthesis of glycosaminoglycans in foraminifera: A review. Marine Micropaleontology 19, 245–255. https://doi.org/10.1016/0377-8398(92)90031-E

Laurent, D., Barré, G., Durlet, C., Cartigny, P., Paris, G., Pironon, J., Gaucher, E., 2023. Unravelling biotic versus abiotic processes in the development of large sulfuric-acid karsts. Geology 51, 262–267.

Laurent, D., Durlet, C., Barré, G., Sorriaux, P., Audra, P., Cartigny, P., Carpentier, C., Paris, G., Collon, P., Rigaudier, T., Pironon, J., Gaucher, E.C., 2021. Epigenic vs. hypogenic speleogenesis governed by H2S/CO2 hydrothermal input and Quaternary icefield dynamics (NE French Pyrenees). Geomorphology 387, 107769. https://doi.org/10.1016/j.geomorph.2021.107769

Le Quéré, C., Harrison, S.P., Colin Prentice, I., Buitenhuis, E.T., Aumont, O., Bopp, L., Claustre, H., Cotrim Da Cunha, L., Geider, R., Giraud, X., Klaas, C., Kohfeld, K.E., Legendre, L., Manizza, M., Platt, T., Rivkin, R.B., Sathyendranath, S., Uitz, J., Watson, A.J., Wolf-Gladrow, D., 2005. Ecosystem dynamics based on plankton functional types for global ocean biogeochemistry models. Global Change Biology 11, 2016–2040. https://doi.org/10.1111/j.1365-2486.2005.1004.x

Leavitt, W.D., Halevy, I., Bradley, A.S., Johnston, D.T., 2013. Influence of sulfate reduction rates on the Phanerozoic sulfur isotope record. Proceedings of the National Academy of Sciences 110, 11244–11249. https://doi.org/10.1073/pnas.1218874110

Lemarchand, D., Gaillardet, J., Lewin, E., Allegre, C.J., 2002. Boron isotope systematics in large rivers: implications for the marine boron budget and paleo-pH reconstruction over the Cenozoic. Chemical Geology 190, 123–140.

Lemarchand, D., Wasserburg, G.J., Papanastassiou, D.A., 2004. Rate-controlled calcium isotope fractionation in synthetic calcite. Geochimica et Cosmochimica Acta 68, 4665–4678. https://doi.org/10.1016/j.gca.2004.05.029

Leyden, E., Farkas, J., Gilbert, S., Hutson, J., Mosley, L.M., 2021. A simple and rapid ICP-MS/MS determination of sulfur isotope ratios (34S/32S) in complex natural waters: A new tool for tracing seawater intrusion in coastal systems. Talanta 235, 122708. https://doi.org/10.1016/j.talanta.2021.122708

Li, G., Elderfield, H., 2013. Evolution of carbon cycle over the past 100 million years. Geochimica et Cosmochimica Acta 103, 11–25. https://doi.org/10.1016/j.gca.2012.10.014

Li, L., Keller, G., 1998. Abrupt deep-sea warming at the end of the Cretaceous 5.

Li, N., Zhang, F., Gao, J., Cao, M., Wei, G.-Y., Wang, H., Zhang, Z., Cheng, M., Xiong, G., Zhou, J., Zhang, H., Peng, Y., Li, C., Shen, S., 2022. Assessing bulk carbonates as archives for seawater sulfur isotopic composition using shallow water cores from the South China Sea. Palaeogeography, Palaeoclimatology, Palaeoecology 598, 111029. https://doi.org/10.1016/j.palaeo.2022.111029

Li, P., Huang, J., Chen, M., Bai, X., 2009. Coincident negative shifts in sulfur and carbon isotope compositions prior to the end-Permian mass extinction at Shangsi Section of Guangyuan, South China. Frontiers of Earth Science in China 3, 51–56. https://doi.org/10.1007/s11707-009-0018-4

Li, S.L., Calmels, D., Han, G., Gaillardet, J., Liu, C.Q., 2008. Sulfuric acid as an agent of carbonate weathering constrained by 13CDIC: Examples from Southwest China. Earth and Planetary Science Letters 270, 189–199.

Light, T., Garcia, M., Prairie, J.C., Martínez-Ruiz, F., Norris, R., 2023. Water column barium sulfate dissolution and shielding by organic matter aggregates: Implications for the pelagic barite proxy. Chemical Geology 636, 121637. https://doi.org/10.1016/j.chemgeo.2023.121637

Liu, X., Fike, D., Li, A., Dong, J., Xu, F., Zhuang, G., Rendle-Bühring, R., Wan, S., 2019. Pyrite sulfur isotopes constrained by sedimentation rates: Evidence from sediments on the East China Sea inner shelf since the late Pleistocene. Chemical Geology 505, 66–75. https://doi.org/10.1016/j.chemgeo.2018.12.014

Liu, Y.-W., Sutton, J.N., Ries, J.B., Eagle, R.A., n.d. Regulation of calcification site pH is a polyphyletic but not always governing response to ocean acidification. Science Advances 6, eaax1314. https://doi.org/10.1126/sciadv.aax1314

Lorens, R.B., Bender, M.L., 1980. The impact of solution chemistry on Mytilus edulis calcite and aragonite. Geochimica et Cosmochimica Acta 44, 1265–1278. https://doi.org/10.1016/0016-7037(80)90087-3

Loste, E., Wilson, R.M., Seshadri, R., Meldrum, F.C., 2003. The role of magnesium in stabilising amorphous calcium carbonate and controlling calcite morphologies. Journal of Crystal Growth 254, 206–218. https://doi.org/10.1016/S0022-0248(03)01153-9

Louvat, P., Allègre, C.J., 1997. Present denudation rates on the island of Réunion determined by river geochemistry: Basalt weathering and mass budget between chemical and mechanical erosions. Geochimica et Cosmochimica Acta 61, 3645–3669.

Louvat, P., Gaillardet, J., Paris, G., Dessert, C., 2011. Boron isotope ratios of surface waters in Guadeloupe, Lesser Antilles. Applied Geochemistry 26, Supplement, S76–S79. https://doi.org/10.1016/j.apgeochem.2011.03.035

Lowenstam, H.A., 1981. Minerals Formed by Organisms. Science 211, 1126–1131. https://doi.org/10.1126/science.7008198

Lowenstam, H.A., Weiner, S., 1989. On biomineralization. Oxford University Press, USA.

Lowenstein, T.K., Timofeeff, M.N., Brennan, S.T., Hardie, L.A., Demicco, R.V., 2001. Oscillations in Phanerozoic Seawater Chemistry: Evidence from Fluid Inclusions. Science 294, 1086–1088.

Loyd, S.J., Berelson, W.M., Lyons, T.W., Hammond, D.E., Corsetti, F.A., 2012. Constraining pathways of microbial mediation for carbonate concretions of the Miocene Monterey Formation using carbonate-associated sulfate. Geochimica et Cosmochimica Acta 78, 77–98. https://doi.org/10.1016/j.gca.2011.11.028

Luo, G., Kump, L.R., Wang, Y., Tong, J., Arthur, M.A., Yang, H., Huang, J., Yin, H., Xie, S., 2010. Isotopic evidence for an anomalously low oceanic sulfate concentration following end-Permian mass extinction. Earth and Planetary Science Letters 300, 101–111. https://doi.org/10.1016/j.epsl.2010.09.041

Lyons, T.W., Walter, L.M., Gellatly, A.M., Martini, A.M., Blake, R.E., 2004. Sites of anomalous organic remineralization in the carbonate sediments of South Florida, USA: the sulfur cycle and carbonate-associated sulfate.

Macalady, J.L., Jones, D.S., Lyon, E.H., 2007. Extremely acidic, pendulous cave wall biofilms from the Frasassi cave system, Italy. Environmental Microbiology 9, 1402–1414.

Mackenzie, F.T., Bischoff, W.D., Bishop, F.C., Loijens, M., Schoonmaker, J., Wollast, R., 1983. Magnesian calcites; low-temperature occurrence, solubility and solid-solution behavior. Reviews in Mineralogy and Geochemistry 11, 97–144.

Macnamara, J., Thode, H.G., 1950. Comparison of the Isotopic Constitution of Terrestrial and Meteoritic Sulfur. Physical Review 78, 307.

Maffre, P., Swanson-Hysell, N.L., Goddéris, Y., 2021. Limited Carbon Cycle Response to Increased Sulfide Weathering Due to Oxygen Feedback. Geophysical Research Letters 48, e2021GL094589. https://doi.org/10.1029/2021GL094589

Mann, J.L., Vocke Jr., R.D., Kelly, W.R., 2009. Revised δ34S reference values for IAEA sulfur isotope reference materials S-2 and S-3. Rapid Communications in Mass Spectrometry 23, 1116–1124. https://doi.org/10.1002/rcm.3977

Mann, S., 1988. Molecular recognition in biomineralization. Nature 332, 119–124. https://doi.org/10.1038/332119a0

Marenco, P.J., Corsetti, F.A., Hammond, D.E., Kaufman, A.J., Bottjer, D.J., 2008a. Oxidation of pyrite during extraction of carbonate associated sulfate. Chemical Geology 247, 124–132. https://doi.org/10.1016/j.chemgeo.2007.10.006

Marenco, P.J., Corsetti, F.A., Kaufman, A.J., Bottjer, D.J., 2008b. Environmental and diagenetic variations in carbonate associated sulfate: An investigation of CAS in the Lower Triassic of the western USA. Geochimica et Cosmochimica Acta 72, 1570–1582. https://doi.org/10.1016/j.gca.2007.10.033

Märki, L., Lupker, M., France-Lanord, C., Lavé, J., Gallen, S., Gajurel, A.P., Haghipour, N., Leuenberger-West, F., Eglinton, T., 2021. An unshakable carbon budget for the Himalaya. Nature Geoscience 14, 745–750. https://doi.org/10.1038/s41561-021-00815-z

Marriott, C.S., Henderson, G.M., Belshaw, N.S., Tudhope, A.W., 2004. Temperature dependence of δ7Li, δ44Ca and Li/Ca during growth of calcium carbonate. Earth and Planetary Science Letters 222, 615–624. https://doi.org/10.1016/j.epsl.2004.02.031

Martin, R.A., Nesbitt, E.A., Campbell, K.A., 2010. The effects of anaerobic methane oxidation on benthic foraminiferal assemblages and stable isotopes on the Hikurangi Margin of eastern New Zealand. Marine Geology 272, 270–284. https://doi.org/10.1016/j.margeo.2009.03.024

Mason, P.R.D., Kaspers, K., van Bergen, M.J., 1999. Determination of sulfur isotope ratios and concentrations in water samples using ICP-MS incorporating hexapole ion optics. Journal of Analytical Atomic Spectrometry 14, 1067–1074.

Mass, T., Drake, J.L., Haramaty, L., Kim, J.D., Zelzion, E., Bhattacharya, D., Falkowski, P.G., 2013. Cloning and Characterization of Four Novel Coral Acid-Rich Proteins that Precipitate Carbonates In Vitro. Current Biology 23, 1126–1131. https://doi.org/10.1016/j.cub.2013.05.007

Mass, T., Giuffre, A.J., Sun, C.-Y., Stifler, C.A., Frazier, M.J., Neder, M., Tamura, N., Stan, C.V., Marcus, M.A., Gilbert, P.U.P.A., 2017. Amorphous calcium carbonate particles form coral skeletons. Proceedings of the National Academy of Sciences 114, E7670–E7678. https://doi.org/10.1073/pnas.1707890114

Masterson, A., Alperin, M.J., Berelson, W.M., Johnston, D.T., 2018. Interpreting multiple sulfur isotope signals in modern anoxic sediments using a full diagenetic model (California-Mexico margin: Alfonso Basin). American Journal of Science 318, 459–490. https://doi.org/10.2475/05.2018.02

Masterson, A.L., Wing, B.A., Paytan, A., Farquhar, J., Johnston, D.T., 2016. The minor sulfur isotope composition of Cretaceous and Cenozoic seawater sulfate. Paleoceanography 31, 779–788. https://doi.org/10.1002/2016PA002945

Mavromatis, V., Purgstaller, B., Dietzel, M., Buhl, D., Immenhauser, A., Schott, J., 2017. Impact of amorphous precursor phases on magnesium isotope signatures of Mg-calcite. Earth and Planetary Science Letters 464, 227–236. https://doi.org/10.1016/j.epsl.2017.01.031

Mazumdar, A., Goldberg, T., Strauss, H., 2008. Abiotic oxidation of pyrite by Fe(III) in acidic media and its implications for sulfur isotope measurements of lattice-bound sulfate in sediments. Chemical Geology 253, 30–37. https://doi.org/10.1016/j.chemgeo.2008.03.014

McConnaughey, T.A., Whelan, J.F., 1997. Calcification generates protons for nutrient and bicarbonate uptake. Earth-Science Reviews 42, 95–117. https://doi.org/10.1016/S0012-8252(96)00036-0

McConnell, J.R., Burke, A., Dunbar, N.W., Köhler, P., Thomas, J.L., Arienzo, M.M., Chellman, N.J., Maselli, O.J., Sigl, M., Adkins, J.F., Baggenstos, D., Burkhart, J.F., Brook, E.J., Buizert, C., Cole-Dai, J., Fudge, T.J., Knorr, G., Graf, H.-F., Grieman, M.M., Iverson, N., McGwire, K.C., Mulvaney, R., Paris, G., Rhodes, R.H., Saltzman, E.S., Severinghaus, J.P., Steffensen, J.P., Taylor, K.C., Winckler, G., 2017. Synchronous volcanic eruptions and abrupt climate change ~17.7 ka plausibly linked by stratospheric ozone depletion. Proceedings of the National Academy of Sciences. https://doi.org/10.1073/pnas.1705595114

McDermott, J.M., Ono, S., Tivey, M.K., Seewald, J.S., Shanks III, W.C., Solow, A.R., 2015. Identification of sulfur sources and isotopic equilibria in submarine hot-springs using multiple sulfur isotopes. Geochimica et Cosmochimica Acta 160, 169–187. https://doi.org/10.1016/j.gca.2015.02.016

McGlynn, S.E., Chadwick, G.L., Kempes, C.P., Orphan, V.J., 2015. Single cell activity reveals direct electron transfer in methanotrophic consortia. Nature 526, 531–535. https://doi.org/10.1038/nature15512

Menegario, A.A., Fernanda Gine, M., Bendassolli, J.A., Claudia S. Bellato, A., Trivelin, P.C.O., 1998. Sulfur isotope ratio (34S:32S) measurements in plant material by inductively coupled plasma mass spectrometry. Journal of Analytical Atomic Spectrometry 13, 1065–1067.

Meybeck, M., 1987. Global chemical weathering of surficial rocks estimated from river dissolved loads. American Journal of Science 287, 401.

Middelburg, J.J., Vlug, T., Jaco, F., van der Nat, W.A., 1993. Organic matter mineralization in marine systems. Global and Planetary Change 8, 47–58. https://doi.org/10.1016/0921-8181(93)90062-S

Millot, R., Gaillardet, J., Dupré, B., Allègre, C.J., 2002. The global control of silicate weathering rates and the coupling with physical erosion: new insights from rivers of the Canadian Shield. Earth and Planetary Science Letters 196, 83–98.

Mills, J.V., DePaolo, D.J., Lammers, L.N., 2021. The influence of Ca:CO3 stoichiometry on Ca isotope fractionation: Implications for process-based models of calcite growth. Geochimica et Cosmochimica Acta 298, 87–111. https://doi.org/10.1016/j.gca.2021.01.016

Mitterer, R.M., 2010. Methanogenesis and sulfate reduction in marine sediments: A new model. Earth and Planetary Science Letters 295, 358–366. https://doi.org/10.1016/j.epsl.2010.04.009

Mondal, S., Anand, P., Chakrabarti, R., 2023. Evaluating the temperature dependence of δ44/40Ca along with δ18O, Mg/Ca, and Sr/Ca in calcite tests of multiple foraminifera species. Chemical Geology 639, 121736. https://doi.org/10.1016/j.chemgeo.2023.121736

Montes-Hernandez, G., Findling, N., Renard, F., 2016. Dissolution-precipitation reactions controlling fast formation of dolomite under hydrothermal conditions. Applied Geochemistry 73, 169–177.

Montes-Hernandez, G., Renard, F., Auzende, A.-L., Findling, N., 2020. Amorphous calcium–magnesium carbonate (ACMC) accelerates dolomitization at room temperature under abiotic conditions. Crystal Growth & Design 20, 1434–1441.

Moran, A., 2000. Calcein as a marker in experimental studies newly-hatched gastropods. Marine Biology 137, 893–898.

Morse, J.W., Wang, Q., Tsio, M.Y., 1997. Influences of temperature and Mg: Ca ratio on CaCO3 precipitates from seawater. Geology 25, 85.

Mucci, A., Canuel, R., Zhong, S., 1989. The solubility of calcite and aragonite in sulfate-free seawater and the seeded growth kinetics and composition of the precipitates at 25°C. Chemical Geology 74, 309–320. https://doi.org/10.1016/0009-2541(89)90040-5

Mucci, A., Morse, J.W., 1983. The incorporation of Mg^{2+} and Sr^{2+} into calcite overgrowths: influences of growth rate and solution composition. Geochimica et Cosmochimica Acta 47, 217–233. https://doi.org/10.1016/0016-7037(83)90135-7

Mummadisetti, M.P., Drake, J.L., Falkowski, P.G., 2021. The spatial network of skeletal proteins in a stony coral. Journal of The Royal Society Interface 18, 20200859. https://doi.org/10.1098/rsif.2020.0859

Naehr, T.H., Eichhubl, P., Orphan, V.J., Hovland, M., Paull, C.K., Ussler, W., Lorenson, T.D., Greene, H.G., 2007. Authigenic carbonate formation at hydrocarbon seeps in continental margin sediments: A comparative study. Deep Sea Research Part II: Topical Studies in Oceanography 54, 1268–1291. https://doi.org/10.1016/j.dsr2.2007.04.010

Nägler, T.F., Eisenhauer, A., Müller, A., Hemleben, C., Kramers, J., 2000. The δ^{44}Ca-temperature calibration on fossil and cultured Globigerinoides sacculifer: New tool for reconstruction of past sea surface temperatures. Geochemistry, Geophysics, Geosystems 1. https://doi.org/10.1029/2000GC000091

Nash, M.C., Troitzsch, U., Opdyke, B.N., Trafford, J.M., Russell, B.D., Kline, D.I., 2011. First discovery of dolomite and magnesite in living coralline algae and its geobiological implications. Biogeosciences 8, 3331–3340. https://doi.org/10.5194/bg-8-3331-2011

Nehrke, G., Keul, N., Langer, G., De Nooijer, L., Bijma, J., Meibom, A., 2013. A new model for biomineralization and trace-element signatures of Foraminifera tests. Biogeosciences 10, 6759–6767.

Neubauer, C., Crémière, A., Wang, X.T., Thiagarajan, N., Sessions, A.L., Adkins, J.F., Dalleska, N.F., Turchyn, A.V., Clegg, J.A., Moradian, A., Sweredoski, M.J., Garbis, S.D., Eiler, J.M., 2020. Stable Isotope Analysis of Intact Oxyanions Using Electrospray Quadrupole-Orbitrap Mass Spectrometry. Anal. Chem. 92, 3077–3085. https://doi.org/10.1021/acs.analchem.9b04486

Newton, R., Bottrell, S., 2007. Stable isotopes of carbon and sulphur as indicators of environmental change: past and present. Journal of the Geological Society 164, 691–708. https://doi.org/10.1144/0016-76492006-101

Ng, G.C., Rosenfeld, C.E., Santelli, C.M., Yourd, A.R., Lange, J., Duhn, K., Johnson, N.W., 2020. Microbial and reactive transport modeling evidence for hyporheic flux-driven cryptic sulfur cycling and anaerobic methane oxidation in a sulfate-impacted wetland-stream system. Journal of Geophysical Research: Biogeosciences 125, e2019JG005185.

Nichols, D., Jarzen, D., Orth, C., Oliver, P., 1986. Palynological and iridium anomalies at Cretaceous-Tertiary boundary, south-central Saskatchewan. Science 231, 714–717.

Nielsen, H., 1973. MODEL EVALUATIONS OF THE SULFUR ISOTOPE BUDGET OF ANCIENT OCEANS II.

Nielsen, H., Ricke, W., 1964. Schwefel-isotopen verhältnisse von evaporiten aus deutschland; Ein beitrag zur kenntnis von δ 34 S im meerwasser-sulfat. Geochimica et Cosmochimica Acta 28, 577–591.

Nielsen, L. C., DePaolo, D.J., De Yoreo, J.J., 2012. Self-consistent ion-by-ion growth model for kinetic isotopic fractionation during calcite precipitation. https://doi.org/10.1016/j.gca.2012.02.009

Nielsen, Laura C., DePaolo, D.J., De Yoreo, J.J., 2012. Self-consistent ion-by-ion growth model for kinetic isotopic fractionation during calcite precipitation. Geochimica et Cosmochimica Acta 86, 166–181. https://doi.org/10.1016/j.gca.2012.02.009

Nielsen, M.R., Sand, K.K., Rodriguez-Blanco, J.D., Bovet, N., Generosi, J., Dalby, K.N., Stipp, S.L.S., 2016. Inhibition of Calcite Growth: Combined Effects of Mg2+ and SO42–. Crystal Growth & Design 16, 6199–6207. https://doi.org/10.1021/acs.cgd.6b00536

Nordt, L., Atchley, S., Dworkin, S., 2003. Terrestrial evidence for two greenhouse events in the latest Cretaceous. GSA today 13, 4.

Ogawa, Y., Takahashi, K., Yamanaka, T., Onodera, J., 2009. Significance of euxinic condition in the middle Eocene paleo-Arctic basin: A geochemical study on the IODP Arctic Coring Expedition 302 sediments. Earth and Planetary Science Letters 285, 190–197. https://doi.org/10.1016/j.epsl.2009.06.011

Ohkouchi, N., Kawamura, K., Kajiwara, Y., Wada, E., Okada, M., Kanamatsu, T., Taira, A., 1999. Sulfur isotope records around Livello Bonarelli (northern Apennines, Italy) black shale at the Cenomanian-Turonian boundary. Geology 27, 535.

O'Hora, H.E., Petersen, S.V., Vellekoop, J., Jones, M.M., Scholz, S.R., 2022. Clumped-isotope-derived climate trends leading up to the end-Cretaceous mass extinction in northwestern Europe. Climate of the Past 18, 1963–1982.

Olivero, E.B., 2012. Sedimentary cycles, ammonite diversity and palaeoenvironmental changes in the Upper Cretaceous Marambio Group, Antarctica. Cretaceous Research 34, 348–366. https://doi.org/10.1016/j.cretres.2011.11.015

Ono, S., Keller, N.S., Rouxel, O., Alt, J.C., 2012. Sulfur-33 constraints on the origin of secondary pyrite in altered oceanic basement. Geochimica et Cosmochimica Acta 87, 323–340. https://doi.org/10.1016/j.gca.2012.04.016

Ono, S., Shanks Iii, W.C., Rouxel, O.J., Rumble, D., 2007. S-33 constraints on the seawater sulfate contribution in modern seafloor hydrothermal vent sulfides. Geochimica et cosmochimica acta 71, 1170–1182. https://doi.org/10.1016/j.gca.2006.11.017

Ono, S., Wing, B., Johnston, D., Farquhar, J., Rumble, D., 2006a. Mass-dependent fractionation of quadruple stable sulfur isotope system as a new tracer of sulfur biogeochemical cycles. Geochimica et Cosmochimica Acta 70, 2238–2252. https://doi.org/10.1016/j.gca.2006.01.022

Ono, S., Wing, B., Rumble, D., Farquhar, J., 2006b. High precision analysis of all four stable isotopes of sulfur (32S, 33S, 34S and 36S) at nanomole levels using a laser fluorination isotope-ratio-monitoring gas chromatography-mass spectrometry. Chemical Geology 225, 30–39. https://doi.org/10.1016/j.chemgeo.2005.08.005

Orphan, V.J., Hinrichs, K.-U., Ussler, W., Paull, C.K., Taylor, L.T., Sylva S. P., Hayes J. M., Delong E. F., 2001. Comparative Analysis of Methane-Oxidizing Archaea and Sulfate-Reducing Bacteria in Anoxic Marine Sediments. Applied and Environmental Microbiology 67, 1922–1934. https://doi.org/10.1128/AEM.67.4.1922-1934.2001

Orphan, V.J., House, C.H., Hinrichs, K.-U., McKeegan, K.D., DeLong, E.F., 2002. Multiple archaeal groups mediate methane oxidation in anoxic cold seep sediments. Proceedings of the National Academy of Sciences 99, 7663–7668. https://doi.org/10.1073/pnas.072210299

Orth, C.J., Gilmore, J.S., Knight, J.D., Pillmore, C.L., Tschudy, R.H., Fassett, J.E., 1981. An iridium abundance anomaly at the palynological Cretaceous-Tertiary boundary in northern New Mexico. Science 214, 1341–1343.

Osburn, M.R., Owens, J., Bergmann, K.D., Lyons, T.W., Grotzinger, J.P., 2015. Dynamic changes in sulfate sulfur isotopes preceding the Ediacaran Shuram Excursion. Geochimica et Cosmochimica Acta 170, 204–224. https://doi.org/10.1016/j.gca.2015.07.039

Owens, J.D., Gill, B.C., Jenkyns, H.C., Bates, S.M., Severmann, S., Kuypers, M.M.M., Woodfine, R.G., Lyons, T.W., 2013. Sulfur isotopes track the global extent and dynamics of euxinia during Cretaceous Oceanic Anoxic Event 2. Proceedings of the National Academy of Sciences 110, 18407–18412. https://doi.org/10.1073/pnas.1305304110

Pardo, A., Keller, G., 2008. Biotic effects of environmental catastrophes at the end of the Cretaceous and early Tertiary: Guembelitria and Heterohelix blooms. Cretaceous Research 29, 1058–1073. https://doi.org/10.1016/j.cretres.2008.05.031

Paris, G., 2023. Data associated to the publication “Determination of unbiased δ34S and Δ33S values using down to 30 nmol of sulfur by MC-ICP-MS.” https://doi.org/10.24396/ORDAR-132

Paris, G., Adkins, J.F., Sessions, A.L., Webb, S.M., Fischer, W.W., 2014a. Neoarchean carbonate–associated sulfate records positive Δ33S anomalies. Science 346, 739–741. https://doi.org/10.1126/science.1258211

Paris, G., Bartolini, A., Donnadieu, Y., Beaumont, V., Gaillardet, J., 2010. Investigating boron isotopes in a middle Jurassic micritic sequence: Primary vs. diagenetic signal. Chemical Geology 275, 117–126.

Paris, G., Fehrenbacher, J.S., Sessions, A.L., Spero, H.J., Adkins, J.F., 2014b. Experimental determination of carbonate-associated sulfate δ34S in planktonic foraminifera shells. Geochemistry, Geophysics, Geosystems 15, 1452–1461. https://doi.org/10.1002/2014gc005295

Paris, G., Fischer, W.W., Johnson, J.E., Webb, S.M., Present, T.M., Sessions, A.L., Adkins, J.F., 2020. Deposition of sulfate aerosols with positive Δ33S in the Neoarchean. Geochimica et Cosmochimica Acta 285, 1–20. https://doi.org/10.1016/j.gca.2020.06.028

Paris, G., Sessions, A.L., Subhas, A.V., Adkins, J.F., 2013. MC-ICP-MS measurement of $\delta^{34}S$ and $\Delta^{33}S$ in small amounts of dissolved sulfate. Chemical Geology 345, 50–61. https://doi.org/10.1016/j.chemgeo.2013.02.022

Pasquier, V., Bryant, R.N., Fike, D.A., Halevy, I., 2021. Strong local, not global, controls on marine pyrite sulfur isotopes. Science Advances 7, eabb7403. https://doi.org/10.1126/sciadv.abb7403

Pasquier, V., Sansjofre, P., Rabineau, M., Revillon, S., Houghton, J., Fike, D.A., 2017. Pyrite sulfur isotopes reveal glacial−interglacial environmental changes. Proceedings of the National Academy of Sciences 114, 5941–5945. https://doi.org/10.1073/pnas.1618245114

Paulsen, P., Kelly, W., 1984. Determination of sulfur as arsenic monosulfide ion by isotope dilution thermal ionization mass spectrometry. Analytical Chemistry 56, 708–713.

Paytan, A., Kastner, M., Campbell, D., Thiemens, M.H., 2004. Seawater sulfur isotope fluctuations in the Cretaceous. Science 304, 1663–1665. https://doi.org/10.1126/science.1095258

Paytan, A., Kastner, M., Campbell, D., Thiemens, M.H., 1998. Sulfur Isotopic Composition of Cenozoic Seawater Sulfate. Science 282, 1459–1462. https://doi.org/10.1126/science.282.5393.1459

Paytan, A., Kastner, M., Martin, E.E., Macdougall, J.D., Herbert, T., 1993. Marine barite as a monitor of seawater strontium isotope composition. Nature 366, 445–449. https://doi.org/10.1038/366445a0

Paytan, A., Mearon, S., Cobb, K., Kastner, M., 2002. Origin of marine barite deposits: Sr and S isotope characterization. Geology 30, 747–750. https://doi.org/10.1130/0091-7613(2002)030<0747:oombds>2.0.co;2

Peck Jr, H., 1962. V. Comparative metabolism of inorganic sulfur compounds in microorganisms. Bacteriological reviews 26, 67–94.

Pérez-Huerta, A., Cusack, M., Jeffries, T.E., Williams, C.T., 2008. High resolution distribution of magnesium and strontium and the evaluation of Mg/Ca thermometry in Recent brachiopod shells. Chemical Geology 247, 229–241. https://doi.org/10.1016/j.chemgeo.2007.10.014

Perrin, J., Rivard, C., Vielzeuf, D., Laporte, D., Fonquernie, C., Ricolleau, A., Cotte, M., Floquet, N., 2017. The coordination of sulfur in synthetic and biogenic Mg calcites: The red coral case. Geochimica et Cosmochimica Acta 197, 226–244. https://doi.org/10.1016/j.gca.2016.10.017

Pester, M., Knorr, K.-H., Friedrich, M., Wagner, M., Loy, A., 2012. Sulfate-reducing microorganisms in wetlands – fameless actors in carbon cycling and climate change. Frontiers in Microbiology 3, 72. https://doi.org/10.3389/fmicb.2012.00072

Philippot, P., Van Zuilen, M., Lepot, K., Thomazo, C., Farquhar, J., Van Kranendonk, M.J., 2007. Early Archaean Microorganisms Preferred Elemental Sulfur, Not Sulfate. Science 317, 1534. https://doi.org/10.1126/science.1145861

Pimminger, M., Grasserbauer, M., Schroll, E., Cerny, I., 1984. Microanalysis in galena by secondary ion mass spectrometry. Analytical Chemistry 56, 407–411.

Pina, C.M., Pimentel, C., Crespo, Á., 2022. The Dolomite Problem: A Matter of Time. ACS Earth Space Chem. 6, 1468–1471. https://doi.org/10.1021/acsearthspacechem.2c00078

Pingitore, N., 1995. Identification of sulfate in natural carbonates by X-ray absorption spectroscopy. Geochimica et Cosmochimica Acta 59, 2477–2483.

Pingitore, N.E., 1978. The behavior of Zn 2+ and Mn 2+ during carbonate diagenesis; theory and applications. Journal of Sedimentary Research 48, 799–814.

Planavsky, N.J., Bekker, A., Hofmann, A., Owens, J.D., Lyons, T.W., 2012. Sulfur record of rising and falling marine oxygen and sulfate levels during the Lomagundi event. Proceedings of the National Academy of Sciences 109, 18300–18305. https://doi.org/10.1073/pnas.1120387109

Planavsky, N.J., McGoldrick, P., Scott, C.T., Li, C., Reinhard, C.T., Kelly, A.E., Chu, X., Bekker, A., Love, G.D., Lyons, T.W., 2011. Widespread iron-rich conditions in the mid-Proterozoic ocean. Nature 477, 448–451. http://www.nature.com/nature/journal/v477/n7365/abs/nature10327.html#supplementary-information

Pope, K.O., Baines, K.H., Ocampo, A.C., Ivanov, B.A., 1997. Energy, volatile production, and climatic effects of the Chicxulub Cretaceous/Tertiary impact. Journal of Geophysical Research: Planets (1991–2012) 102, 21645–21664. https://doi.org/10.1029/97JE01743

Present, T.M., Adkins, J.F., Fischer, W.W., 2020. Variability in Sulfur Isotope Records of Phanerozoic Seawater Sulfate. Geophysical Research Letters 47, e2020GL088766. https://doi.org/10.1029/2020GL088766

Present, T.M., Gutierrez, M., Paris, G., Kerans, C., Grotzinger, J.P., Adkins, J.F., 2019. Diagenetic controls on the isotopic composition of carbonate-associated sulphate in the Permian Capitan Reef Complex, West Texas. Sedimentology 0. https://doi.org/10.1111/sed.12615

Present, T.M., Paris, G., Burke, A., Fischer, W.W., Adkins, J.F., 2015. Large Carbonate Associated Sulfate isotopic variability between brachiopods, micrite, and other sedimentary components in Late Ordovician strata. Earth and Planetary Science Letters 432, 187–198. https://doi.org/10.1016/j.epsl.2015.10.005

Prohaska, T., Latkoczy, C., Stingeder, G., 1999. Precise sulfur isotope ratio measurements in trace concentration of sulfur by inductively coupled plasma double focusing sector field mass spectrometry. Journal of Analytical Atomic Spectrometry 14, 1501–1504.

Punekar, J., Keller, G., Khozyem, H.M., Adatte, T., Font, E., Spangenberg, J., 2016. A multi-proxy approach to decode the end-Cretaceous mass extinction. Palaeogeography, Palaeoclimatology, Palaeoecology 441, 116–136. https://doi.org/10.1016/j.palaeo.2015.08.025

Purton, L.M., Shields, G.A., Brasier, M.D., Grime, G.W., 1999. Metabolism controls Sr/Ca ratios in fossil aragonitic mollusks. Geology 27, 1083–1086.

Qi, H.P., Coplen, T.B., 2003. Evaluation of the 34S/32S ratio of Soufre de Lacq elemental sulfur isotopic reference material by continuous flow isotope-ratio mass spectrometry. Chemical Geology 199, 183–187. http://dx.doi.org/10.1016/S0009-2541(03)00075-5

Raab, M., Spiro, B., 1991. Sulfur isotopic variations during seawater evaporation with fractional crystallization. Chemical Geology: Isotope Geoscience section 86, 323–333. https://doi.org/10.1016/0168-9622(91)90014-N

Rae, J.W., Zhang, Y.G., Liu, X., Foster, G.L., Stoll, H.M., Whiteford, R.D., 2021. Atmospheric CO_2 over the past 66 million years from marine archives. Annual Review of Earth and Planetary Sciences 49, 609–641.

Raiswell, R., Berner, R.A., 1986. Pyrite and organic matter in Phanerozoic normal marine shales. Geochimica et Cosmochimica Acta 50, 1967–1976. https://doi.org/10.1016/0016-7037(86)90252-8

Rathburn, A.E., Corliss, B.H., 1994. The ecology of living (stained) deep-sea benthic foraminifera from the Sulu Sea. Paleoceanography 9, 87–150. https://doi.org/10.1029/93PA02327

Rathmann, S., Hess, S., Kuhnert, H., Mulitza, S., 2004. Mg/Ca ratios of the benthic foraminifera Oridorsalis umbonatus obtained by laser ablation from core top sediments: Relationship to bottom water temperature. Geochemistry, Geophysics, Geosystems 5. https://doi.org/10.1029/2004GC000808

Rathmann, S., Kuhnert, H., 2008. Carbonate ion effect on Mg/Ca, Sr/Ca and stable isotopes on the benthic foraminifera Oridorsalis umbonatus off Namibia. Marine Micropaleontology 66, 120–133. https://doi.org/10.1016/j.marmicro.2007.08.001

Raven, M.R., Adkins, J.F., Werne, J.P., Lyons, T.W., Sessions, A.L., 2015. Sulfur isotopic composition of individual organic compounds from Cariaco Basin sediments. Organic Geochemistry 80, 53–59. https://doi.org/10.1016/j.orggeochem.2015.01.002

Raven, M.R., Fike, D.A., Gomes, M.L., Webb, S.M., Bradley, A.S., McClelland, H.-L.O., 2018. Organic carbon burial during OAE2 driven by changes in the locus of organic matter sulfurization. Nature Communications 9, 3409. https://doi.org/10.1038/s41467-018-05943-6

Raven, M.R., Keil, R.G., Webb, S.M., 2021. Microbial sulfate reduction and organic sulfur formation in sinking marine particles. Science 371, 178–181. https://doi.org/10.1126/science.abc6035

Raymo, M.E., Ruddiman, W.F., Froelich, P.N., 1988. Influence of late Cenozoic mountain building on ocean geochemical cycles. Geology 16, 649–653.

Raz, S., Hamilton, P.C., Wilt, F.H., Weiner, S., Addadi, L., 2003. The Transient Phase of Amorphous Calcium Carbonate in Sea Urchin Larval Spicules: The Involvement of Proteins and Magnesium Ions in Its Formation and Stabilization. Advanced Functional Materials 13, 480–486. https://doi.org/10.1002/adfm.200304285

Reeder, R.J., Lamble, G.M., Lee, J.-F., Staudt, W.J., 1994. Mechanism of SeO42− substitution in calcite: An XAFS study. Geochimica et Cosmochimica Acta 58, 5639–5646. https://doi.org/10.1016/0016-7037(94)90256-9

Rees, C.E., 1973. A steady-state model for sulphur isotope fractionation in bacterial reduction processes. Geochimica et Cosmochimica Acta 37, 1141–1162. https://doi.org/10.1016/0016-7037(73)90052-5

Regenberg, M., Nürnberg, D., Schönfeld, J., Reichart, G.-J., 2007. Early diagenetic overprint in Caribbean sediment cores and its effect on the geochemical composition of planktonic foraminifera. Biogeosciences 4, 957–973. https://doi.org/10.5194/bg-4-957-2007

Renne, P.R., Deino, A.L., Hilgen, F.J., Kuiper, K.F., Mark, D.F., Mitchell, W.S., Morgan, L.E., Mundil, R., Smit, J., 2013. Time Scales of Critical Events Around the Cretaceous-Paleogene Boundary. Science 339, 684. https://doi.org/10.1126/science.1230492

Renne, P.R., Sprain, C.J., Richards, M.A., Self, S., Vanderkluysen, L., Pande, K., 2015. State shift in Deccan volcanism at the Cretaceous-Paleogene boundary, possibly induced by impact. Science 350, 76. https://doi.org/10.1126/science.aac7549

Rennie, V.C.F., Paris, G., Sessions, A.L., Abramovich, S., Turchyn, A.V., 2014. Foraminiferal calcite provides new insight into the coupled carbon & sulfur isotope evolution of the ocean in the Palaeogene. Presented at the Agouron Symposium.

Rennie, V.C.F., Paris, G., Sessions, A.L., Abramovich, S., Turchyn, A.V., Adkins, J.F., 2018. Cenozoic record of δ34S in foraminiferal calcite implies an early Eocene shift to deep-ocean sulfide burial. Nature Geoscience. https://doi.org/10.1038/s41561-018-0200-y

Rennie, V.C.F., Turchyn, A.V., 2014. The preservation of δ34S and δ18O in carbonate-associated sulfate during marine diagenesis: A 25 Myr test case using marine sediments. Earth and Planetary Science Letters 395, 13–23. https://doi.org/10.1016/j.epsl.2014.03.025

Riccardi, A.L., Arthur, M.A., Kump, L.R., 2006. Sulfur isotopic evidence for chemocline upward excursions during the end-Permian mass extinction. Geochimica et Cosmochimica Acta 70, 5740–5752. https://doi.org/10.1016/j.gca.2006.08.005

Richards, M.A., Alvarez, W., Self, S., Karlstrom, L., Renne, P.R., Manga, M., Sprain, C.J., Smit, J., Vanderkluysen, L., Gibson, S.A., 2015. Triggering of the largest Deccan eruptions by the Chicxulub impact. Geological Society of America Bulletin 127, 1507–1520. https://doi.org/10.1130/B31167.1

Richardson, J.A., Lepland, A., Hints, O., Prave, A.R., Gilhooly, W.P., Bradley, A.S., Fike, D.A., 2021. Effects of early marine diagenesis and site-specific depositional controls on carbonate-associated sulfate: Insights from paired S and O isotopic analyses. Chemical Geology 584, 120525. https://doi.org/10.1016/j.chemgeo.2021.120525

Richardson, J.A., Newville, M., Lanzirotti, A., Webb, S.M., Rose, C.V., Catalano, J.G., Fike, D.A., 2019a. The source of sulfate in brachiopod calcite: Insights from μ-XRF imaging and XANES spectroscopy. Chemical Geology 529, 119328. https://doi.org/10.1016/j.chemgeo.2019.119328

Richardson, J.A., Newville, M., Lanzirotti, A., Webb, S.M., Rose, C.V., Catalano, J.G., Fike, D.A., 2019b. Depositional and diagenetic constraints on the abundance and spatial variability of carbonate-associated sulfate. Chemical Geology 523, 59–72. https://doi.org/10.1016/j.chemgeo.2019.05.036

Robinson, B., 1995. Sulphur isotope standards. International Atomic Energy Agency TECDOC 825 39–45.

Rollion-Bard, C., Chaussidon, M., France-Lanord, C., 2011. Biological control of internal pH in scleractinian corals: Implications on paleo-pH and paleo-temperature reconstructions. Comptes Rendus Geoscience 343, 397–405. https://doi.org/10.1016/j.crte.2011.05.003

Rollion-Bard, C., Chaussidon, M., France-Lanord, C., 2003. pH control on oxygen isotopic composition of symbiotic corals. Earth and Planetary Science Letters 215, 275–288. https://doi.org/10.1016/S0012-821X(03)00391-1

Rollion-Bard, C., Erez, J., 2010. Intra-shell boron isotope ratios in benthic foraminifera: Implications for paleo-pH reconstructions. Geochimica et Cosmochimica Acta 74, 1530–1536.

Rose, C.V., Fischer, W.W., Finnegan, S., Fike, D.A., 2019a. Records of carbon and sulfur cycling during the Silurian Ireviken Event in Gotland, Sweden. Geochimica et Cosmochimica Acta 246, 299–316. https://doi.org/10.1016/j.gca.2018.11.030

Rose, C.V., Webb, S.M., Newville, M., Lanzirotti, A., Richardson, J.A., Tosca, N.J., Catalano, J.G., Bradley, A.S., Fike, D.A., 2019b. Insights into past ocean proxies from micron-scale mapping of sulfur species in carbonates. Geology 47, 833–837. https://doi.org/10.1130/G46228.1

Ross, M.B., Glennon, B.M., Murciano-Goroff, R., Berkes, E.G., Weinberg, B.A., Lane, J.I., 2022. Women are credited less in science than men. Nature 608, 135–145. https://doi.org/10.1038/s41586-022-04966-w

Rucker, D.D., Galinsky, A.D., Magee, J.C., 2018. Chapter Two - The Agentic–Communal Model of Advantage and Disadvantage: How Inequality Produces Similarities in the Psychology of Power, Social Class, Gender, and Race, in: Olson, J.M. (Ed.), Advances in Experimental Social Psychology. Academic Press, pp. 71–125. https://doi.org/10.1016/bs.aesp.2018.04.001

Russell, A.D., Hönisch, B., Spero, H.J., Lea, D.W., 2004. Effects of seawater carbonate ion concentration and temperature on shell U, Mg, and Sr in cultured planktonic foraminifera. Geochimica et Cosmochimica Acta 68, 4347–4361. https://doi.org/10.1016/j.gca.2004.03.013

Sakuma, H., Andersson, M.P., Bechgaard, K., Stipp, S.L.S., 2014. Surface Tension Alteration on Calcite, Induced by Ion Substitution. J. Phys. Chem. C 118, 3078–3087. https://doi.org/10.1021/jp411151u

Sandberg, P.A., 1985. Nonskeletal aragonite and pCO_2 in the Phanerozoic and Proterozoic. The carbon cycle and atmospheric CO_2: Natural variations archean to present; Proceedings of the Chapman Conference on Natural Variations in Carbon Dioxide and the Carbon Cycle, Tarpon Springs, FL, January 9-13, 1984 (A86-39426 18-46). Washington, DC, American Geophysical Union, 1985, p. 585-594.

Santos, A.A., Venceslau, S.S., Grein, F., Leavitt, W.D., Dahl, C., Johnston, D.T., Pereira, I.A.C., 2015. A protein trisulfide couples dissimilatory sulfate reduction to energy conservation. Science 350, 1541–1545. https://doi.org/10.1126/science.aad3558

Sato, A., Nagasaka, S., Furihata, K., Nagata, S., Arai, I., Saruwatari, K., Kogure, T., Sakuda, S., Nagasawa, H., 2011. Glycolytic intermediates induce amorphous calcium carbonate formation in crustaceans. Nature Chemical Biology 7, 197–199. https://doi.org/10.1038/nchembio.532

Saulnier, S., Rollion-Bard, C., Vigier, N., Chaussidon, M., 2012. Mg isotope fractionation during calcite precipitation: An experimental study. Geochimica et Cosmochimica Acta 91, 75–91. https://doi.org/10.1016/j.gca.2012.05.024

Savarino, J., Romero, A., Cole-Dai, J., Bekki, S., Thiemens, M.H., 2003. UV induced mass-independent sulfur isotope fractionation in stratospheric volcanic sulfate. Geophysical Research Letters 30, 2131. https://doi.org/10.1029/2003gl018134

Schidlowski, M., Junge, C., Pietrek, H., 1977. Sulfur isotope variations in marine sulfate evaporites and the Phanerozoic oxygen budget. Journal of Geophysical Research 82, 2557–2565.

Schobben, M., Stebbins, A., Ghaderi, A., Strauss, H., Korn, D., Korte, C., 2015. Flourishing ocean drives the end-Permian marine mass extinction. Proceedings of the National Academy of Sciences 112, 10298–10303. https://doi.org/10.1073/pnas.1503755112

Schoene, B., Eddy, M.P., Samperton, K.M., Keller, C.B., Keller, G., Adatte, T., Khadri, S.F.R., 2019. U-Pb constraints on pulsed eruption of the Deccan Traps across the end-Cretaceous mass extinction. Science 363, 862. https://doi.org/10.1126/science.aau2422

Schrag, D.P., Higgins, John.A., Macdonald, F.A., Johnston, D.T., 2013. Authigenic Carbonate and the History of the Global Carbon Cycle. Science 339, 540–543. https://doi.org/10.1126/science.1229578

Schubert, C.J., Vazquez, F., Lösekann-Behrens, T., Knittel, K., Tonolla, M., Boetius, A., 2011. Evidence for anaerobic oxidation of methane in sediments of a freshwater system (Lago di Cadagno). FEMS Microbiology Ecology 76, 26–38. https://doi.org/10.1111/j.1574-6941.2010.01036.x

Schulte, P., Alegret, L., Arenillas, I., Arz, J.A., Barton, P.J., Bown, P.R., Bralower, T.J., Christeson, G.L., Claeys, P., Cockell, C.S., Collins, G.S., Deutsch, A., Goldin, T.J., Goto, K., Grajales-Nishimura, J.M., Grieve, R.A.F., Gulick, S.P.S., Johnson, K.R., Kiessling, W., Koeberl, C., Kring, D.A., MacLeod, K.G., Matsui, T., Melosh, J., Montanari, A., Morgan, J.V., Neal, C.R., Nichols, D.J., Norris, R.D., Pierazzo, E., Ravizza, G., Rebolledo-Vieyra, M., Reimold, W.U., Robin, E., Salge, T., Speijer, R.P., Sweet, A.R., Urrutia-Fucugauchi, J., Vajda, V., Whalen, M.T., Willumsen, P.S., 2010. The Chicxulub Asteroid Impact and Mass Extinction at the Cretaceous-Paleogene Boundary. Science 327, 1214. https://doi.org/10.1126/science.1177265

Sepkoski, J.J., 1996. Patterns of Phanerozoic extinction: a perspective from global data bases, in: Walliser, O.H. (Ed.), Global Events and Event Stratigraphy in the Phanerozoic. Springer, Berlin, pp. 35–51.

Sexton, P.F., Wilson, P.A., Pearson, P.N., 2006. Microstructural and geochemical perspectives on planktic foraminiferal preservation:“Glassy” versus “Frosty.” Geochemistry, Geophysics, Geosystems 7.

Shen, S.-Z., Ramezani, J., Chen, J., Cao, C.-Q., Erwin, D.H., Zhang, H., Xiang, L., Schoepfer, S.D., Henderson, C.M., Zheng, Q.-F., 2019. A sudden end-Permian mass extinction in South China. GSA Bulletin 131, 205–223.

Shen, Y., Buick, R., Canfield, D.E., 2001. Isotopic evidence for microbial sulphate reduction in the early Archaean era. Nature 410, 77–81. https://doi.org/10.1038/35065071

Sim, M.S., 2019. Effect of sulfate limitation on sulfur isotope fractionation in batch cultures of sulfate reducing bacteria. Geosciences Journal 23, 687–694. https://doi.org/10.1007/s12303-019-0015-x

Sim, M.S., Bosak, T., Ono, S., 2011a. Large Sulfur Isotope Fractionation Does Not Require Disproportionation. Science 333, 74. https://doi.org/10.1126/science.1205103

Sim, M.S., Ogata, H., Lubitz, W., Adkins, J.F., Sessions, A.L., Orphan, V.J., McGlynn, S.E., 2019. Role of APS reductase in biogeochemical sulfur isotope fractionation. Nature Communications 10, 44. https://doi.org/10.1038/s41467-018-07878-4

Sim, M.S., Ono, S., Donovan, K., Templer, S.P., Bosak, T., 2011b. Effect of electron donors on the fractionation of sulfur isotopes by a marine Desulfovibrio sp. Geochimica et Cosmochimica Acta 75, 4244–4259. https://doi.org/10.1016/j.gca.2011.05.021

Sim, M.S., Paris, G., Adkins, J.F., Orphan, V.J., Sessions, A.L., 2017. Quantification and isotopic analysis of intracellular sulfur metabolites in the dissimilatory sulfate reduction pathway. Geochimica et Cosmochimica Acta 206, 57–72. https://doi.org/10.1016/j.gca.2017.02.024

Sim, M.S., Woo, D.K., Kim, B., Jeong, H., Joo, Y.J., Hong, Y.W., Choi, J.Y., 2023. What Controls the Sulfur Isotope Fractionation during Dissimilatory Sulfate Reduction? ACS Environ. Au 3, 76–86. https://doi.org/10.1021/acsenvironau.2c00059

Sime, N.G., De La Rocha, C.L., Galy, A., 2005. Negligible temperature dependence of calcium isotope fractionation in 12 species of planktonic foraminifera. Earth and Planetary Science Letters 232, 51–66. https://doi.org/10.1016/j.epsl.2005.01.011

Simonet Roda, M., Griesshaber, E., Ziegler, A., Rupp, U., Yin, X., Henkel, D., Häussermann, V., Laudien, J., Brand, U., Eisenhauer, A., Checa, A.G., Schmahl, W.W., 2019. Calcite fibre formation in modern brachiopod shells. Scientific Reports 9, 598. https://doi.org/10.1038/s41598-018-36959-z

Skulan, J., DePaolo, D.J., Owens, T.L., 1997. Biological control of calcium isotopic abundances in the global calcium cycle. Geochimica et Cosmochimica Acta 61, 2505–2510. https://doi.org/10.1016/S0016-7037(97)00047-1

Smit, J., Hertogen, J., 1980. An extraterrestrial event at the Cretaceous–Tertiary boundary. Nature 285, 198–200. https://doi.org/10.1038/285198a0

Smith, M.E., Moore, E.W., Swart, P.K., 2022. Constraining diagenesis within shallow water carbonate environments: Insights from clumped and sulfur isotopes. Chemical Geology 614, 121183. https://doi.org/10.1016/j.chemgeo.2022.121183

Song, Huyue, Du, Y., Algeo, T.J., Tong, J., Owens, J.D., Song, Haijun, Tian, L., Qiu, H., Zhu, Y., Lyons, T.W., 2019. Cooling-driven oceanic anoxia across the Smithian/Spathian boundary (mid-Early Triassic). Earth-Science Reviews 195, 133–146. https://doi.org/10.1016/j.earscirev.2019.01.009

Spero, H.J., 1998. Life history and stable isotope geochemistry of planktonic foraminifera. The Paleontological Society Papers 4, 7–36.

Spero, H.J., 1988. Ultrastructural examination of chamber morphogenesis and biomineralization in the planktonic foraminiferOrbulina universa. Mar. Biol. 99, 9–20. https://doi.org/10.1007/bf00644972

Spero, H.J., Eggins, S.M., Russell, A.D., Vetter, L., Kilburn, M.R., Hönisch, B., 2015. Timing and mechanism for intratest Mg/Ca variability in a living planktic foraminifer. Earth and Planetary Science Letters 409, 32–42. https://doi.org/10.1016/j.epsl.2014.10.030

Sprain, C.J., Renne, P.R., Vanderkluysen, L., Pande, K., Self, S., Mittal, T., 2019. The eruptive tempo of Deccan volcanism in relation to the Cretaceous-Paleogene boundary. Science 363, 866. https://doi.org/10.1126/science.aav1446

Staudt, W.J., Reeder, R.J., Schoonen, M.A.A., 1994. Surface structural controls on compositional zoning of SO42− and SeO42− in synthetic calcite single crystals. Geochimica et Cosmochimica Acta 58, 2087–2098. https://doi.org/10.1016/0016-7037(94)90287-9

Stehli, F.G., Hower, J., 1961. Mineralogy and early diagenesis of carbonate sediments. Journal of Sedimentary Research 31, 358–371.

Stichler, W., 1995. Interlaboratory comparison of new materials for carbon and oxygen isotope ratio measurements. Reference and intercomparison materials for stable isotopes of light elements 825, 67–74.

Stolper, D.A., Eiler, J.M., Higgins, J.A., 2018. Modeling the effects of diagenesis on carbonate clumped-isotope values in deep- and shallow-water settings. Geochimica et Cosmochimica Acta 227, 264–291. https://doi.org/10.1016/j.gca.2018.01.037

Strauss, H., 1997. The isotopic composition of sedimentary sulfur through time. Palaeogeography, Palaeoclimatology, Palaeoecology 132, 97–118. https://doi.org/10.1016/s0031-0182(97)00067-9

Stroobants, N., Dehairs, F., Goeyens, L., Vanderheijden, N., Van Grieken, R., 1991. Barite formation in the Southern Ocean water column. Marine Chemistry 35, 411–421. https://doi.org/10.1016/S0304-4203(09)90033-0

Sundquist, E.T., 1985. Geological Perspectives on Carbon Dioxide and the Carbon Cycle, in: The Carbon Cycle and Atmospheric CO_2: Natural Variations Archean to Present, Geophysical Monograph Series. pp. 55–59. https://doi.org/10.1029/GM032p0005

Swart, P.K., 2015. The geochemistry of carbonate diagenesis: The past, present and future. Sedimentology 62, 1233–1304. https://doi.org/10.1111/sed.12205

Szanda, G., Rajki, A., Gallego-Sandín, S., Garcia-Sancho, J., Spät, A., 2009. Effect of cytosolic Mg2+ on mitochondrial Ca^{2+} signaling. Pflügers Archiv - European Journal of Physiology 457, 941–954. https://doi.org/10.1007/s00424-008-0551-0

Takano, B., 1985. Geochemical implications of sulfate in sedimentary carbonates. Chemical Geology 49, 393–403. https://doi.org/10.1016/0009-2541(85)90001-4

Takano, B., Asano, Y., Watanuki, K., 1980. Characterization of sulfate ion in travertine. Contributions to Mineralogy and Petrology 72, 197–203. https://doi.org/10.1007/BF00399480

Tambutté, E., Tambutté, S., Segonds, N., Zoccola, D., Venn, A., Erez, J., Allemand, D., 2012. Calcein labelling and electrophysiology: insights on coral tissue permeability and calcification. Proceedings of the Royal Society B: Biological Sciences 279, 19–27.

Tambutté, S., Tambutté, E., Zoccola, D., Caminiti, N., Lotto, S., Moya, A., Allemand, D., Adkins, J., 2007. Characterization and role of carbonic anhydrase in the calcification process of the azooxanthellate coral Tubastrea aurea. Marine Biology 151, 71–83. https://doi.org/10.1007/s00227-006-0452-8

Tamenori, Y., Yoshimura, T., 2018. Sulfur speciation in growth layers of shell cross section of the long-lived bivalve Margaritifera laevis using synchrotron spectromicroscopy analysis. Geochimica et Cosmochimica Acta 237, 357–369. https://doi.org/10.1016/j.gca.2018.07.002

Tamenori, Y., Yoshimura, T., Luan, N.T., Hasegawa, H., Suzuki, A., Kawahata, H., Iwasaki, N., 2014. Identification of the chemical form of sulfur compounds in the Japanese pink coral (Corallium elatius) skeleton using μ-XRF/XAS speciation mapping. Journal of Structural Biology 186, 214–223. https://doi.org/10.1016/j.jsb.2014.04.001

Tanaka, K., Okaniwa, N., Miyaji, T., Murakami-Sugihara, N., Zhao, L., Tanabe, K., Schöne, B.R., Shirai, K., 2019. Microscale magnesium distribution in shell of the Mediterranean mussel Mytilus galloprovincialis: An example of multiple factors controlling Mg/Ca in biogenic calcite. Chemical Geology 511, 521–532. https://doi.org/10.1016/j.chemgeo.2018.10.025

Tang, J., Dietzel, M., Böhm, F., Köhler, S.J., Eisenhauer, A., 2008. Sr^{2+}/Ca^{2+} and $^{44}Ca/^{40}Ca$ fractionation during inorganic calcite formation: II. Ca isotopes. Geochimica et Cosmochimica Acta 72, 3733–3745. https://doi.org/10.1016/j.gca.2008.05.033

ter Kuile, B., Erez, J., Padan, E., 1989. Mechanisms for the uptake of inorganic carbon by two species of symbiont-bearing foraminifera. Marine Biology 103, 241–251. https://doi.org/10.1007/BF00543354

Ter Kuile, B.H., Erez, J., 1991. Carbon Budgets for Two Species of Benthonic Symbiont-Bearing Foraminifera. The Biological Bulletin 180, 489–495. https://doi.org/10.2307/1542350

Thaler, C., Paris, G., Dellinger, M., Dissard, D., Berland, S., Marie, A., Labat, A., Bartolini, A., preprint. Impact of seawater sulfate concentration on sulfur concentration and isotopic composition in calcite of two cultured benthic foraminifera. EGUsphere 2023, 1–29.

Thiemens, M.H., 1999. Mass-Independent Isotope Effects in Planetary Atmospheres and the Early Solar System. Science 283, 341–345. https://doi.org/10.1126/science.283.5400.341

Thode, H., Monster, J., 1964. The sulfur isotope abundances in evaporites and in ancient oceans. Presented at the Proceedings of geochemistry conference commemorating the centenary of VI Vernadskii's birth, p. 630.

Thode, H., Monster, S., 1965. Sulfur-isotope geochemistry of petroleum, evaporites, and ancient seas. Amer. Assoc. Petrol. Geol. Bull 42, 2619–2629.

Thode, H.G., Macnamara, J., Fleming, W.H., 1953. Sulphur isotope fractionation in nature and geological and biological time scales. Geochimica et Cosmochimica Acta 3, 235–243. https://doi.org/10.1016/0016-7037(53)90042-8

Thode, H.G., Monster, J., Dunford, H.B., 1961. Sulphur isotope geochemistry. Geochimica et Cosmochimica Acta 25, 159–174. https://doi.org/10.1016/0016-7037(61)90074-6

Thode, H.G., Rees, C.E., 1971. Measurement of sulphur concentrations and the isotope ratios 33S/32S, 34S/32S and 36S/32S in Apollo 12 samples. Earth and Planetary Science Letters 12, 434–438. https://doi.org/10.1016/0012-821x(71)90029-x

Timofeeff, M.N., Lowenstein, T.K., da Silva, M.A.M., Harris, N.B., 2006. Secular variation in the major-ion chemistry of seawater: Evidence from fluid inclusions in Cretaceous halites. Geochimica et Cosmochimica Acta 70, 1977–1994. https://doi.org/10.1016/j.gca.2006.01.020

Tipper, E.T., Galy, A., Gaillardet, J., Bickle, M.J., Elderfield, H., Carder, E.A., 2006. The magnesium isotope budget of the modern ocean: Constraints from riverine magnesium isotope ratios. Earth and Planetary Science Letters 250, 241–253.

Tipper, E.T., Stevenson, E.I., Alcock, V., Knight, A.C.G., Baronas, J.J., Hilton, R.G., Bickle, M.J., Larkin, C.S., Feng, L., Relph, K.E., Hughes, G., 2021. Global silicate weathering flux overestimated because of sediment–water cation exchange. Proceedings of the National Academy of Sciences 118, e2016430118. https://doi.org/10.1073/pnas.2016430118

Tochon-Danguy, D., Campion, L., Very, J., 1976. Mise en évidence d'ions SO4 dans le test du foraminifère planctonique Orbulina universa d'Orbigny.

Torres, M.A., Moosdorf, N., Hartmann, J., Adkins, J.F., West, A.J., 2017. Glacial weathering, sulfide oxidation, and global carbon cycle feedbacks. Proceedings of the National Academy of Sciences 114, 8716–8721. https://doi.org/10.1073/pnas.1702953114

Torres, M.A., Paris, G., Adkins, J.F., Fischer, W.W., 2018. Riverine evidence for isotopic mass balance in the Earth's early sulfur cycle. Nature Geoscience. https://doi.org/10.1038/s41561-018-0184-7

Torres, M.A., West, A.J., Clark, K.E., Paris, G., Bouchez, J., Ponton, C., Feakins, S.J., Galy, V., Adkins, J.F., 2016. The acid and alkalinity budgets of weathering in the Andes–Amazon system: Insights into the erosional control of global biogeochemical cycles. Earth and Planetary Science Letters 450, 381–391. https://doi.org/10.1016/j.epsl.2016.06.012

Torres, M.A., West, A.J., Li, G., 2014. Sulphide oxidation and carbonate dissolution as a source of CO_2 over geological timescales. Nature 507, 346–349. https://doi.org/10.1038/nature13030

Tostevin, R., Turchyn, A.V., Farquhar, J., Johnston, D.T., Eldridge, D.L., Bishop, J.K.B., McIlvin, M., 2014. Multiple sulfur isotope constraints on the modern sulfur cycle. Earth and Planetary Science Letters 396, 14–21. https://doi.org/10.1016/j.epsl.2014.03.057

Toyama, K., Paytan, A., Sawada, K., Hasegawa, T., 2020. Sulfur isotope ratios in co-occurring barite and carbonate from Eocene sediments: A comparison study. Chemical Geology 535, 119454. https://doi.org/10.1016/j.chemgeo.2019.119454

Toyofuku, T., Matsuo, M.Y., de Nooijer, L.J., Nagai, Y., Kawada, S., Fujita, K., Reichart, G.-J., Nomaki, H., Tsuchiya, M., Sakaguchi, H., Kitazato, H., 2017. Proton pumping accompanies calcification in foraminifera. Nature Communications 8, 14145. https://doi.org/10.1038/ncomms14145

Trong Nguyen, L., Rahman, M.A., Maki, T., Tamenori, Y., Yoshimura, T., Suzuki, A., Iwasaki, N., Hasegawa, H., 2014. Distribution of trace element in Japanese red coral Paracorallium japonicum by μ-XRF and sulfur speciation by XANES: Linkage

between trace element distribution and growth ring formation. Geochimica et Cosmochimica Acta 127, 1–9. https://doi.org/10.1016/j.gca.2013.11.023

Trudinger, P.A., Chambers, L.A., 1973. Reversibility of bacterial sulfate redaction and its relevance to isotope fractionation. Geochimica et Cosmochimica Acta 37, 1775–1778. https://doi.org/10.1016/0016-7037(73)90162-2

Turchyn, A.V., Bradbury, H.J., Walker, K., Sun, X., 2021. Controls on the Precipitation of Carbonate Minerals Within Marine Sediments. Frontiers in Earth Science 9. https://doi.org/10.3389/feart.2021.618311

Turchyn, A.V., DePaolo, D.J., 2019. Seawater Chemistry Through Phanerozoic Time. Annu. Rev. Earth Planet. Sci. 47, 197–224. https://doi.org/10.1146/annurev-earth-082517-010305

Turchyn, A.V., Schrag, D.P., 2006. Cenozoic evolution of the sulfur cycle: Insight from oxygen isotopes in marine sulfate. Earth and Planetary Science Letters 241, 763–779. https://doi.org/10.1016/j.epsl.2005.11.007

Turchyn, A.V., Schrag, D.P., 2004. Oxygen Isotope Constraints on the Sulfur Cycle over the Past 10 Million Years. Science 303, 2004–2007. https://doi.org/10.1126/science.1092296

Turchyn, A.V., Schrag, D.P., Coccioni, R., Montanari, A., 2009. Stable isotope analysis of the Cretaceous sulfur cycle. Earth and Planetary Science Letters 285, 115–123. https://doi.org/10.1016/j.epsl.2009.06.002

Turchyn, A.V., Tipper, E.T., Galy, A., Lo, J.-K., Bickle, M.J., 2013. Isotope evidence for secondary sulfide precipitation along the Marsyandi River, Nepal, Himalayas. Earth and Planetary Science Letters 374, 36–46. https://doi.org/10.1016/j.epsl.2013.04.033

Uchikawa, J., Zeebe, R.E., 2012. The effect of carbonic anhydrase on the kinetics and equilibrium of the oxygen isotope exchange in the CO_2–H_2O system: Implications for $\delta^{18}O$ vital effects in biogenic carbonates. Geochimica et Cosmochimica Acta 95, 15–34. https://doi.org/10.1016/j.gca.2012.07.022

Ueno, Y., Aoyama, S., Endo, Y., Matsu'ura, F., Foriel, J., 2015. Rapid quadruple sulfur isotope analysis at the sub-micromole level by a flash heating with CoF_3. Chemical Geology 419, 29–35. https://doi.org/10.1016/j.chemgeo.2015.10.032

Ullmann, C.V., Campbell, H.J., Frei, R., Hesselbo, S.P., Pogge von Strandmann, P.A.E., Korte, C., 2013. Partial diagenetic overprint of Late Jurassic belemnites from New Zealand: Implications for the preservation potential of δ^7Li values in calcite fossils. Geochimica et Cosmochimica Acta 120, 80–96. https://doi.org/10.1016/j.gca.2013.06.029

Ullmann, C.V., Korte, C., 2015. Diagenetic alteration in low-Mg calcite from macrofossils: a review. Geological Quarterly 59, 3–20.

Urey, H.C., Lowenstam, H.A., Epstein, S., McKinney, C.R., 1951. Measurement of paleotemperatures and temperatures of the Upper Cretaceous of England, Denmark, and the Southeastern United States. GSA Bulletin 62, 399–416. https://doi.org/10.1130/0016-7606(1951)62[399:MOPATO]2.0.CO;2

Utrilla, R., Pierre, C., Orti, F., Pueyo, J.J., 1992. Oxygen and sulphur isotope compositions as indicators of the origin of Mesozoic and Cenozoic evaporites from Spain. Chemical Geology 102, 229–244. https://doi.org/10.1016/0009-2541(92)90158-2

Uyama, T., Kitagawa, H., Sugahara, K., 2007. 3.05 - Biosynthesis of Glycosaminoglycans and Proteoglycans, in: Kamerling, H. (Ed.), Comprehensive Glycoscience. Elsevier, Oxford, pp. 79–104. https://doi.org/10.1016/B978-044451967-2/00036-2

van Dijk, I., Barras, C., de Nooijer, L.J., Mouret, A., Geerken, E., Oron, S., Reichart, G.-J., 2019. Coupled calcium and inorganic carbon uptake suggested by magnesium and sulfur incorporation in foraminiferal calcite. Biogeosciences 16, 2115–2130. https://doi.org/10.5194/bg-16-2115-2019

van Dijk, I., de Nooijer, L.J., Boer, W., Reichart, G.-J., 2017. Sulfur in foraminiferal calcite as a potential proxy for seawater carbonate ion concentration. Earth and Planetary Science Letters 470, 64–72. https://doi.org/10.1016/j.epsl.2017.04.031

Van Leeuwen, T.N., Moed, H.F., Tijssen, R.J.W., Visser, M.S., Van Raan, A.F.J., 2001. Language biases in the coverage of the Science Citation Index and its consequencesfor international comparisons of national research performance. Scientometrics 51, 335–346. https://doi.org/10.1023/A:1010549719484

van Zelm, R., Huijbregts, M.A.J., den Hollander, H.A., van Jaarsveld, H.A., Sauter, F.J., Struijs, J., van Wijnen, H.J., van de Meent, D., 2008. European characterization factors for human health damage of PM10 and ozone in life cycle impact assessment. Atmospheric Environment 42, 441–453. https://doi.org/10.1016/j.atmosenv.2007.09.072

Vasconcelos, C., McKenzie, J.A., Bernasconi, S., Grujic, D., Tiens, A.J., 1995. Microbial mediation as a possible mechanism for natural dolomite formation at low temperatures. Nature 377, 220–222.

Vavouraki, A.I., Putnis, C.V., Putnis, A., Koutsoukos, P.G., 2008. An Atomic Force Microscopy study of the growth of calcite in the presence of sodium sulfate. Chemical Geology 253, 243–251. https://doi.org/10.1016/j.chemgeo.2008.05.013

Vellekoop, J., Woelders, L., Açikalin, S., Smit, J., van de Schootbrugge, B., Yilmaz, I.Ö., Brinkhuis, H., Speijer, R.P., 2017. Ecological response to collapse of the biological pump following the mass extinction at the Cretaceous–Paleogene boundary. Biogeosciences 14, 885–900. https://doi.org/10.5194/bg-14-885-2017

Venceslau, S.S., Stockdreher, Y., Dahl, C., Pereira, I.A.C., 2014. The "bacterial heterodisulfide" DsrC is a key protein in dissimilatory sulfur metabolism. Biochimica et Biophysica Acta (BBA) - Bioenergetics 1837, 1148–1164. https://doi.org/10.1016/j.bbabio.2014.03.007

Vielzeuf, D., Garrabou, J., Gagnon, A., Ricolleau, A., Adkins, J., Günther, D., Hametner, K., Devidal, J.-L., Reusser, E., Perrin, J., Floquet, N., 2013. Distribution of sulphur and magnesium in the red coral. Chemical Geology 355, 13–27. https://doi.org/10.1016/j.chemgeo.2013.07.008

Vigier, N., Rollion-Bard, C., Levenson, Y., Erez, J., 2015. Lithium isotopes in foraminifera shells as a novel proxy for the ocean dissolved inorganic carbon (DIC). Comptes Rendus Geoscience 347, 43–51. https://doi.org/10.1016/j.crte.2014.12.001

Vinogradov, V.I., 2007. Was there a conflict at the Neoproterozoic-Cambrian boundary: Evidence from sulfur isotope composition? Lithology and Mineral Resources 42, 1–14. https://doi.org/10.1134/S0024490207010014

von Blanckenburg, F., 2006. The control mechanisms of erosion and weathering at basin scale from cosmogenic nuclides in river sediment. Earth and Planetary Science Letters 242, 224–239. https://doi.org/10.1016/j.epsl.2005.11.017

Waldeck, A.R., Hemingway, J.D., Yao, W., Paytan, A., Johnston, D.T., 2022. The triple oxygen isotope composition of marine sulfate and 130 million years of microbial control. Proceedings of the National Academy of Sciences 119, e2202018119. https://doi.org/10.1073/pnas.2202018119

Walker, J.C.G., Hays, P.B., Kasting, J.F., 1981. A negative feedback mechanism for the long-term stabilization of Earth's surface temperature. Journal of Geophysical Research 86, 9776–9782.

Wang, D., Hamm, L.M., Giuffre, A.J., Echigo, T., Rimstidt, J.D., De Yoreo, J.J., Grotzinger, J., Dove, P.M., 2012. Revisiting geochemical controls on patterns of carbonate deposition through the lens of multiple pathways to mineralization. Faraday Discuss. 159, 371–386. https://doi.org/10.1039/C2FD20077E

Wanless, R.K., Thode, H.G., 1953. A mass spectrometer for high precision isotope ratio determinations. Journal of Scientific Instruments 30, 395.

Warren, J., 2000. Dolomite: occurrence, evolution and economically important associations. Earth-Science Reviews 52, 1–81. https://doi.org/10.1016/S0012-8252(00)00022-2

Watkins, J.M., DePaolo, D.J., Watson, E.B., 2017. Kinetic fractionation of non-traditional stable isotopes by diffusion and crystal growth reactions. Reviews in Mineralogy and Geochemistry 82, 85–125.

Weber, J.N., Schmalz, R., 1968. Factors affecting the carbon and oxygen isotopic composition of marine carbonate sediments; Part III, Eniwetok Atoll. Journal of Sedimentary Research 38, 1270–1279.

Wegener, G., Krukenberg, V., Riedel, D., Tegetmeyer, H.E., Boetius, A., 2015. Intercellular wiring enables electron transfer between methanotrophic archaea and bacteria. Nature 526, 587–590. https://doi.org/10.1038/nature15733

Weiner, S., Addadi, L., 2011. Crystallization pathways in biomineralization. Annual review of materials research 41, 21–40.

Weiner, S., Dove, P.M., 2003. An Overview of Biomineralization Processes and the Problem of the Vital Effect. Reviews in Mineralogy and Geochemistry 54, 1–29. https://doi.org/10.2113/0540001

Weiner, S., Erez, J., 1984. Organic matrix of the shell of the foraminifer, Heterostegina depressa. The Journal of Foraminiferal Research 14, 206–212. https://doi.org/10.2113/gsjfr.14.3.206

Weiner, S., Levi-Kalisman, Y., Raz, S., Addadi, L., 2003. Biologically Formed Amorphous Calcium Carbonate. Connective Tissue Research 44, 214–218. https://doi.org/10.1080/03008200390181681

West, A.J., Galy, A., Bickle, M., 2005. Tectonic and climatic controls on silicate weathering. Earth and Planetary Science Letters 235, 211–228.

Wieder, R.K., Yavitt, J.B., Lang, G.E., 1990. Methane production and sulfate reduction in two Appalachian peatlands. Biogeochemistry 10, 81–104.

Wing, B.A., Farquhar, J., 2015. Sulfur isotope homogeneity of lunar mare basalts. Geochimica et Cosmochimica Acta 170, 266–280. https://doi.org/10.1016/j.gca.2015.09.003

Wing, B.A., Halevy, I., 2014. Intracellular metabolite levels shape sulfur isotope fractionation during microbial sulfate respiration. Proceedings of the National Academy of Sciences 111, 18116–18125. https://doi.org/10.1073/pnas.1407502111

Winland, H.D., 1969. Stability of calcium carbonate polymorphs in warm, shallow seawater. Journal of Sedimentary Research 39.

Witts, J.D., Newton, R.J., Mills, B.J.W., Wignall, P.B., Bottrell, S.H., Hall, J.L.O., Francis, J.E., Alistair Crame, J., 2018. The impact of the Cretaceous–Paleogene (K–Pg) mass extinction event on the global sulfur cycle: Evidence from Seymour Island, Antarctica. Geochimica et Cosmochimica Acta 230, 17–45. https://doi.org/10.1016/j.gca.2018.02.037

Wortmann, U.G., Chernyavsky, B.M., 2011. The significance of isotope specific diffusion coefficients for reaction-transport models of sulfate reduction in marine sediments. Geochimica et Cosmochimica Acta 75, 3046–3056. https://doi.org/10.1016/j.gca.2011.03.007

Wortmann, U.G., Chernyavsky, B.M., 2007. Effect of evaporite deposition on Early Cretaceous carbon and sulphur cycling. Nature 446, 654–656. https://doi.org/10.1038/nature05693

Wortmann, U.G., Paytan, A., 2012. Rapid Variability of Seawater Chemistry Over the Past 130 Million Years. Science 337, 334–336. https://doi.org/10.1126/science.1220656

Wotte, T., Shields-Zhou, G.A., Strauss, H., 2012. Carbonate-associated sulfate: Experimental comparisons of common extraction methods and recommendations toward a standard analytical protocol. Chemical Geology 326–327, 132–144. https://doi.org/10.1016/j.chemgeo.2012.07.020

Wuebbles, D.J., Hayhoe, K., 2002. Atmospheric methane and global change. Earth-Science Reviews 57, 177–210.

Yao, W., Markovic, S., Paytan, A., Erhardt, A.M., Wortmann, U.G., 2021. Quantifying pyrite oxidation on continental shelves during the onset of Antarctic glaciation in the Eocene-Oligocene transition. Earth and Planetary Science Letters 568, 117015. https://doi.org/10.1016/j.epsl.2021.117015

Yao, W., Paytan, A., 2020. Possible triggers of the seawater sulfate S-isotope increase between 55 and 40 million years ago. Chemical Geology 552, 119788. https://doi.org/10.1016/j.chemgeo.2020.119788

Yao, W., Paytan, A., Griffith, E.M., Martínez-Ruiz, F., Markovic, S., Wortmann, U.G., 2020a. A revised seawater sulfate S-isotope curve for the Eocene. Chemical Geology 532, 119382. https://doi.org/10.1016/j.chemgeo.2019.119382

Yao, W., Paytan, A., Wortmann, U.G., 2020b. Effects of a transient marine sulfur reservoir on seawater δ18OSO4 during the Paleocene-Eocene Thermal Maximum. Geochimica et Cosmochimica Acta 269, 257–269. https://doi.org/10.1016/j.gca.2019.10.019

Yao, W., Paytan, A., Wortmann, U.G., 2018. Large-scale ocean deoxygenation during the Paleocene-Eocene Thermal Maximum. Science 361, 804. https://doi.org/10.1126/science.aar8658

Yoshimura, T., Maeda, A., Tamenori, Y., Suzuki, A., Fujita, K., Kawahata, H., 2019. Partitioning and Chemical Environments of Minor Elements in Individual Large Benthic Foraminifera Cultured in Temperature-Controlled Tanks. Frontiers in Earth Science 7.

Yoshimura, T., Tamenori, Y., Kawahata, H., Suzuki, A., 2014. Fluctuations of sulfate, S-bearing amino acids and magnesium in a giant clam shell. Biogeosciences 11, 3881–3886.

Yoshimura, T., Tamenori, Y., Suzuki, A., Nakashima, R., Iwasaki, N., Hasegawa, H., Kawahata, H., 2013. Element profile and chemical environment of sulfur in a giant clam shell: Insights from μ-XRF and X-ray absorption near-edge structure. Chemical Geology 352, 170–175. https://doi.org/10.1016/j.chemgeo.2013.05.035

Zachos, J.C., Arthur, M.A., Dean, W.E., 1989. Geochemical evidence for suppression of pelagic marine productivity at the Cretaceous/Tertiary boundary. Nature 337, 61–64. https://doi.org/10.1038/337061a0

Zachos, J.C., Pagani, M., Sloan, L., Thomas, E., Billups, K., 2001. Trends, Rhythms, and Aberrations in Global Climate 65 Ma to Present. Science 292, 686–693. https://doi.org/10.1126/science.1059412

Zeebe, R.E., Sanyal, A., 2002. Comparison of two potential strategies of planktonic foraminifera for house building: Mg2+ or H+ removal? Geochimica et Cosmochimica Acta 66, 1159–1169. https://doi.org/10.1016/S0016-7037(01)00852-3

Zeebe, R.E., Wolf-Gladrow, D.A., 2001. CO_2 in seawater: equilibrium, kinetics, isotopes, Oceanography series. Elsevier science B.V., Amsterdam.

Ziegler, P.A., 1988. Evolution of the Arctic-North Atlantic and the western Tethys.

Zorlu, J., 2007. Sedimentpetrographische und geochemische Untersuchungen an unterschiedlich überprägten Triasdolomiten der Ost-und Südalpen.

Abstract/résumé

Abstract

The carbon and oxygen cycles have controlled the composition of the ocean-atmosphere system throughout Earth's history. They are linked by widely studied processes: (1) photosynthesis and its associated opposed flux, the oxidation of organic matter, and (2) carbonate precipitation coupled with weathering and its counter-flux, reversed weathering. The third flux/counter flux, less well characterized, is the formation and burial of pyrite, which releases oxygen and CO_2 on geological timescales and its counter-flux, the oxidation of pyrite at the surface of continents, which disrupts weathering and lead to atmospheric oxygen consumption.

This memoire presents how I helped develop measurements of sulfur isotope ratios in rivers to improve our understanding of the modern carbon, oxygen and sulfur cycles and how I improved the use of carbonate associated sulfate as an archive for past sulfur isotope ratios of seawater. Additionally, I contributed to a better understanding of biomineralization, and paved the way to extract multiple paleoenvironmental signals from carbonate rocks. Not only can we now reliably reconstruct past sulfur isotope ratios of seawater from carbonates, but we can also use isotopes to unpack the various steps of diagenetic alteration and thus collect key information about the activity of microorganisms in deep ocean sediments. Collectively, my work has enhanced our understanding of the relationships between past and modern sulfur, carbon and oxygen cycles.

Résumé

Les cycles du carbone et de l'oxygène ont contrôlé la composition du système océan-atmosphère tout au long de l'histoire de la Terre. Ils sont liés par des processus amplement étudiés : (1) la photosynthèse et la respiration, et (2) la précipitation carbonatée couplée à l'altération. Le troisième flux/contre-flux essentiel est la formation et l'enfouissement de la pyrite, qui libère de l'oxygène et du CO_2 aux échelles de temps géologiques et son contre-flux, l'oxydation de la pyrite à la surface des continents, qui perturbe l'altération et entraîne une consommation d'O_2. Les rapports isotopiques du soufre sont un outil essentiel pour étudier le cycle du soufre actuel ou ancien. Ce mémoire présente comment j'ai contribué au développement des rapports isotopiques du soufre mesurés dans les rivières pour améliorer notre compréhension des cycles du carbone, de l'oxygène et du soufre actuels et comment j'ai contribué à améliorer l'utilisation du sulfate associé au carbonate comme archive des rapports isotopiques du soufre passés de l'eau de mer. Ces travaux ont non seulement contribué à une meilleure compréhension de la biominéralisation, mais ils ouvrent la voie à l'extraction de signaux paléoenvironnementaux multiples à partir des roches carbonatées. Il est ainsi non seulement possible de désormais reconstruire de manière fiable les rapports isotopiques du soufre de l'eau de mer au cours des temps géologiques, mais également d'accéder à des informations clés sur la diagenèse et l'activité des micro-organismes dans les sédiments des océans profonds et ainsi commencer à ouvrir cette partie jusque-là cachée des cycles anciens et actuels du soufre, du carbone et de l'oxygène.